Finite-temperature theory
of bosons in optical lattices

Daniel Baillie

UNIVERSITY
of
OTAGO

Te Whare Wānanga o Otāgo

NEW ZEALAND

a thesis submitted for the degree of

Master of Science

at the University of Otago, Dunedin,

New Zealand.

September 11, 2009

Abstract

Beautiful experiments have shown that bosons in optical lattices provide a physical system with an unprecedented degree of control; that they can generate strongly correlated states; and that, as long-term goals, they may be useful for simulating other many-body systems, or realising a quantum computer. Recently a practical scheme for measuring temperature in an optical lattice has been demonstrated [1], which marks an important milestone necessary for the detailed study of the thermodynamics of this system.

In this thesis, we consider both the translationally-invariant lattice, and the combined harmonic trap and optical lattice. We use an extended Bose-Hubbard Hamiltonian which goes beyond the usual Bose-Hubbard approach, and is valid for shallower lattices and higher temperatures, by allowing for beyond nearest-neighbour hopping and excited bands, and we have developed an approximation scheme for off-site interactions. We derive the equations of the Popov approximation to the Hartree-Fock-Bogoliubov method for our Hamiltonian, and diagonalise these equations in the local density approximation (LDA).

We examine the density of states of the optical lattice in detail and in various limits. We derive new results on the structure of the density of states, and, in the ideal case, we compare the density of states from the full diagonalisation with our LDA calculation.

We make an efficient numerical implementation of our theory and compare the results with the full diagonalisation (for the non-interacting case) and with the limited experimental results currently available. We consider the significance of beyond nearest-neighbour hopping and excited bands and illustrate the properties of our model.

In contrast to the trapped gas with no lattice, few thermodynamic results for cold bosons in an optical lattice have been calculated. We analytically derive the first practical formula for the critical temperature in an optical lattice by using simplified shapes for the density of states. We derive corrections for the influence of excited bands, the finite-size effect and mean-field interactions. In all of these cases, we compare our results to full numerical calculations and show that the validity range of our method is complementary to that of the effective-mass approximation, so that the simple descriptions extend over a wide range.

Acknowledgements

Contents

Contents

Contents

Abbreviations

The only abbreviations we use are for the local density approximation (LDA) and the first Brillouin zone (BZ). We list our notation in table 1. We do not include notation that is well known (on the level of m for the mass of an atom or $z = e^{\beta\mu}$ for the fugacity); used only near to where it is defined, or used only in appendices C and D. The reference is to the page number where defined, or to the equation if in parentheses.

Table 1: Table of notation

Notation	Description	Ref.
$\hat{a}_{b,i}$	destruction operator for an atom in band b at site i	(2.4)
a_j, a	lattice spacing in direction j and their geometric mean	(2.1)
a_s	s-wave scattering length	14
b_j, b	band index in direction j and d-dimensional band-index vector ($b = 0$ is the ground band for any d)	14
d	number of dimensions (number of harmonically trapped dimensions in sections 7.2 and 7.4)	11, 75
$E_{b,j}, E_b(\mathbf{k}, \mathbf{r})$	Hartree-Fock or Bogoliubov energy for band b, mode j and its LDA equivalent for quasi-momentum $\mathbf{k}$	(3.28), (3.40)
$E_{R,j}, E_R$	recoil energy in direction j and their geometric mean	12
g	no lattice interaction parameter, $g = 4\pi\hbar^2 a_s/m$	14
$g_b(K)$	translationally-invariant lattice density of states, band b	(4.1)
$g_{\mathrm{LDA}}(E)$	combined harmonic lattice LDA density of states	(4.12)
$g_{\mathrm{trap}}(V_{\mathrm{tr}})$	harmonic trap density of states for potential energy V_{tr}	(4.13)
$J_{b,i,i'}, J_{b,y}^l$	hopping matrix between sites i, i' for band b and between neighbours l sites apart in direction y	(2.6), 18
J	ground-band hopping matrix element for a cubic lattice	17
$\hat{K}_{0,i}, \hat{K}_{1,i}, \hat{K}_{2,b,i}$	site i grand-canonical Hamiltonian with 0,1,2 $\hat{\delta}_{b,i}$ factors	33
$K_b(\mathbf{k})$	non-interacting translationally-invariant lattice energy	(3.34)
K_b^{min}	minimum of $K_b(\mathbf{k})$ for band b	47, 87
$\hat{\mathcal{L}}_{b,i}$	Hartree-Fock energy operator for band b at site i	(3.16)
$\mathcal{L}_b(\mathbf{k}, \mathbf{r})$	LDA equivalent of $\hat{\mathcal{L}}_{b,i}$ for quasi-momentum $\mathbf{k}$	(3.39)
$\mathrm{m}_i, \mathrm{m}_i^*$	anomalous density at site i and its complex conjugate	32
m_j^*, m^*	effective mass in direction j and their geometric mean	(4.8)
$\bar{n}_{\mathrm{BE}}(E)$	Bose-Einstein distribution at energy E	34
$\hat{n}_{b,i}, \tilde{n}_{b,i}$	number operator and non-condensate number	16, 31

Table 1: *continued*

Notation	Description	Ref.
$\tilde{n}_b(\mathbf{r})$	band b non-condensate LDA per-site density envelope	37
$\tilde{n}_T^U(\mathbf{r},\mu),$	ground-band non-condensate LDA envelope for the per-	90
$\tilde{N}_T^U(\mu)$	site density and total number (sections 7.5, 7.6 only)	
$\tilde{N}_b, \tilde{N}$	non-condensate atom number for band b and all bands	31, (3.6)
$n_c(\mathbf{r})$	condensate LDA per-site density envelope	37
N_c	total number of condensate atoms	(3.4)
N_s	number of sites in the translationally-invariant lattice	14,
	(combined harmonic lattice thermal sites in chapter 7)	75
$r_j, \bar{r}$	direction j position and distance from trap units origin	54
$S(w)$	spread function for the mean-field interaction shift	(7.65)
$T_L^0, T_c^0, T_c^{\text{fs}}, T_c$	critical temperature: non-interacting deep lattice limit,	(7.30),
	thermal limit, finite-size; mean-field interacting	89
$U_{\substack{i_1,i_2,i_3,i_4 \\ b_1,b_2,b_3,b_4}}$	general interaction parameter for sites i and bands b	(2.10)
$U_{bb'}, U$	bands b, b' and ground-band on-site interaction parameter	(2.14),17
U', U''	all site interaction parameters	(F.7,F.9)
$u_{b,i,j}, v_{b,i,j}$	Hartree-Fock/Bogoliubov amplitudes	(3.24)
$u_b, v_b(\mathbf{k}, \mathbf{r})$	LDA envelopes for Hartree-Fock/Bogoliubov amplitudes	37
$V_{\text{latt}}(\mathbf{r}), V_j, V$	lattice potential, lattice depth and its geometric mean	(2.1)
$V_{\text{tr}}(\mathbf{r}), v_i$	harmonic-trap potential (0 if no trap), $v_i = V_{\text{tr}}(\mathbf{R}_i)$	13, 15
$w_b(\mathbf{r} - \mathbf{R}_i)$	Wannier function for band b localised at site i	(2.4,D.1)
W, W_b	width of the ground band and band b respectively	49, (7.7)
w, w_L, w_c^0, w_c	thermal width $w = W/k_B T$ at temperatures T, T_L^0, T_c^0, T_c	74,84,94
$z_i, z(\mathbf{r})$	condensate amplitude, $z_i = \left\langle \hat{a}_{0,i} \right\rangle$ and its LDA envelope	30, 37
$\hat{\alpha}_{b,j}$	Hartree-Fock/Bogoliubov operator for band b, mode j	(3.24)
$\hat{\delta}_{b,i}$	non-condensate destruction operator for band b at site i	30
$\zeta_\alpha(z)$	Bose function, $\zeta_\alpha(z) = \sum_{n=1}^\infty z^n/n^\alpha$	(I.1)
μ_{fs}	chemical potential for finite-size effect, $\mu_{\text{fs}} = 3\hbar\bar{\omega}^*/2$	(5.18)
$\Phi(\mathbf{r})$	condensate amplitude (order parameter), $\Phi(\mathbf{r}) = \left\langle \hat{\Psi}(\mathbf{r}) \right\rangle$	30
$\psi_{b,\mathbf{k}}(\mathbf{r})$	translationally-invariant lattice Bloch wavefunction	(C.3)
$\hat{\Psi}(\mathbf{r}), \tilde{\psi}(\mathbf{r}),$	total and non-condensate bosonic field operator at $\mathbf{r}$	13, 30
$\omega_j, \omega, \bar{\omega},$	harmonic trap frequency in direction j, their geometric	13,59,
$\omega_j^*, \omega^*, \bar{\omega}^*$	and arithmetic mean and their effective frequencies	(4.15)
ω_R	recoil frequency, $\omega_R = E_R/\hbar$	12

Chapter 1

Introduction

1.1 Bose-Einstein condensation

Extending Bose's work on photons [2],[1] Einstein introduced what we now call bosons in 1924 [4], and in 1925 he predicted the phenomenon of Bose-Einstein condensation: that when the density of an ideal gas is increased at fixed temperature, 'an increasing number of molecules goes into the quantum [. . .] state without kinetic energy [. . .]. A separation occurs; a part "condenses", the rest remains a "saturated ideal gas" [. . .].' [5]. In this thesis we will consider atoms which are composite bosons, being composed of an even number of fermions (electrons and nucleons) as discussed in appendix A.

In 1938, London suggested that the superfluidity of liquid ^{4}He 'very probably has to be regarded as the condensation phenomenon of the Bose-Einstein statistics, distorted, of course, by the presence of molecular forces and by the fact that it manifests itself in the liquid and not in the gaseous state.' [6, 7].

We do not attempt to detail here the huge amount of work that has been done in the intervening years; rather we mention some contributions which are extremely important to our work. In 1947, Bogoliubov derived a method appropriate to 'a "nearly perfect" Bose-Einstein gas' whereby '[. . .]the excited states of the [. . .] molecules can be treated as a perfect gas composed of "elementary excitations" – "quasi-particles" [. . . that] are also subjected to Bose statistics.' [8].

For a given density, the temperature at which condensation occurs (the 'critical tem-

---

[1]For all articles cited which are German in the original, the translations in [3] were used.

perature') for an ideal gas was soon shown to be very different for a gas in a box than for a gas subject to a harmonic potential, and very different for lower-dimensional problems [9]. In particular, it was shown that there is no condensation for an ideal gas in a one or two-dimensional box, or in a one-dimensional harmonic potential. These differences are of crucial importance to our work.

For a weakly-interacting Bose gas, the Gross-Pitaevskii equation was derived; this describes the entire condensate with a single wavefunction at zero temperature and uses a pseudo-potential whereby the interaction between two particles is replaced by a delta function at the origin [10, 11].
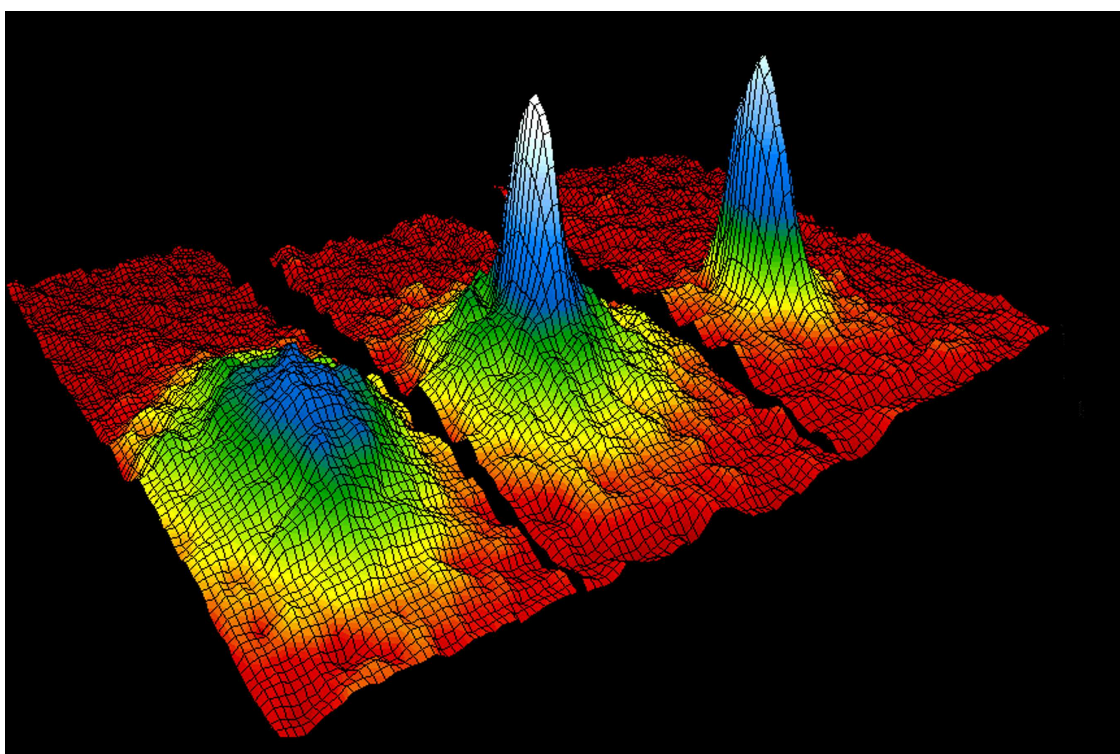
Figure 1.1: Velocity distribution of the cloud of atoms just before the appearance of the condensate (left), just after the appearance of the condensate (centre), and for a nearly pure condensate (right) [12, 13]

An incredible impetus to the experimental and theoretical work on weakly-interacting Bose gases occurred with the experimental realisation of Bose-Einstein condensation in a dilute atomic gas in 1995 [12, 14, 15]. Almost all experiments creating Bose-Einstein condensates have had a harmonic trap to confine the particles. With an aspherical trap, the momentum density of the condensate is anisotropic (as a result of the Heisenberg uncertainty principle), whereas the momentum density of the thermal atoms is

isotropic.[2] Figure 1.1 shows this definitive signature with time of flight images revealing a clearly anisotropic momentum distribution after condensation. This experimental realisation has lead to some amazing applications with Bose-Einstein condensates, with observations of: interference between condensates [16]; 'atom lasers' [17]; vortices [18]; collective excitations [19]; collapsing and exploding condensates 'Bosenova' [20, 21]; tunable scattering with Feshbach resonances [22–24]; three-body loss rates [25]; condensation of molecules from fermionic atoms [26, 27] and optical lattices.

1.2 Optical lattices

If a gas of atoms is subjected to standing waves due to opposing lasers at a suitable frequency, as in figure 1.2, the result is a periodic optical-lattice potential.[3] This is analogous to the periodic structure of a solid-state crystal. In contrast to a crystal, however, an optical lattice has an unprecedented degree of control: the atomic density can be varied; the depth of the periodic potential can be controlled using the laser intensity; the lattice spacing can be controlled using the laser wavelength or direction and the interaction strength may be controlled with a Feshbach resonance [29–31].[4] This level of control

Figure 1.2: Schematic of laser setup for an optical lattice [28]

is valuable for understanding condensed-matter problems. Furthermore, optical lattices are simpler than crystals in some respects, being, for example, free of impurities and of a pure sinusoidal shape.

In addition to the optical-lattice potential, it is necessary to have an overall confining potential. In optical-lattice experiments to date, the confining potential has been approximately harmonic for low energies, arising from the combined effect of focused laser beams and magnetic trap potentials. The additional harmonic potential adds significant complication to the theoretical problem, since the combined potential is no

---

[2]This can be shown using, for example, the local density approximation for the thermal atoms.

[3]Discussed in section 2.1.

[4]The use of a Feshbach resonance for bosons has been achieved without an optical lattice and is proposed with an optical lattice as discussed in the references given. In addition, the effective interaction varies with the lattice depth as considered below.

longer truly periodic. For atoms confined to a plane, we can visualise the combined trap and harmonic optical lattice potential using a surface above the plane representing the strength of the combined potential. This reveals an egg-carton-like structure with additional harmonic confinement, as schematically shown in figure 1.3.[5]
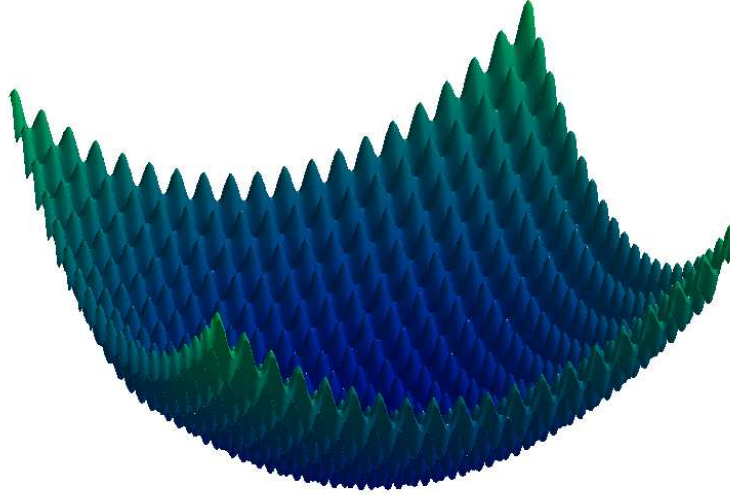
Figure 1.3: Combined harmonic lattice potential in two dimensions

However, the energy structure of the optical lattice with no harmonic confinement (the 'translationally-invariant' lattice) has some relevance locally in the trap. For sufficiently deep lattices, the energy levels of the translationally-invariant lattice separate into bands, and, for a degenerate system, the atomic density becomes more concentrated near the centre of lattice sites. In this regime, the many-body Hamiltonian for the system is well approximated by the Bose-Hubbard Hamiltonian [32–35], a simple model which includes local interactions and hopping between nearest-neighbour sites. The Bose-Hubbard model is widely applicable, but neglects off-site interactions, hopping beyond nearest-neighbour sites and excited bands – approximations that are not always well justified at the critical temperature.

As the depth of the optical lattice increases, the effective interaction increases (since the atomic density is higher at the centre of a lattice site at the expense of density nearer the lattice barriers) and the hopping term decreases. The result is a transition from a weakly-interacting regime, where the kinetic energy dominates interactions, to

---

[5]The potential shown is for a very weak lattice, since the lattice variation for an experimentally relevant lattice depth and trap (as discussed in sections 2.1 and 2.2) would be too rapid to display for a discernable harmonic variation.
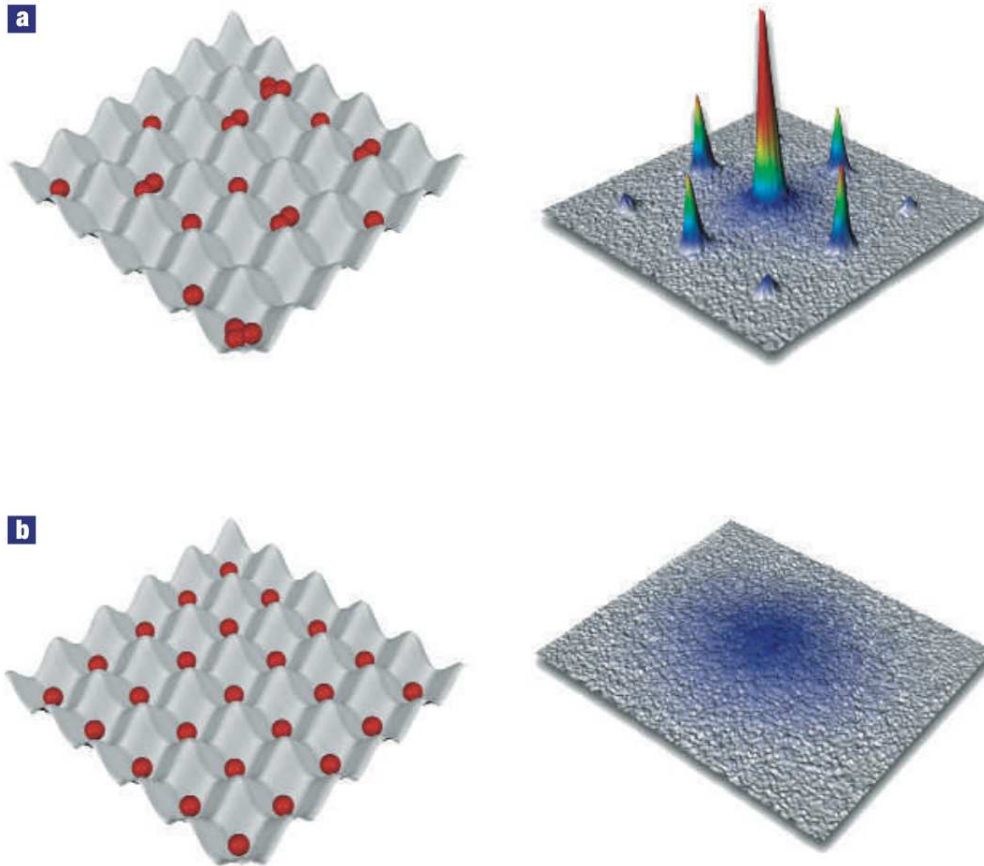
Figure 1.4: Atom number at each site (left) and interference pattern (imaged after time of flight, right) of the superfluid (a) and Mott-insulator (b) states [28]

a strongly-correlated regime, where interactions dominate. In the weakly-interacting case, for sufficiently low temperatures, there is a Bose-Einstein condensate superfluid state [34, 36–38], where the condensate atoms all have the same wavefunction, which is spread out over the lattice; this is a coherent phase which interferes as shown in figure 1.4(a), and the atom number at each site fluctuates. In the strongly-correlated regime, the phase is incoherent, but, for sufficiently low temperatures, there is a Mott-insulator state, where each lattice site is filled with a fixed number of atoms as shown in figure 1.4(b).

The transition from a superfluid to a Mott-insulator has been observed experimentally [39], as shown in figure 1.5. In subfigure (a), there is no lattice, and the lattice depth increases in each subfigure until the maximum depth in (h). As the lattice depth is increased, the interference pattern due to phase coherence is initially clearly visible. From subfigure (e), the interference maxima decrease until for (g) and (h) the atoms are

incoherent. What is truly amazing about this is that, if the lattice depth is reduced, the phase coherence returns, demonstrating that its loss was not due to irreversible processes.
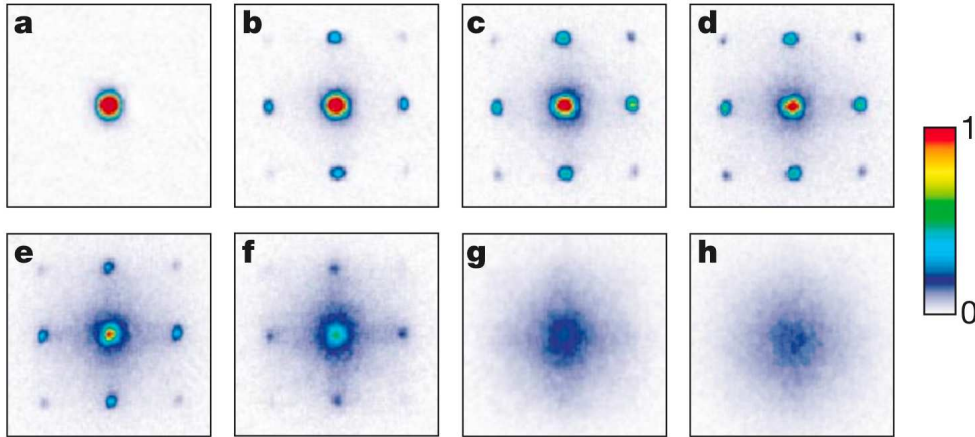
Figure 1.5: Absorption images of matter wave interference patterns as the optical lattice depth is increased [39]

In the superfluid phase of a non-interacting gas, the ground state is fully condensed at zero temperature. For an interacting gas, competing effects emerge: a state with some atoms promoted out of the single particle ground state increases the single particle energy, but can decrease the interaction energy. Bogoliubov theory predicts that, due to this competition, even at zero temperature there are some atoms which are not in the condensate (these atoms are the 'quantum depletion') [8]. As the lattice depth increases, the increase in the effective interaction, and decrease in the (single particle) hopping term, both put the competition in favour of quantum depletion. The quantum depletion therefore increases with lattice depth, long before the onset of the Mott-insulator state discussed above. This effect has been shown experimentally [40] with results reproduced in figure 1.6.

In addition to this fascinating transition, optical lattices promise to be an experimental method for the simulation of other many-body Hamiltonians. There have been numerous applications for the versatile optical lattice already, including observation of: strongly correlated systems such as the Tonks-Girardeau gas [41]; number squeezing [42]; superexchange [43]; and steps towards quantum computing [44, 45].
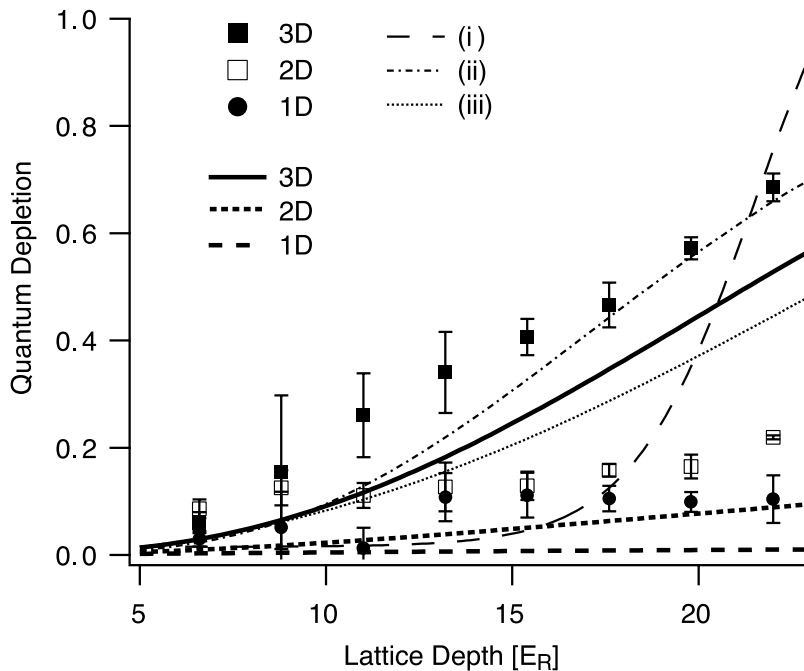
Figure 1.6: Quantum depletion of a ^{23}Na condensate in an optical lattice near zero temperature. The squares and circles correspond to experimental data and the thick lines show the Bogoliubov result (we do not consider the lines (i)-(iii) here) [40]

An exact diagonalisation of even the Bose-Hubbard Hamiltonian is currently computationally unattainable for more than a few particles and sites. Quantum Monte-Carlo for the combined harmonic lattice problem in three dimensions has been limited to approximately 20 sites in each direction [46, 47]. The density-matrix renormalisation group method has not currently been solved in three dimensions [48, 49] although recent work on a special case in two dimensions has been reported [50]. Due to the difficulty of exact calculations with the Bose-Hubbard Hamiltonian, Bogoliubov approaches, commonly used for the trapped system without a lattice [51], have been used for the lattice system in the superfluid regime. For the combined harmonic lattice, this has been limited to one dimension: adiabatic loading was considered in [52] with 19 atoms and superfluidity and condensation was considered in [53] with 41 sites and ten atoms.

To model sufficient atoms for thermodynamics, and since, as we shall see, the dimension of the system has a profound effect on its properties, it is necessary to simplify further. The local density approximation (LDA) has been shown to give reasonable agreement with experimental results for the trapped, no lattice case [54–56], although it restricts

the validity of results to temperatures well above the energy spacing of the Hamiltonian. Duan and co-workers [57, 58] have considered the combined harmonic lattice in the LDA using the Bose-Hubbard assumption. Although they concentrate on the effect of condensation on the interference pattern, they do produce condensate fractions, the depletion fraction and number densities. Other LDA work with interacting bosons in the combined harmonic lattice has used the decoupling approximation [59], or has treated tunnelling as a perturbation [60], so is more applicable in the Mott-insulator regime.

1.3   Overview

In this thesis, we develop theory for Bose-Einstein condensates in optical lattices, both with and without an additional harmonic potential. We go beyond the Bose-Hubbard Hamiltonian and critically assess the importance of hopping beyond nearest-neighbour sites, excited bands and off-site interactions. Our results justify the regimes of applicability of the Bose-Hubbard Hamiltonian and indicate that in many accessible regimes, beyond Bose-Hubbard Hamiltonian effects are important. Most results we produce apply to systems of one, two or three spatial dimensions, but for numerical results, we generally concentrate on the three-dimensional case.

We start from the many-body Hamiltonian for bosons in an optical lattice, derive the extended Bose Hubbard Hamiltonian, and make the Popov approximation to the Hartree-Fock Bogoliubov method. We diagonalise the resulting Hamiltonian in the LDA. Our approach is more general than the related work of Duan and co-workers [57, 58]: their work is based on the Bose-Hubbard model and uses the simpler case of fixed number density at the trap centre (so that the chemical potential iteration is local). The efficient numerical implementation of our theory allows us to model the fixed total number case, while providing a more general treatment of beyond nearest-neighbour tunnelling and the influence of excited bands.

We derive new results on the rich structure of the combined harmonic lattice density of states. We compare the LDA combined harmonic lattice density of states to the density of states from the full diagonalisation for the ideal gas. We numerically implement our model and compare the thermodynamic results with the full diagonalisation of the ideal gas and with limited experimental results available.

We derive analytical results for the ideal number density, condensate fraction and critical temperature, and for the finite-size effect and mean-field interaction shift. We give simple iterative procedures for including excited bands. We compare all of these against the full numerical approach. We show that the nature of useful approximations for the translationally-invariant and combined harmonic lattices differ distinctly. For the translationally-invariant case, the lowest energy states are singularly important, for which we verify that an effective-mass treatment is accurate over a broad regime. In contrast, for the combined harmonic lattice, the entire ground-band structure is typically important, for which we develop simple band shape approximations. In both the translationally-invariant and the combined harmonic lattices, we show that the effective-mass treatment and the simple band shape approximations work in complementary regimes.

1.4 Outline

We begin by presenting the many-body Hamiltonian for bosons in an optical lattice in chapter two. We show the conversion to the extended Bose-Hubbard Hamiltonian, by changing to a localised basis. We compare our approach with other extended Bose-Hubbard work. We discuss the hopping, trap, and interaction parameters appearing in the Hamiltonian, and consider approximations that are often used in other work.

We make mean-field approximations to the extended Bose-Hubbard Hamiltonian in chapter three, using the Popov approximation to the Hartree-Fock-Bogoliubov method [61]. We diagonalise the mean-field Hamiltonian in the LDA.

We show the translationally-invariant lattice density of states, in chapter four. We consider nearest-neighbour only, effective-mass and high-energy approximations. We derive results on the LDA combined harmonic lattice density of states, which we compare to the full diagonalisation of the non-interacting Hamiltonian.

In chapter five we show some important features of our numerical implementation, we give our algorithm for finding thermodynamic results in an optical lattice, and we compare our implementation to that of [57, 58].

We present numerical results from our model in chapter six. We compare our predictions of thermal properties with results from the full diagonalisation for the ideal gas. We show the significance of the parameters and assumptions in the Hamiltonian and the

effect of the Bogoliubov approach.

We derive analytical results for number density, condensate fraction and mean-field critical temperature in chapter seven. We start by exploring the validity of the well-known effective-mass approximation, and consider an existing very deep lattice limit [62]. We then consider simple band shapes and use these to derive a simple formula for the non-interacting critical temperature, first ignoring excited bands, then deriving adjustments for excited bands, the finite-size effect and the mean-field interaction shift. We compare to results from our full numerical model.

We present our conclusions and outlook in chapter 8.

In the appendices, we consider some background material and mathematical details and extensions.

1.5 Papers arising

Two papers arising from this thesis, and subsequent work, are in review and available on arXiv, based on the theory and numerical results from chapters 2 to 6 [63] and analytical critical-temperature work of chapter 7 [64]. Additional work related to the finite-temperature, mean-field description of a quasi-two-dimensional gas was undertaken during this masters thesis (that work is not discussed here) and is published in Phys. Rev. A [65].

Chapter 2

Bosons in optical lattices

In this chapter we derive the many-body Hamiltonian for bosons in an optical lattice with two body interaction. In this work we consider the effect of inclusion of excited bands, beyond nearest-neighbour hopping, and approximate off-site interactions, by developing an extended version of the usual Bose-Hubbard Hamiltonian. Our approach is more general than existing extended Bose-Hubbard work [66–69]. We then consider the values of the numerical parameters in the Hamiltonian in considerable detail, including investigation of approximations that are commonly used in the literature, and give our own novel improvements to these approximations. Our investigation of approximations in the treatment of the harmonic trap by the extended Bose-Hubbard model is the first to our knowledge.

2.1 Lattice potential

We consider an optical lattice formed by orthogonal standing waves. In each direction, the standing wave is created by two opposing lasers. The laser wavelength λ_j (in direction j) is off-resonant with respect to an atomic transition. The resulting potential in d dimensions, up to an additive constant, is (from appendix B):

$$V_{\text{latt}}(\mathbf{r}) \equiv \sum_{j=1}^{d} V_j \sin^2\left(\frac{\pi r_j}{a_j}\right), \tag{2.1}$$

where V_j is the lattice depth and $a_j \equiv \lambda_j/2$ is the lattice spacing in direction j. We set $V \equiv \left(\prod_j V_j\right)^{1/d}$ and $a \equiv \left(\prod_j a_j\right)^{1/d}$. Most of our results can be generalised to the

non-separable case, but the notation would be more complex [70, 71] (and the method of calculation of the density of states, discussed in chapter 4, would be specific to the experimental configuration).

We will generally present results in recoil units, with the unit of length being a_j/π and the unit of energy $E_{R,j} \equiv h^2/2m\lambda_j^2$ where m is the atomic mass (we have $m = 86.909\,\text{u}$ for ^{87}Rb [72] and $m = 22.990\,\text{u}$ for ^{23}Na [73]). We set $E_R \equiv \left(\prod_j E_{R,j}\right)^{1/d}$, and the recoil frequency to $\omega_R \equiv E_R/\hbar$.

Except where specifically stated otherwise, our formulae are generally valid for non-cubic lattices and lower-dimensional systems.[1] By a cubic lattice, we mean the underlying Bravais lattice has cubic symmetry (or the equivalent in lower dimensions, such as the square case) and that the lattice spacings, a_j, and depths, V_j, are the same in each axial direction. All of our numerical results are for separable cubic lattices. The three-dimensional experiments for which we give parameters in table 2.1 generally have a cubic-lattice potential, apart from minor frequency shifts to eliminate cross-interference between different beams which have a relative effect on the lattice spacing of $\lesssim 10^{-7}$.

Table 2.1: Typical experimental lattice parameters [72, 73]

atom	transition	lattice lasers	E_R/h
^{87}Rb	D$_2$ 5^2S$_{1/2} \rightarrow 5^2$P$_{3/2}$ at 780.24 nm	852 nm [39, 74]	3.2 kHz
		850 nm [75–77]	3.2 kHz
		840 nm [42]	3.3 kHz
		826 nm [78]	3.4 kHz
^{23}Na	D$_2$ (3^2S$_{1/2} \rightarrow 3^2$P$_{3/2}$) at 589.16 nm, and D$_1$(3^2S$_{1/2} \rightarrow 3^2$P$_{1/2}$) at 589.8 nm	594.7 nm [79]	24.4 kHz
		1064 nm [40]	7.7 kHz

2.2 Harmonic-trap potential

Experimentally, atoms are subject to a crossed optical dipole [40, 79] harmonic trap (due to the focused lasers used to make the lattices) and often a magnetic trap also

---

[1]However, we do not consider quasi-reduced-dimensional systems, where some directions are partially accessible, that is, $k_B T$ is of the order of the level spacing.

[74, 75]. The resulting potential is $V_{\text{tr}}(\mathbf{r}) \equiv \frac{1}{2} m \sum_j \omega_j^2 r_j^2$, where ω_j is the harmonic trap frequency in direction j. In three-dimensional experiments, the trap is often spherical or radially symmetric, with, for example $\omega_x = \omega_y \neq \omega_z$. We set $\omega = \left(\prod_j \omega_j \right)^{1/d}$. We consider the aspherical case in d dimensions, but, as for the lattice parameters discussed above, we do not allow for quasi-reduced-dimensionality. In this thesis we consider both the lattice with with $V_{\text{tr}}(\mathbf{r}) = 0$, which we call the 'translationally-invariant lattice',[2] and the experimentally relevant combined harmonic-trap and optical-lattice potential, which we call the 'combined harmonic lattice'.

From a sample of three-dimensional lattice experiments, we find the harmonic trapping frequencies to be generally between $2\pi \times 18\,\text{Hz}$ and $2\pi \times 155\,\text{Hz}$ [39, 40, 74, 78, 79], giving ω/ω_R between 0.005 and 0.02. The maximum anisotropy, ω_j/ω_k, for these experiments is less than 50%.

An iso-surface of the combined harmonic lattice potential is shown for an ellipsoidal harmonic trap in figure 2.1. For a given potential energy, the volume of a site is reduced when the harmonic potential is greater.
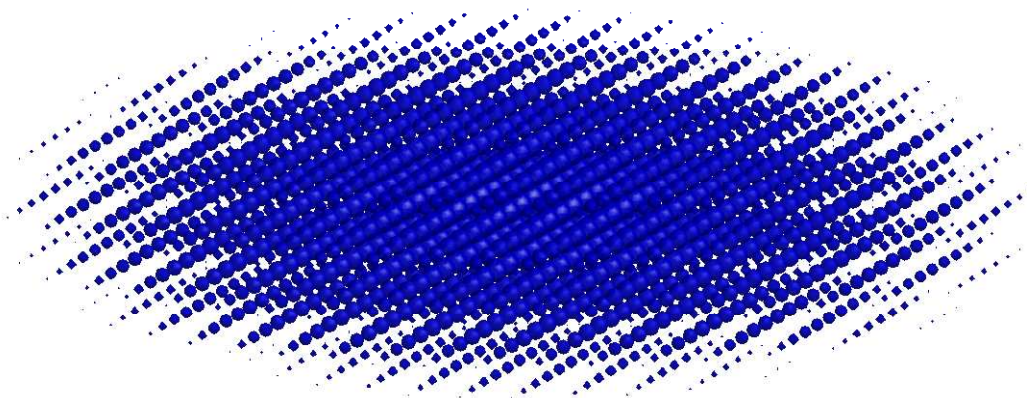
Figure 2.1: An iso-surface of the combined harmonic lattice potential in three dimensions

2.3 Many-body Hamiltonian

In this work we consider only bosons, with field operator $\hat{\Psi}(\mathbf{r})$ such that [80]:

$$\left[\hat{\Psi}(\mathbf{r}), \hat{\Psi}(\mathbf{r}') \right] = 0, \quad \left[\hat{\Psi}(\mathbf{r}), \hat{\Psi}^\dagger(\mathbf{r}') \right] = \delta(\mathbf{r} - \mathbf{r}'). \tag{2.2}$$

---

[2]This is standard terminology, but the lattice without a harmonic trap is only invariant under translations of a direct lattice vector.

As we are considering low energy collisions in a cold dilute gas, we consider two-body forces only and we use the pseudo-potential, to lowest order depending only on the s-wave scattering length, a_s, giving a Hamiltonian with a contact potential [81]:

$$\hat{H} = \int d\mathbf{r}\hat{\Psi}^\dagger(\mathbf{r}) \left[-\frac{\hbar^2\nabla^2}{2m} + V_{\text{latt}}(\mathbf{r}) + V_{\text{tr}}(\mathbf{r}) \right] \hat{\Psi}(\mathbf{r}) + \frac{g}{2} \int d\mathbf{r}\hat{\Psi}^\dagger(\mathbf{r})\hat{\Psi}^\dagger(\mathbf{r})\hat{\Psi}(\mathbf{r})\hat{\Psi}(\mathbf{r}),$$
(2.3)

where $g \equiv 4\pi\hbar^2 a_s/m$. For ^{87}Rb, $a_s = 5.77$ nm from the triplet configuration and for ^{23}Na, we use the maximally stretched $a_s = 2.75$ nm [72, 73, 82].

2.4 Wannier basis

We expand the boson field operators in a basis of the Wannier functions, $w_b(\mathbf{r} - \mathbf{R}_i)$, of the non-interacting translationally-invariant lattice (D.1), so that for bands b and sites $\mathbf{R}_i$ we have (as in [66]):

$$\hat{\Psi}(\mathbf{r}) = \sum_{b,i} \hat{a}_{b,i} w_b(\mathbf{r} - \mathbf{R}_i), \quad \hat{\Psi}^\dagger(\mathbf{r}) = \sum_{b,i} \hat{a}_{b,i}^\dagger w_b^*(\mathbf{r} - \mathbf{R}_i),$$
(2.4)

where the creation operator for an atom in band b at site i is given by $\hat{a}_{b,i}$. We note that b and i are discrete d-dimensional vectors. We will refer to the ground band as $b = 0$ by which we mean $b_j = 0$ for all j. Also, for the translationally-invariant lattice with N_s sites, we will let $i = 1, \ldots, N_s$. We require that:

$$\left[\hat{a}_{b,i}, \hat{a}_{b',i'}^\dagger \right] = \delta_{bb'}\delta_{ii'}, \quad \left[\hat{a}_{b,i}, \hat{a}_{b',i'} \right] = 0,$$
(2.5)

which ensures (2.2), since then $\left[\hat{\Psi}(\mathbf{r}), \hat{\Psi}^\dagger(\mathbf{r}') \right] = \sum_{b,i} w_b(\mathbf{r} - \mathbf{R}_i)w_b^*(\mathbf{r}' - \mathbf{R}_i) = \delta(\mathbf{r} - \mathbf{r}')$ from (D.10). The Wannier basis is a localised basis for sufficiently deep lattices, as depicted in figure 2.2. For a given lattice depth, there is less localisation for excited bands as shown in figure D.3. Using a localised basis significantly simplifies the treatment of interactions when off-site interactions are ignored.

The Wannier states are 'quasi-stationary', since, as we show in appendix D, they are not eigenstates of the Hamiltonian, so that there are transitions between the different Wannier states in the same band due to the single-particle evolution. In particular, the matrix element for hopping from site $\mathbf{R}_{i'}$ to site $\mathbf{R}_i$ for band b is defined as:

$$J_{b,i,i'} \equiv - \int d\mathbf{r}\, w_b^*(\mathbf{r} - \mathbf{R}_i) \left[-\frac{\hbar^2\nabla^2}{2m} + V_{\text{latt}}(\mathbf{r}) \right] w_b(\mathbf{r} - \mathbf{R}_{i'}).$$
(2.6)
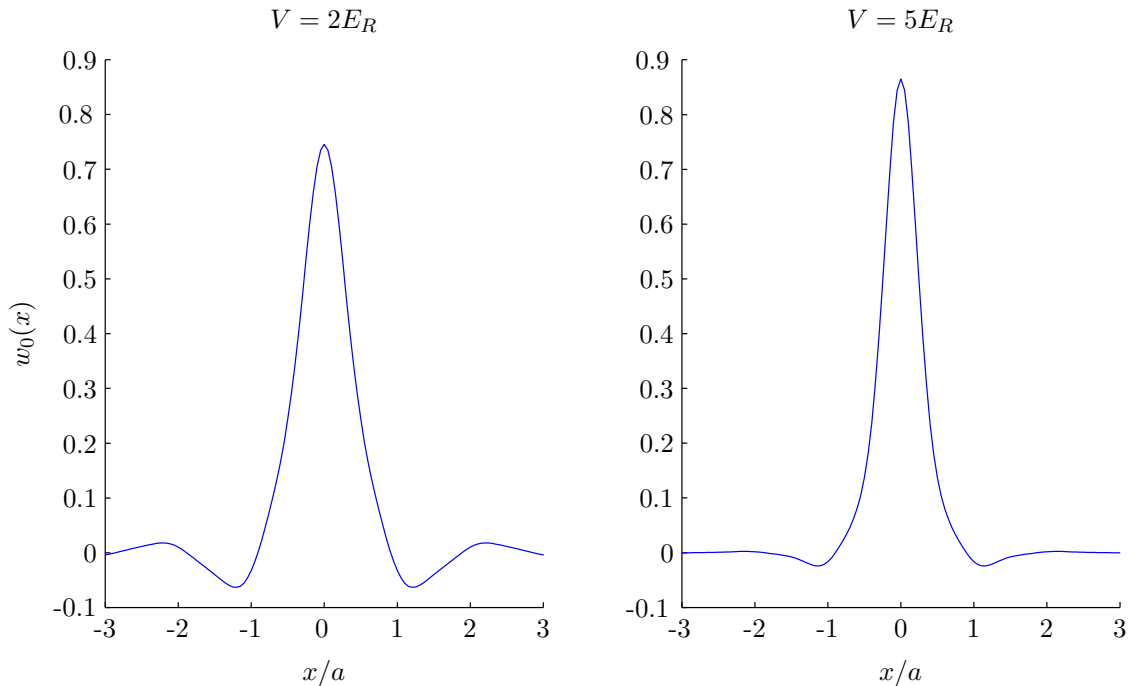
Figure 2.2: Ground-band Wannier functions

We show in the appendix (D.16) that there is no inter-band hopping with the (non-interacting, translationally-invariant lattice) definition of the Wannier functions we are using. A change of variables in (2.6) shows that this formula is dependent on $\mathbf{R}_i$ and $\mathbf{R}_{i'}$ only through the difference $\mathbf{R}_i - \mathbf{R}_{i'}$.

2.5 Extended Bose-Hubbard Hamiltonian

We now express the Hamiltonian in terms of the operators $\hat{a}_{b,i}$ by inserting (2.4) into (2.3) and we consider the resulting terms in this section.

We assume the trap is slowly varying relative to the lattice spacings a_j so that:

$$\int d\mathbf{r}\, V_{\text{tr}}(\mathbf{r}) w_b^*(\mathbf{r} - \mathbf{R}_i) w_{b'}(\mathbf{r} - \mathbf{R}_{i'}) \approx v_i \int d\mathbf{r}\, w_b^*(\mathbf{r} - \mathbf{R}_i) w_{b'}(\mathbf{r} - \mathbf{R}_{i'}) = v_i \delta_{bb'} \delta_{ii'}, \quad (2.7)$$

using (D.7) where $v_i \equiv V_{\text{tr}}(\mathbf{R}_i)$. The approximations in (2.7) will be discussed in section 2.9. We define:

$$\hat{N} \equiv \int d\mathbf{r}\, \hat{\Psi}^\dagger(\mathbf{r})\hat{\Psi}(\mathbf{r}) = \sum_{b,b',i,i'} \hat{a}_{b,i}^\dagger \hat{a}_{b',i'} \int d\mathbf{r} w_b^*(\mathbf{r} - \mathbf{R}_i) w_{b'}(\mathbf{r} - \mathbf{R}_{i'}) = \sum_{b,i} \hat{n}_{b,i}, \quad (2.8)$$

where $\hat{n}_{b,i} \equiv \hat{a}_{b,i}^{\dagger}\hat{a}_{b,i}$. Then, expressing the Hamiltonian in the grand-canonical distribution to conserve total particle number, $\hat{K} \equiv \hat{H} - \mu\hat{N}$:

$$\hat{K} = \sum_{b,i} \left[-\sum_{i'} \left(J_{b,i,i'}\hat{a}_{b,i}^{\dagger}\hat{a}_{b,i'} \right) + \hat{n}_{b,i}(v_i - \mu) \right] + \frac{1}{2} \sum_{\substack{i_1,i_2,i_3,i_4 \\ b_1,b_2,b_3,b_4}} \hat{a}_{b_1,i_1}^{\dagger}\hat{a}_{b_2,i_2}^{\dagger}\hat{a}_{b_3,i_3}\hat{a}_{b_4,i_4} U_{\substack{i_1,i_2,i_3,i_4 \\ b_1,b_2,b_3,b_4}},$$

(2.9)

where:

$$U_{\substack{i_1,i_2,i_3,i_4 \\ b_1,b_2,b_3,b_4}} \equiv g \int d\mathbf{r}\, w_{b_1}^{*}(\mathbf{r} - \mathbf{R}_{i_1})w_{b_2}^{*}(\mathbf{r} - \mathbf{R}_{i_2})w_{b_3}(\mathbf{r} - \mathbf{R}_{i_3})w_{b_4}(\mathbf{r} - \mathbf{R}_{i_4}). \qquad (2.10)$$

If we restrict to on-site interactions, (2.9) reduces to $\hat{K} = \sum_i \hat{K}_i$ where:

$$\hat{K}_i \equiv \sum_{b} \left[-\sum_{i'} \left(J_{b,i,i'}\hat{a}_{b,i}^{\dagger}\hat{a}_{b,i'} \right) + \hat{n}_{b,i}(v_i - \mu) \right] + \frac{1}{2} \sum_{b_1,b_2,b_3,b_4} \hat{a}_{b_1,i}^{\dagger}\hat{a}_{b_2,i}^{\dagger}\hat{a}_{b_3,i}\hat{a}_{b_4,i} U_{\substack{i,i,i,i \\ b_1,b_2,b_3,b_4}},$$

(2.11)

where the interaction parameter is:

$$U_{\substack{i,i,i,i \\ b_1,b_2,b_3,b_4}} \equiv g \int d\mathbf{r}\, w_{b_1}^{*}(\mathbf{r})w_{b_2}^{*}(\mathbf{r})w_{b_3}(\mathbf{r})w_{b_4}(\mathbf{r}), \qquad (2.12)$$

as in [83].

2.6 Comparison to other approaches

The extended Bose-Hubbard Hamiltonian (2.11) is the basis for the work in this thesis: we will make approximations to it in chapter 3 (although we also consider off-site interactions in section 2.10.5 and appendix F). In this section, we consider approximations that have been made in previous work. Assuming that interactions are perturbative relative to the band-gap energy scale, so that we may ignore collisional couplings between bands in the many body state, we get:

$$\frac{1}{2} \sum_{b_1,b_2,b_3,b_4} \hat{a}_{b_1,i}^{\dagger}\hat{a}_{b_2,i}^{\dagger}\hat{a}_{b_3,i}\hat{a}_{b_4,i} U_{\substack{i,i,i,i \\ b_1,b_2,b_3,b_4}}$$

$$\approx \frac{1}{2} \sum_{b} \hat{a}_{b,i}^{\dagger}\hat{a}_{b,i}^{\dagger}\hat{a}_{b,i}\hat{a}_{b,i} U_{bb} + \sum_{\substack{b,b' \\ b \neq b'}} \hat{a}_{b,i}^{\dagger}\hat{a}_{b',i}^{\dagger}\hat{a}_{b,i}\hat{a}_{b',i} U_{bb'} + \sum_{\substack{b,b' \\ b \neq b'}} \hat{a}_{b,i}^{\dagger}\hat{a}_{b,i}^{\dagger}\hat{a}_{b',i}\hat{a}_{b',i} U_{bb'}$$

$$= \frac{1}{2} \sum_{b} \hat{n}_{b,i}(\hat{n}_{b,i} - 1)U_{bb} + \sum_{\substack{b,b' \\ b \neq b'}} \hat{n}_{b,i}\hat{n}_{b',i} U_{bb'} + \sum_{\substack{b,b' \\ b \neq b'}} \hat{a}_{b,i}^{\dagger}\hat{a}_{b,i}^{\dagger}\hat{a}_{b',i}\hat{a}_{b',i} U_{bb'}, \qquad (2.13)$$

where:

$$U_{bb'} \equiv g \int \mathrm{d}\mathbf{r} \ |w_b(\mathbf{r})w_{b'}(\mathbf{r})|^2 , \qquad (2.14)$$

as for the result derived in [68] (although, by $\sum_{bb',b\neq b'}$ they seem to mean either $\sum_{b>b'}$ or $\frac{1}{2}\sum_{bb',b\neq b'}$).

Other extended Bose-Hubbard work has used various simplifications of (2.11): [66] uses nearest-neighbour hopping and nearest-neighbour interactions, [69] uses ground band only, nearest-neighbour hopping and nearest-neighbour interactions and [67] uses ground band only and nearest-neighbour interactions.

Limiting to the ground band, nearest-neighbour hopping (and ignoring the energy offset $J_{0,i,i}$), and on-site interactions only, the Hamiltonian reduces to the Bose-Hubbard model [32, 33] which for the cubic lattice is:

$$\hat{K} = -J \sum_{\langle i,i'\rangle} \hat{a}_{0,i}^{\dagger}\hat{a}_{0,i'} + \sum_{i} \hat{n}_{0,i}(v_i - \mu) + \frac{U}{2}\sum_{i} \hat{n}_{0,i}(\hat{n}_{0,i} - 1), \qquad (2.15)$$

where $J \equiv J_{0,i,i'}$ is the cubic-lattice ground-band hopping matrix element for nearest-neighbours i and i' (labelled $\langle i,i'\rangle$), and $U \equiv U_{00}$.

2.7 Mott-insulator transition

In this thesis, we consider atoms in the normal and superfluid states. For a sufficiently deep lattice, there is a transition to a Mott-insulator phase [34]. In a three-dimensional cubic lattice, this occurs for the unit-filled system when $U/6J > 5.83$ at $T = 0$ [38]. For typical experimental parameters, the transition occurs in ^{87}Rb when $V \gtrsim 13E_R$ (when $V > 16E_R$ for ^{23}Na with the far blue detuning of [40]). The lattice depth for the Mott-insulator transition is increased for higher filling factors.

2.8 Hopping matrix

We first consider the importance of beyond nearest-neighbour hopping in section 2.8.1. We then consider alternative approximations for the nearest-neighbour ground-band hopping matrix element, J. These can be useful rules of thumb, but, in this work, we will always use the exact form, (2.6), for calculations of the hopping matrix.

2.8.1 Beyond nearest-neighbour hopping

In this section, we consider the ratio of beyond nearest to nearest-neighbour hopping matrix elements (we also discuss the significance of beyond nearest-neighbour hopping in sections 4.2, 6.2 and D.2).

In section 2.5 we defined the band b hopping matrix element between sites i and i' by $J_{b,i,i'}$, which is the form that will be most useful for our theory, and the cubic-lattice ground-band nearest-neighbour hopping matrix element, J, which is useful in the deep lattice limit. Here we will also define the band b hopping between neighbours l sites apart in axial direction j to be $J_{b,j}^l$ (for example $J_{b,y}^l = J_{b,000,0l0}$ and, for the cubic lattice, $J = J_{0,j}^1$),[3] which we will use for considering the significance of beyond nearest-neighbour hopping.

The ratio of beyond nearest-neighbour to nearest-neighbour hopping in shown in figure 2.3.[4]
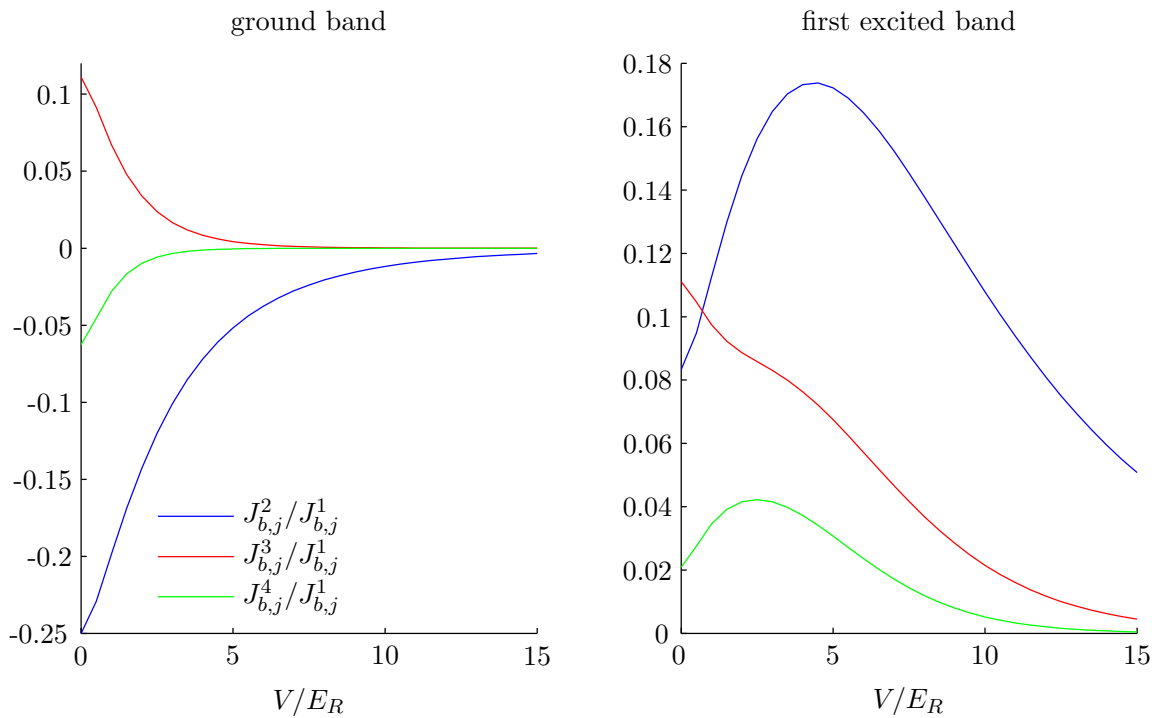
Figure 2.3: Ratio of beyond nearest- to nearest-neighbour hopping

---

[3]When we use this notation, we are implicitly assuming that the energy spectrum is invariant under inversion of quasi-momentum, in view of (D.15).

[4]For the first excited band, the hopping matrix element in a non-excited direction is the same as for the ground band, so the excited direction used for the first excited band is the hopping matrix direction, j.

We see from figure 2.3 that the ground-band next-nearest-neighbour hopping matrix element is as much as 25% of its nearest-neighbour counterpart at $V = 0$, but decreases rapidly with increasing V. Beyond next-nearest-neighbour hopping is less significant. For the excited band, some of the ratios can increase initially.

2.8.2 Numerical fit

For the ground-band nearest-neighbour hopping matrix, a numerical fit of the exact form over the range $5E_R < V < 15E_R$ is:

$$\frac{J}{E_R} \approx \frac{2.48}{\sqrt{\pi}} \left(\frac{V}{E_R} \right)^{1.04} e^{-2.11\sqrt{V/E_R}}, \tag{2.16}$$

with coefficient of determination, $R^2 > 1 - 10^{-5}$. Equivalent results to two significant figures are given with unspecified lattice-depth validity range in [84].

2.8.3 Deep lattice limit

In the nearest-neighbour hopping approximation, the width of the one-dimensional ground band is $4J$ from (D.19), so from [85] as $V \to \infty$:

$$\frac{J}{E_R} \to \frac{4}{\sqrt{\pi}} \left[\left(\frac{V}{E_R} \right)^{3/4} - 0.45 \left(\frac{V}{E_R} \right)^{1/4} + O\left(\frac{V}{E_R} \right)^{-1/2} \right] e^{-2\sqrt{V/E_R}}, \tag{2.17}$$

the first term of which is given in [86].

2.8.4 Gaussian approximation

For a sufficiently deep lattice, the energy of the ground band is low within the lattice potential. Near the bottom of a lattice potential well, we see from (2.1) that (taking $\mathbf{r} \approx \mathbf{0}$ as an example), $V_{\text{latt}}(\mathbf{r}) \approx \sum_{j=1}^{3} V_j(\pi r_j/a_j)^2$. As the lattice depth increases, the ground band narrows toward the ground-state energy of this potential. We approximate the ground-band Wannier function with the ground-state wavefunction of this harmonic potential:

$$w_0(\mathbf{r}) \approx \left(\frac{\pi}{a^2} \sqrt{\frac{V}{E_R}} \right)^{d/4} e^{-\sum_j \sqrt{V_j/E_{R,j}}(\pi r_j/a_j)^2/2}. \tag{2.18}$$

The approximation of the ground-band Wannier function by a Gaussian is illustrated further in appendix D. For the hopping matrix, if we also approximate the lattice potential with a quadratic barrier, we find (E.3) for the cubic lattice:

$$J \approx \left(\frac{\pi^2}{4} - 1 \right) V e^{-\frac{\pi^2}{4} \sqrt{V/E_R}}. \tag{2.19}$$

The origin of the numerical coefficient shown in (2.19) is given in appendix E and is used in [87]. However, since the Gaussians which approximate the Wannier functions at different sites are not orthogonal, any constant addition to the Hamiltonian will change the J estimate, so the coefficient is not well determined. If we use a Gram-Schmidt orthogonalisation to get a pair of orthogonal functions, we find that the hopping matrix element is zero (shown in appendix E). The scaling of the exponential shown, $\pi^2/4 \approx$ 2.47 (used in [38]) is a poor approximation to the true large V scaling in (2.17), since the true Wannier functions are fatter tailed than the Gaussian approximation (the tails, important for the hopping matrix, are where the potential is not approximately harmonic). A comparison of the hopping matrix approximations is shown in figure 2.4. We see that (2.16) and (2.17) are good approximations (and the first term of (2.17) has the correct large V behaviour) and that (2.19) is a poor approximation.
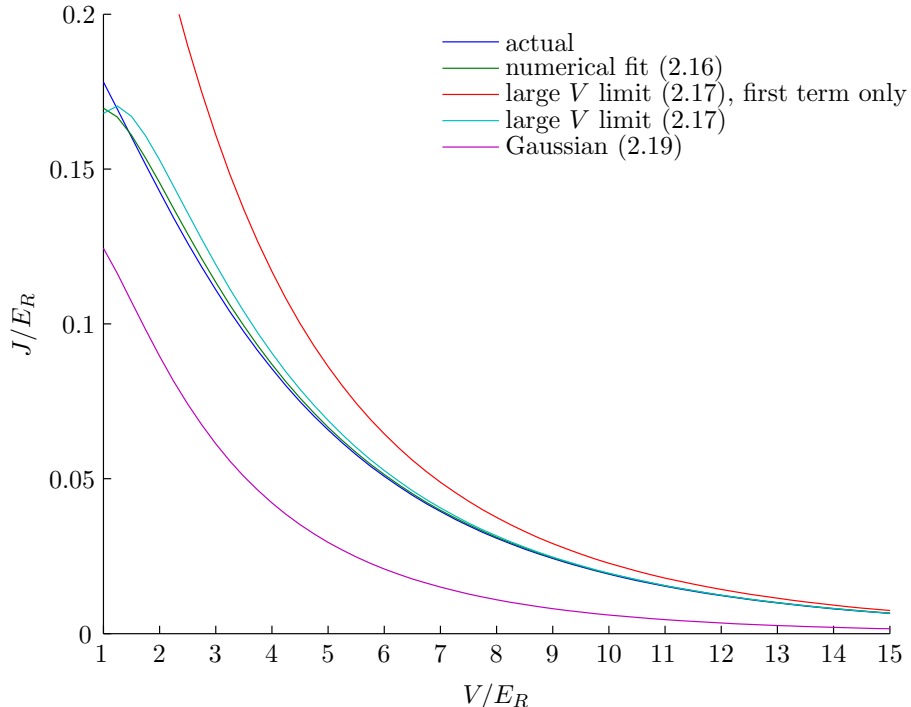
Figure 2.4: Nearest-neighbour, ground-band hopping matrix approximations

2.9 Harmonic trap

In this work, we will always use the local energy form (2.7) to represent the harmonic trap. However, there are approximations involved in (2.7) which we consider in this section.

2.9.1 On-site variation

Here we consider the accuracy of (2.7) when $i = i'$ and $b = b'$. To the extent that this is in error due to variation on the trap site, the error could be removed by setting:

$$v_{b,i} = \int d\mathbf{r}\, V_{\mathrm{tr}}(\mathbf{r}) \left| w_b(\mathbf{r} - \mathbf{R}_i) \right|^2. \tag{2.20}$$

However, to the extent that (2.7) is in error due to the Wannier functions not being fully localised on the site, to be consistent, it would be necessary to allow for the off-site contribution, considered in the next section.

We now quantify the extent of the error. There are three components to the integral in (2.7), one for each trap direction and the three components are additive. Considering the x component, for example, we have (using X_i for the x component of $\mathbf{R}_i$):

$$\int d\mathbf{r}\, \frac{1}{2} m \omega_x^2 x^2 \left| w_b(\mathbf{r} - \mathbf{R}_i) \right|^2 = \frac{1}{2} m \omega_x^2 \int_{-\infty}^{\infty} dx\, x^2 \left| w_b(x - X_i) \right|^2$$

$$= \frac{1}{2} m \omega_x^2 \int_{-\infty}^{\infty} dx'\, x'^2 \left| w_b(x') \right|^2 + \frac{1}{2} m \omega_x^2 X_i^2, \tag{2.21}$$

where we have made the transformation $x - X_i \rightarrow x'$ to obtain the last line and have used the fact that $x \left| w_b(x) \right|^2$ is odd and that $w_b(\mathbf{r})$ is normalised. For the ground band, we can recover (2.7) by absorbing the constant $\frac{1}{2} m \omega_x^2 \int_{-\infty}^{\infty} dx'\, x'^2 \left| w_b(x') \right|^2$ into the chemical potential. For excited bands there will be an error of

$$\frac{1}{2} m \omega_x^2 \int_{-\infty}^{\infty} dx'\, x'^2 \left[\left| w_b(x') \right|^2 - \left| w_0(x') \right|^2 \right], \tag{2.22}$$

which is applied to $\hat{n}_{b,i}$ in the Hamiltonian.

In figure 2.5 we plot the ratio $\int_{-\infty}^{\infty} dx\, x^2 \left[\left| w_1(x) \right|^2 - \left| w_0(x) \right|^2 \right] / a^2$ as a function of V. The divisor of a^2 means if the ratio is 1, v_i is wrong by $\frac{1}{2} m \omega_x^2 a^2$.
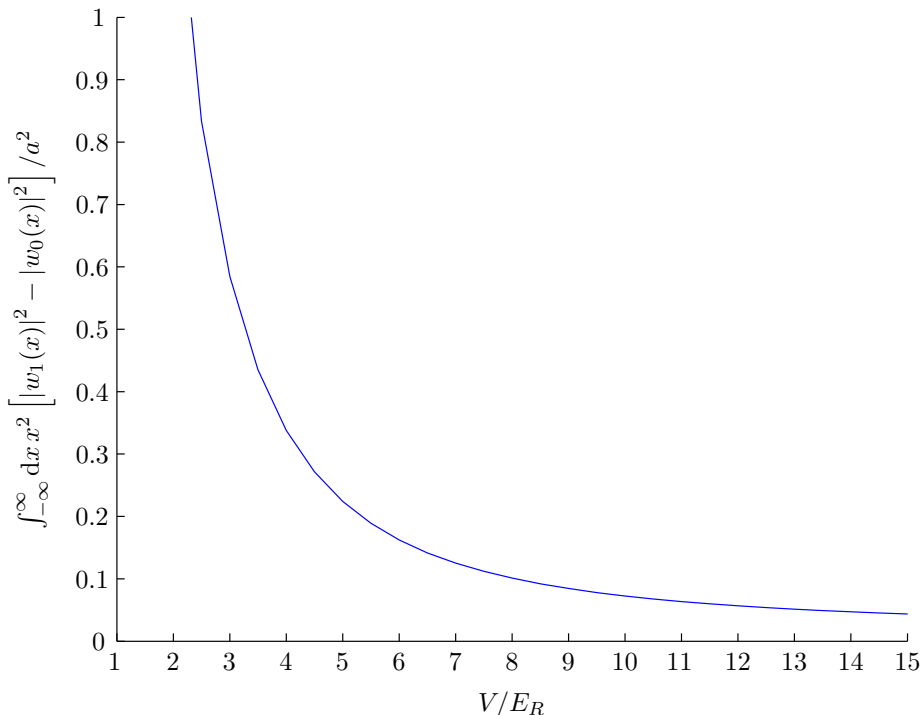
Figure 2.5: First excited band error due to on-site variation of the trap

2.9.2 Off-site contribution

Now, we consider the case with $i \neq i'$ but with $b = b'$. This contribution could be included by introducing hopping matrix element adjustments that vary by site, given by:

$$v_{b,i,i'} \equiv \int d\mathbf{r}\, V_{\mathrm{tr}}(\mathbf{r}) w_b^*(\mathbf{r} - \mathbf{R}_i) w_b(\mathbf{r} - \mathbf{R}_{i'}) \tag{2.23}$$

instead of using $v_{b,i}$ (that is, the diagonal element of $v_{b,i,i'}$).

To quantify the error of ignoring the off-diagonal elements of $v_{b,i,i'}$, we note again that the components of the trap contributing to the integral in the three directions are additive. We only get a potential error in the x component if components in the other directions of i and i' are equal. Then, for $X_i \neq X_{i'}$:

$$
\begin{aligned}
\int d\mathbf{r}\, \frac{1}{2} m\omega_x^2 x^2 w_b^*(\mathbf{r} - \mathbf{R}_i) w_b(\mathbf{r} - \mathbf{R}_{i'}) &= \frac{1}{2} m\omega_x^2 \int_{-\infty}^{\infty} dx\, x^2 w_b^*(x - X_i) w_b(x - X_{i'}) \\
&= \frac{1}{2} m\omega_x^2 \int_{-\infty}^{\infty} dx\, x^2 w_b^*(x) w_b(x - (X_{i'} - X_i)),
\end{aligned}
\tag{2.24}
$$

since $w_b(x - X_i)$ and $w_b(x - X_{i'})$ are orthogonal and $w_b^*(x - X_i)w_b(x - X_{i'})$ is even about $(X_i + X_{i'})/2$ as $w_b(x)$ is either even or odd.[5] In figure 2.6 we plot the ratio $\left|\int_{-\infty}^{\infty} \mathrm{d}x\, x^2 w_b^*(x) w_b(x - a)\right| / a^2$ as a function of V.
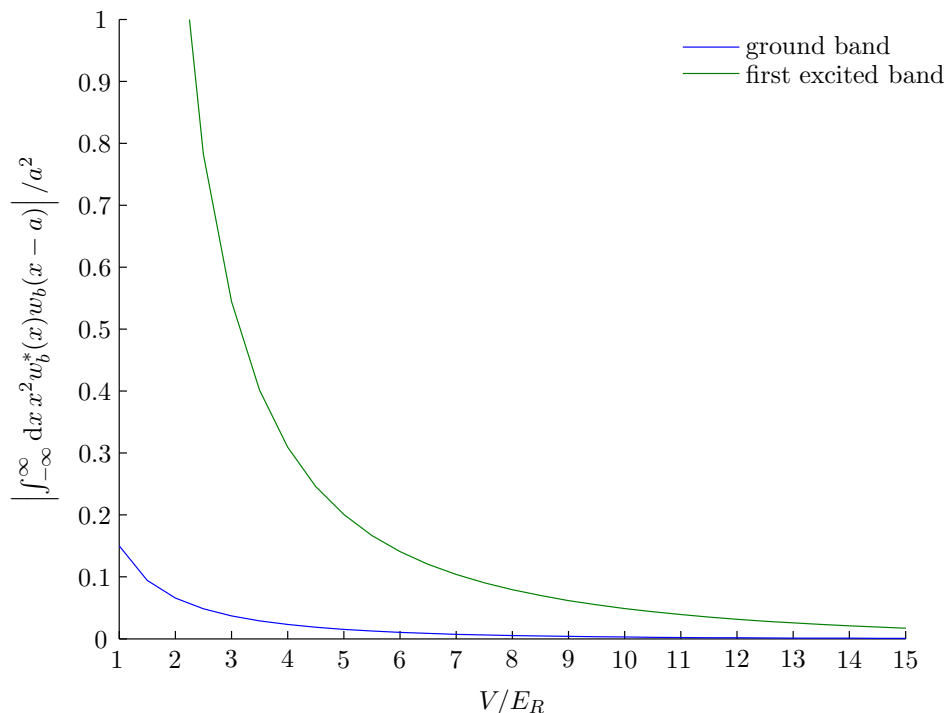
Figure 2.6: Error due to contribution from adjacent sites

2.9.3 Inter-band contribution

Now we consider the case with $b \neq b'$, but with $i = i'$. To allow for this contribution, it would be necessary to include matrix elements between bands in the Hamiltonian.

To quantify the error, we consider the additive component in the x direction, and we only get a potential error if the other components of band b and b' are equal. Then, with b_x being the x component of b and $b_x \neq b'_x$:

$$\int \mathrm{d}\mathbf{r}\, \frac{1}{2} m\omega_x^2 x^2 w_b^*(\mathbf{r} - \mathbf{R}_i) w_{b'}(\mathbf{r} - \mathbf{R}_i) = \frac{1}{2} m\omega_x^2 \int_{-\infty}^{\infty} \mathrm{d}x\, x^2 w_{b_x}^*(x - X_i) w_{b'_x}(x - X_i)$$

$$= \frac{1}{2} m\omega_x^2 \int_{-\infty}^{\infty} \mathrm{d}x\, (x + X_i)^2 w_{b_x}^*(x) w_{b'_x}(x). \quad (2.25)$$

---

[5] $f(-x) = \pm f(x), g(x) = f(x-a)f(x+a) \implies f(x-a) = \pm f(-x+a), f(x+a) = \pm f(-x-a) \implies g(-x) = f(-x-a)f(-x+a) = f(x+a)f(x-a) = g(x)$

23

Considering, for example $b_x = 0$ (the ground band), and $b'_x = 1$ (the first excited band) $w_0^*(x)w_1(x)$ is odd so the above becomes $m\omega_x^2 X_i \int_{-\infty}^{\infty} dx\, x w_0^*(x)w_1(x)$. In figure 2.7 we plot the ratio $\int_{-\infty}^{\infty} dx\, x w_0^*(x)w_1(x)/a$ as a function of V, and note that when occupation of excited bands is low, its significance will be reduced.
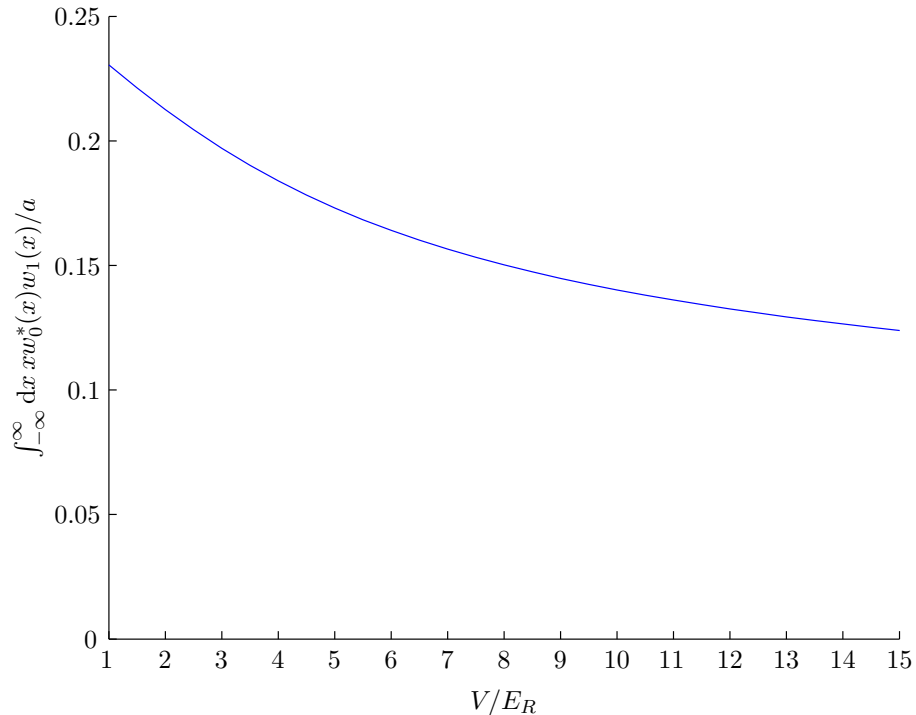
Figure 2.7: Error due to overlap between Wannier functions from the ground and first excited bands

2.10 Interaction coefficients

In this work, we will always use the exact form (2.12) for calculation of interaction coefficients. However, we consider approximations and limits in this section.

2.10.1 Numerical fit

A numerical fit of the ground-band on-site interaction coefficient over the range $5E_R < V < 15E_R$ gives, for the three-dimensional case:

$$\frac{U}{E_R} \approx 2.33 \frac{a_s}{a} \left(\frac{V}{E_R} \right)^{0.96}, \tag{2.26}$$

with coefficient of determination, $R^2 > 0.999$.

24

2.10.2 Gaussian approximation

As in section 2.8.4, if we approximate the Wannier function by (2.18), then:

$$U \approx g \int \mathrm{d}\mathbf{r} \, |w_0(\mathbf{r})|^4 \approx g \left(\frac{\pi}{2a^2} \right)^{d/2} \left(\frac{V}{E_R} \right)^{d/4}, \tag{2.27}$$

and in three dimensions this gives $U \approx 2\sqrt{2\pi}(V/E_R)^{3/4} E_R a_s/a$ as in [88, 89].

2.10.3 No lattice limit

In appendix F.2 we show that, in the limit when there is no lattice, the numerical approach we follow in this thesis gives the same results as those we would get from existing no-lattice LDA calculations [56] if $U_{bb'} = g/a^d$ for all b, b'. This is equivalent to:

$$\frac{U_{bb'} a^{d-2}}{E_R a_s} = \frac{8}{\pi}. \tag{2.28}$$

In appendix F.2 we proceed to show that the correct limit is obtained when we consider interactions with all sites. In this section we consider what the shortfall is when only on-site interactions are included.

We have $w_0(x) = \mathrm{sinc}\,(\pi x/a)/\sqrt{a}$ from (D.25), so the on-site only component for the ground band is:

$$U = g \int |w_0(\mathbf{r})|^4 \, \mathrm{d}\mathbf{r} = g \left[\int_{-\infty}^{\infty} \left| \frac{1}{\sqrt{a}} \mathrm{sinc}\,(\pi x/a) \right|^4 \mathrm{d}x \right]^d$$

$$= g \left(\frac{2}{3a} \right)^d, \tag{2.29}$$

so that, in three dimensions, $Ua^d/g = (2/3)^3 \approx 30\%$, showing that on-site component makes up 30% of the total interaction in the no-lattice limit. From (D.25), in three dimensions, the on-site interaction component between the ground band and an excited $00n$ band (ground band in two directions and band n in one direction) is:

$$U_{000,00n} = g \left[\int_{-\infty}^{\infty} w_0^4(x)\mathrm{d}x \right]^2 \int_{-\infty}^{\infty} w_0^2(x)w_n^2(x)\mathrm{d}x$$

$$= g \left(\frac{2}{3a} \right)^2 \frac{5}{12a} = g\frac{5}{27a^3} = \frac{40}{27\pi} \frac{a_s}{a} E_R. \tag{2.30}$$

So, the on-site ground to $00n$ band interactions make up $5/27 = 18\%$ of the total ground to $00n$ band interactions in the no lattice limit.

The two types of on-site interactions between first excited bands in three dimensions are:

$$U_{00n,00n} = g \left[\int_{-\infty}^{\infty} w_0^4(x) \mathrm{d}x \right]^2 \int_{-\infty}^{\infty} w_n^4(x) \mathrm{d}x$$

$$= g \left(\frac{2}{3a} \right)^2 \frac{1}{2a} = g \frac{2}{9a^3} = \frac{16}{9\pi} \frac{a_s}{a} E_R, \tag{2.31}$$

and

$$U_{0n0,00n} = g \int_{-\infty}^{\infty} w_0^4(x) \mathrm{d}x \left[\int_{-\infty}^{\infty} w_0^2(x) w_n^2(x) \mathrm{d}x \right]^2$$

$$= g \frac{2}{3a} \left(\frac{5}{12a} \right)^2 = g \frac{25}{216a^3} = \frac{25}{27\pi} \frac{a_s}{a} E_R, \tag{2.32}$$

so the on-site interactions are 22% and 12% of the respective totals.

2.10.4   Using Wannier functions

The three-dimensional ground-band interaction coefficients are shown in figure 2.8. The on-site interaction coefficient tends to the expected value, (2.29), at $V = 0$. We also show the all-site interaction coefficients, discussed in section 2.10.5, which tend to the expected value (2.28) at $V = 0$. Compared to the Gaussian approximation, the Wannier functions are fatter tailed and therefore lower at the peak for a given normalisation (as shown in figure D.2). This increased peak height for the Gaussian approximation is accentuated by taking the fourth power in the integral for U, and we can see that the Gaussian approximation significantly overstates the interaction coefficient.

The three-dimensional excited-band interaction coefficients are shown for reference in figure 2.9. The results all tend to the expected limits at $V = 0$. The gap between all-site and on-site interaction coefficients is maintained for higher V/E_R than for the ground-band, since the excited-band Wannier functions are less localised.

2.10.5   Off-site interactions

We derive an approximation scheme for off-site interactions in appendix F. The result is a modification of the interaction coefficients, as shown in figure 2.8. As discussed in section F.2, if we use the all-site interaction coefficients in our model at $V = 0$, with a certain interpretation of the number densities, the formulae are exactly the
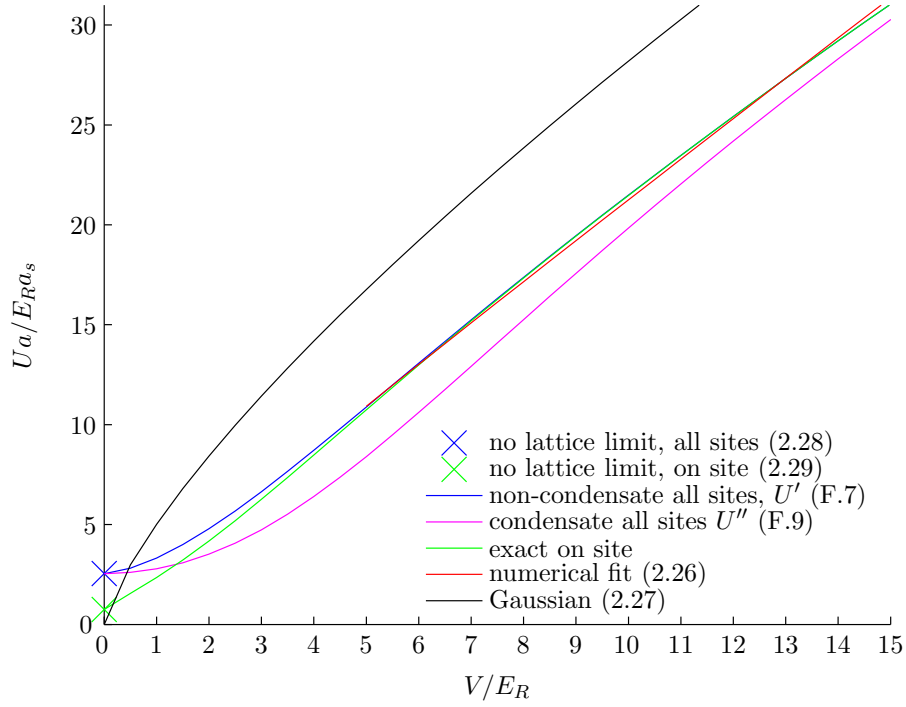
Figure 2.8: Ground-band interaction coefficients in three dimensions
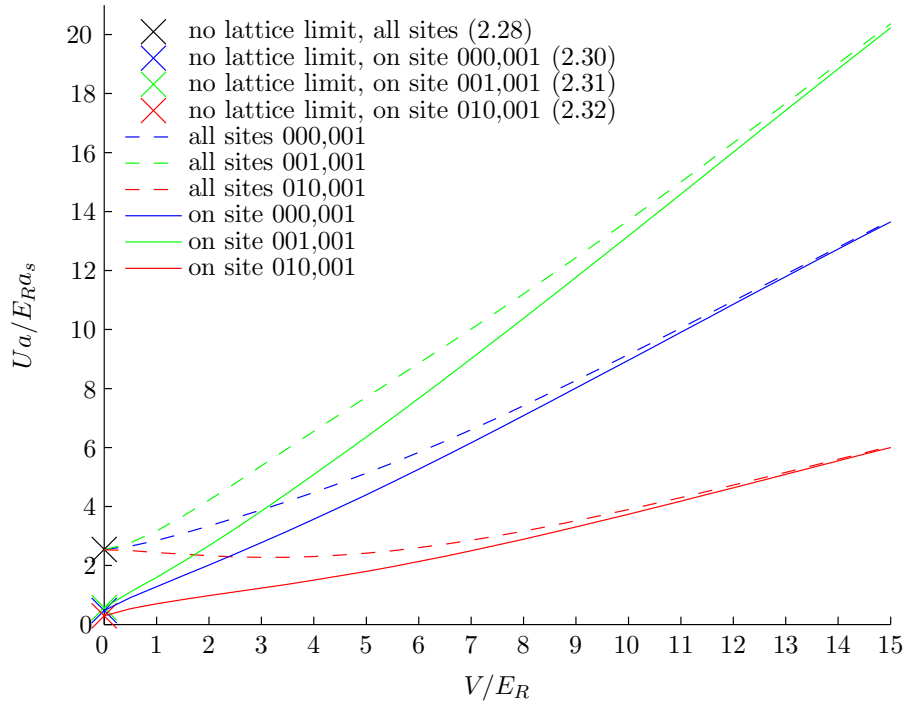
Figure 2.9: Excited-band interaction coefficients. The integers in the legend specify the components b_x, b_y, b_z of each band

same as those for existing no-lattice calculations. For the non-condensate (for example, for calculating critical temperatures from above), the on-site and all-site interaction coefficients are very similar for $V \gtrsim 5E_R$. We do not pretend to have solved the problem of an interacting gas in a lattice with $V \lesssim E_R$, since the Wannier basis we use is not localised in such a regime (we discuss interactions in a shallow lattice in section 7.1.1). However, our off-site interaction coefficients provide a useful interpolation scheme which is accurate in the no-lattice case and for moderate to deep lattices. The validity of other aspects of formulae in shallow lattices must still be considered; for example, our analytical results will not be accurate if interactions in the excited bands are significant.

For the condensate, interference between sites, mediated by the tails of distant Wannier states, can reduce the interaction coefficient, as discussed in section F.1.

All of our numerical results in this thesis use on-site interaction coefficients.

2.11 Summary

We have described the optical-lattice and harmonic-trap potentials and given their typical experimental parameters. We have derived an extended Bose-Hubbard Hamiltonian which goes beyond the usual Bose-Hubbard approach, so will be valid for shallower lattices and at higher temperatures, by allowing for beyond nearest-neighbour hopping, excited bands, and by giving an interpolation scheme for off-site interactions. We have carefully considered the extended Bose-Hubbard model parameters, including the hopping matrix, the harmonic trap and interactions and have investigated the approximations often used to obtain the Bose-Hubbard model parameters.

Chapter 3

Mean-field approximation

For more than a few particles and sites, the Hamiltonian (2.9) cannot be solved exactly. Quantum Monte-Carlo has generally been used for the one-dimensional problem [90–92]. Three-dimensional solutions have been produced, but have been limited to approximately 20 sites in each direction [46, 47]. For the translationally-invariant lattice, the number of particles modelled is up to order 10^4 [47, 93], but for the combined harmonic lattice, the number of particles is limited to approximately 500 [94]. The density-matrix renormalisation group method has not currently been solved in three dimensions [48, 49] although recent work with hard-core bosons in two dimensions has been reported [50].

Due to the difficulty of exact calculations with the Bose-Hubbard Hamiltonian, we use the Popov approximation to the Hartree-Fock Bogoliubov method. The discrete version of this method has been used for the ground band of the combined harmonic lattice, but has been limited to one dimension: adiabatic loading was considered in [52] with 19 atoms and the superfluidity and condensation was considered in [53] with 41 sites and ten atoms. Our derivation of the quadratic Hamiltonian for the extended Bose-Hubbard model is the first to our knowledge.

Since, as we shall see, the dimension of the system has a profound effect on its properties, and since we wish to numerically consider thermodynamics so that we require many more atoms and sites, we continue this chapter by introducing the LDA. We then diagonalise the Hamiltonian within the LDA. A necessary condition for the LDA treatment to be valid is that $k_B T \gg \hbar \bar{\omega}^*$ (the energy spacing, $\hbar \bar{\omega}^*$, is defined on page 59). Ours is the first LDA treatment of the extended Bose-Hubbard model, and the

first for the Bose-Hubbard model via the position basis.

Allowing for off-site interactions within a local calculation involves significant approximations and an involved derivation which is discussed in appendix F. In this chapter we derive the results for on-site interactions, starting from the Hamiltonian (2.11).

3.1 Mean-field approach: condensate and non-condensate

We assume that the local number of condensate atoms is either macroscopic or zero [8, 95], so that the field operator, $\hat{\Psi}(\mathbf{r})$, can be separated into a c-number condensate component (the order parameter), $\Phi(\mathbf{r})$, and a non-condensate field operator, $\tilde{\psi}(\mathbf{r})$, defined by the usual broken symmetry approach, $\Phi(\mathbf{r}) \equiv \left\langle \hat{\Psi}(\mathbf{r}) \right\rangle$, $\tilde{\psi}(\mathbf{r}) \equiv \hat{\Psi}(\mathbf{r}) - \Phi(\mathbf{r})$ so that $\left\langle \tilde{\psi}(\mathbf{r}) \right\rangle = 0$.

The assumption that $\Phi(\mathbf{r})$ is a c-number is inaccurate near the edges of the condensate, where the local condensate density, $|\Phi(\mathbf{r})|^2$, is small and just below the critical temperature, as the condensate component is then small everywhere, since fluctuations are important in such regions.

We expand the condensate amplitude and the non-condensate field-operator in a Wannier basis:

$$\Phi(\mathbf{r}) = \sum_i z_i w_0(\mathbf{r} - \mathbf{R}_i), \quad \tilde{\psi}(\mathbf{r}) = \sum_{b,i} \hat{\delta}_{b,i} w_b(\mathbf{r} - \mathbf{R}_i), \quad \tilde{\psi}^\dagger(\mathbf{r}) = \sum_{b,i} \hat{\delta}_{b,i}^\dagger w_b^*(\mathbf{r} - \mathbf{R}_i).$$
(3.1)

From (2.4) and the orthogonality, (D.7), and completeness, (D.8), of the Wannier functions, we get $z_i \equiv \left\langle \hat{a}_{0,i} \right\rangle$ for the ground band and $\hat{\delta}_{0,i} \equiv \hat{a}_{0,i} - z_i$ [96], and $\hat{\delta}_{b,i} \equiv \hat{a}_{b,i}$ above the ground band. Using (2.5), we get the usual commutation relations:

$$\left[\hat{\delta}_{b,i}, \hat{\delta}_{b',i'}^\dagger \right] = \delta_{bb'} \delta_{ii'}, \quad \left[\hat{\delta}_{b,i}, \hat{\delta}_{b',i'} \right] = 0.$$
(3.2)

The condensate density is:

$$|\Phi(\mathbf{r})|^2 = \sum_{i,i'} z_i^* z_{i'} w_0^*(\mathbf{r} - \mathbf{R}_i) w_0(\mathbf{r} - \mathbf{R}_{i'}),$$
(3.3)

allowing for the non-locality of the Wannier states, and:

$$N_c \equiv \int d\mathbf{r} \, |\Phi(\mathbf{r})|^2 = \sum_i |z_i|^2.$$
(3.4)

We note that $|z_i|^2$ is not the number of condensate atoms per site, but it is a good approximation for a deep lattice, when the term $w_0^*(\mathbf{r}-\mathbf{R}_i)w_0(\mathbf{r}-\mathbf{R}_{i'})$ is approximately zero for $i \neq i'$ and $|w_b(\mathbf{r}-\mathbf{R}_i)|^2 \approx 0$ except for $\mathbf{r} \approx \mathbf{R}_i$.

For both the condensate and the non-condensate, we assume that interactions are perturbative relative to the band-gap energy scale (a necessary condition for this is that the band gap is small compared to $2U_{0b}|z_i|^2 + 2\sum_{b'}U_{bb'}\tilde{n}_{b',i}$), so that we may ignore collisional couplings between bands in the many-body state. The advantage of including excited bands in our approach is that, if temperatures are sufficiently high for our calculations to show that excited bands are highly occupied, this is an indication that the validity of ignoring collisional couplings should be considered.

For the non-condensate, we assume that the thermal coherence length is sufficiently short (long range coherence is absorbed by the condensate) that the non-condensate one-body density matrix is diagonal in lattice site indices $\left\langle \hat{\delta}_{b,i}^{\dagger}\hat{\delta}_{b',i'} \right\rangle = \tilde{n}_{b,i}\delta_{bb'}\delta_{ii'}$, where we define $\tilde{n}_{b,i} \equiv \left\langle \hat{\delta}_{b,i}^{\dagger}\hat{\delta}_{b,i} \right\rangle$. Note that δ_{ij} is the delta function and $\hat{\delta}_{b,i}$ is the destruction operator. The non-condensate density is then given by:

$$\left\langle \tilde{\psi}^{\dagger}(\mathbf{r})\tilde{\psi}(\mathbf{r}) \right\rangle = \sum_{b,b',i,i'} \left\langle \hat{\delta}_{b,i}^{\dagger}\hat{\delta}_{b',i'} \right\rangle w_b^*(\mathbf{r}-\mathbf{R}_i)w_{b'}(\mathbf{r}-\mathbf{R}_{i'}) = \sum_{b,i} \tilde{n}_{b,i}|w_b(\mathbf{r}-\mathbf{R}_i)|^2, \quad (3.5)$$

so that:

$$\tilde{N} \equiv \int d\mathbf{r} \left\langle \tilde{\psi}^{\dagger}(\mathbf{r})\tilde{\psi}(\mathbf{r}) \right\rangle = \sum_{b,i} \tilde{n}_{b,i}, \quad (3.6)$$

and we define $\tilde{N}_b \equiv \sum_i \tilde{n}_{b,i}$. Following the same arguments given for the condensate, for a sufficiently deep lattice $\tilde{n}_{b,i}$ is approximately the number of non-condensate atoms in band b at site i.

To express the Hamiltonian in terms of the amplitudes z_i, and operators, $\hat{\delta}_{b,i}$, we take the interaction term from (2.11):

$$\frac{1}{2}\sum_{b_1,b_2,b_3,b_4} \hat{a}_{b_1,i}^{\dagger}\hat{a}_{b_2,i}^{\dagger}\hat{a}_{b_3,i}\hat{a}_{b_4,i} U_{b_1,b_2,b_3,b_4}^{i,i,i,i}$$

$$= \frac{1}{2}|z_i|^4 U_{00} + \sum_b \left[z_i^*\hat{\delta}_{b,i} + z_i\hat{\delta}_{b,i}^{\dagger} \right]|z_i|^2 U_{0,0,0,b}^{i,i,i,i}$$

$$+ \sum_{b,b'} \left[\frac{1}{2}\mathrm{m}_i^*\hat{\delta}_{b,i}\hat{\delta}_{b',i} + \frac{1}{2}\mathrm{m}_i\hat{\delta}_{b,i}^{\dagger}\hat{\delta}_{b',i}^{\dagger} + 2|z_i|^2\hat{\delta}_{b,i}^{\dagger}\hat{\delta}_{b',i} \right] U_{0,0,b,b'}^{i,i,i,i}$$

$$+ \sum_{b_1,b_2,b_3} \left[z_i^*\hat{\delta}_{b_1,i}^{\dagger}\hat{\delta}_{b_2,i}\hat{\delta}_{b_3,i} + z_i\hat{\delta}_{b_1,i}^{\dagger}\hat{\delta}_{b_2,i}^{\dagger}\hat{\delta}_{b_3,i} \right] U_{0,b_1,b_2,b_3}^{i,i,i,i} + \frac{1}{2}\sum_{b_1,b_2,b_3,b_4} \hat{\delta}_{b_1,i}^{\dagger}\hat{\delta}_{b_2,i}^{\dagger}\hat{\delta}_{b_3,i}\hat{\delta}_{b_4,i}U_{b_1,b_2,b_3,b_4}^{i,i,i,i},$$

where $m_i \equiv z_i^2$, $m_i^* \equiv z_i^{*2}$ and we have taken advantage of our real Wannier functions, (D.22), so that the order of subscripts in $U_{b_1,b_2,b_3,b_4}^{i,i,i,i}$ is not important.

3.2 Quadratic Hamiltonian

The Hamiltonian still includes up to fourth powers in the operators $\hat{\delta}_{b,i}$. We make a quadratic Hamiltonian simplification by making a mean-field approximation motivated by Wick's theorem [56, 61]. This is valid in the weakly-interacting regime; therefore, our work is not valid in the strongly-correlated Mott-insulator case. For the translationally-invariant, no lattice case at $T = 0$, the small parameter for a perturbative approach is $n_c a_s^3 \ll 1$ and for $k_B T \gg n_c g$ the small parameter is $\sqrt{n_c a_s^3} k_B T / n_c g \ll 1$ [97]. We are not aware of any literature specifying the small parameter for a lattice. We use:

$$
\hat{\delta}_{b_1,i}^\dagger \hat{\delta}_{b_2,i}^\dagger \hat{\delta}_{b_3,i} \hat{\delta}_{b_4,i} \approx \left\langle \hat{\delta}_{b_1,i}^\dagger \hat{\delta}_{b_2,i}^\dagger \right\rangle \hat{\delta}_{b_3,i} \hat{\delta}_{b_4,i} + \left\langle \hat{\delta}_{b_1,i}^\dagger \hat{\delta}_{b_3,i} \right\rangle \hat{\delta}_{b_2,i}^\dagger \hat{\delta}_{b_4,i} + \left\langle \hat{\delta}_{b_1,i}^\dagger \hat{\delta}_{b_4,i} \right\rangle \hat{\delta}_{b_2,i}^\dagger \hat{\delta}_{b_3,i}
$$

$$
+ \left\langle \hat{\delta}_{b_2,i}^\dagger \hat{\delta}_{b_3,i} \right\rangle \hat{\delta}_{b_1,i}^\dagger \hat{\delta}_{b_4,i} + \left\langle \hat{\delta}_{b_2,i}^\dagger \hat{\delta}_{b_4,i} \right\rangle \hat{\delta}_{b_1,i}^\dagger \hat{\delta}_{b_3,i} + \left\langle \hat{\delta}_{b_3,i} \hat{\delta}_{b_4,i} \right\rangle \hat{\delta}_{b_1,i}^\dagger \hat{\delta}_{b_2,i}^\dagger
$$

$$
\approx \tilde{n}_{b_1,i} \hat{\delta}_{b_2,i}^\dagger \hat{\delta}_{b_2,i} \left(\delta_{b_1 b_3} \delta_{b_2 b_4} + \delta_{b_1 b_4} \delta_{b_2 b_3} \right) + \tilde{n}_{b_2,i} \hat{\delta}_{b_1,i}^\dagger \hat{\delta}_{b_1,i} \left(\delta_{b_2 b_3} \delta_{b_1 b_4} + \delta_{b_2 b_4} \delta_{b_1 b_3} \right)
$$
$$\tag{3.7}$$

$$
\implies \sum_{b_1,b_2,b_3,b_4} \hat{\delta}_{b_1,i}^\dagger \hat{\delta}_{b_2,i}^\dagger \hat{\delta}_{b_3,i} \hat{\delta}_{b_4,i} U_{b_1,b_2,b_3,b_4}^{i,i,i,i} \approx 4 \sum_{b,b'} \tilde{n}_{b',i} \hat{\delta}_{b,i}^\dagger \hat{\delta}_{b,i} U_{bb'}, \tag{3.8}
$$

where we have used a Popov approximation to eliminate the terms $\left\langle \hat{\delta}_{b,i}^\dagger \hat{\delta}_{b,i}^\dagger \right\rangle$ and $\left\langle \hat{\delta}_{b,i} \hat{\delta}_{b,i} \right\rangle$, and we have neglected pairs with different band indices, since we ignore collisional couplings between bands in the many-body state as discussed above.

Similarly, by analogy with Wick's theorem [98], we can simplify the third order terms:

$$
z_i^* \hat{\delta}_{b_1,i}^\dagger \hat{\delta}_{b_2,i} \hat{\delta}_{b_3,i} \approx z_i^* \left\langle \hat{\delta}_{b_1,i}^\dagger \hat{\delta}_{b_2,i} \right\rangle \hat{\delta}_{b_3,i} + z_i^* \left\langle \hat{\delta}_{b_1,i}^\dagger \hat{\delta}_{b_3,i} \right\rangle \hat{\delta}_{b_2,i} + z_i^* \left\langle \hat{\delta}_{b_2,i} \hat{\delta}_{b_3,i} \right\rangle \hat{\delta}_{b_1,i}^\dagger
$$

$$
\approx z_i^* \tilde{n}_{b_1,i} \left[\hat{\delta}_{b_3,i} \delta_{b_1 b_2} \delta_{b_3 0} + \hat{\delta}_{b_2,i} \delta_{b_1 b_3} \delta_{b_2 0} \right] \tag{3.9}
$$

$$
\implies \sum_{b_1,b_2,b_3} z_i^* \hat{\delta}_{b_1,i}^\dagger \hat{\delta}_{b_2,i} \hat{\delta}_{b_3,i} U_{0,b_1,b_2,b_3}^{i,i,i,i} \approx 2 z_i^* \hat{\delta}_{0,i} \sum_b \tilde{n}_{b,i} U_{0b}, \tag{3.10}
$$

and:

$$
\sum_{b_1,b_2,b_3} z_i \hat{\delta}_{b_1,i}^\dagger \hat{\delta}_{b_2,i}^\dagger \hat{\delta}_{b_3,i} U_{0,b_1,b_2,b_3}^{i,i,i,i} \approx 2 z_i \hat{\delta}_{0,i}^\dagger \sum_b \tilde{n}_{b,i} U_{0b}, \tag{3.11}
$$

and we set the linear terms $\left[z_i^* \hat{\delta}_{b,i} + z_i \hat{\delta}_{b,i}^\dagger \right] |z_i|^2$ to zero for $b \neq 0$ and the quadratic terms $|z_i|^2 \hat{\delta}_{b,i}^\dagger \hat{\delta}_{b',i}$, $m_i^* \hat{\delta}_{b,i} \hat{\delta}_{b',i}$ and $m_i \hat{\delta}_{b,i}^\dagger \hat{\delta}_{b',i}^\dagger$ to zero for $b \neq b'$ by the same assumption

that interactions are perturbative relative to the band-gap energy scale. Our interaction term then becomes:

$$\frac{1}{2} \sum_{b_1,b_2,b_3,b_4} \hat{a}^\dagger_{b_1,i} \hat{a}^\dagger_{b_2,i} \hat{a}_{b_3,i} \hat{a}_{b_4,i} U_{b_1,b_2,b_3,b_4} \approx \left[\frac{1}{2} |z_i|^2 + z_i^* \hat{\delta}_{0,i} + z_i \hat{\delta}^\dagger_{0,i} \right] |z_i|^2 U_{00}$$

$$+ \sum_b \left[\frac{1}{2} \mathrm{m}_i^* \hat{\delta}^2_{b,i} + \frac{1}{2} \mathrm{m}_i \hat{\delta}^{\dagger 2}_{b,i} + 2 |z_i|^2 \hat{\delta}^\dagger_{b,i} \hat{\delta}_{b,i} + 2 z_i^* \tilde{n}_{b,i} \hat{\delta}_{0,i} + 2 z_i \tilde{n}_{b,i} \hat{\delta}^\dagger_{0,i} \right] U_{0b}$$

$$+ 2 \sum_{b,b'} \tilde{n}_{b',i} \hat{\delta}^\dagger_{b,i} \hat{\delta}_{b,i} U_{bb'}. \tag{3.12}$$

Separating the Hamiltonian (2.11) by the number of depletion operators $\hat{\delta}^\dagger_i$ and $\hat{\delta}_i$ appearing and by band, $\hat{K}_i = \hat{K}_{0,i} + \hat{K}_{1,i} + \hat{K}^\dagger_{1,i} + \sum_b \hat{K}_{2,b,i}$, we get:

$$\hat{K}_{0,i} \equiv z_i^* \left[-\sum_{i'} J_{0,i,i'} \hat{S}_{i',i} + v_i - \mu + \frac{U_{00}}{2} |z_i|^2 \right] z_i, \tag{3.13}$$

$$\hat{K}_{1,i} \equiv \hat{\delta}^\dagger_{0,i} \left[-\sum_{i'} J_{0,i,i'} \hat{S}_{i',i} + v_i - \mu + U_{00} |z_i|^2 + 2 \sum_b U_{0b} \tilde{n}_{b,i} \right] z_i, \tag{3.14}$$

$$\hat{K}_{2,b,i} \equiv \hat{\delta}^\dagger_{b,i} \hat{\mathcal{L}}_{b,i} \hat{\delta}_{b,i} + \frac{U_{0b}}{2} \left[\hat{\delta}^{\dagger 2}_{b,i} \mathrm{m}_i + \hat{\delta}^2_{b,i} \mathrm{m}_i^* \right], \tag{3.15}$$

where:

$$\hat{\mathcal{L}}_{b,i} \equiv -\sum_{i'} J_{b,i,i'} \hat{S}_{i',i} + v_i - \mu + 2 U_{0b} |z_i|^2 + 2 \sum_{b'} U_{bb'} \tilde{n}_{b',i}, \tag{3.16}$$

and $\hat{S}_{i',i}$ is the shift operator from the site $\mathbf{R}_i$ to $\mathbf{R}_{i'}$, for example $\hat{S}_{i',i} \hat{\delta}_{b,i} = \hat{\delta}_{b,i'}$.

3.3 Gross-Pitaevskii equation

By minimising the energy functional $\mathrm{d} \langle \hat{K} \rangle / \mathrm{d} z_i^* = 0$, using $\langle \hat{\delta}^\dagger_{0,i} \rangle = \langle \hat{\delta}_{0,i} \rangle = 0$, so that $\langle \hat{K}_{1,i} + \hat{K}^\dagger_{1,i} \rangle = 0$ and noting which terms in $\hat{K}_{2,b,i}$ have no z_i^* dependence, we obtain the generalised Gross-Pitaevskii equation at site i:

$$\left[-\sum_{i'} J_{0,i,i'} \hat{S}_{i',i} + v_i - \mu + U_{00} |z_i|^2 + 2 \sum_b U_{0b} \tilde{n}_{b,i} \right] z_i = 0. \tag{3.17}$$

We note that if z_i satisfies the generalised Gross-Pitaevskii equation, then the terms $\hat{K}_{1,i}$ and $\hat{K}^\dagger_{1,i}$ are zero and the next contribution comes from $\hat{K}_{2,b,i}$.

The generalised Gross-Pitaevskii has the Thomas-Fermi solution:

$$|z_i|^2 = \frac{1}{U_{00}} \max \left(0, \mu - v_i - 2 \sum_b U_{0b} \tilde{n}_{b,i} \right), \tag{3.18}$$

where μ is determined by $N = \sum_i |z_i|^2 + \sum_{b,i} \tilde{n}_{b,i}$.

3.4 Hartree-Fock

The Hartree-Fock treatment is obtained by ignoring the terms[1] $\hat{\delta}_{b,i}^{\dagger 2} \mathrm{m}_i$ and $\hat{\delta}_{b,i}^2 \mathrm{m}_i^*$ in $\hat{K}_{2,b,i}$ which can then be diagonalised by a single particle transformation, setting $\hat{\delta}_{b,i} = \sum_j' u_{b,i,j} \hat{\alpha}_{b,j}$ (where the symbol $\sum_j'$ indicates a sum over modes excluding the condensate). The operators $\hat{\alpha}_{b,j}$ are chosen to satisfy:

$$\left[\hat{\alpha}_{b,j}, \hat{\alpha}_{b',j'}^{\dagger}\right] = \delta_{bb'}\delta_{jj'}, \qquad \left[\hat{\alpha}_{b,j}, \hat{\alpha}_{b',j'}\right] = 0, \tag{3.19}$$

and the $u_{b,i,j}$ modes are an orthonormal basis, that is $\sum_i u_{b,i,j}^* u_{b,i,j'} = \delta_{jj'}$, satisfying:

$$\hat{\mathcal{L}}_{b,i} u_{b,i,j} = E_{b,j} u_{b,i,j}, \tag{3.20}$$

so that:

$$\sum_i \hat{K}_{2,b,i} = \sum_j{}' E_{b,j} \hat{\alpha}_{b,j}^{\dagger} \hat{\alpha}_{b,j}. \tag{3.21}$$

Taking the condensate to satisfy the generalised GPE, we have:

$$\hat{K} = \sum_i z_i^* \left[-\sum_{i'} J_{0,i,i'} \hat{S}_{i',i} + v_i - \mu + \frac{U_{00}}{2} |z_i|^2 \right] z_i + \sum_{b,j}{}' E_{b,j} \hat{\alpha}_{b,j}^{\dagger} \hat{\alpha}_{b,j}. \tag{3.22}$$

Since the Hamiltonian is diagonal in band b and mode j, we can treat the Hartree-Fock modes as non-interacting which leads to $\left\langle \hat{\alpha}_{b,j}^{\dagger} \hat{\alpha}_{b',j'} \right\rangle = \delta_{bb'}\delta_{jj'} \bar{n}_{\mathrm{BE}}(E_{b,j})$ where $\bar{n}_{\mathrm{BE}}(E) \equiv (e^{\beta E} - 1)^{-1}$ and $\left\langle \hat{\alpha}_{b,j} \hat{\alpha}_{b',j'} \right\rangle = \left\langle \hat{\alpha}_{b,j}^{\dagger} \hat{\alpha}_{b',j'}^{\dagger} \right\rangle = 0$, so the non-condensate density is given by:

$$\tilde{n}_{b,i} = \sum_j{}' |u_{b,i,j}|^2 \, \bar{n}_{\mathrm{BE}}(E_{b,j}). \tag{3.23}$$

3.5 Bogoliubov diagonalisation

In general it is desirable to go beyond the Hartree-Fock treatment when the condensate is present. To do this, we retain the terms $\hat{\delta}_{b,i}^{\dagger 2} \mathrm{m}_i$ and $\hat{\delta}_{b,i}^2 \mathrm{m}_i^*$ in the Hamiltonian, which

---

[1] We note that this is different from the Popov approximation which eliminates only the expected value of the terms $\hat{\delta}_{b,i}^{\dagger 2}$ and $\hat{\delta}_{b,i}^2$.

can be diagonalised using a quasi-particle transformation [8]:

$$\hat{\delta}_{b,i} = \sideset{}{'}\sum_j \left(u_{b,i,j}\hat{\alpha}_{b,j} + v^*_{b,i,j}\hat{\alpha}^\dagger_{b,j} \right), \quad \hat{\delta}^\dagger_{b,i} = \sideset{}{'}\sum_j \left(u^*_{b,i,j}\hat{\alpha}^\dagger_{b,j} + v_{b,i,j}\hat{\alpha}_{b,j} \right), \qquad (3.24)$$

where we refer to the $\hat{\alpha}_{b,j}$ as the quasi-particle operators and the $u_{b,i,j}, v_{b,i,j}$ as the quasi-particle modes. We require that (3.19) holds, as for the Hartree-Fock case so that:[2]

$$\left[\hat{\delta}_{b,i}, \hat{\delta}^\dagger_{b',i'} \right] = \delta_{bb'} \sideset{}{'}\sum_j \left(u_{b,i,j}u^*_{b,i',j} - v^*_{b,i,j}v_{b,i',j} \right)$$

$$\implies \sideset{}{'}\sum_j \left(u_{b,i,j}u^*_{b,i',j} - v^*_{b,i,j}v_{b,i',j} \right) = \delta_{ii'}, \qquad (3.25)$$

and $\left[\hat{\delta}_{b,i}, \hat{\delta}_{b,i'} \right] = \sideset{}{'}\sum_j \left(u_{b,i,j}v^*_{b,i',j} - v^*_{b,i,j}u_{b,i',j} \right) = 0$. The quasi-particle modes are normalised:

$$\sum_i \left(|u_{b,i,j}|^2 - |v_{b,i,j}|^2 \right) = 1. \qquad (3.26)$$

The quasi-particle transformation, brings $\hat{K}_{2,b,i}$ into the form:

$$\hat{K}_{2,b,i} = \sideset{}{'}\sum_{j,k} \left[\hat{\alpha}^\dagger_{b,j}\hat{\alpha}_{b,k} \left(u^*_{b,i,j}\hat{\mathcal{L}}_{b,i}u_{b,i,k} + \frac{U_{0b}}{2}\left\{ \mathrm{m}_i u^*_{b,i,j}v_{b,i,k} + \mathrm{m}^*_i v^*_{b,i,j}u_{b,i,k} \right\} \right) \right.$$

$$+ \hat{\alpha}_{b,j}\hat{\alpha}^\dagger_{b,k} \left(v_{b,i,j}\hat{\mathcal{L}}_{b,i}v^*_{b,i,k} + \frac{U_{0b}}{2}\left\{ \mathrm{m}_i v_{b,i,j}u^*_{b,i,k} + \mathrm{m}^*_i u_{b,i,j}v^*_{b,i,k} \right\} \right)$$

$$+ \hat{\alpha}_{b,j}\hat{\alpha}_{b,k} \left(v_{b,i,j}\hat{\mathcal{L}}_{b,i}u_{b,i,k} + \frac{U_{0b}}{2}\left\{ \mathrm{m}_i v_{b,i,j}v_{b,i,k} + \mathrm{m}^*_i u_{b,i,j}u_{b,i,k} \right\} \right)$$

$$\left. + \hat{\alpha}^\dagger_{b,j}\hat{\alpha}^\dagger_{b,k} \left(u^*_{b,i,j}\hat{\mathcal{L}}_{b,i}v^*_{b,i,k} + \frac{U_{0b}}{2}\left\{ \mathrm{m}_i u^*_{b,i,j}u^*_{b,i,k} + \mathrm{m}^*_i v^*_{b,i,j}v^*_{b,i,k} \right\} \right) \right]. \quad (3.27)$$

We choose the modes to satisfy the Bogoliubov-de Gennes equations (see section 3.5.1 for a discussion of orthogonalisation of these equations):

$$\hat{\mathcal{L}}_{b,i}u_{b,i,j} + U_{0b}\mathrm{m}_i v_{b,i,j} = E_{b,j}u_{b,i,j}, \qquad (3.28)$$

$$\hat{\mathcal{L}}_{b,i}v_{b,i,j} + U_{0b}\mathrm{m}^*_i u_{b,i,j} = -E_{b,j}v_{b,i,j}. \qquad (3.29)$$

We show that the Hamiltonian is diagonal with these solutions in appendix G:

$$\hat{K} = -\sum_{i,i'} J_{0,i,i'}z^*_i z_{i'} + \sum_i \left[v_i - \mu + \frac{U_{00}}{2}|z_i|^2 \right] |z_i|^2 + \sideset{}{'}\sum_{b,j} E_{b,j} \left[\hat{\alpha}^\dagger_{b,j}\hat{\alpha}_{b,j} - \sum_i |v_{b,i,j}|^2 \right],$$

$$(3.30)$$

---

[2]Using $\left[\sum_j A_j, \sum_k B_k \right] = \sum_{j,k} [A_j, B_k]$.

and we can treat the quasi-particles as non-interacting which leads to:

$$\tilde{n}_{b,i} = {\sum_{j,k}}' \left\langle \left(u^*_{b,i,j} \hat{\alpha}^\dagger_{b,j} + v_{b,i,j} \hat{\alpha}_{b,j} \right) \left(u_{b,i,k} \hat{\alpha}_{b,k} + v^*_{b,i,k} \hat{\alpha}^\dagger_{b,k} \right) \right\rangle$$

$$= {\sum_{j}}' \left(|u_{b,i,j}|^2 + |v_{b,i,j}|^2 \right) \bar{n}_{\text{BE}}(E_{b,j}) + |v_{b,i,j}|^2 . \tag{3.31}$$

3.5.1 Quasi-particle orthogonality

The references [98, 99] explain that, for a general potential, equations (3.28) and (3.29) give quasi-particle functions which are orthogonal to the condensate only in a generalised sense, $\sum_i z^*_i u_{b,i,j} + z_i v_{b,i,j} = 0$. To be orthogonal in the sense $\sum_i z^*_i u_{b,i,j} = \sum_i z_i v_{b,i,j} = 0$, adjustments are required, for example [96, 100]:

$$E_{0,j} u_{0,i,j} \rightarrow E_{0,j} u_{0,i,j} + U_{00} \sum_i |z_i|^2 \left(z^*_i u_{0,i,j} - z_i v_{0,i,j} \right) z_i, \tag{3.32}$$

for (3.28) and a similar adjustment for (3.29). We do not follow this approach since, in our LDA solution below, we approximate by using an orthogonal Bloch form for the modes.

3.6 Local density approximation

3.6.1 Overview

The LDA has been extensively used for (non-lattice) harmonically trapped Bose gases. The essence of this approximation is the replacements $-\hbar^2 \nabla^2/2m \rightarrow p^2/2m$ in the Hamiltonian with $\mathbf{r}$ and $\mathbf{p}$ treated as classical variables. The extension of this approach to the lattice case is made by the replacement $-\hbar^2 \nabla^2/2m + V_{\text{latt}}(\mathbf{r}) \rightarrow K_b(\mathbf{k})$ where $\mathbf{k}$ is the quasi-momentum, b the quantised band index and $K_b(\mathbf{k})$ the Bloch spectrum. In what follows, we present our assumptions in making this replacement more precisely.

3.6.2 Bloch approximation

We set j to be the Bloch momentum, $\mathbf{k}$, and make the LDA by seeking solutions where u and v have the Bloch form:

$$u_{b,i',\mathbf{k}} = e^{i\mathbf{k} \cdot (\mathbf{R}_{i'} - \mathbf{R}_i)} u_{b,i,\mathbf{k}}, \qquad v_{b,i',\mathbf{k}} = e^{i\mathbf{k} \cdot (\mathbf{R}_{i'} - \mathbf{R}_i)} v_{b,i,\mathbf{k}}. \tag{3.33}$$

This assumption is exact for the translationally-invariant case, and we justify the approximation by comparing our non-interacting density of states to the numerical diagonalisation of the full combined harmonic lattice problem in section 4.6.

To make progress, it is useful to consider the Bloch waves (appendix C), $\psi_{b,\mathbf{k}}(\mathbf{r})$, of the homogeneous non-interacting lattice Hamiltonian:

$$\left[-\frac{\hbar^2 \nabla^2}{2m} + V_{\text{latt}}(\mathbf{r}) \right] \psi_{b,\mathbf{k}}(\mathbf{r}) = K_b(\mathbf{k}) \psi_{b,\mathbf{k}}(\mathbf{r}), \qquad (3.34)$$

with corresponding energy, $K_b(\mathbf{k})$. We find from (3.33) and (D.17) that:

$$-\sum_{i'} J_{b,i,i'} u_{b,i',\mathbf{k}} = K_b(\mathbf{k}) u_{b,i,\mathbf{k}}. \qquad (3.35)$$

We then have:

$$\hat{\mathcal{L}}_{b,i} u_{b,i,\mathbf{k}} = \left[K_b(\mathbf{k}) + v_i - \mu + 2U_{0b} |z_i|^2 + 2\sum_{b'} U_{bb'} \tilde{n}_{b',i} \right] u_{b,i,\mathbf{k}}. \qquad (3.36)$$

3.6.3 Envelope functions

We define a function $\tilde{n}_b(\mathbf{r})$ which is a proxy with the continuous variable $\mathbf{r}$ for the number of non-condensate atoms per site: $\tilde{n}_b(\mathbf{R}_i) = \tilde{n}_{b,i}$. Introducing these envelope functions greatly simplifies our formalism by allowing us to use continuous functions to exploit the trap symmetry which is broken by the lattice. Then, for a sufficiently small lattice spacing:

$$\frac{1}{a^d} \int d\mathbf{r}\, \tilde{n}_b(\mathbf{r}) \approx \sum_i \tilde{n}_b(\mathbf{R}_i) = \sum_i \tilde{n}_{b,i} = \tilde{N}_b, \qquad (3.37)$$

where $a^d = \prod_j a_j$ is the volume of a unit cell of the optical lattice. Similarly, we define the condensate mode envelope $z(\mathbf{r})$ where $z(\mathbf{R}_i) = z_i$ and $n_c(\mathbf{r}) \equiv |z(\mathbf{r})|^2$ so that:

$$\frac{1}{a^d} \int d\mathbf{r}\, n_c(\mathbf{r}) \approx \sum_i |z(\mathbf{R}_i)|^2 = \sum_i |z_i|^2 = N_c. \qquad (3.38)$$

We also define the envelope functions $u_b(\mathbf{k}, \mathbf{r})$ and $v_b(\mathbf{k}, \mathbf{r})$ where $u_b(\mathbf{k}, \mathbf{R}_i) = u_{b,i,\mathbf{k}}$ and $v_b(\mathbf{k}, \mathbf{R}_i) = v_{b,i,\mathbf{k}}$ and from (3.36) we have $\hat{\mathcal{L}}_{b,i} \to \mathcal{L}_b(\mathbf{k}, \mathbf{r})$ where:

$$\mathcal{L}_b(\mathbf{k}, \mathbf{r}) = K_b(\mathbf{k}) + V_{\text{tr}}(\mathbf{r}) - \mu + 2U_{0b} n_c(\mathbf{r}) + 2\sum_{b'} U_{bb'} \tilde{n}_{b'}(\mathbf{r}). \qquad (3.39)$$

Envelope functions represent the discrete functions but do not contain the fast Wannier state variation. However, apart from exceptional imaging techniques, such as the

stunning results of high-resolution scanning electron microscopy [101], normal optical imaging techniques would not distinguish density variation at the order of one site. If we require the detailed spatial density, rather than just site occupation, once we have the envelope functions, we can calculate $|\Phi(\mathbf{r})|^2 = \sum_{i,i'} z^*(\mathbf{R}_i) z(\mathbf{R}_{i'}) w_0^*(\mathbf{r} - \mathbf{R}_i) w_0(\mathbf{r} - \mathbf{R}_{i'})$ from (3.3) and $\left\langle \tilde{\psi}^\dagger(\mathbf{r}) \tilde{\psi}(\mathbf{r}) \right\rangle = \sum_{b,i} \tilde{n}_b(\mathbf{R}_i) \left| w_b(\mathbf{r} - \mathbf{R}_i) \right|^2$ from (3.5).

3.6.4 Bogoliubov spectrum

Making use of the envelope functions from the previous section, the Bogoliubov-de Gennes equations (3.28) and (3.29) take the algebraic form:

$$\mathcal{L}_b(\mathbf{k}, \mathbf{r}) u_b(\mathbf{k}, \mathbf{r}) + U_{0b} z^2(\mathbf{r}) v_b(\mathbf{k}, \mathbf{r}) = E_b(\mathbf{k}, \mathbf{r}) u_b(\mathbf{k}, \mathbf{r}), \tag{3.40}$$

$$\mathcal{L}_b(\mathbf{k}, \mathbf{r}) v_b(\mathbf{k}, \mathbf{r}) + U_{0b} z^{*2}(\mathbf{r}) u_b(\mathbf{k}, \mathbf{r}) = -E_b(\mathbf{k}, \mathbf{r}) v_b(\mathbf{k}, \mathbf{r}). \tag{3.41}$$

Solving the characteristic equation yields:

$$E_b(\mathbf{k}, \mathbf{r}) = \sqrt{\mathcal{L}_b^2(\mathbf{k}, \mathbf{r}) - [U_{0b} n_c(\mathbf{r})]^2}$$

$$= \sqrt{\left[K_b(\mathbf{k}) + V_{\text{tr}}(\mathbf{r}) - \mu + 2 U_{0b} n_c(\mathbf{r}) + 2 \sum_{b'} U_{bb'} \tilde{n}_{b'}(\mathbf{r}) \right]^2 - [U_{0b} n_c(\mathbf{r})]^2}. \tag{3.42}$$

From $v_b^*(\mathbf{k}, \mathbf{r}) \times (3.40) - u_b(\mathbf{k}, \mathbf{r}) \times (3.41)^*$, choosing u_b and v_b to satisfy the normalisation condition $|u_b(\mathbf{k}, \mathbf{r})|^2 - |v_b(\mathbf{k}, \mathbf{r})|^2 = 1$ (as in [56] for the no lattice case):

$$u_b(\mathbf{k}, \mathbf{r}) v_b^*(\mathbf{k}, \mathbf{r}) = -\frac{U_{0b} z^2(\mathbf{r})}{2 E_b(\mathbf{k}, \mathbf{r})}. \tag{3.43}$$

Substituting this into $u_b(\mathbf{k}, \mathbf{r}) \times (3.41)^*$ and $v_b^*(\mathbf{k}, \mathbf{r}) \times (3.40)$, we have:

$$|u_b(\mathbf{k}, \mathbf{r})|^2 = \frac{\mathcal{L}_b(\mathbf{k}, \mathbf{r}) + E_b(\mathbf{k}, \mathbf{r})}{2 E_b(\mathbf{k}, \mathbf{r})}$$

$$= \frac{K_b(\mathbf{k}) + V_{\text{tr}}(\mathbf{r}) - \mu + 2 U_{0b} n_c(\mathbf{r}) + 2 \sum_{b'} U_{bb'} \tilde{n}_{b'}(\mathbf{r}) + E_b(\mathbf{k}, \mathbf{r})}{2 E_b(\mathbf{k}, \mathbf{r})}, \tag{3.44}$$

$$|v_b(\mathbf{k}, \mathbf{r})|^2 = \frac{\mathcal{L}_b(\mathbf{k}, \mathbf{r}) - E_b(\mathbf{k}, \mathbf{r})}{2 E_b(\mathbf{k}, \mathbf{r})}$$

$$= \frac{K_b(\mathbf{k}) + V_{\text{tr}}(\mathbf{r}) - \mu + 2 U_{0b} n_c(\mathbf{r}) + 2 \sum_{b'} U_{bb'} \tilde{n}_{b'}(\mathbf{r}) - E_b(\mathbf{k}, \mathbf{r})}{2 E_b(\mathbf{k}, \mathbf{r})}. \tag{3.45}$$

Setting $v_b(\mathbf{k}, \mathbf{r}) = 0$, we find $|u_b(\mathbf{k}, \mathbf{r})|^2 = 1$ and $E_b(\mathbf{k}, \mathbf{r}) = \mathcal{L}_b(\mathbf{k}, \mathbf{r})$, yielding the Hartree-Fock solution (3.20).

It has been stated that the Thomas-Fermi approximation is consistent with the LDA:

Where the local-density approximation is used for the whole excitation spectrum, not only the high-lying part, then it is necessary for consistency to treat also the condensate in the corresponding approximation, which is the finite-temperature Thomas-Fermi approximation. [102]

We use the Thomas-Fermi solution for all of our interacting calculations, which we restate using the envelope functions, starting from (3.18) to find:

$$n_c(\mathbf{r}) = \frac{1}{U_{00}} \max \left[0, \mu - V_{\mathrm{tr}}(\mathbf{r}) - 2 \sum_b U_{0b} \tilde{n}_b(\mathbf{r}) \right]. \tag{3.46}$$

For the non-condensate, using (3.31) and the envelope functions we have:

$$\tilde{n}_b(\mathbf{r}) \approx \left(\frac{a}{2\pi} \right)^d \int_{\mathrm{BZ}} d\mathbf{k} \left\{ \left[|u_b(\mathbf{k}, \mathbf{r})|^2 + |v_b(\mathbf{k}, \mathbf{r})|^2 \right] \bar{n}_{\mathrm{BE}}[E_b(\mathbf{k}, \mathbf{r})] + |v_b(\mathbf{k}, \mathbf{r})|^2 \right\}. \tag{3.47}$$

3.7 Summary

We have used the usual broken symmetry approach to separate the mean-field condensate from the non-condensate. We have used a mean-field approach to simplify the extended Bose-Hubbard Hamiltonian to quadratic form with the Popov approximation to the Hartree-Fock-Bogoliubov method. We have expressed the resulting Hamiltonian in LDA form and introduced envelope functions to exploit the trap symmetry. Finally, we have diagonalised the quadratic Hamiltonian in the LDA to find the Bogoliubov energy spectrum.

Chapter 4

Density of states

The density of states of an optical lattice is an essential tool which we will use throughout the rest of this thesis. In this chapter we first introduce the density of states, which we will calculate using the method of section 5.2 for use in our numerical results in chapter 6. We then show typical examples of the density of states, so that we can judge the appropriateness of the approximations we will make in chapter 7. We do this separately for one, two and three-dimensional optical lattices. Then we demonstrate the significance of allowing for beyond nearest-neighbour hopping which we introduced in section 2.5 and considered in section 2.8.1. We develop new results on the approximate structure of the combined harmonic density of states. Finally we compare the density of states from LDA to the full diagonalisation of the non-interacting problem. This will be an important piece of evidence of the validity of the approximations that we described in section 3.6.

4.1   Definition

By 'density of states', we refer to the per-volume density of states for the non-interacting, translationally-invariant[1] lattice which we define as [103]:

$$g_b(K) \equiv \frac{1}{(2\pi)^d} \int_{\mathrm{BZ}} \mathrm{d}\mathbf{k}\, \delta[K - K_b(\mathbf{k})], \tag{4.1}$$

where we take $K_b(\mathbf{k})$ from its definition (3.34). When an integrand depends on $\mathbf{k}$ only through $K_b(\mathbf{k})$ we can change variables to $K = K_b(\mathbf{k})$ since we then have, for any

---

[1]We consider the combined harmonic lattice density of states only in section 4.6.

function $Q_b[K_b(\mathbf{k}), \mathbf{r}]$:

$$\int_{-\infty}^{\infty} dK\, g_b(K) Q_b(K, \mathbf{r}) = \frac{1}{(2\pi)^d} \int_{-\infty}^{\infty} dK \int_{\mathrm{BZ}} d\mathbf{k}\, \delta[K - K_b(\mathbf{k})] Q_b(K, \mathbf{r})$$

$$= \frac{1}{(2\pi)^d} \int_{\mathrm{BZ}} d\mathbf{k}\, Q_b[K_b(\mathbf{k}), \mathbf{r}]. \tag{4.2}$$

Applying this to (3.47):

$$\tilde{n}_b(\mathbf{r}) = a^d \int_{-\infty}^{\infty} dK\, g_b(K) \left\{ \left[|u_b(K, \mathbf{r})|^2 + |v_b(K, \mathbf{r})|^2 \right] \bar{n}_{\mathrm{BE}}[E_b(K, \mathbf{r})] + |v_b(K, \mathbf{r})|^2 \right\}. \tag{4.3}$$

We emphasise that this is making no additional approximation: the approximations of section 3.6 allow us to use the density of states. In the Hartree-Fock approximation, or above the critical temperature:

$$\tilde{n}_b(\mathbf{r}) = a^d \int_{-\infty}^{\infty} dK\, g_b(K) \bar{n}_{\mathrm{BE}}[E_b(K, \mathbf{r})]. \tag{4.4}$$

4.2 Translationally-invariant lattice

To calculate the density of states, we first need the energy dispersion, $K_b(\mathbf{k})$. We note that the potential (2.1) is separable, so that the solution of (3.34) has Bloch wavefunction (appendix C) $\psi_{b_x, \mathbf{k}}(\mathbf{r}) = \prod_j \psi_{b_j, k_j}(j)$ and energy $K_b(\mathbf{k}) = \sum_j K_{b_j}(k_j)$ with, for the x direction, for example:

$$-\frac{\hbar^2}{2m} \frac{d^2 \psi_{b_x, k_x}(x)}{dx^2} + V_x \sin^2\left(\frac{\pi x}{a_x}\right) \psi_{b_x, k_x}(x) = K_{b_x}(k_x) \psi_{b_x, k_x}(x), \tag{4.5}$$

which is the well-studied Mathieu's equation [104–106].[2] We show the energies of the lowest three bands in figure 4.1, for $V_x = 2E_{R,x}$ and $V_x = 15E_{R,x}$.

[2]On converting (4.5) to the standard Mathieu form, the amplitude is $-V_x/4E_{R,x}$ (often labelled q) and the 'characteristic value' (energy eigenvalue, often labelled a) is $[K_{b_x}(k_x) - \frac{1}{2}V_x]/E_{R,x}$.
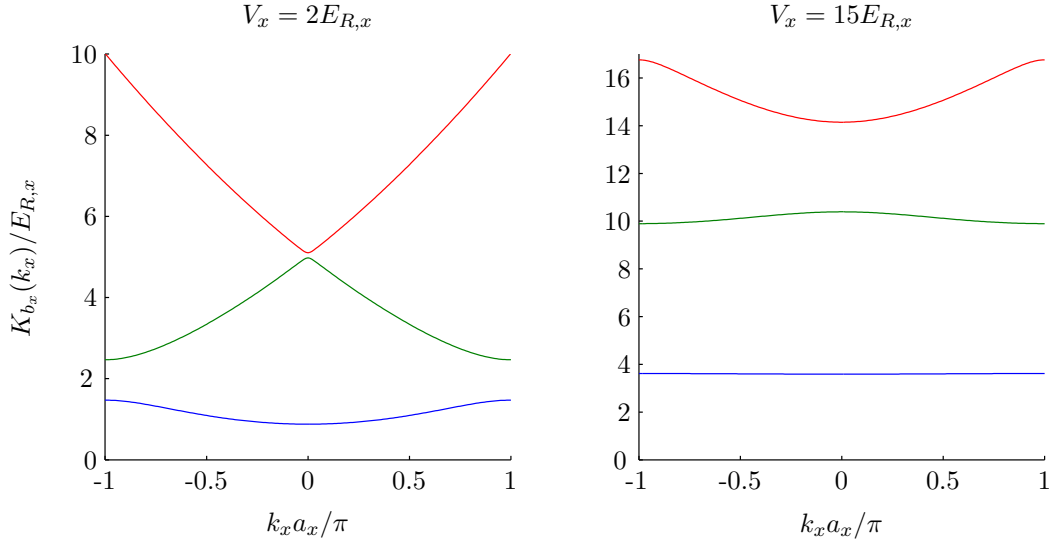
Figure 4.1: Energy dispersion relation in one dimension for the first three bands

For the cubic lattice in three dimensions, we show the minimum and maximum energies of the lowest energy bands as a function of the lattice depth in figure 4.2.
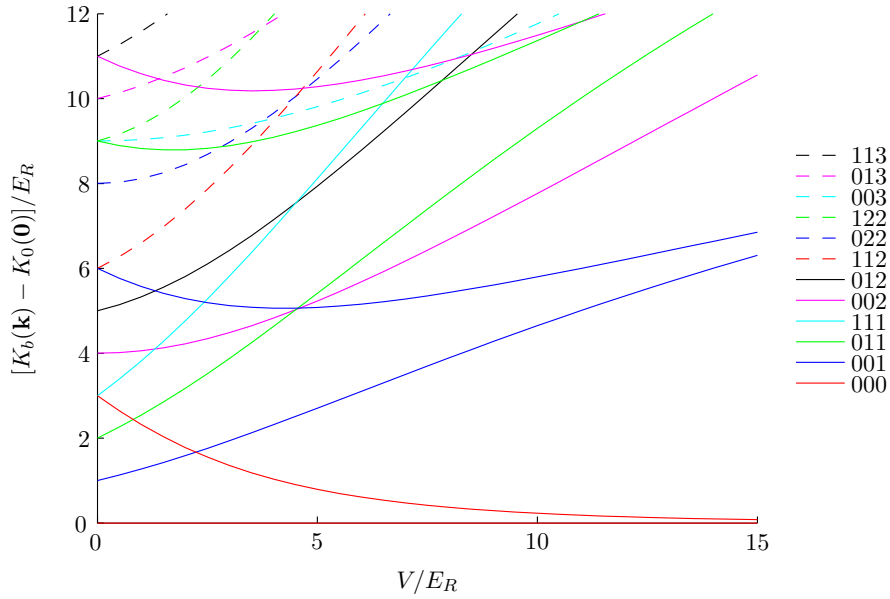
Figure 4.2: Minimum and maximum energies of the lowest energy bands for the three-dimensional cubic lattice. The integers in the legend specify the components b_x, b_y, b_z of the band b.

We numerically calculate the density of states, as will be discussed in section 5.2, and

show the results in figure 4.3.
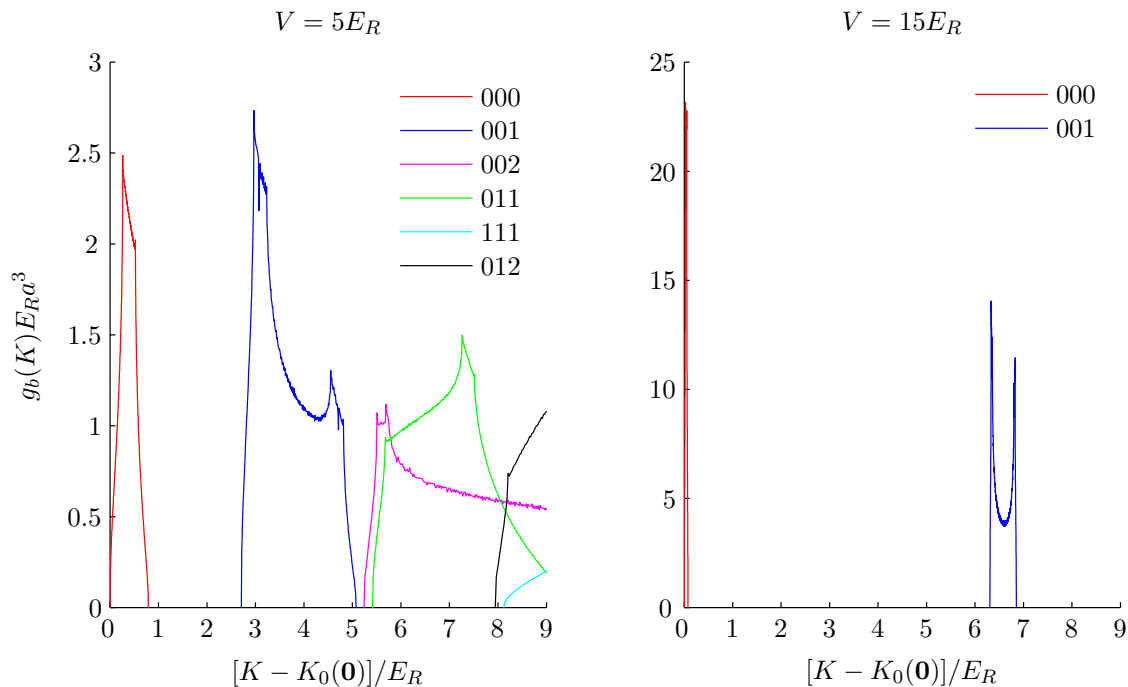
Figure 4.3: Density of states for the three-dimensional cubic lattice

4.3 Tight binding

From (D.20), the dispersion can be written as a Fourier cosine series, with the hopping matrix elements as coefficients:

$$K_b(\mathbf{k}) = -\sum_j \left[J_{b_j,j}^0 + 2 \sum_{l>0} J_{b_j,j}^l \cos(l k_j a_j) \right]. \tag{4.6}$$

In the tight-binding limit,[3] beyond nearest-neighbour hopping is ignored.[4] In one dimension the density of states is then, from (4.1):[5]

$$g_b(K) = \frac{1}{2\pi a \left| J_{b,x}^1 \right| \sqrt{1 - \left[(K + J_{b,x}^0)/2 J_{b,x}^1 \right]^2}}, \tag{4.7}$$

---

[3]We show some results in this section for general bands, but the tight-binding limit generally refers to the ground band. For excited bands we note that $J_{b,x}^1$ is positive for even b and negative for odd b. The validity of the tight-binding limit must be checked for each band, since highly excited bands are closer to the free-particle density of states as discussed in section 4.5.

[4]For the importance of beyond nearest-neighbour hopping, see also sections 2.8.1, 6.2 and figure D.1.

[5]Using the substitution $u = -\cos(ka)$, $\mathrm{d}u = a\sqrt{1 - u^2}\,\mathrm{d}k$.

44

which has infinite Van Hove singularities at the maximum and minimum energies of the band $K = -J^0_{b,x} \pm 2J^1_{b,x}$, which can also be seen from the zero derivative in 4.6. The density of states (4.7) is shown in figure 4.4.
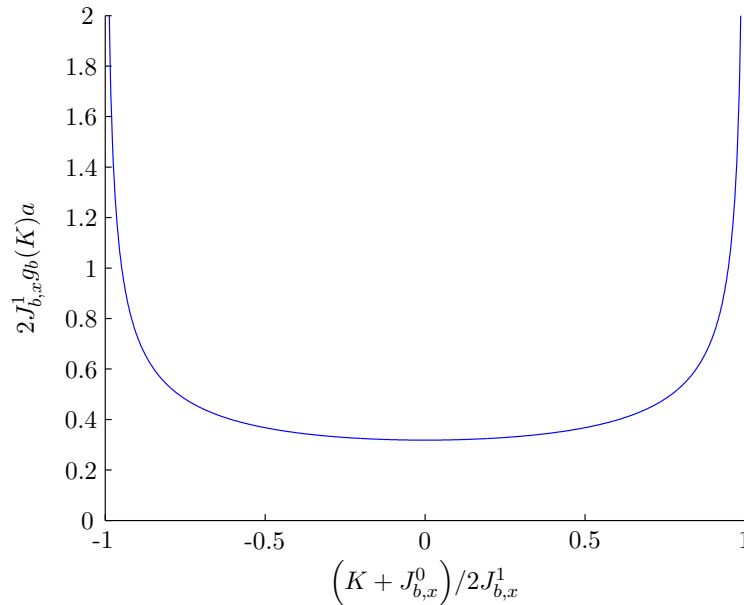
Figure 4.4: Tight-binding density of states in one dimension

In two dimensions, the cubic-lattice density of states[6] is shown in figure 4.5. There is an infinite Van Hove singularity at $K = -2J^0_{b,j}$ and non-zero density at the band edges.
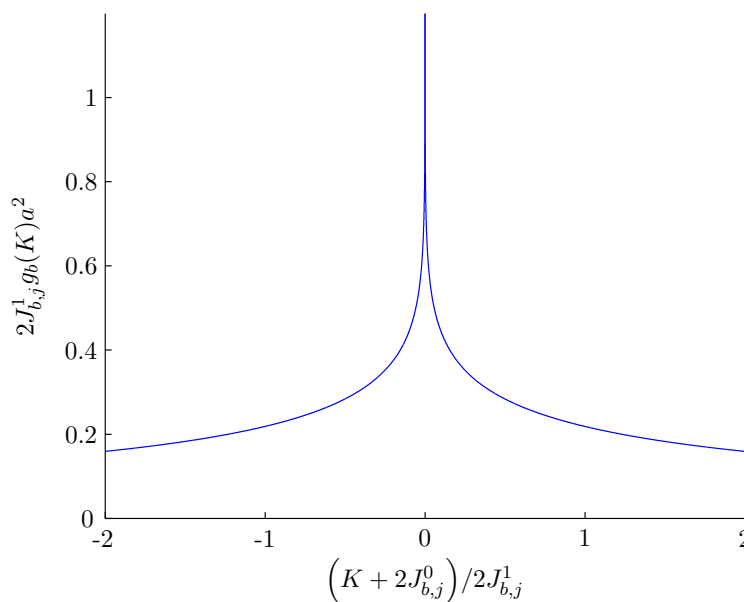
Figure 4.5: Isotropic tight-binding density of states in two dimensions

---

[6]By convolution we can express it as a complete elliptic integral of the first kind.

In three dimensions, the case of primary interest in this work, we compare the tight-binding density of states to the actual density of states in figure 4.6 for the cubic-lattice ground band. For $V \gtrsim 5E_R$, the effect of beyond nearest-neighbours is much reduced, except for very low energies, for which the effective-mass approach of the next section may be more appropriate.
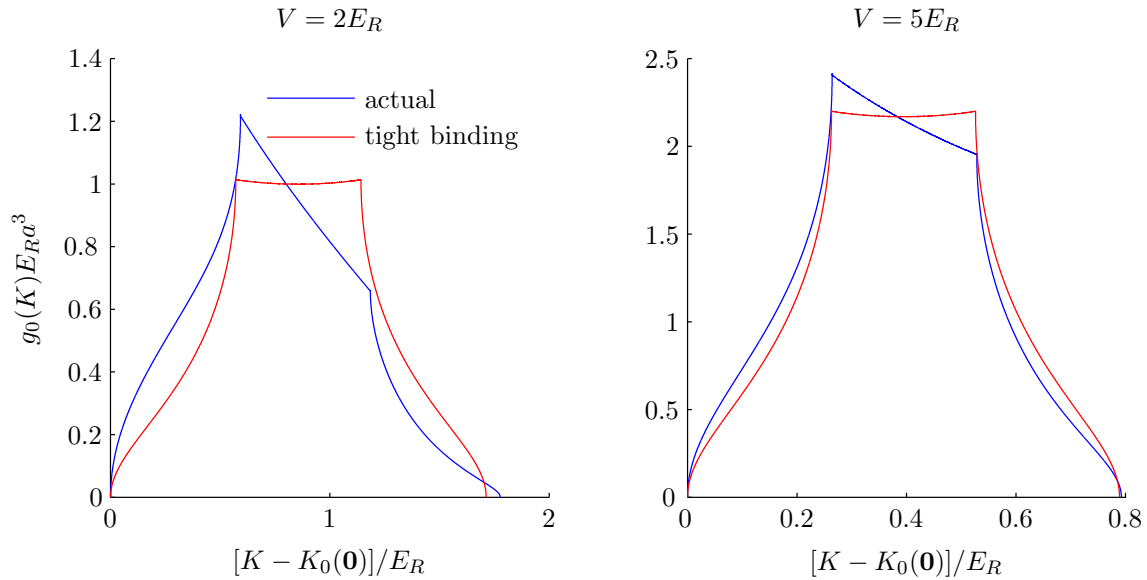
Figure 4.6: Isotropic ground-band density of states in three dimensions

4.4 Effective mass

Near any point, $\mathbf{k}_0$, in the dispersion where we have $\nabla K_b(\mathbf{k}_0) = \mathbf{0}$, the Taylor series about that point gives:

$$K_b(\mathbf{k}) \approx K_b(\mathbf{k}_0) + \hbar^2 \sum_j \frac{(k_j - k_{0,j})^2}{2m_j^*}, \tag{4.8}$$

where the effective mass at $\mathbf{k}_0$ in direction j, m_j^*, is defined by [103] (the off-diagonal terms are zero since the potential is separable) as discussed in appendix H:

$$\frac{1}{m_j^*} = \frac{1}{\hbar^2} \left[\frac{\partial^2 K_b(\mathbf{k})}{\partial k_j^2} \right]_{\mathbf{k}=\mathbf{k}_0}, \tag{4.9}$$

so that for a free particle, $m_j^* = m$. From the full form of (4.6), we see that $\nabla K_b(\mathbf{k}_0) = \mathbf{0}$ whenever $k_j = 0$ or $k_j = \pi/a_j$ for all j. From figure 4.1 we can see that, for excited bands in shallow lattices, there is only a small region around $\mathbf{k}_0$ for which this is a good approximation.

46

At the minimum energy of a band, $K_b^{\min} = K_b(\mathbf{k}_0)$, if due to the second derivative test we have $m_j^* > 0$ for all j from (4.9), and we assume that the effective mass applies for all K in some region near $K_b^{\min}$, then for that region of K, from (4.1) and (4.8):

$$g_b(K) = \frac{1}{\Gamma(d/2)(2\pi)^{d/2}\,(\hbar^2/m^*)^{d/2}} \max\left(K - K_b^{\min}, 0\right)^{d/2-1},\qquad (4.10)$$

where $m^* = \left(\prod_j m_j^*\right)^{1/d}$. This shows that the van Hove singularities at the minimum energy are qualitatively the same for the effective-mass assumption as for the tight-binding assumption: infinite in one dimension, a finite jump in two dimensions and an infinite derivative in three dimensions.

4.5 High energies

For high energies, $K \gg \sum_j V_j$, the most significant effect of the lattice on the density of states is the spatially averaged energy of the lattice potential, $\frac{1}{2}\sum_j V_j$ as shown in figure 4.7.
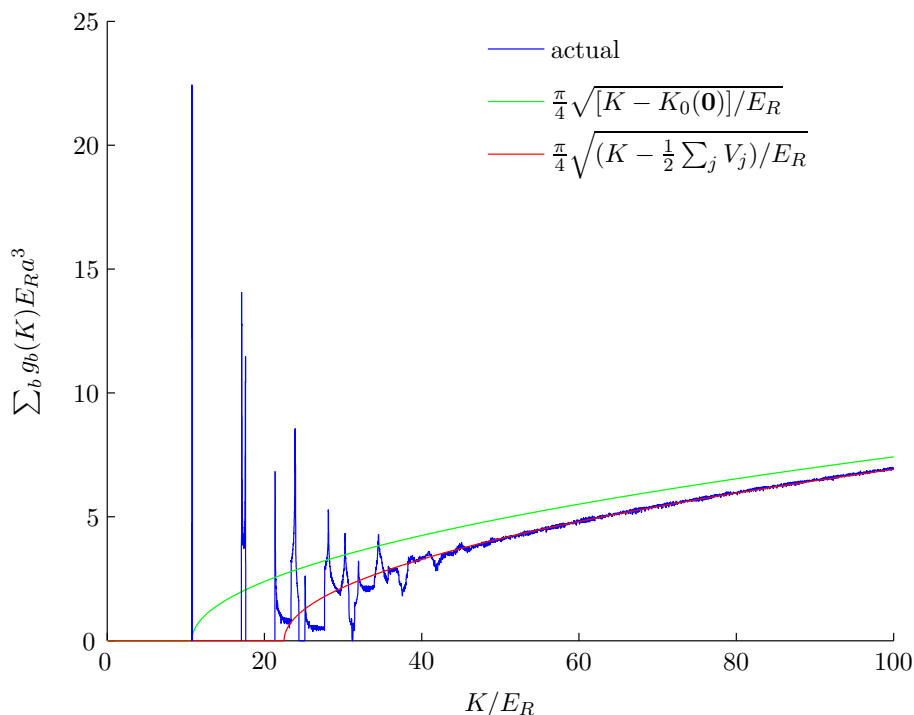
Figure 4.7: Isotropic density of states in three dimensions for $V = 15E_R$. The analytic expressions are the free-particle density of states shifted by the minimum energy eigenvalue and the spatially averaged energy of the lattice.

4.6 Combined harmonic lattice

In this section, we calculate the density of states for the combined harmonic trap and optical lattice potential.[7] We use the LDA density of states only in this section and only for checking against the full diagonalisation.

For the harmonically trapped case, in the non-interacting LDA, when we wish to calculate some function, $Q[K_b(\mathbf{k}) + V_{\mathrm{tr}}(\mathbf{r})]$ of the energy, such as the total thermal number from (3.37), we have:

$$\frac{1}{(2\pi)^d} \sum_b \int d\mathbf{r} \int d\mathbf{k}\, Q[K_b(\mathbf{k}) + V_{\mathrm{tr}}(\mathbf{r})] = \int dE\, Q(E)\, g_{\mathrm{LDA}}(E), \qquad (4.11)$$

from (4.2) where $g_{\mathrm{LDA}}(E)$ is given by the convolution:

$$g_{\mathrm{LDA}}(E) \equiv \frac{1}{(2\pi)^d} \sum_b \int d\mathbf{r} \int_{\mathrm{BZ}} d\mathbf{k}\, \delta[E - K_b(\mathbf{k}) - V_{\mathrm{tr}}(\mathbf{r})]$$

$$= \sum_b \int_0^E dV_{\mathrm{tr}}\, g_{\mathrm{trap}}(V_{\mathrm{tr}}) g_b(E - V_{\mathrm{tr}}), \qquad (4.12)$$

and we define and calculate the harmonic trap density of states as:

$$g_{\mathrm{trap}}(V_{\mathrm{tr}}) \equiv \int d\mathbf{r}\, \delta[V_{\mathrm{tr}} - V_{\mathrm{tr}}(\mathbf{r})] = \frac{(2\pi)^{d/2}}{\Gamma(d/2)\,(m\omega^2)^{d/2}} V_{\mathrm{tr}}^{d/2-1}. \qquad (4.13)$$

4.6.1 Expected structure

Since the combined density of states, $g_{\mathrm{LDA}}(E)$, has a rich structure, we consider what we expect at various energies. In a region where the effective-mass approximation, (4.10), applies, the contribution to $g_{\mathrm{LDA}}(E)$ from band b is:

$$\frac{1}{[\Gamma(d/2)]^2(\hbar\omega)^d} \left(\frac{m^*}{m}\right)^{d/2} \int_0^{E-K_b^{\min}} dV\, [V(E - V_{\mathrm{tr}} - K_b^{\min})]^{d/2-1}$$

$$= \frac{1}{(d-1)!(\hbar\omega^*)^d} \left(E - K_b^{\min}\right)^{d-1}, \qquad (4.14)$$

where the effective trap frequencies are defined by:

$$\omega_j^* \equiv \sqrt{\frac{m}{m_j^*}}\,\omega_j, \qquad (4.15)$$

---

[7]Some features of the combined harmonic lattice density of states in the one-dimensional tight-binding case (and the two-dimensional case, numerically) are discussed in [107].

as in [84] and $\omega^* = \left(\prod_j \omega_j^*\right)^{1/d}$. We therefore expect the initial contribution from each band (just after $K_b^{\min}$) to the combined density of states to scale like a harmonically-trapped particle, with power $d-1$.

If we assume that the bands are rectangular with width W_b and minimum energy $K_b^{\min}$, so that $g_b(K) = 1/W_b a^d$ for $K_b^{\min} < K < K_b^{\min} + W_b$ and $g_b(K) = 0$ otherwise, then from (4.12) and (4.13):

$$g_{\text{LDA}}(E) = \frac{2(2\pi)^{d/2}}{d\Gamma(d/2)\left(m\omega^2 a^2\right)^{d/2}} \sum_b \frac{\max\left(E - K_b^{\min}, 0\right)^{d/2} - \max\left(E - K_b^{\min} - W_b, 0\right)^{d/2}}{W_b}$$

(4.16)

$$\approx \frac{(2\pi)^{d/2}}{\Gamma(d/2)\left(m\omega^2 a^2\right)^{d/2}} \sum_b \left(E - K_b^{\min} - \frac{W_b}{2}\right)^{d/2-1}$$

$$= \frac{1}{a^d} \sum_b g_{\text{trap}}\left(E - K_b^{\min} - \frac{W_b}{2}\right),$$

(4.17)

for $E \gg K_b^{\min} + W_b$. So, we expect the eventual contribution of the band (far after $K_b^{\min} + W_b$) to the combined density of states to scale like the trap, with power $d/2-1$. The high-energy contribution is therefore like the density of states for a particle in a harmonic trap with no kinetic energy, we call this the 'trap-only' region.

For energies beyond the effective-mass region, but with $K_b^{\min} < E < K_b^{\min} + W_b$, the combined density of states depends on the detailed structure of the band $g_b(K)$ with an approximation given by (4.16).[8]

So, the initial contribution from the band is effective-mass like and the high-energy contribution from the band is trap-only like. We estimate the crossover point between these two regimes by equating the single-band contribution from equations (4.14) and (4.17). In three dimensions,[9] there is no intersection for the first excited bands for $V \gtrsim 5E_R$ and, for the ground band:

$$E_{\text{cross}} = K_0^{\min} + \frac{W_0}{2} + \frac{1}{128\pi^2}\left(\frac{m^* a^2}{\hbar^2}\right)^3 \left(E_{\text{cross}} - K_0^{\min}\right)^4. \tag{4.20}$$

---

[8]For $K_b^{\min} < E < K_b^{\min} + W_b$ the rectangular assumption implies that the contribution to $g_{\text{LDA}}(E)$ from band b is proportional to $(E - K_b^{\min})^{d/2}$. For three dimensions, this is a blend between the effective-mass (power $d-1$) behaviour near the start of the band and the trap-only (power $d/2-1$) behaviour far after the band. For lower dimensions, the rectangular assumption is poor from figures 4.4 and 4.5.

[9]In one and two dimensions, one of the approximations (4.14) and (4.17) is constant so the solution

Figure 4.8: Isotropic LDA density of states in three dimensions

Using the tight-binding approximations $W_b = 4 \sum_j \left| J^1_{b_j,j} \right|$ (D.21) and $m^*_j = \hbar^2 / \left(2 J^1_{b,j} a^2_j \right)$ (H.4) for the cubic lattice and assuming that the cross over is near the middle of the band $E_{\text{cross}} - K^{\min}_0 \approx W_0/2$ (which seems reasonable from (4.21) and is confirmed in

is simple (although the approximation is poor as discussed in footnote 8):

$$E^{d=1}_{\text{cross}} - K^{\min}_b = \frac{W_b}{2} + \frac{2\hbar^2}{m^* a^2} \approx \frac{3W_b}{2}, \tag{4.18}$$

$$E^{d=2}_{\text{cross}} - K^{\min}_b = \hbar\sqrt{\frac{2\pi}{m^* a^2}} \approx \sqrt{\frac{\pi W_0}{2}}, \tag{4.19}$$

where the last form in each case uses the tight-binding approximation given for three dimensions and, for two dimensions is valid only for the square-lattice ground band.

figure 4.8):

$$E_{\text{cross}} \approx K_0^{\text{min}} + \left(\frac{1}{2} + \frac{27}{256\pi^2} \right) W_0 \approx K_0^{\text{min}} + 0.51\, W_0, \tag{4.21}$$

which has the same scaling, but is slightly lower than $E_{\text{cross}} \approx 0.86\, W_0$, given in [62].

The actual LDA density of states is compared to the expressions (4.14), (4.16), (4.17) and (4.21) in figure 4.8 for the cubic lattice in three dimensions.

For high energies, once there have been many bands, we consider the assumption that the bands start at the free-particle positions, adjusted by the average energy of the lattice (as in section 4.5), $K_b^{\text{min}} = \sum_j \left(\frac{1}{2} V_j + \hbar^2 \pi^2 b_j^2 / 2m a_j^2 \right)$. We keep the other assumptions leading to (4.17) and approximate the sum in (4.17) by an integral over the region of bands b such that $0 < K_b^{\text{min}} < E$, then we recover the density of states for a trap with no lattice ((4.14) with $m = m^*$). Evaluating this integral in band space, we find:

$$g_{\text{LDA}}(E) = \frac{1}{(d-1)!(\hbar\omega)^d} \left(E - \frac{1}{2} \sum_j V_j \right)^{d-1}, \tag{4.22}$$

so, the eventual contribution of all bands has power $d-1$, like the density of states of a harmonically-trapped particle.

4.6.2 Comparative results

We compare the full diagonalisation to the LDA density of states in figure 4.9. For the low energy LDA results, we also show the contribution from the ground band. For the low energy plots (the left subplots of figure 4.9), we show up to the start of the second excited band. We plot the product $g_{\text{LDA}}(E)\omega^d$, since, for the LDA case, $g_{\text{LDA}}(E)\omega^d$ is independent of ω from (4.13). For the full diagonalisation, we can see no dependence of the full density of states multiplied by ω^3 for varying ω apart from granularity due to the few discrete energies for large ω at low energy.

The LDA results show excellent agreement with the full diagonalisation. We note that the approximation (4.22) becomes valid in the $V = 15 E_R$ case beyond the region of this plot. The effective-mass region is not visible on the plot for $V = 15 E_R$ due to the scale.
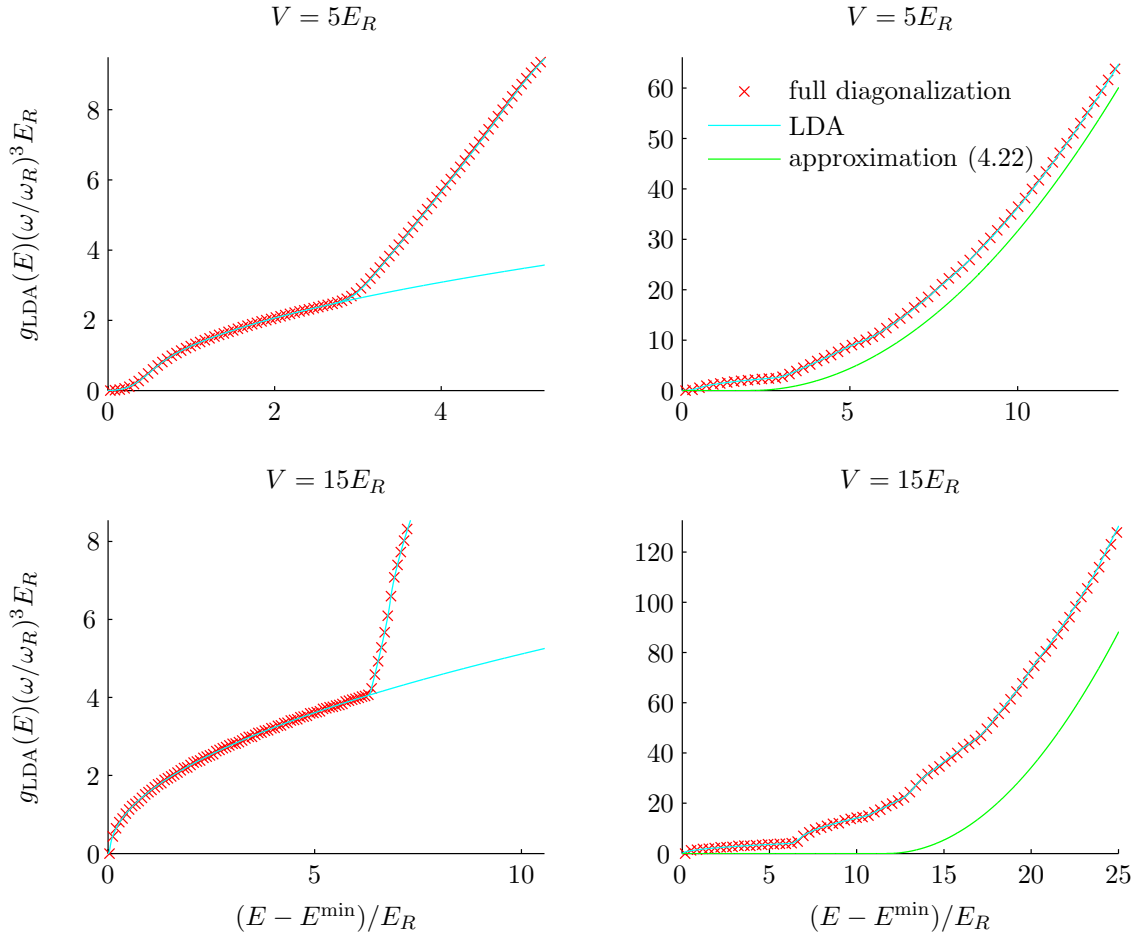
Figure 4.9: Combined harmonic cubic-lattice density of states in three dimensions. The left subplots show region from the ground to the first excited bands and the right subplots show many bands. The LDA is so good that it is obscured by the full diagonalization results in all cases. For the left subplots, we also show the LDA ground band results for reference. We show the high energy approximation (4.22) only on the right subplots.

4.7 Summary

We have simplified the calculation of thermal results through the use of the density of states. We have shown numerical results for the density of states and considered the tight-binding, effective-mass and high-energy limits. We have explained the structure of the combined density of states, and shown that the full diagonalisation has excellent agreement with the LDA.

Chapter 5

Numerical implementation

In this chapter, we outline the numerical implementation of our finite-temperature formalism described in section 3.6.

5.1 Translationally-invariant energies

We use the translationally-invariant energies from the non-interacting Bloch solutions to find the density of states, which we use for the full numerical calculation. To do this, we use the Fourier series [103] of the Bloch wavefunction:

$$\psi_{b,\mathbf{k}} = \sum_{\mathbf{K}} c_{b,\mathbf{k}-\mathbf{K}} \, e^{\mathrm{i}(\mathbf{k}-\mathbf{K})\cdot\mathbf{r}}, \tag{5.1}$$

for $\mathbf{K}$ on the reciprocal lattice[1] to restate Schrödinger's equation (4.5) as the recurrence relation:

$$\left[\frac{\hbar^2}{2m}(k_x - K_x)^2 - K_{b_x}(k_x) + \frac{V_x}{2} \right] c_{b,k_x-K_x} - \frac{V_x}{4} \left(c_{b,k_x-K_x+2\pi/a} + c_{b,k_x-K_x-2\pi/a} \right) = 0. \tag{5.2}$$

We form a tri-diagonal matrix[2] with super-diagonal and sub-diagonal terms all equal to $-V_x/4E_{R,x}$ and diagonal entries equal to $\ldots, (\bar{k}_x - 4)^2, (\bar{k}_x - 2)^2, \bar{k}_x^2, (\bar{k}_x + 2)^2, (\bar{k}_x + 4)^2, \ldots$ where $\bar{k}_x = k_x a_x / \pi$ so that $-1 \leq \bar{k}_x < 1$. The eigenvalues of this matrix are then $[K_{b_x}(k_x) - \frac{1}{2}V_x]/E_{R,x}$ and the eigenvectors give the Fourier coefficients of the

---

[1]That is, $\mathbf{K}$ has elements which are integer multiples of $2\pi/a_j$.

[2]The tri-diagonal nature of this matrix is not, of course, a nearest-neighbour only assumption. We are in quasi-momentum space, and the matrix is tri-diagonal because the lattice potential is sinusoidal.

corresponding wavefunctions. The (algebraically) smallest eigenvalue is from the ground band, the second smallest is from the first excited band, etc. The more bands that are required, the more terms that need to be retained in the matrix before truncating.

5.2 Translationally-invariant density of states

From (4.1), using the rectangular Dirac delta sequence [103, 108] with an energy spacing ΔK, for each band:

$$g_b(K) = \frac{1}{(2\pi)^d} \lim_{\Delta K \to 0} \frac{1}{\Delta K} \int_{\text{BZ}} d\mathbf{k} \begin{cases} 1 & \text{if } |K - K_b(\mathbf{k})| < \frac{1}{2}\Delta K, \\ 0 & \text{otherwise,} \end{cases} \tag{5.3}$$

$$\approx \frac{1}{(2\pi)^d} \frac{\prod_{j=1}^d \Delta k_j}{\Delta K} \sum_{\mathbf{k} \in \text{BZ}} \begin{cases} 1 & \text{if } |K - K_b(\mathbf{k})| < \frac{1}{2}\Delta K, \\ 0 & \text{otherwise,} \end{cases} \tag{5.4}$$

for small $\Delta k_j, \Delta K$. We actually calculate the one-dimensional density of states ($d = 1$ in (5.4)) and get the higher-dimensional results with the convolutions $g_{b_x b_y}(K) = \int du\, g_{b_x}(K - u)g_{b_y}(u)$ and $g_b(K) = \int du\, g_{b_x b_y}(K - u)g_{b_z}(u)$.

5.3 Trap units

From (3.46) and (3.47), $\tilde{n}_b(\mathbf{r})$ and $n_c(\mathbf{r})$ depend on $\mathbf{r}$ only through $V_{\text{tr}}(\mathbf{r}) = \frac{1}{2}m(\omega_x^2 x^2 + \omega_y^2 y^2 + \omega_z^2 z^2)$, so we define the scaled co-ordinates $\bar{x} = x\omega_x/\omega, \bar{y} = y\omega_y/\omega, \bar{z} = z\omega_z/\omega, \bar{r}^2 = \bar{x}^2 + \bar{y}^2 + \bar{z}^2$ so that $V_{\text{tr}}(\bar{r}) = \frac{1}{2}m\omega^2\bar{r}^2$ and $d\bar{x}d\bar{y}d\bar{z} = dxdydz$. Our formulae then become:

$$n_c(\bar{r}) = \frac{1}{U_{00}} \max\left[0, \mu - V_{\text{tr}}(\bar{r}) - 2\sum_b U_{0b}\tilde{n}_b(\bar{r})\right], \tag{5.5}$$

$$\mathcal{L}_b(K, \bar{r}) = K + V_{\text{tr}}(\bar{r}) - \mu + 2U_{0b}n_c(\bar{r}) + 2\sum_{b'} U_{bb'}\tilde{n}_{b'}(\bar{r}), \tag{5.6}$$

$$E_b(K, \bar{r}) = \sqrt{\mathcal{L}_b^2(K, \bar{r}) - [U_{0b}n_c(\bar{r})]^2}, \tag{5.7}$$

$$\tilde{n}_b(\bar{r}) = a^d \int_{-\infty}^{\infty} dK\, g_b(K) \left\{ \frac{\mathcal{L}_b(K, \bar{r})}{E_b(K, \bar{r})} \bar{n}_{\text{BE}}[E_b(K, \bar{r})] + \frac{\mathcal{L}_b(K, \bar{r}) - E_b(K, \bar{r})}{2E_b(K, \bar{r})} \right\}. \tag{5.8}$$

We can then calculate the total number using:

$$N_c = \frac{2\pi^{d/2}}{\Gamma(d/2)a^d} \int_0^\infty d\bar{r}\, \bar{r}^{d-1} n_c(\bar{r}), \tag{5.9}$$

$$\tilde{N}_b = \frac{2\pi^{d/2}}{\Gamma(d/2)a^d} \int_0^\infty d\bar{r}\, \bar{r}^{d-1} \tilde{n}_b(\bar{r}), \tag{5.10}$$

which is now a problem in the two dimensions K and $\bar{r}$.

5.4 Interaction parameters

We calculate the one-dimensional Wannier functions from (D.22) and use their separability (D.11) to get the on-site interaction as:

$$U_{bb'} = g \int d\mathbf{r}\, |w_b(\mathbf{r})w_{b'}(\mathbf{r})|^2 = g \prod_{j=1}^d \int dr_j \left| w_{b_j}(r_j)w_{b'_j}(r_j) \right|^2. \tag{5.11}$$

For the non-condensate off-site interaction, discussed in appendix F, we calculate:

$$\begin{aligned}
U'_{bb'} &= g \sum_i \int d\mathbf{r}\, |w_b(\mathbf{r})w_{b'}(\mathbf{r} - \mathbf{R}_i)|^2 \\
&= g \prod_{j=1}^d \sum_{i=0}^\infty \int dr_j \left| w_{b_j}(r_j)w_{b'_j}(r_j - R_{i,j}) \right|^2,
\end{aligned} \tag{5.12}$$

where we need many sites, $\mathbf{R}_i$, to reproduce the $V = 0$ results given in appendix F.

For the cubic lattice in three dimensions, the densities of the three bands $001, 010$ and 100 must be equal, that is, $\tilde{n}_{001}(\bar{r}) = \tilde{n}_{010}(\bar{r}) = \tilde{n}_{100}(\bar{r})$. Thus we can use this symmetry to simplify our calculation of higher bands. For a given one of these bands, $\frac{1}{3}$ of the atomic population is in the same band and $\frac{2}{3}$ is in one of the other first excited bands so that:

$$\begin{aligned}
&U_{001,001}\tilde{n}_{001}(\bar{r}) + U_{001,010}\tilde{n}_{010}(\bar{r}) + U_{001,100}\tilde{n}_{100}(\bar{r}) \\
&= (U_{001,001} + 2U_{001,010}) \frac{\tilde{n}_{001}(\bar{r}) + \tilde{n}_{010}(\bar{r}) + \tilde{n}_{100}(\bar{r})}{3},
\end{aligned} \tag{5.13}$$

since $U_{001,010} = U_{001,100}$. We therefore treat the three excited bands together and use $(U_{001,001} + 2U_{001,010})/3$ for their self-interaction parameter.

5.5 Thomas-Fermi simplification

We use a Thomas-Fermi approximation for the condensate for all our interacting calculations, as discussed in section 3.6. From (3.42), if $n_c(\bar{r})$ is zero (e.g. above T_c or outside the Thomas-Fermi radius), we have the Hartree-Fock result. Otherwise, adding $n_c(\bar{r})$ to both sides of (5.5) and rearranging:

$$V_{\text{tr}}(\bar{r}) - \mu + 2U_{00}n_c(\bar{r}) + 2\sum_b U_{0b}\tilde{n}_b(\bar{r}) = U_{00}n_c(\bar{r}), \tag{5.14}$$

so, for the ground band, from (5.6):

$$\mathcal{L}_0(K,\bar{r}) = K + U_{00}n_c(\bar{r}), \tag{5.15}$$

$$E_0(K,\bar{r}) = \sqrt{K^2 + 2KU_{00}n_c(\bar{r})}, \tag{5.16}$$

which is a useful simplification, and is automatically self-consistent with $n_c(\bar{r})$.

To compare to the LDA work of [58], we rearrange the equation for the non-condensate density calculated:

$$\tilde{n}_0(\bar{r}) = a^d \int_{-\infty}^{\infty} dK\, g_0(K) \left\{ \frac{K + U_{00}n_c(\bar{r})}{E_0(K,\bar{r})} \bar{n}_{\text{BE}}[E_0(K,\bar{r})] + \frac{K + U_{00}n_c(\bar{r}) - E_0(K,\bar{r})}{2E_0(K,\bar{r})} \right\},$$

$$= a^d \int_{-\infty}^{\infty} dK\, g_0(K) \frac{1}{2} \left\{ \frac{K + U_{00}n_c(\bar{r})}{E_0(K,\bar{r})} \coth\left[\frac{\beta E_0(K,\bar{r})}{2}\right] - 1 \right\}, \tag{5.17}$$

and we see that, although a different derivation has been used, if we restrict to the ground band and to nearest-neighbour hopping, then our result is the same as that of [58]. Our derivation has the advantage that (5.8) applies for excited bands and beyond nearest-neighbour hopping. Also, we have used the density of states to reduce the problem to two dimensions, which is perhaps why we are able to fix the total number of particles whereas [58], using a four-dimensional calculation, calculates the simpler case of fixed number density at the trap centre (so that the chemical potential iteration is local). Finally, our use of trap units allows modelling of aspherical harmonic traps, whereas their approach is stated for a spherical trap.

5.6 Procedure

We fix the parameters $N, V_j, a_j, a_s, \omega_j$ and m throughout the entire calculation. For the cubic lattice, we calculate the density of states $g_b(K)$ and the interaction parameters $U_{bb'}$ once and use them for any cubic-lattice calculation. For the non-cubic lattice, we calculate the density of states and interaction parameters when required.

We present our algorithm for the LDA calculation in figure 5.1. We note that, once we have a choice for the chemical potential, the calculation is completely local. Therefore, in contrast to the Gross-Pitaevskii equation approach of [56], we do not check the target for the total number N until the calculations at each site are self-consistent.

When we 'choose' a value in the algorithm, we avoid fixed-point where possible (since it may not converge) and use the Brent method [109]. We use fixed-point only to get consistency of the interactions between bands: after the check 'Has $\tilde{n}_b(\bar{r})$ converged $\forall b$?', the calculated values for $\tilde{n}_b(\bar{r})$ are used for the next iteration.

While we give the general formulae in figure 5.1, we use the simplification of section 5.5 for the ground band.

For the translationally-invariant lattice, we use almost the same calculation, with $V_{\text{tr}}(\mathbf{r})$ set to zero, and use only one spatial point, $\bar{r}$. However, due to the importance of the low energy states, as discussed in appendix J, we make the substitution $u^4 = K$ and use $\int \mathrm{d}K \to \int 4u^3 \mathrm{d}u$ so that the integrand isn't divergent.
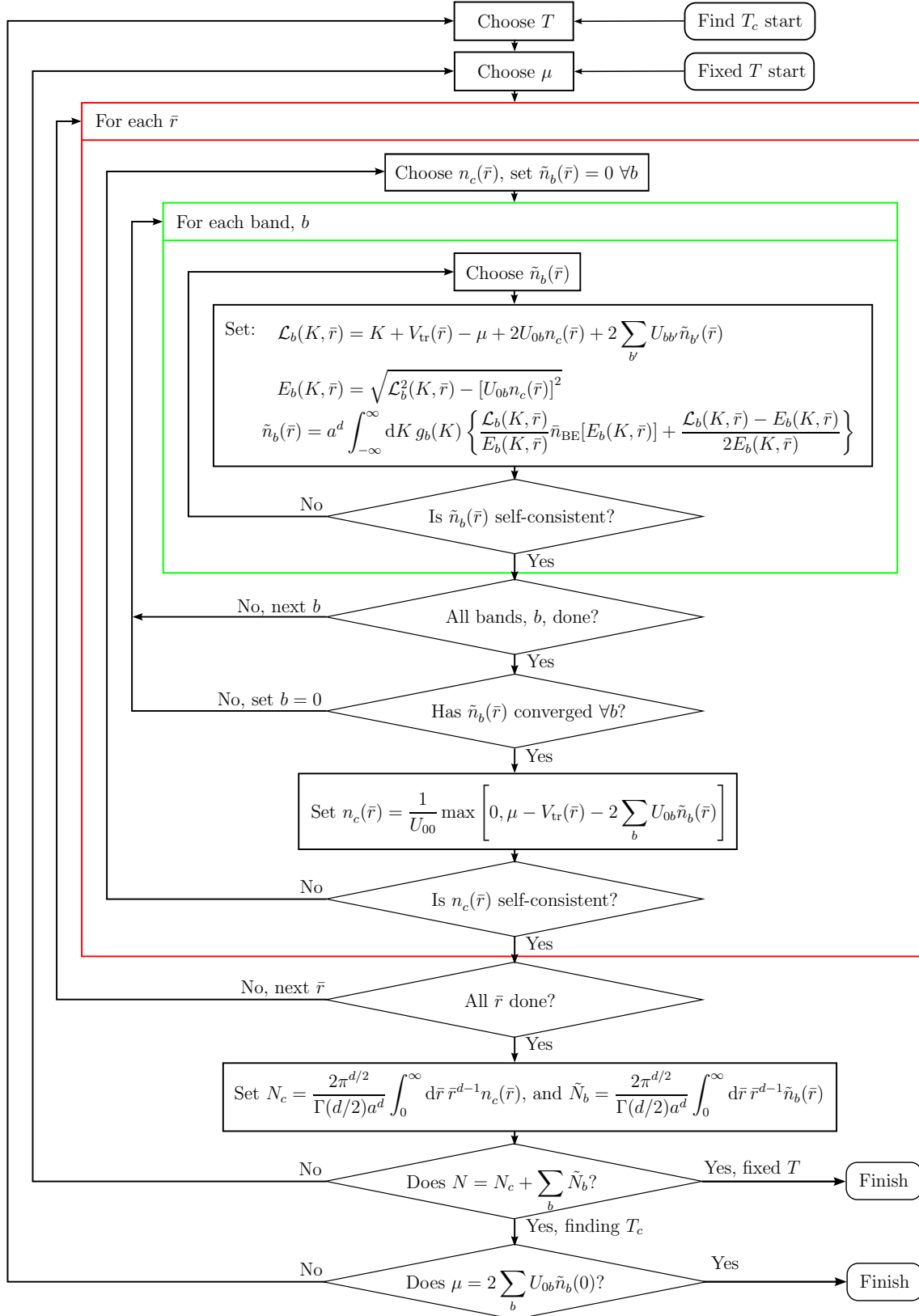
Figure 5.1: Procedure for LDA calculation

5.7 Finite-size effect

For the non-interacting gas in a combined harmonic lattice, we allow for the effect of a positive chemical potential at condensation, equal to the minimum energy:

$$\mu_{\mathrm{fs}} \equiv \frac{d}{2}\hbar\bar{\omega}^*, \tag{5.18}$$

where ω_j^* are the effective trapping frequencies, defined in (4.15), and $\bar{\omega}^*$ is their arithmetic mean. We limit the domain of the integral (5.8) to $K + V_{\mathrm{tr}}(\mathbf{r}) > \mu_{\mathrm{fs}}$, which has a negligible effect on results compared to the effect of increasing the chemical potential.

For the interacting gas, it is normal to consider the finite-size effect and mean-field interaction shift as independent additive corrections, [54], which we do analytically in section 7.6. For our numerical model, motivated by the non-interacting case, we could increase the point of condensation to $\mu = \mu_{\mathrm{fs}} + 2\sum_b U_{0b}\tilde{n}_b(0)$. We would then have to use:

$$n_c(\bar{r}) = \frac{1}{U_{00}}\max\left[0, \mu - \mu_{\mathrm{fs}} - V_{\mathrm{tr}}(\bar{r}) - 2\sum_b U_{0b}\tilde{n}_b(\bar{r})\right], \tag{5.19}$$

for our Thomas-Fermi calculation, so that the point of condensation is consistent between the condensate and non-condensate. However, μ_{fs} in (5.19) should be the difference between the Gross-Pitaevskii and Hartree-Fock minimum energies, and (5.18) is not a good estimate of that difference. Therefore, we do not follow this approach, and in our numerical model for the interacting gas, we do not allow for the finite-size effect.

We do not consider the finite-size effect due to factors other than the positive chemical potential.

5.8 Summary

We have made an efficient numerical implementation of our theory which we have clearly depicted in figure 5.1. By using the density of states and trap units, the LDA problem has been reduced to two dimensions, even for a non-cubic lattice with an aspherical harmonic trap. For the simpler Bose-Hubbard case, including ground band only, and nearest-neighbours only, we have shown that our theory reduces to an existing result [58].

Chapter 6

Numerical results

In this chapter we present results demonstrating the application of our mean-field theory to experimentally realistic regimes of a Bose gas in a three-dimensional combined harmonic lattice potential. Our results quantify lattice and interaction effects on the thermal properties of the system.

We demonstrate the accuracy of the numerical procedure described in section 5.6 for predicting thermal properties, by comparing with the full diagonalisation for the ideal gas. We show the significance of various assumptions, display some important features of cold bosons in optical lattices and compare our methods with experiment. We refrain from discussing the critical temperature here, which we deal with in detail in chapter 7.

6.1 Finite-size effect

We consider the effect on the non-interacting condensate fraction of a positive chemical potential at condensation, as discussed in section 5.7.

We plot the condensate fraction for $\omega = 0.02\omega_R$ and $V = 15E_R$ in figure 6.1.[1] We chose a small number of atoms, $N = 1000$, to accentuate the finite-size effect.

---

[1] We also considered the plots for other lattice depths and trap frequencies, but the plot was similar in each case, except for scaling due to the different critical temperatures.
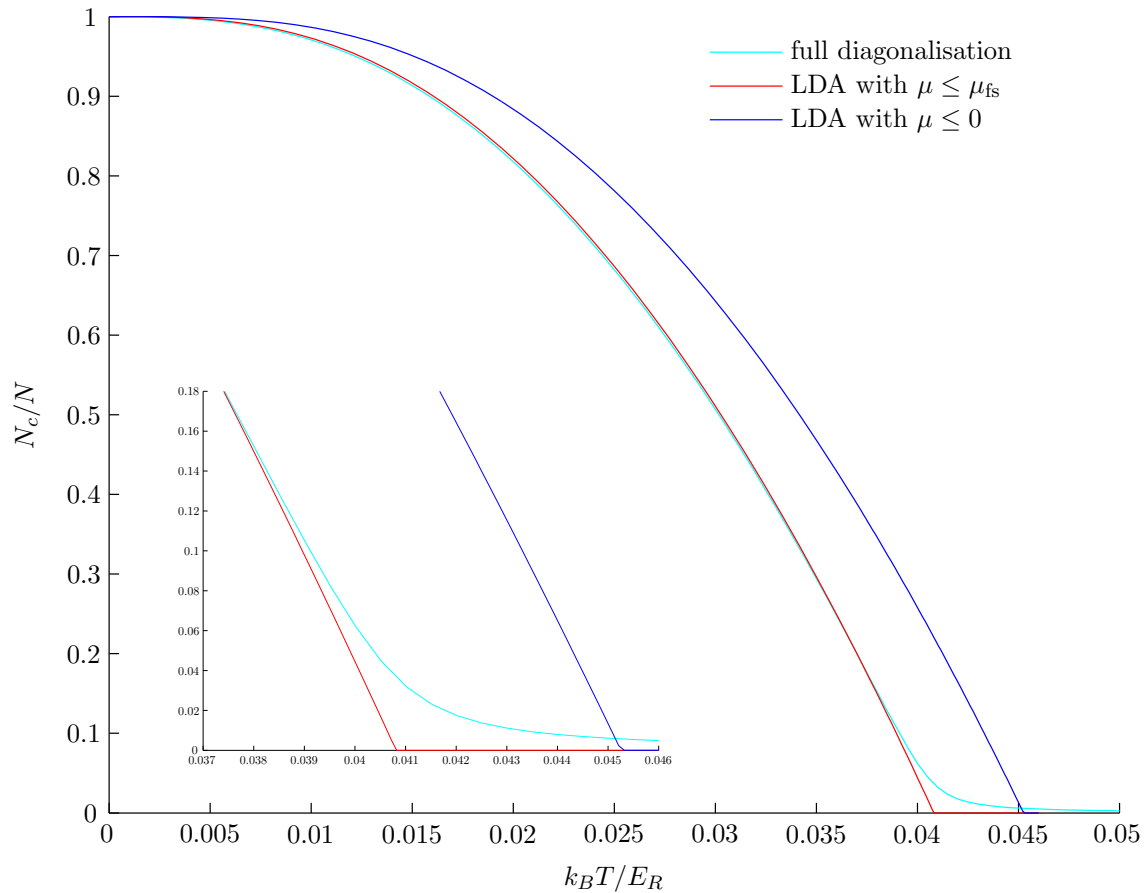
Figure 6.1: Condensate fraction for a non-interacting combined harmonic cubic-lattice in three dimensions with $N = 1000$, $\omega = 0.02\omega_R$ and $V = 15E_R$. The inset shows the region near the critical temperature in more detail.

We see that the positive chemical potential describes the bulk of the finite-size effect well. The LDA calculation with the finite-size effect gives excellent agreement with the condensate fraction from the full diagonalisation, except that LDA result shows a phase transition (that is, discontinuous behaviour) at the critical temperature, whereas the full diagonalisation shows a more gradual change.

6.2 Beyond nearest-neighbour hopping

In this section, we consider the effect on the non-interacting condensate fraction of beyond nearest-neighbour hopping (we use all neighbours for our numerical calculations

in all other sections).

We only consider the case where excited bands are insignificant. Using nearest-neighbour hopping for excited bands would be difficult to justify, based on figure 2.3. Also, figure 4.7 shows that, for sufficiently high energies, excited bands are free-particle-like, which demonstrates the increased significance of beyond nearest-neighbour hopping.

We show the condensate fraction for $N = 10^5$ and $\omega = 0.01\omega_R$ in figure 6.2. We see that beyond nearest-neighbour hopping is significant for $V = 2E_R$ and much less so for $V = 5E_R$. For $V = 10E_R$ (not shown), the condensate fractions are barely distinguishable on an equivalent plot. The decrease in significance of beyond nearest-neighbour hopping with increasing V/E_R, agrees with what we expect from figures 2.3, 4.6 and D.1.
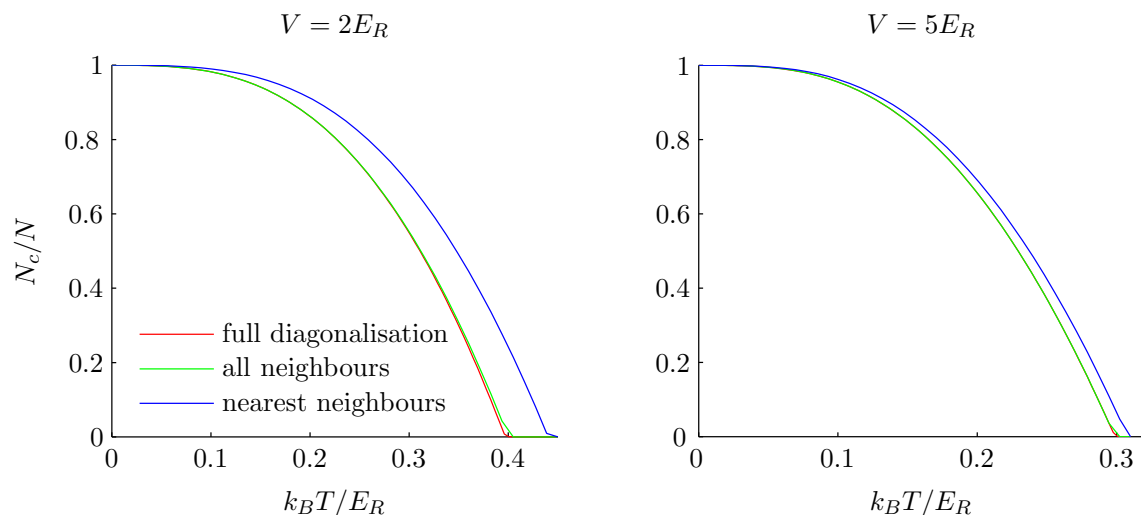
Figure 6.2: Non-interacting condensate fraction for $N = 10^5$ and $\omega = 0.01\omega_R$. The full diagonalisation curve is almost obscured by the all-neighbours result.

6.3   Excited bands

In this section, we consider the significance of excited bands. We do not compare to the full diagonalisation, since the separation into bands for that calculation is not well defined. Since we are not comparing to the full diagonalisation, we show interacting results. The higher the temperature, the more important excited bands are, since they are more thermodynamically accessible. We therefore consider the significance of ex-

cited bands at the critical temperature. From figure 4.2, which showed us the band sizes and gaps, for a given temperature in the order of up to a few recoil units, increasing the lattice depth decreases the significance of excited bands.

We show the thermal number of atoms in excited bands as a proportion of the thermal number in the ground band in figure 6.3.
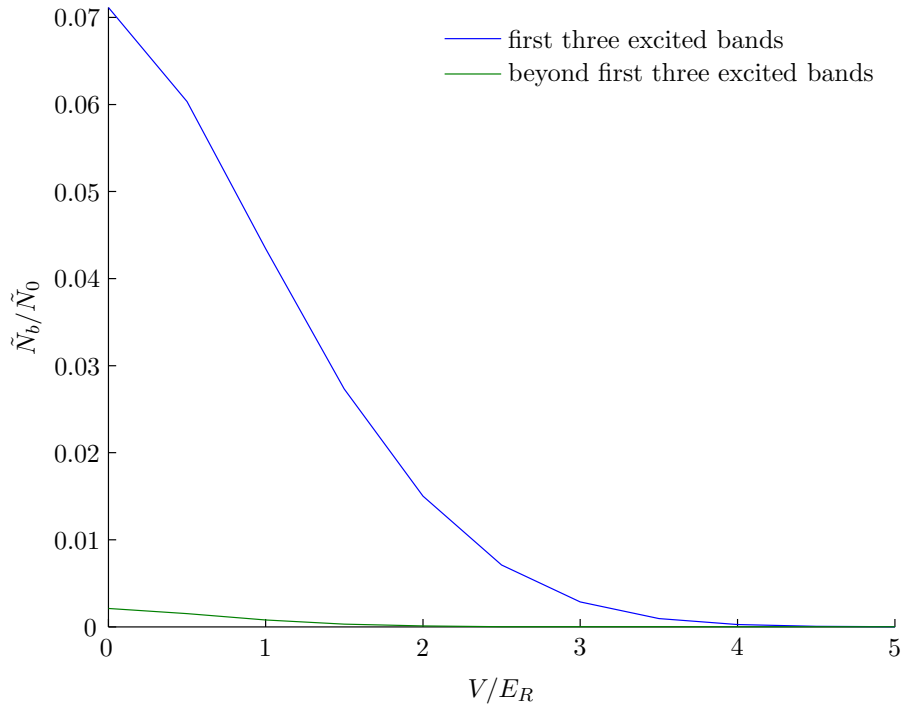
Figure 6.3: Ratio of number of thermal atoms in excited bands to thermal atoms in the ground band at the critical temperature for the experimental setup of [39]

The calculations are for ^{87}Rb with $a_s = 5.77$ nm and the parameters of [39] with an optical lattice wavelength of $\lambda = 2a = 852$ nm and a spherical trap with frequency $\omega = 2\pi \times 24$ Hz. We used their maximum number of atoms, $N = 2 \times 10^5$. We see that excited bands become insignificant for $V \gtrsim 3E_R$. The significance of excited bands at condensation would increase for an increased number of particles or a tighter trap, due to the increased critical temperature. For sufficiently high temperatures beyond the condensation region, excited bands become very significant.

6.4 Quantum depletion

The experimental measurement of quantum depletion was reported in [40]. They loaded atoms into a lattice, which was linearly ramped up to a lattice depth of $V \approx 20E_R$ and linearly ramped back down. 'This ramp sequence was interrupted at various times by a sudden switch-off of all lattice and trapping potentials' [40]. By observing the diffuse background peak of the momentum distribution of time-of-flight images, the populations of the condensed and non-condensed atoms were estimated. When the lattice was fully ramped back down, up to 20% of the atoms were observed as thermal depletion. 'Linear interpolation was used to subtract this small heating contribution (up to 10% at the maximum lattice depth)' to obtain the quantum depletion [40]. Their results are presented in figure 6.4.[2]

We have calculated the zero temperature quantum depletion to compare with their experimental results. We have reproduced the translationally-invariant lattice calculations of [40] to a level indistinguishable on the plot. The combined harmonic lattice calculation (solid black curve) of [40] applies 'the result from the homogeneous system to shells of different occupancy numbers using the local density approximation'. We used our LDA calculations[3] to give improved agreement with experimental results (red curve).[4] However, our calculations are still not within error bars for some measurements, perhaps due to the linear interpolation in the experiment to allow for the thermal depletion, as described above. The agreement at shallow lattices is worse, where the theory should be best. We hope that future experiments in this area with a qualitative focus will enable careful comparison with theory and be able to clearly distinguish thermal and quantum depletion.

---

[2]We removed their one and two-dimensional data and calculations from their plot, which we do not consider.

[3]We have assumed $N = 1.7 \times 10^5$ atoms, which is mentioned in the paper. Although the number of atoms throughout is unclear, using their maximum number of atoms, $N = 5 \times 10^5$, makes only a small change to the results, being close to the curve (ii).

[4]We note that our methods are not valid after the Mott-insulator transition. Although the $n = 1$ Mott-insulator transition is at $V = 16.4E_R$, the 'measurements were performed at a peak lattice site occupancy number ~ 7' [40], and the Mott-insulator transition is at $V > 20E_R$ for $n \geq 3$, which extends our validity regime somewhat. The smoothed Mott-insulator fraction was calculated by [40] and is shown in figure 6.4.
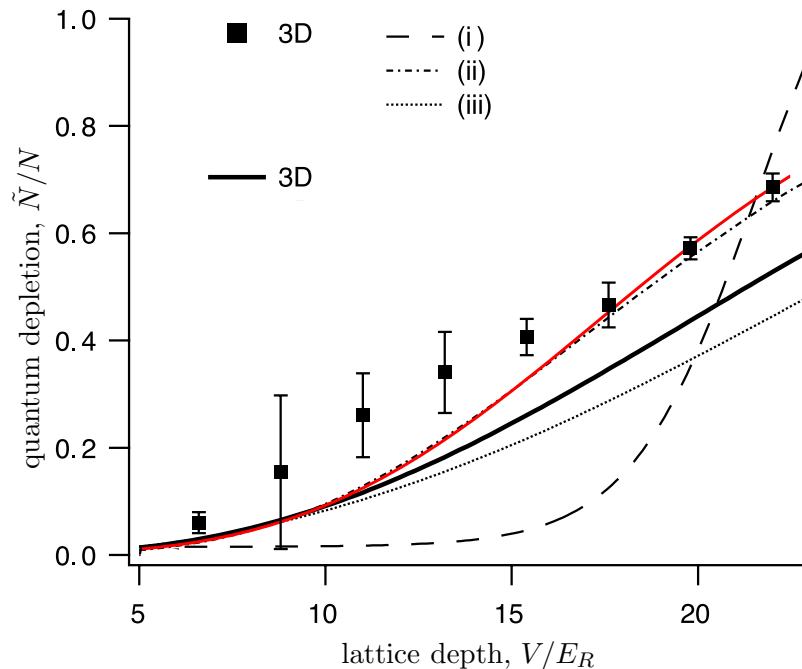
Figure 6.4: Quantum depletion of ^{23}Na in a three-dimensional optical lattice. The data points with error bars give the experimental quantum depletion. The curves are: '(i) the (smoothed out) Mott-insulator fraction'; (ii) 'the calculated quantum depletion for a *homogeneous* system of per-site occupancy number $n = 1$ and (iii) $n = 7$'. The solid curves are combined harmonic lattice calculations: the black curve from [40] and the red curve is our result.

6.5   Effect of quasi-particles

In addition to the quantum depletion, which was considered at zero temperature in section 6.4, the Bogoliubov quasi-particles modify the energy dispersion as in (3.42). We compare the quantum depletion to the residual Bogoliubov effect in this section (using the parameters of [39], as discussed in section 6.3).

In figure 6.5 we show the condensate fraction and the condensate plus quantum depletion fraction. At zero temperature, the only effect of quasi-particles is the quantum depletion. The methods with and without quasi-particles give the same results above the critical temperature and the same critical temperature,[5] since equations (5.7) and

---

[5]The critical temperature is the same if we define it as the lowest temperature for which all particles can be accommodated as thermal atoms. We note the consistency issues near the critical temperature discussed in [110].
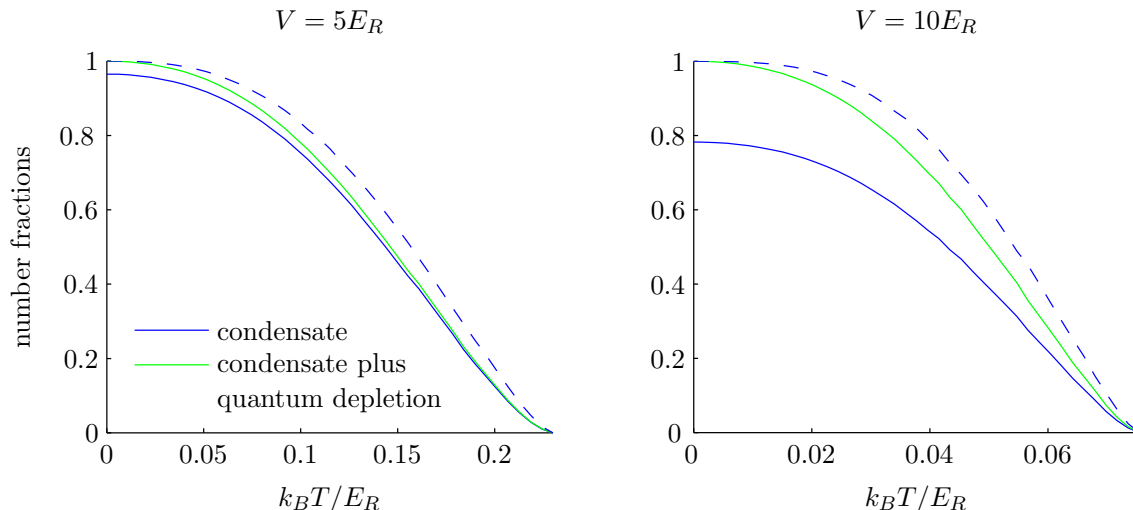
Figure 6.5: Condensate and quantum depletion fractions for the parameters of [39]. Solid lines are for the Popov approximation to Hartree-Fock-Bogoliubov method and dashed lines are for the Hartree-Fock method.

(5.8) are the same when there is no condensate. In figure 6.5 we can see the zero temperature increase in quantum depletion due to the increase in lattice depth (as in figure 6.4) and we can see that the nature of the Bogoliubov quasi-particle spectrum (3.42) also increases thermal depletion relative to the Hartree-Fock prediction.

In figure 6.6 we show the total spatial density, and that of the condensate and quantum depletion.[6] The quantum depletion follows the condensate density from (3.42) and (3.45). A larger lattice depth increases the effective interaction, decreasing the core density and, for the Hartree-Fock case, forces all of the thermal depletion away from the condensate region. We note that condensate fractions and number densities have been previously produced in [58] for the similar, but simpler case of fixed number density at the trap centre (so that the chemical potential iteration is local), nearest-neighbours and ground band only (although, as we have shown, beyond nearest-neighbours and excited bands are not too significant at these lattice depths). The characteristic lengths reported in [58] suggest a lattice spacing that is two orders of magnitude less than that used in experiments, and we have not attempted to reproduce their results.

---

[6]The total density curves all integrate to $N = 2 \times 10^5$, the much higher Hartree-Fock condensate density near the core is made up for by the slightly lower density further away due to the r^2 term in the integral.
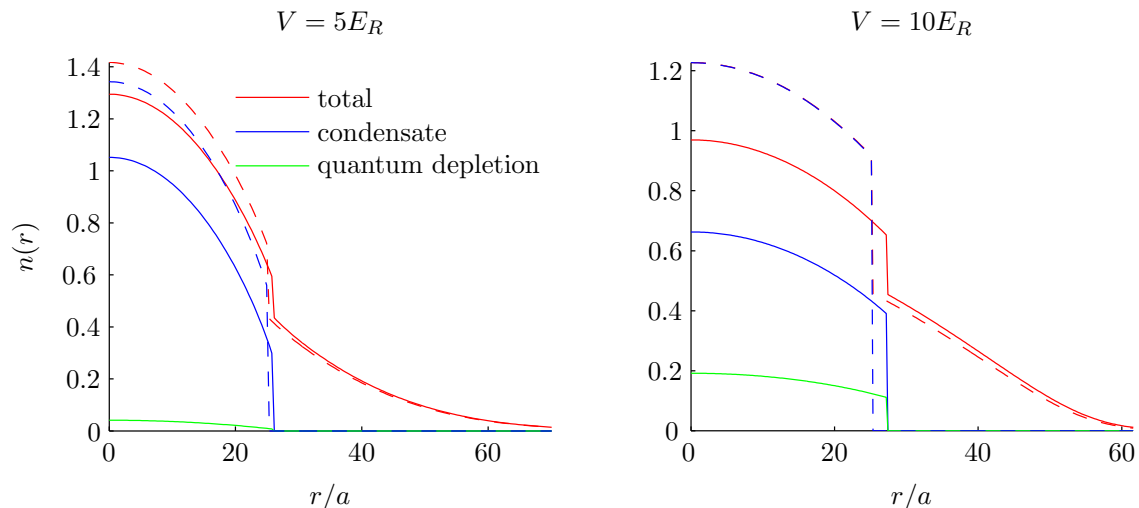
Figure 6.6: Spatial densities for the parameters of [39] at $T = 0.8T_c$. Solid lines are for the Popov approximation to Hartree-Fock-Bogoliubov method and dashed lines are for the Hartree-Fock method.

6.6 Summary

We have shown the accuracy of the LDA method in comparison with the full diagonalisation after allowing for the finite-size effect. We have quantitatively shown the decreasing significance of beyond nearest-neighbour hopping and excited bands as the lattice depth increases. We have compared our prediction of quantum depletion with experiment. We have examined the effect of Bogoliubov quasi-particles, so that the quantum depletion and extra thermal depletion may be separately identified.

Chapter 7

Critical temperature

In this chapter, we present analytical results for the ideal number density, condensate fraction and critical temperature, and for the finite-size effect and mean-field interaction shift. We give simple iterative procedures for including excited bands. We compare all of these results and methods against the full numerical approach given in chapter 5.

We show that the nature of useful approximations for the translationally-invariant and combined harmonic lattices differ distinctly. For the translationally-invariant case, the lowest energy states are singularly important, for which we verify that an effective-mass treatment is accurate over a broad regime. In contrast, for the combined harmonic lattice, the entire ground-band structure is typically important, for which we develop simple band shape approximations. In both the translationally-invariant and the combined harmonic lattices, we show that the effective-mass treatment and the simple band shape approximations work in complementary regimes.

7.1   Effective mass

The effective-mass approximation was considered in section 4.4 and formulae for the effective mass are given in appendix H. To consider its range of validity, we plot extracts of the one-dimensional translationally-invariant lattice spectrum in figure 7.1. We see that the approximation is only valid for energies low in the ground band. Even for V_x as small as $E_{R,x}$, the approximation is poor for $k_x \gtrsim 0.7\pi/a_x$ and is certainly poor

for excited bands (worse than the free-particle dispersion).[1] However, we note that the effective-mass approximation is not just for shallow lattices, provided the important energies are sufficiently small. Even for V_x as large as $15E_{R,x}$, the approximation is still reasonable for quasi-momentum $k_x \lesssim 0.3\pi/a_x$, but the range of energies which these quasi-momentum correspond to is much less since the band is much narrower from figure 4.2.
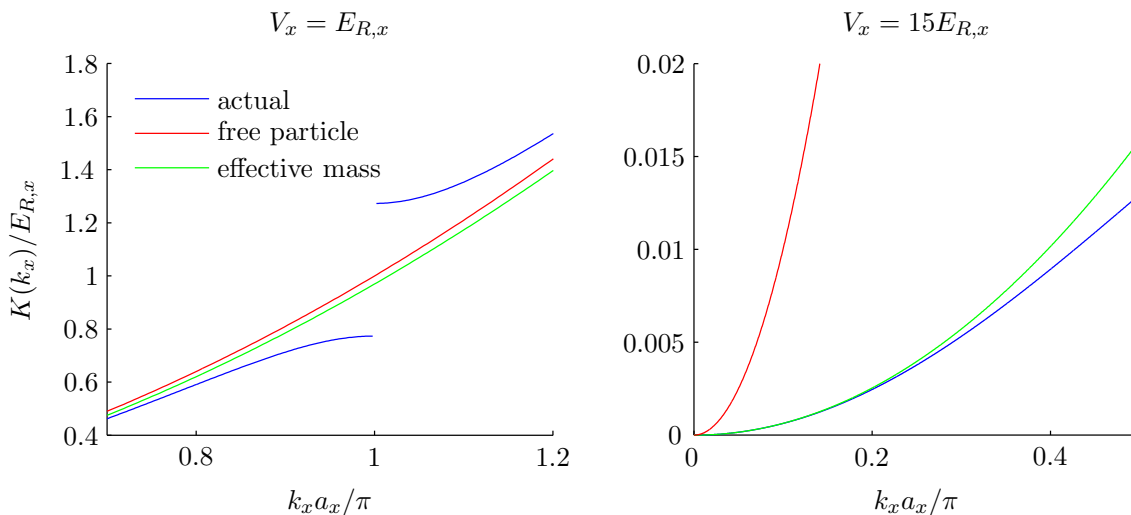
Figure 7.1: One-dimensional translationally-invariant lattice spectrum

We use the effective-mass density of states from (4.10). For the translationally-invariant case, from (3.37) and (4.4)

$$\frac{\tilde{N}}{N_s a^3} = \left(\frac{m^*}{m}\right)^{d/2} \lambda_T^{-d} \zeta_{d/2}(z), \tag{7.1}$$

where $z = e^{\beta\mu}$, $\lambda_T = h/\sqrt{2\pi m k_B T}$ and $\zeta_\alpha(z) = \sum_{n=1}^{\infty} z^n/n^\alpha$ is the Bose function (some properties of this function are discussed in appendix I). Solving for the critical temperature, so that $\tilde{N} = N$ and $\mu \to 0$, there is no condensation in one and two dimensions and in three dimensions we have the well known result [111]:

$$T_c^0 = \frac{2\pi\hbar^2}{k_B m^*} \left[\frac{N}{N_s a^3 \zeta(3/2)}\right]^{2/3}. \tag{7.2}$$

---

[1]We could recalculate the effective mass and set the energy to the correct level at the start and end of each band (and blend the approximations together at the middle of the band), but this would not be nearly so tractable, and in many cases it would still not be very accurate near the middle of the bands.

We compare the critical-temperature results to our full numerical calculation in figure 7.2. The results obviously coincide at $V = 0$ and the effective mass is a good approximation for $V \lesssim E_R$ since there the lattice has a perturbative effect. The approximation is also good when the critical temperature is well within the band (we consider the bandwidth in figure 7.4). The effective-mass results show a reasonable approximation of the full numerical calculation in figure 7.2, even where the critical temperature is well above ground band. This is because the low energy states are extremely important to the calculation since the integrand to arrive at (7.1) is divergent as $K \to 0$ and therefore the low K region has a substantial contribution to the total integral.[2] Even though the remainder of the actual density of states is very different, this is suppressed relative to the $K \to 0$ behaviour.
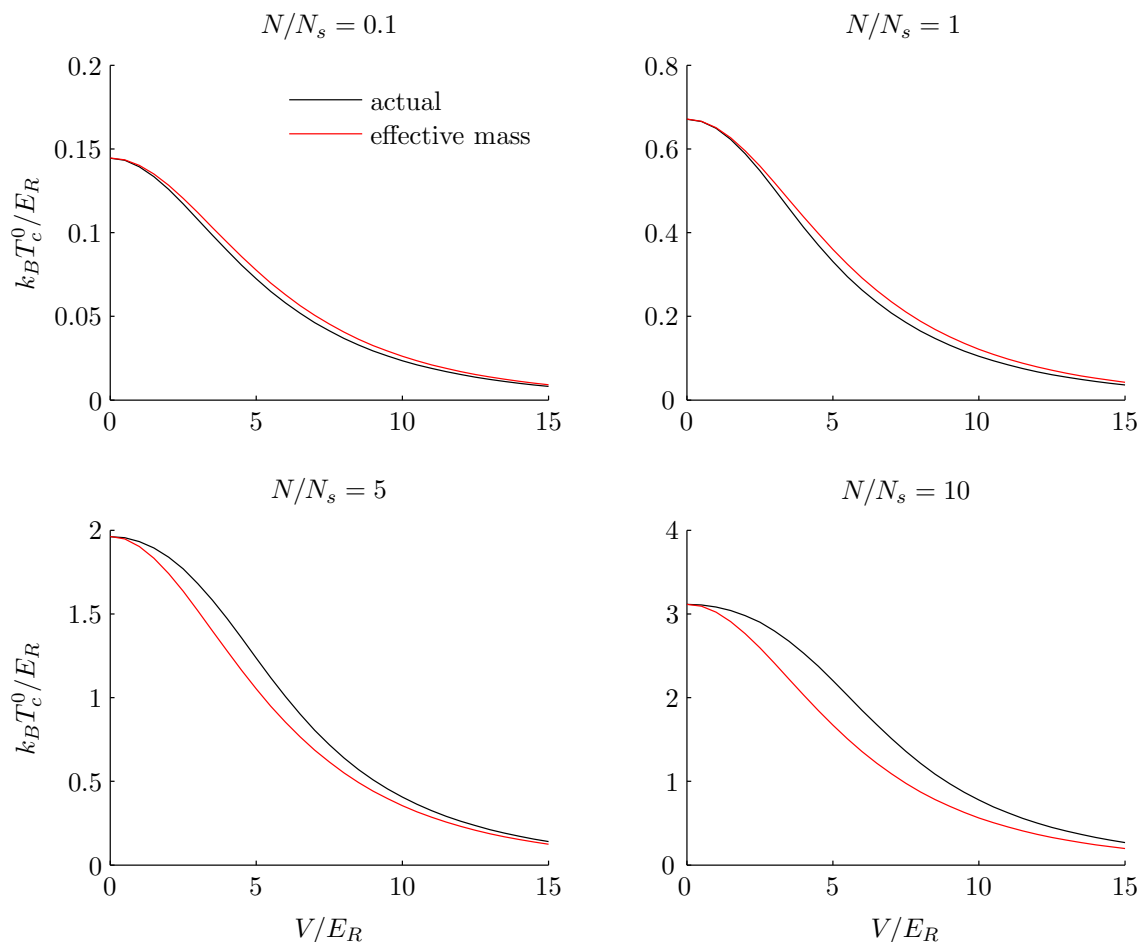
Figure 7.2: Comparison of actual to effective-mass critical temperature for a three-dimensional translationally-invariant lattice

---

[2] Since the density of states (4.10) reflects the true density of states for low energies, the integrand in this region is $g(K)/(e^{\beta K} - 1) \sim k_B T/\sqrt{K}$ which is divergent as $K \to 0$ and we have for low K $\int_0^K \mathrm{d}K' g(K')/(e^{\beta K'} - 1) \sim k_B T \sqrt{K}$. For more detail and graphs of the integrand, see appendix J.

For the combined harmonic lattice, from (3.37) and (4.4) (or from (4.14)):

$$\tilde{N} = \left(\frac{m^*}{m}\right)^{d/2} \left(\frac{k_B T}{\hbar \omega}\right)^d \zeta_d(z),$$

(7.3)

so that there is no condensation in one dimension and in two or three dimensions, the critical temperature is the well known result [112]:

$$T_c^0 = \frac{\hbar \omega^*}{k_B} \left[\frac{N}{\zeta(d)}\right]^{1/d},$$

(7.4)

where the effective trap frequencies were defined in (4.15). For three dimensions, we compare the effective-mass results to our full numerical calculation in figure 7.3.
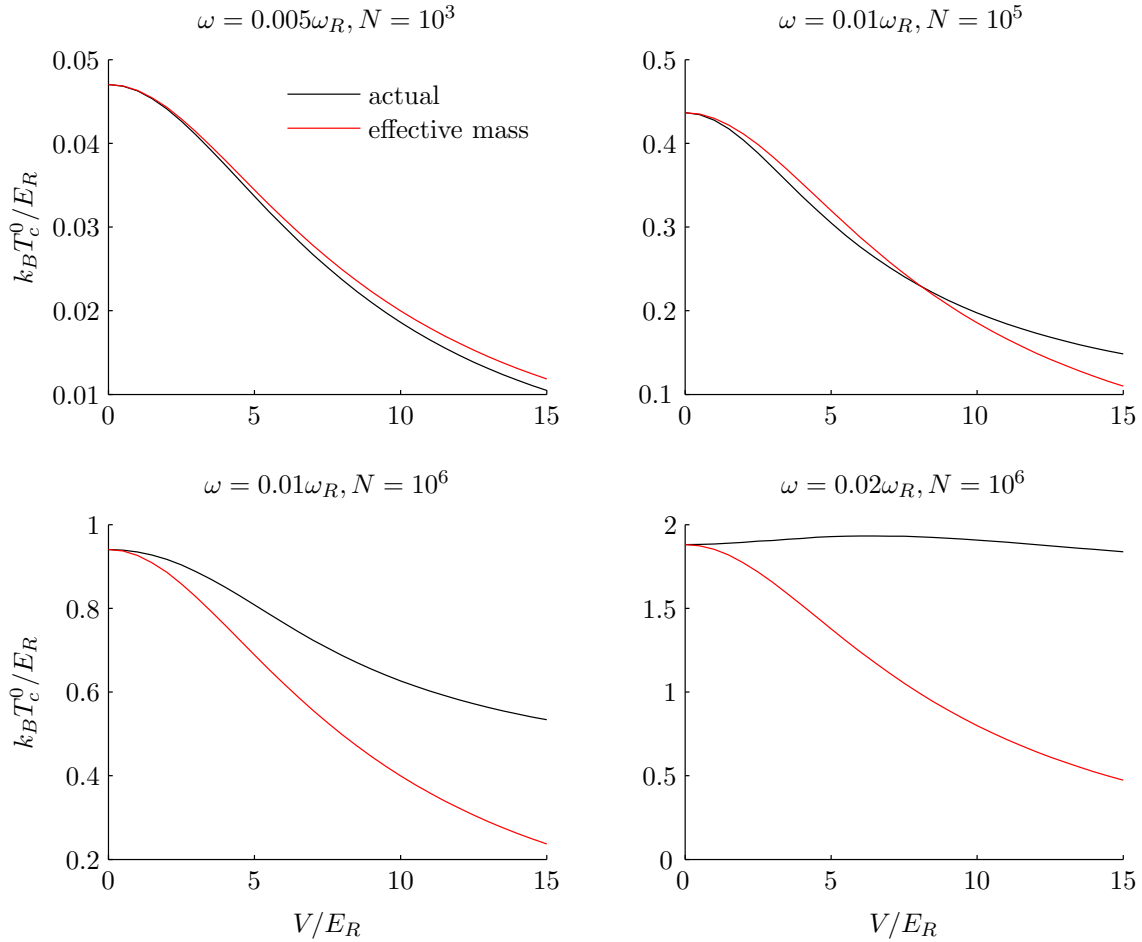
Figure 7.3: Comparison of actual to effective-mass critical temperature for a three-dimensional combined harmonic lattice

We again see that the agreement is good for $V \lesssim E_R$ and when the critical temperature is well within the ground band. The approximation is generally poor when the critical

temperature is out of the ground band. For the combined harmonic lattice, the low energy states mentioned above and in footnote 2 are not so important since the low energy region is not divergent.[3]

For the finite-size effect in three dimensions, using the methodology of [113] (which considered the finite-size effect in the no lattice case) with the modified density of states:

$$\frac{\delta T_c^{\text{fs}}}{T_c^0} \approx -\frac{\bar{\omega}^*}{\omega^*}\frac{\zeta(2)}{2\zeta(3)^{2/3}}N^{-1/3} \approx -0.73\frac{\bar{\omega}^*}{\omega^*}N^{-1/3}. \tag{7.5}$$

Since, for a cubic lattice, this is independent of V, we do not plot it here, but show it on figure 7.12.

7.1.1 Shallow lattice interaction

In this section, we motivate a shallow lattice coupling constant, g^*, which is a modification of the no lattice coupling constant, g. We consider the three-dimensional no harmonic trap case, with all of the atoms in the condensate. In the shallow lattice limit, where $\mu > V_{\text{latt}}(\mathbf{r})$, it is permissible to make the continuous Thomas-Fermi approximation for the condensate, $n_c(\mathbf{r}) = (\mu - V_{\text{latt}}(\mathbf{r}))/g$, whereas, for deeper lattices, the discrete approximation (3.18) becomes valid. The condensate energy in the no lattice case is $gN^2/2N_s a^3$ [114], so averaging over the lattice, we require that:

$$g^*\frac{N^2}{N_s a^3} = g \int \mathrm{d}\mathbf{r}\, n_c(\mathbf{r})^2$$

$$\implies g^* = \frac{N_s a^3}{gN^2}\int \mathrm{d}\mathbf{r}\left[\mu - \frac{1}{2}\sum_j V_j - \frac{1}{2}\sum_j V_j \cos\left(\frac{2\pi r_j}{a_j}\right)\right]^2$$

$$= g\left[1 + \frac{1}{8}\left(\frac{N_s a^3}{Ng}\right)^2 \sum_j V_j^2\right], \tag{7.6}$$

where we have used $N = \int \mathrm{d}\mathbf{r}\, n_c(\mathbf{r}) \implies \mu - \frac{1}{2}\sum_j V_j = Ng/N_s a^3$. We see in (7.6) the interplay between the squared magnitude of the lattice $\sum_j V_j^2$ and the squared average no-lattice interaction energy $(gN/N_s a^3)^2)$.

We do not have a numerical model valid in this regime. The above shows some first steps towards understanding the interacting gas in a shallow lattice.

---

[3]Since the K integrand is divergent only when $r \to 0$ and this region is suppressed by the r^2 term in $\int_0^\infty \mathrm{d}r\, r^2 \int \mathrm{d}K g(K)/(e^{\beta(K+V_{\text{tr}}(\mathbf{r}))} - 1)$.

7.2 Simplified ground-band shape

As we have seen in figure 4.3, for a deep lattice, the density of states becomes separated into disjoint bands. In this section we ignore the finite-size effect and interactions and we assume that the energy of the excited bands is sufficiently high relative to the critical temperature that they can be ignored. We will consider adjustments for these effects in later sections. Work for section 7.1 suggests that, particularly for the combined harmonic lattice, there is a wide regime where it is not sufficient to consider only the effective-mass region of the band. This suggests that modelling the overall shape of the whole band is likely to be important. We therefore use simplified shapes for the whole ground band. Our approach will not, however, be fully accurate when the critical temperature is so low that the fine structure of the ground band becomes important.

As we can see from figure 4.3, the width of the ground band becomes very narrow for deep lattices. As the most simple approximation, we use a delta function at zero energy for the density of states which we call the zero-delta approximation. We then consider two additional approaches. The first is a delta function at the middle of the band which we call the centred-delta approximation. The second is to spread the density evenly over the band, which we call the rectangular band assumption.[4] We then consider approximate band shapes that are more representative of the band structure: the quadratic and triangular bands. These two assumed shapes have similar complexity and are both included so that we can see the effect on results of these band shapes.

In all cases, except the zero-delta approximation, we expand the results as a series in the quantity we call the 'thermal width', $w = W/k_B T$. As $w \to 0$ the results become the zero-delta results. The series expansion is convergent when w is not too large, which is also when approximations inherent in the simple band shapes are less important.

The value for the width, W, used in our calculations is chosen so that the average energy of our approximate band shape (which is always at the midpoint of the approximate band since the shapes we use are symmetrical) is equal to the average energy of the actual density of states:

$$\frac{W}{2} = a^d \int dK \, K g_0(K). \tag{7.7}$$

For large lattice depths, the density of states is approximately symmetric and the use of

---

[4]These are extremes of simplicity, but not necessarily of value. For example, the infinite Van Hove singularities discussed later in this section may cause more extreme results.

(7.7) is equivalent to using the difference between the maximum and minimum energy of the band. For shallow lattices, the density of states has significant asymmetry as shown in figure 7.4. The cubic-lattice tight-binding result, $W = 12J$ from (D.19), is often used in the literature and is shown for comparison.
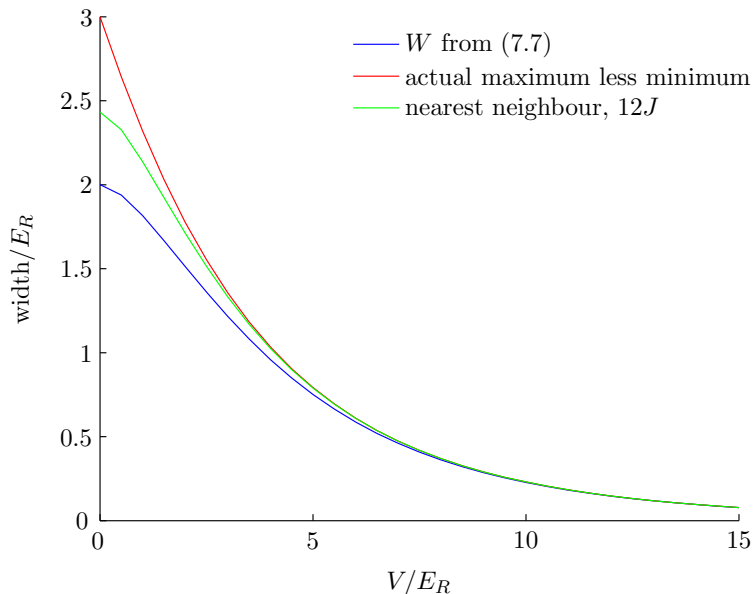
Figure 7.4: Width of the ground band

We set d to be the number of dimensions which are harmonically trapped. For example, $d = 0$ for the translationally-invariant lattice and $d = 3$ for the combined harmonic lattice in three dimensions. Our band shapes are chosen by comparison to the actual density of states in three dimensions. Therefore the results should be used with caution in one or two dimensions. The actual band shape for a one-dimensional optical lattice has infinite Van Hove singularities at the bottom of the ground band, and at the minimum and maximum energy of every band in the tight-binding limit (from figure 4.4), so would be better approximated by a shape including delta functions at both of those points. The actual ground-band shape for a square lattice in the tight-binding limit is infinite at the middle of the band (from figure 4.5), so would be better approximated by a shape including a delta function there. We intend to derive further results for one and two-dimensional optical lattices as part of later work.

For a translationally-invariant lattice, we set N_s to be the number of sites. For the combined harmonic lattice, we set $N_s = [\pi k_B T/(m\omega^2 a^2/2)]^{d/2}$ which is a measure of the thermally accessible number of sites and, as we shall see below, is a factor in combined harmonic lattice results which takes the place of the translationally-invariant lattice number of sites.

7.2.1 Zero-delta band shape

For sufficiently deep lattices, the spread in kinetic energy becomes negligible compared to other relevant energy scales. As an extreme approximation, we then take the kinetic dispersion to be zero, $K_b(\mathbf{k}) = 0$ [62, 115]. We can then represent the density of states with a delta function at the lowest energy of the band, $g_0(K) = \delta(K)/a^d$ from (4.1) using $\int_{\mathrm{BZ}} \mathrm{d}\mathbf{k} = (2\pi/a)^d$. Then using (4.4), we calculate the number of thermal atoms per site in the ground band:

$$\tilde{n}_0(\mathbf{r}) = \int \frac{a^d g_0(K)\mathrm{d}K}{z^{-1}\exp\{\beta[K + V_{\mathrm{tr}}(\mathbf{r})]\} - 1}$$
$$= \frac{1}{z^{-1}\exp[\beta V_{\mathrm{tr}}(\mathbf{r})] - 1}. \tag{7.8}$$

We use (3.37) to calculate the total number of thermal atoms. For the translationally-invariant lattice, we set $V_{\mathrm{tr}}(\mathbf{r}) = 0$ throughout the volume so that the integrand is constant and we recognise $\zeta_0(z) = 1/(z^{-1} - 1)$. For the combined harmonic lattice, we convert the integrand into a geometric series in $z\exp[-\beta V_{\mathrm{tr}}(\mathbf{r})]$, integrate one dimension at a time in case of anisotropy and recognise the Bose function from (I.1). We find, for both the translationally-invariant and combined harmonic lattice:

$$\tilde{N}_0 = \frac{1}{a^d}\int \mathrm{d}\mathbf{r}\,\tilde{n}_0(\mathbf{r})$$
$$= N_s \zeta_{d/2}(z), \tag{7.9}$$

which was shown, for the three-dimensional combined harmonic lattice, in [62]. This assumption of no kinetic energy dispersion only becomes valid for $V \gg 15E_R$, which is well beyond our regime of interest and gives no indication of the variation with lattice depth, so we consider improvements.

7.2.2 Centred-delta band shape

Rather than setting the dispersion to zero as section 7.2.1, if we set the dispersion throughout the first Brillouin zone to be its average value, $K_b(\mathbf{k}) = W/2$ in (4.1), then the density of states becomes a delta function at the centre of the ground band,[5]

---

[5]This differs from the zero-delta band shape, because, in both cases, the energy origin is set by $\mu \to 0$.

$g_0(K) = \delta(K - W/2)/a^d$. Then from (4.4):

$$\tilde{n}_0(\mathbf{r}) = \frac{1}{z^{-1} \exp[\beta V_{\mathrm{tr}}(\mathbf{r}) + w/2] - 1}. \tag{7.10}$$

This is equivalent to setting the exponential in (4.4) to its value in the middle of the band, combined with any density of states (noting that the density of states must integrate to unity). From (3.37), using the same approach as discussed for the zero-delta case above:

$$\tilde{N}_0 = N_s \zeta_{d/2}\big(z e^{-w/2}\big). \tag{7.11}$$

We note that the three-dimensional combined harmonic lattice result with $\mu \to 0$, $\tilde{N}_0 = N_s \zeta_{3/2}\big(e^{-w/2}\big)$, has been obtained previously using a completely different method in [116] (from the first term of a Bessel function expansion in a tight-binding approximation). When $\mu \to 0$, we expand for the translationally-invariant case as:

$$\tilde{N}_0 = \frac{N_s}{e^{w/2} - 1} = N_s \left[\frac{2}{w} - \frac{1}{2} + O(w) \right], \tag{7.12}$$

and for the combined harmonic lattice we expand using (I.8), which gives convergent series for $w < 4\pi$, in one dimension as:

$$\tilde{N}_0 = N_s \left[\sqrt{\frac{2\pi}{w}} + \zeta(1/2) - \frac{\zeta(-1/2)w}{2} + O\big(w^2\big) \right], \tag{7.13}$$

in two dimensions as:

$$\tilde{N}_0 = N_s \left[-\ln \frac{w}{2} + \frac{w}{4} + O\big(w^2\big) \right], \tag{7.14}$$

and in three dimensions as:

$$\tilde{N}_0 = N_s \left[\zeta(3/2) - \sqrt{2\pi w} - \frac{\zeta(1/2)w}{2} + O\big(w^2\big) \right]. \tag{7.15}$$

We expect the centred-delta assumption to be a poor approximation at least for $k_B T \lesssim W$, since the shape of the band will then be important and the assumed shape is extremely simplified.

7.2.3 Rectangular band shape

After the delta function densities of states assumed in sections 7.2.1 and 7.2.2, the next most simple band shape is a rectangle.

By a rectangular band shape, we mean $g_0(K) = 1/Wa^d$ for $0 < K < W$ and zero otherwise, as we used in section 4.6, and as shown in figure 7.5. Although, due to our definitions, the area and average value are necessarily the same for the actual and approximate density of states, the approximation is poor.

Figure 7.5: Comparison of exact cubic-lattice to rectangular density of states

From (4.4) and (I.1):

$$\tilde{n}_0(\mathbf{r}) = \frac{1}{w} \left[\zeta_1\!\left(z e^{-\beta V_{\mathrm{tr}}(\mathbf{r})}\right) - \zeta_1\!\left(z e^{-\beta V_{\mathrm{tr}}(\mathbf{r})-w}\right) \right]. \tag{7.16}$$

We again use (3.37) to calculate the total number of thermal atoms. For the translationally-invariant lattice, we use the same approach as for the zero-delta band assumption. For the combined harmonic lattice, we use (I.1) to convert the integrand into a series, again integrate one dimension at a time in case of anisotropy, and convert the result back into a Bose function using (I.1) to find:

$$\tilde{N}_0 = \frac{N_s}{w} \left[\zeta_{1+d/2}(z) - \zeta_{1+d/2}\!\left(z e^{-w}\right) \right]. \tag{7.17}$$

We consider $\tilde{N}_0$ in the limit $\mu \to 0$. The translationally-invariant case is divergent. For the one and two-dimensional combined harmonic lattices, the series have the same functional form as (7.13) and (7.14) (but different coefficients), using (I.8). We do not show the results here, since it does not alter the conclusions we wish to make on the reduced-dimensional cases. For the three-dimensional combined harmonic lattice, (I.8) gives the following series, which is here convergent for $w < 2\pi$:

$$\tilde{N}_0 = N_s \left[\zeta(3/2) - \frac{4\sqrt{\pi w}}{3} - \frac{\zeta(1/2)w}{2} + O\!\left(w^2\right) \right]. \tag{7.18}$$

We consider more accurate approximations in the next sections.

7.2.4 Quadratic band shape

The simplest differentiable function that has exactly two zeros is the quadratic, which is the band shape we choose here. By this we mean $g_0(K) = 6K(W - K)/W^3 a^d$ for $0 < K < W$ and zero otherwise. This approximation to the true density of states is shown in figure 7.6. The approximation is much improved compared to the rectangular density of states.

Figure 7.6: Comparison of exact cubic-lattice to quadratic density of states

Using (4.4) and (I.1):

$$\tilde{n}_0(\mathbf{r}) = \frac{6}{w^3} \left[w\zeta_2\big(ze^{-\beta V_{\text{tr}}(\mathbf{r})}\big) - 2\zeta_3\big(ze^{-\beta V_{\text{tr}}(\mathbf{r})}\big) + w\zeta_2\big(ze^{-\beta V_{\text{tr}}(\mathbf{r})-w}\big) + 2\zeta_3\big(ze^{-\beta V_{\text{tr}}(\mathbf{r})-w}\big) \right].$$

(7.19)

Then, from (3.37) and (I.1) using the same approach as for the rectangular case:

$$\tilde{N}_0 = \frac{6N_s}{w^3} \left[w\zeta_{2+d/2}(z) - 2\zeta_{3+d/2}(z) + w\zeta_{2+d/2}\big(ze^{-w}\big) + 2\zeta_{3+d/2}\big(ze^{-w}\big) \right].$$

(7.20)

Letting $\mu \to 0$, and using (I.8) we expand in series (convergent for $w < 2\pi$). For the translationally-invariant case:

$$\tilde{N}_0 = N_s \left[\frac{3}{w} - \frac{1}{2} + \frac{w}{24} + O\big(w^3\big) \right].$$

(7.21)

79

For one and two-dimensional combined harmonic lattices, the series again have the same form as (7.13) and (7.14) with different coefficients and we do not show the results here. For the three-dimensional combined harmonic lattice:

$$\tilde{N}_0 = N_s \left[\zeta(3/2) - \frac{48\sqrt{\pi w}}{35} - \frac{\zeta(1/2)w}{2} + O(w^2) \right].$$

(7.22)

7.2.5   Triangular band shape

There is a family of simplified band assumptions made up of piecewise polynomials for which we can get thermodynamic results as sums of Bose functions. The simplest of this family is the triangular band approximation, by which we mean:

$$g_0(K) = \frac{4}{W^2 a^d} \begin{cases} K & K < W/2, \\ W - K & W/2 < K < W, \\ 0 & \text{otherwise.} \end{cases}$$

(7.23)

The approximation to the true density of states is shown in figure 7.7. Compared to the quadratic band assumption, the skewness of the actual density of states means the triangular approximation is better for deep that for shallow lattices. By $V = 5E_R$ the approximation appears reasonable.
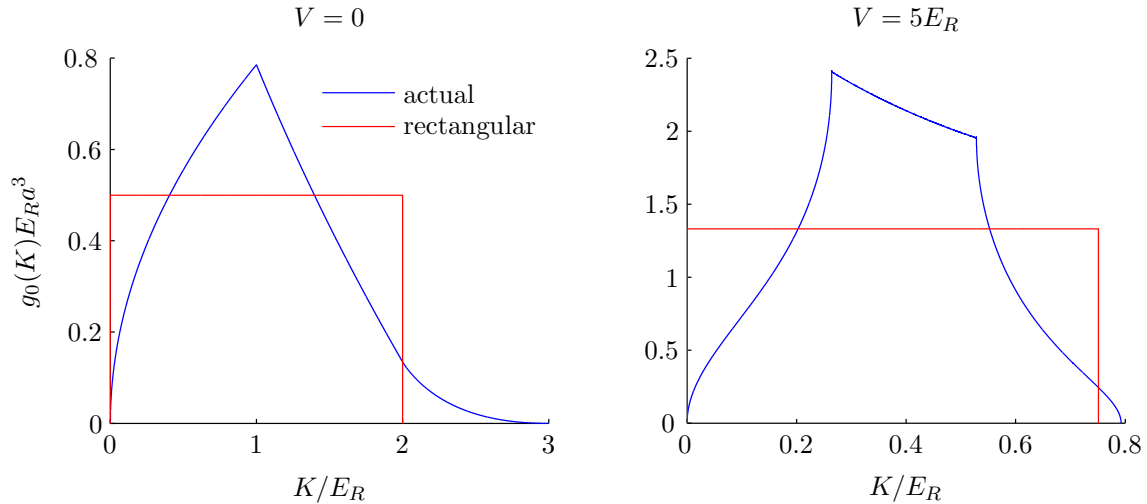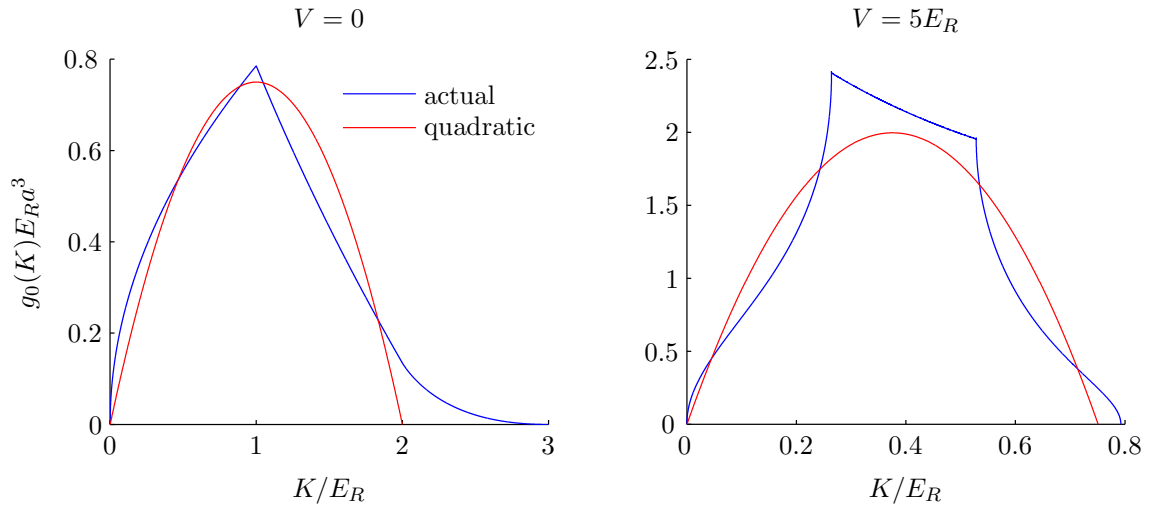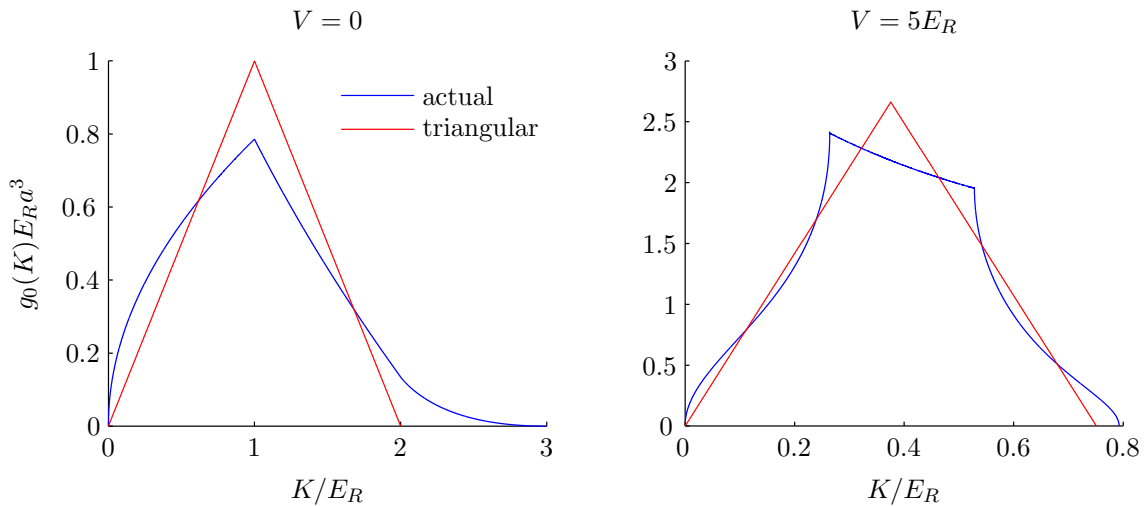

Figure 7.7: Comparison of exact cubic-lattice to triangular density of states

Using (4.4) and (I.1):

$$\tilde{n}_0(\mathbf{r}) = \frac{4}{w^2} \left[\zeta_2\big(ze^{-\beta V_{\text{tr}}(\mathbf{r})}\big) - 2\zeta_2\big(ze^{-\beta V_{\text{tr}}(\mathbf{r})-w/2}\big) + \zeta_2\big(ze^{-\beta V_{\text{tr}}(\mathbf{r})-w}\big) \right].$$

(7.24)

Then using (3.37) and (I.1) as for the other cases:

$$\tilde{N}_0 = \frac{4N_s}{w^2} \left[\zeta_{2+d/2}(z) - 2\zeta_{2+d/2}\big(ze^{-w/2}\big) + \zeta_{2+d/2}\big(ze^{-w}\big) \right]. \tag{7.25}$$

For $\mu \to 0$, again using (I.8) (convergent for $w < 2\pi$), for the translationally-invariant lattice:

$$\tilde{N}_0 = N_s \left[\frac{4\ln 2}{w} - \frac{1}{2} + \frac{w}{24} + O\big(w^3\big) \right], \tag{7.26}$$

and for the three-dimensional combined harmonic lattice:

$$\tilde{N}_0 = N_s \left[\zeta(3/2) - \frac{8\left(4 - \sqrt{2}\right)\sqrt{\pi w}}{15} - \frac{\zeta(1/2)w}{2} + O\big(w^2\big) \right]. \tag{7.27}$$

7.3 Non-interacting, ground-band-only critical temperature

7.3.1 Translationally-invariant

For the zero-delta band assumption with a translationally-invariant lattice, there is no condensation since, with the entire band at zero energy, any number of particles can be accommodated in the thermal cloud by making the chemical potential sufficiently close to zero. Likewise, for the rectangular band shape, or any approximate band shape with finite density at and beyond zero energy there is no condensation.[6] For the other band shapes, we may numerically solve (7.11), (7.17), (7.20) or (7.25). This is only valid for three dimensions, since we know from the effective mass results that there is no condensation in a one or two dimensional translationally-invariant lattice. For the centred-delta band shape we have from (7.12):

$$T_c^0 = \frac{W}{2k_B \ln(1 + N_s/N)}. \tag{7.28}$$

For comparison with approximate solutions for the other band shapes below, for $w \lesssim 1$ (say $N/N_s \geq 2$) the approximate solution is:

$$T_c^0 \approx \frac{W}{2k_B} \left(\frac{N}{N_s} + \frac{1}{2} \right). \tag{7.29}$$

---

[6]If the minimum height is $A > 0$ over some energy region including zero, $[0, K']$, then the density is $\tilde{n}_0(\mathbf{r}) > \int_0^{K'} A\mathrm{d}K/(e^{\beta(K-\mu)} - 1) \to \infty$ as $\mu \to 0$.

From the quadratic translationally-invariant results, for $w \lesssim 1$, the critical temperature is[7] $T_c^0 \approx W \left(N/N_s + \frac{1}{2} \right) /3k_B$ using (7.21) and for the triangular case the equivalent result is $T_c^0 \approx W \left(N/N_s + \frac{1}{2} \right) /4k_B \ln 2 \approx 0.36 W \left(N/N_s + \frac{1}{2} \right) /k_B$.

We plot the translationally-invariant critical temperatures as a function of lattice depth in figure 7.8. The approximate quadratic band formula $W \left(N/N_s + \frac{1}{2} \right) /3k_B$ is reasonable for $V \gtrsim 5 E_R$ except that for the $N/N_s = 0.1$ case, for which (7.20) would need to be solved. The importance of the low energy states to the translationally-invariant lattice, was discussed in section 7.1, where we observed that it improved the effective-mass results. For the approximate band shapes, the importance of the low energy states is to our disadvantage, since we approximate the low energy states poorly (in none of our simplified band assumptions in section 7.2 do we have $g(K) \propto \sqrt{K}$ for small K). We notice the difference between the $V = 0$ quadratic and triangular results in figure 7.8 further demonstrating the importance of the assumed band shape in this case. The importance of the accuracy of the band shape decreases when V increases, since the ratio $W/k_B T_c^0$ decreases.

7.3.2 One and two-dimensional combined harmonic lattice

In the one-dimensional case, we know from the effective mass results that there is no condensation. For two dimensions, we may numerically solve (7.11), (7.17), (7.20) or (7.25) for the critical temperature. We leave analytic results, numerical comparison and more accurate band shapes for the two-dimensional combined harmonic lattice for future work.

7.3.3 Three-dimensional combined harmonic lattice

For the zero-delta band shape we solve (7.9) to find the non-interacting critical temperature in that limit, as in [62]:

$$T_L^0 = \frac{m\omega^2 a^2}{2\pi k_B} \left[\frac{N}{\zeta(3/2)} \right]^{2/3}. \tag{7.30}$$

---

[7]From (7.19), for $w \gg 1$ we get the approximate critical temperature for the quadratic case $T_c^0 \to W\sqrt{N/6\zeta(2)N_s}/k_B \approx 0.32W\sqrt{N/N_s}/k_B$ (for the triangular case, the multiplier is $1/\sqrt{4\zeta(2)} \approx 0.39$ from (7.24)). However, for $w \gg 1$, the simplified band assumptions become poor approximations.
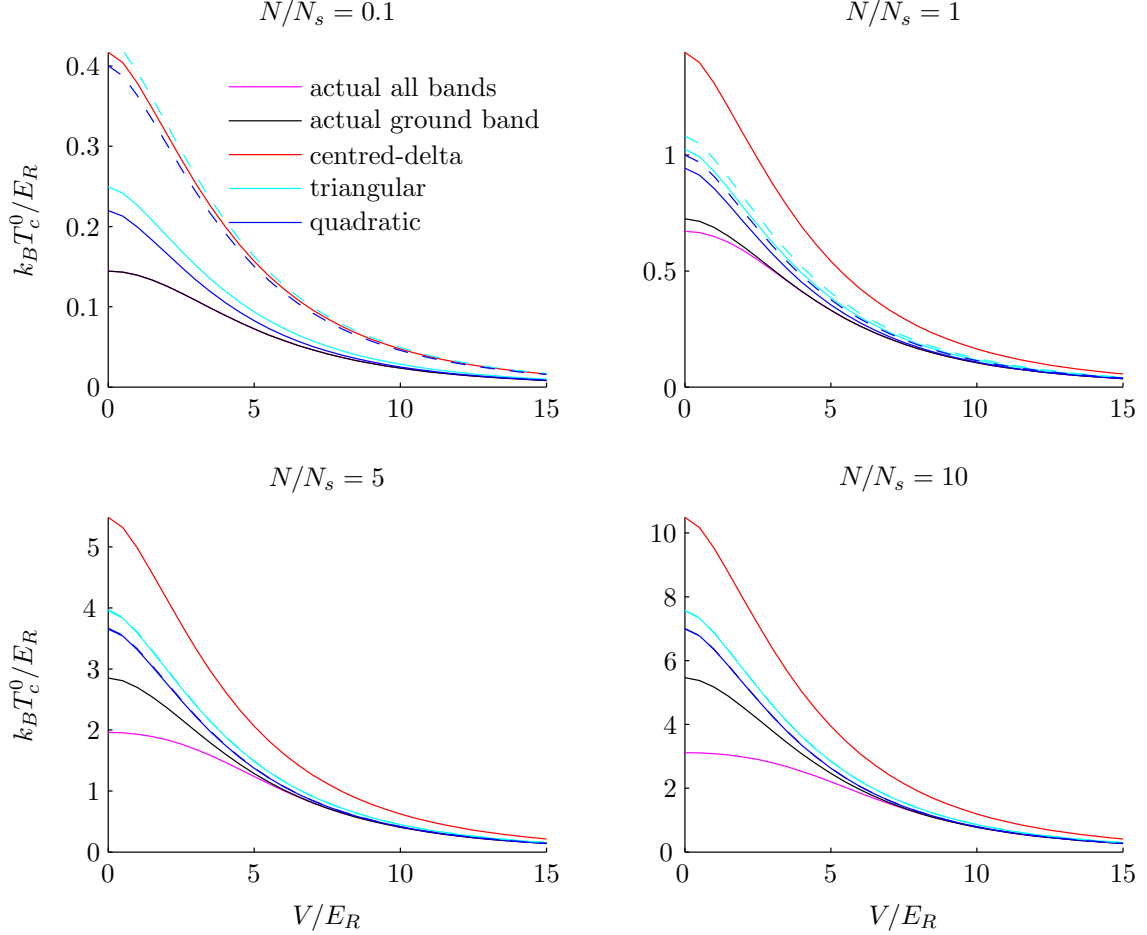
Figure 7.8: Three-dimensional translationally-invariant cubic-lattice ground-band non-interacting critical temperatures as a function of lattice depth. Solid curves were found by solving the Bose functions (7.20), (7.25) and (7.28). For the quadratic and triangular shapes, dashed curves are give the small w results $T_c^0 \approx W \left(N/N_s + \frac{1}{2} \right) / 3k_B$ and $T_c^0 \approx W \left(N/N_s + \frac{1}{2} \right) / 4k_B \ln 2$ respectively. In the $N/N_s = 0.1$ plot, the actual all and ground bands results are indistinguishable. For $N/N_s = 5$ and $N/N_s = 10$, the small w results are indistinguishable from the Bose function results.

From equations (7.15), (7.18), (7.22) and (7.27) in the previous sections, we get a series for the number of thermal atoms as a function of temperature when $\mu \to 0$. In the thermodynamic limit, this gives the total number of atoms, at the critical temperature. In each of these cases, the formula is of the form:

$$N = (k_B T)^{3/2} \left[A + B\sqrt{\frac{W}{k_B T}} + C\frac{W}{k_B T} + D\left(\frac{W}{k_B T}\right)^2 + O(w^3) \right]. \tag{7.31}$$

When we set $w \to 0$, we get the zero-delta result (7.30) in each case, showing that we have chosen functions whose limiting form is the delta function. For finite w this gives a series in integer powers of $\sqrt{W}$ about the zero-delta, $W = 0$, result. This can be viewed as an implicit Taylor series for the non-interacting critical temperature, T_c^0 about the zero-delta non-interacting critical temperature, T_L^0. Then, for the function $k_B T(\sqrt{W})$, the derivative of which at $W = 0$ is $k_B T'(0) = \left[dk_B T / d\sqrt{W} \right]_{W=0}$ we have:

$$k_B T_c^0 = k_B T_L^0 + k_B T'(0)\sqrt{W} + \frac{1}{2}k_B T''(0)W + \frac{1}{3!}k_B T'''(0)W^{3/2} + O(W^2). \quad (7.32)$$

The required derivatives are:

$$k_B T'(\sqrt{W}) = -\frac{\partial N / \partial \sqrt{W}}{\partial N / \partial k_B T}$$

$$= -\frac{Bk_B T + 2C\sqrt{W k_B T} + 4DW^{3/2}/\sqrt{k_B T}}{3A\sqrt{k_B T}/2 + B\sqrt{W} + CW/2\sqrt{k_B T} - DW^2/2(k_B T)^{3/2}}, \quad (7.33)$$

$$k_B T''(0) = \left[\frac{\partial k_B T'(\sqrt{W})}{\partial \sqrt{W}} \right]_{W=0} + \left[\frac{\partial k_B T'(\sqrt{W})}{\partial k_B T} \right]_{W=0} k_B T'(0) = \frac{2(B^2 - 2AC)}{3A^2}, \quad (7.34)$$

$$k_B T'''(0) = \left[\frac{\partial k_B T''(\sqrt{W})}{\partial \sqrt{W}} \right]_{W=0} + \left[\frac{\partial k_B T''(\sqrt{W})}{\partial k_B T} \right]_{W=0} k_B T'(0) = \frac{4}{27}\frac{18ABC - 5B^3}{A^3\sqrt{k_B T}}. \quad (7.35)$$

So, the effect of the band shape on the critical temperature is:

$$\frac{T_c^0 - T_L^0}{T_L^0} = -\frac{2B}{3A}\sqrt{w_L} + \frac{B^2 - 2AC}{3A^2}w_L + \frac{36ABC - 10B^3}{81A^3}w_L^{3/2} + O(w_L^2), \quad (7.36)$$

where $w_L = W/k_B T_L^0$.

For the quadratic band assumption, we have from (7.22):

$$-\frac{2B}{3A} = \frac{32\sqrt{\pi}}{35\zeta(3/2)} \approx 0.620, \quad (7.37)$$

$$\frac{B^2 - 2AC}{3A^2} = \frac{\zeta(3/2)\zeta(1/2) + 2304\pi/1225}{3(\zeta(3/2))^2} \approx 0.102, \quad (7.38)$$

$$\frac{36ABC - 10B^3}{81A^3} = 32\sqrt{\pi}\frac{\zeta(3/2)\zeta(1/2) + 256\pi/245}{105\zeta(3/2)^3} \approx -0.016, \quad (7.39)$$

so that we have:

$$(T_c^0 - T_L^0)/T_L^0 \approx 0.620\sqrt{w_L} + 0.102w_L - 0.016w_L^{3/2} + O(w_L^2). \quad (7.40)$$

Similarly for the triangular band assumption, from (7.27) we have:

$$\left(T_c^0 - T_L^0\right)/T_L^0 \approx 0.624\sqrt{w_L} + 0.105w_L - 0.015w_L^{3/2} + O\left(w_L^2\right), \qquad (7.41)$$

and we see that the coefficients are very similar. For a check on the extremities of the assumptions, we note that for the centred-delta assumption, we have from (7.15):

$$\left(T_c^0 - T_L^0\right)/T_L^0 \approx 0.640\sqrt{w_L} + 0.121w_L - 0.010w_L^{3/2} + O\left(w_L^2\right), \qquad (7.42)$$

and for the rectangular band assumption, we have from (7.18):

$$\left(T_c^0 - T_L^0\right)/T_L^0 \approx 0.603\sqrt{w_L} + 0.086w_L - 0.021w_L^{3/2} + O\left(w_L^2\right). \qquad (7.43)$$

These series are convergent for $w < 2\pi$ [117].[8] For small w_L, by considering the size of the coefficients above, we can omit some of the higher powers of w_L in these series. For example, the $w_L^{3/2}$ adjustment is small for $w_L < 1$. For large w_L, we can numerically solve the equations (7.11), (7.17), (7.20) and (7.25).

We plot these critical temperatures and compare to the full numerical non-interacting critical temperatures in figure 7.9. We use the extremes of experimental values of the trapping frequency and consider a wide range of the number of particles. We see that the centred-delta (7.11) and rectangular (7.17) do indeed provide extreme limits on the results. Since the density of states is nearly symmetrical (figure 7.6) for $V \geq 5E_R$ we expect the quadratic and triangular band shapes to give a good approximation for these lattice depths. For shallower lattices, we expect the approximation to remain acceptable when the critical temperature is greater than the width of the band (ignoring excited bands which are significant for shallow lattices and are considered in section 7.4). The width of the cubic-lattice ground band for $V = 0$ is $W = 2.0E_R$ (from figure 7.4) and we see that the quadratic and triangular results are reasonable even until $T_c^0 \approx W/2k_B$.

The quadratic assumption (7.20) is better than the triangular assumption (7.25) for low V (at least when $V < 5E_R$) and the triangular assumption is better for high V (both approximations are excellent in this range, so the difference is not observable on figure 7.9, for example when $V > 10E_R$).[9]

The series expansions (7.40), (7.41), (7.42) and (7.43) (dashed lines in figure 7.9) give very good results for $k_B T_c^0 > W/2$, virtually indistinguishable from the full

---

[8]The centred-delta series is convergent for $w < 4\pi$ since only $w/2$ appears in the Bose function, but the full centred-delta form (7.11) is more approximate than the quadratic and triangular forms.

[9]The triangular band assumption is better than the quadratic assumption throughout if we are trying to approximate the nearest-neighbours density of states.
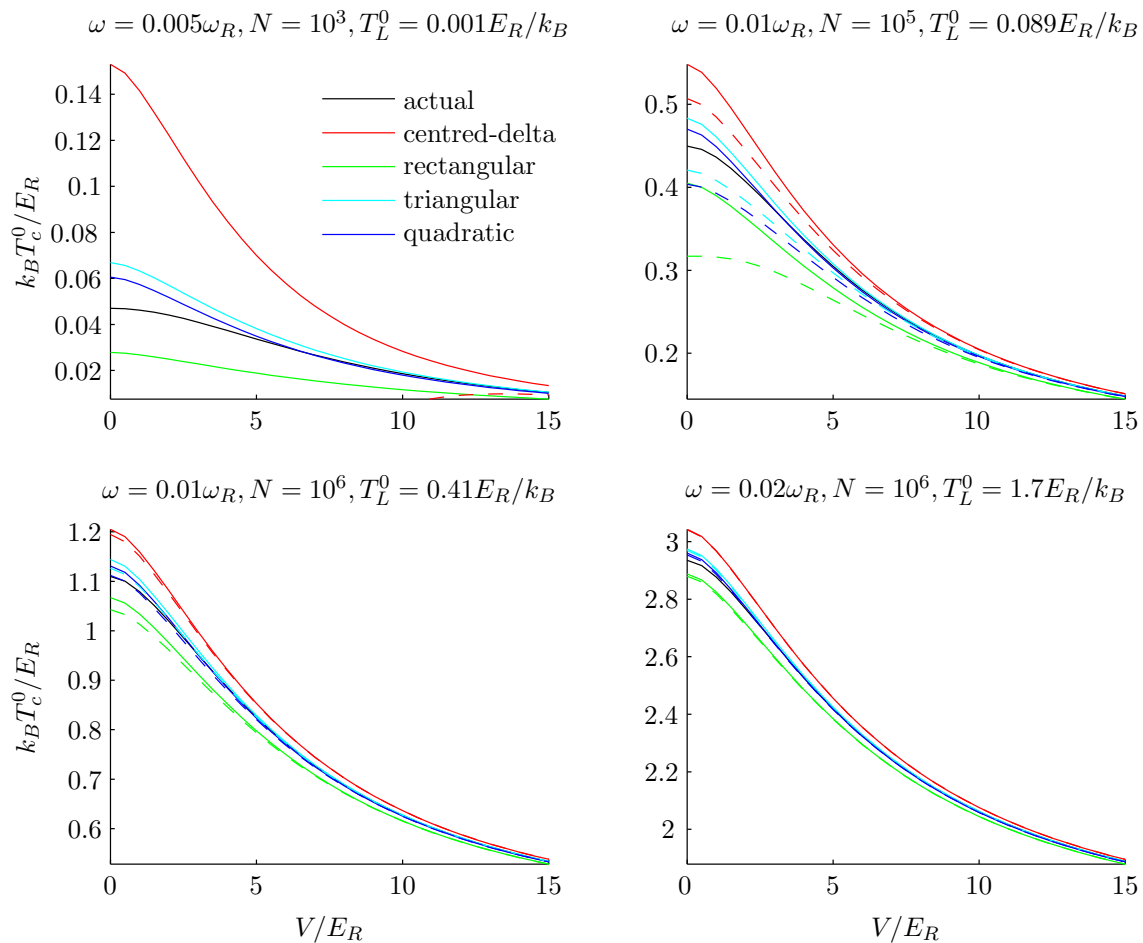
Figure 7.9: Three-dimensional combined harmonic cubic-lattice ground-band non-interacting critical temperatures as a function of lattice depth. Solid approximate forms are calculated by numerically solving (7.11), (7.17), (7.20) and (7.25). Dashed lines are calculated from (7.42), (7.43), (7.40) and (7.41). The dashed lines are indistinguishable from the solid curves for the lower-right plot, and the dashed lines approximations results are off the scale of the top-left plot.

Bose function solutions (equations (7.11), (7.17), (7.20) and (7.25)) even at $V = 0$ for $\omega = 0.02\omega_R, N = 10^6$ where $k_B T_c^0 > 0.7W$. The expansions are not convergent for $k_B T_c^0 < W/2\pi$ (except as discussed in footnote 8) and for the case with $\omega = 0.005\omega_R, N = 10^3$, the series expansions (the dashed lines in figure 7.9) are so poor that only the approximate form of the centred-delta result appears briefly on the plot, and the rest of the approximate shapes do not appear at all.

7.4 Excited bands

As in section 4.6, we set W_b to be the width of excited band b and $K_b^{\min}$ to be the minimum energy of the band. With a rectangular band assumption using (4.4) and (I.1) the thermal number per site at $\mathbf{r}$ in the excited bands is:

$$\tilde{n}_{b>0}(\mathbf{r}) = \sum_{b>0} \frac{k_B T}{W_b} \left[\zeta_1 \left(z e^{-\beta[V_{\mathrm{tr}}(\mathbf{r}) + K_b^{\min}]} \right) - \zeta_1 \left(z e^{-\beta[V_{\mathrm{tr}}(\mathbf{r}) + K_b^{\min} + W_b]} \right) \right]. \qquad (7.44)$$

Then using (3.37) and (I.1), the total thermal number in the excited bands is:

$$\tilde{N}_{b>0} = N_s \sum_{b>0} \frac{k_B T}{W_b} \left[\zeta_{1+d/2} \left(z e^{-\beta K_b^{\min}} \right) - \zeta_{1+d/2} \left(z e^{-\beta(K_b^{\min} + W_b)} \right) \right]. \qquad (7.45)$$

In the case where all excited bands are well above the current temperature ($k_B T \ll K_b^{\min}$ for $b > 0$), using the first term in (I.1) we have:

$$\tilde{N}_{b>0} \approx N_s \sum_{b>0} \frac{k_B T}{W_b} z e^{-\beta K_b^{\min}} \left(1 - e^{-\beta W_b} \right). \qquad (7.46)$$

A comparison of the actual to the approximate density of states, using the above approximation for the excited bands and the quadratic approximation for the ground band is given in figure 7.10. Of course, the approximation we are actually using is more drastic than we have used for the ground band since we use the first term of the Bose series in (7.47).
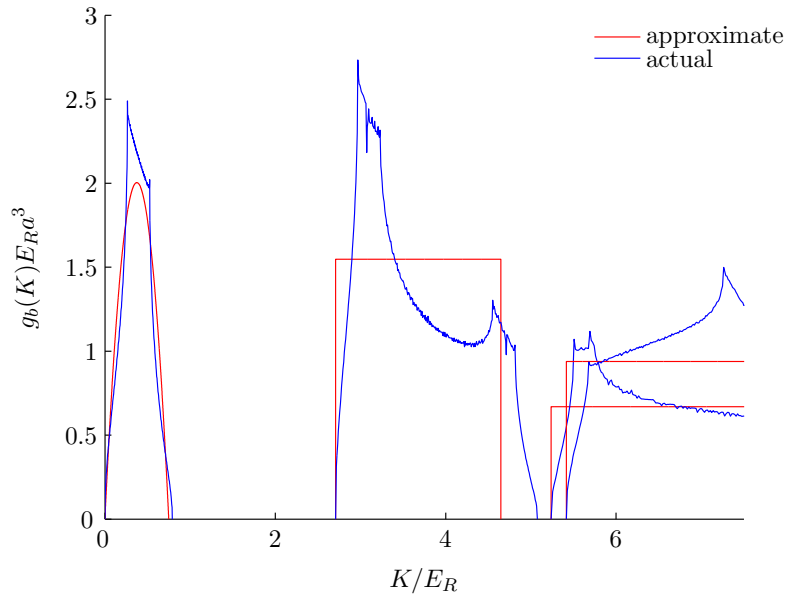
Figure 7.10: Quadratic approximation for the ground band and rectangular approximation for the exited bands for $V = 5E_R$ for the cubic lattice in three dimensions

To estimate the non-interacting critical temperature allowing for excited bands, we first obtain T_c^0 ignoring the excited bands using one of the methods above (for example (7.40)) then we calculate the number of atoms in the ground band, N_0, by adjusting for excited bands using, with $\mu \to 0$:

$$N_0 = N - N_s \sum_{b>0} \frac{k_B T_c^0}{W_b} e^{-K_b^{\min}/k_B T_c^0} \left(1 - e^{-W_b/k_B T_c^0}\right). \tag{7.47}$$

We then recalculate T_c^0 using, for example, (7.40) but replacing N in (7.40) with N_0. If $N - N_0$ is large then iteration on T_c^0 is recommended.

For the translationally-invariant lattice, over the range of parameters that we consider in figure 7.8, in the regions where adjustment for excited bands would be significant (all within $V \lesssim 5E_R$), the ground-band only approximations themselves are a poor representation of the actual ground-band critical temperatures (as we showed in figure 7.8). We therefore do not present approximate translationally-invariant lattice results allowing for excited bands. We accept that our simple band shape translationally-invariant lattice results are only reasonable for $V \gtrsim 5E_R$. However, we have shown in figure 7.2 that the effective-mass approximation is generally reasonable for $V \lesssim 5E_R$.

For the combined harmonic lattice, we compare results using this approximate approach to the full numerical calculation in figure 7.11. We use the quadratic assumption for the ground band by solving (7.20). For the extreme case $\omega = 0.005\omega_R$ the excited bands make negligible difference to any of the actual or approximate results for $N < 10^6$, so, unlike figure 7.9, we present the $N = 10^6$ result for that trapping frequency. We have iterated on T_c^0 where necessary (when the effect of excited bands is significant). The agreement between the full numerical calculation and the approximate calculation using (7.47) is excellent except near $V = 0$.
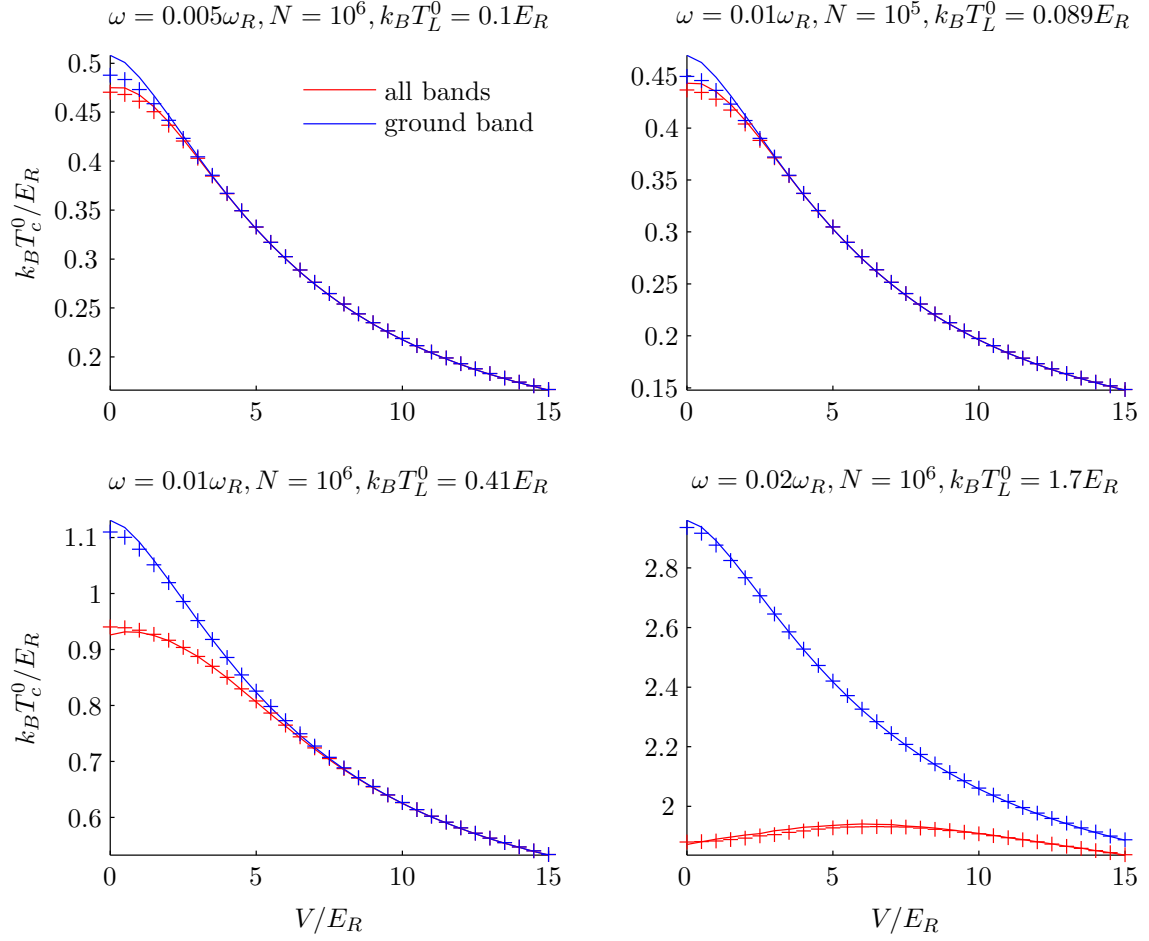
Figure 7.11: Effect of excited bands on the non-interacting critical temperature in a combined harmonic lattice using (7.47). Solid lines solve (7.20) for the ground band and use the method described in the text for excited bands, + results are from the full numerical calculation

7.5 Finite-size effect

In this section we find the effect on the critical temperature, $\delta T_c^{\text{fs}} = T_c^{\text{fs}} - T_c^0$, of a positive chemical potential at condensation, equal to the energy of the ground state, $\mu_{\text{fs}} = 3\hbar\bar{\omega}^*/2$ (from (5.18), as we consider only the three-dimensional combined harmonic lattice). We only consider the finite-size effect due to a positive chemical potential (which was shown to give good agreement to the full diagonalisation in section 6.1). We consider only the effect on the ground band.

We introduce some explicit notation used only in this section, in section 7.6 on the interaction shift, and in the corresponding explanatory appendices. Generally through-

out this thesis, a given formula has one temperature, one chemical potential and one interaction coefficient. In these sections, we explore the effect of changing the chemical potential and the interaction coefficient on the temperature, so we introduce explicit notation for these sections only. For the ground-band thermal atoms calculated at temperature T, chemical potential μ and interaction coefficient U, we label the ground-band thermal number per site at $\mathbf{r}$ (elsewhere labelled $\tilde{n}_0(\mathbf{r})$ where 0 refers to the ground band) to be $\tilde{n}_T^U(\mathbf{r}, \mu)$ and the total ground-band thermal number (elsewhere labelled $\tilde{N}_0$) to be $\tilde{N}_T^U(\mu)$. In this section we keep $U = 0$, we consider $U > 0$ in section 7.6.

We expand in a Taylor series about the $\mu \to 0$ critical temperature, T_c^0:

$$\tilde{N}_{T_c^{\text{fs}}}^0(\mu_{\text{fs}}) = \tilde{N}_{T_c^0}^0(0) + \delta T_c^{\text{fs}} \left[\frac{\partial \tilde{N}_T^0(0)}{\partial T} \right]_{T=T_c^0} + \mu_{\text{fs}} \left[\frac{\partial \tilde{N}_{T_c^0}^0(\mu)}{\partial \mu} \right]_{\mu=0}. \tag{7.48}$$

By the definition of the respective critical temperatures, we have $\tilde{N}_{T_c^0}^0(0) = N = \tilde{N}_{T_c^{\text{fs}}}^0(\mu_{\text{fs}})$ so that:

$$\delta T_c^{\text{fs}} = -\mu_{\text{fs}} \frac{\left[\dfrac{\partial \tilde{N}_{T_c^0}^0(\mu)}{\partial \mu} \right]_{\mu=0}}{\left[\dfrac{\partial \tilde{N}_T^0(0)}{\partial T} \right]_{T=T_c^0}}. \tag{7.49}$$

For the quadratic band assumption, from (7.20), (I.7) and (I.8) we get the following expressions for the required derivatives (the results in terms of Bose functions, valid for a wider range of w are given in appendix K.3):

$$\left[\frac{\partial \tilde{N}_T^0(\mu)}{\partial \mu} \right]_{\mu=0} = \frac{N_s}{k_B T} \left[\frac{8\sqrt{\pi}}{5\sqrt{w}} + \zeta(1/2) + O(w) \right], \tag{7.50}$$

$$\frac{\partial \tilde{N}_T^0(0)}{\partial T} = \frac{N_s}{T} \left[\frac{3}{2}\zeta(3/2) - \frac{48\sqrt{\pi w}}{35} - \frac{\zeta(1/2)}{4}w + O(w^2) \right]. \tag{7.51}$$

From (7.49), (7.50) and (7.51) we get:

$$\delta T_c^{\text{fs}} = -\frac{\mu_{\text{fs}}}{k_B} \left[\frac{16\sqrt{\pi}}{15\zeta(3/2)\sqrt{w_c^0}} + \frac{2\zeta(1/2)}{3\zeta(3/2)} + \frac{512\pi}{525\zeta(3/2)^2} + O\left(\sqrt{w_c^0}\right) \right]$$

$$\approx -\frac{\mu_{\text{fs}}}{k_B} \left[\frac{0.72}{\sqrt{w_c^0}} + 0.076 \right], \tag{7.52}$$

where $w_c^0 = W/k_B T_c^0$. In appendix K.4, we derive similar results for the triangular

band assumption:

$$\delta T_c^{\text{fs}} = -\frac{\mu_{\text{fs}}}{k_B}\left[\frac{16(2-\sqrt{2})\sqrt{\pi}}{9\zeta(3/2)\sqrt{w_c^0}} + \frac{2\zeta(1/2)}{3\zeta(3/2)} + \frac{512(5-3\sqrt{2})\pi}{405\zeta(3/2)^2} + O\left(\sqrt{w_c^0}\right)\right]$$

$$\approx -\frac{\mu_{\text{fs}}}{k_B}\left[\frac{0.71}{\sqrt{w_c^0}} + 0.068\right]. \tag{7.53}$$

For a cubic lattice, using the nearest-neighbour effective mass from (H.4), so that $\bar{\omega}^* = \bar{\omega}\pi\sqrt{J/E_R}$ (we have defined $\bar{\omega} = (\omega_x + \omega_y + \omega_z)/3$) and using the nearest-neighbour assumption $W = 12J$ from (D.19), we have $\mu_{\text{fs}} = \sqrt{3W/E_R}\pi\hbar\bar{\omega}/4$. In this limit, the highest order finite-size shift in (7.52) is independent of W (except as W influences T_c^0):

$$\delta T_c^{\text{fs}} \approx -\frac{\sqrt{3}\pi\hbar\bar{\omega}}{4k_B}\left\{\frac{16\sqrt{\pi}}{15\zeta(3/2)}\sqrt{\frac{k_B T_c^0}{E_R}} + \left[\frac{2\zeta(1/2)}{3\zeta(3/2)} + \frac{512\pi}{525\zeta(3/2)^2}\right]\sqrt{\frac{W}{E_R}} + O(W)\right\}. \tag{7.54}$$

In the zero-delta, $W \to 0$, limit, we have using (7.30):

$$\frac{\delta T_c^{\text{fs}}}{T_L^0} = -\frac{8\sqrt{3}\pi}{15\zeta(3/2)^{2/3}}\frac{\bar{\omega}}{\omega}N^{-1/3} \approx -1.53\frac{\bar{\omega}}{\omega}N^{-1/3}. \tag{7.55}$$

The equivalent result for the triangular band approximation is:

$$\frac{\delta T_c^{\text{fs}}}{T_L^0} = -\frac{8\sqrt{3}(2-\sqrt{2})\pi}{9\zeta(3/2)^{2/3}}\frac{\bar{\omega}}{\omega}N^{-1/3} \approx -1.49\frac{\bar{\omega}}{\omega}N^{-1/3}. \tag{7.56}$$

We compare the finite-size effect using the quadratic assumption to the full numerical calculation in figure 7.12. The shift given by (7.52) is a reasonable approximation to the ground-band shift where the series expansion is valid. The zero-delta limit is not valid in the extreme $\omega = 0.005\omega_R, N = 10^3$ case, but with these parameters, the series expansion is not valid throughout. The effective-mass finite-size effect (7.5) is exact at $V = 0$ for the all bands results and we can see that it remains a good approximation for the $\omega = 0.005\omega_R, N = 10^3$ case.
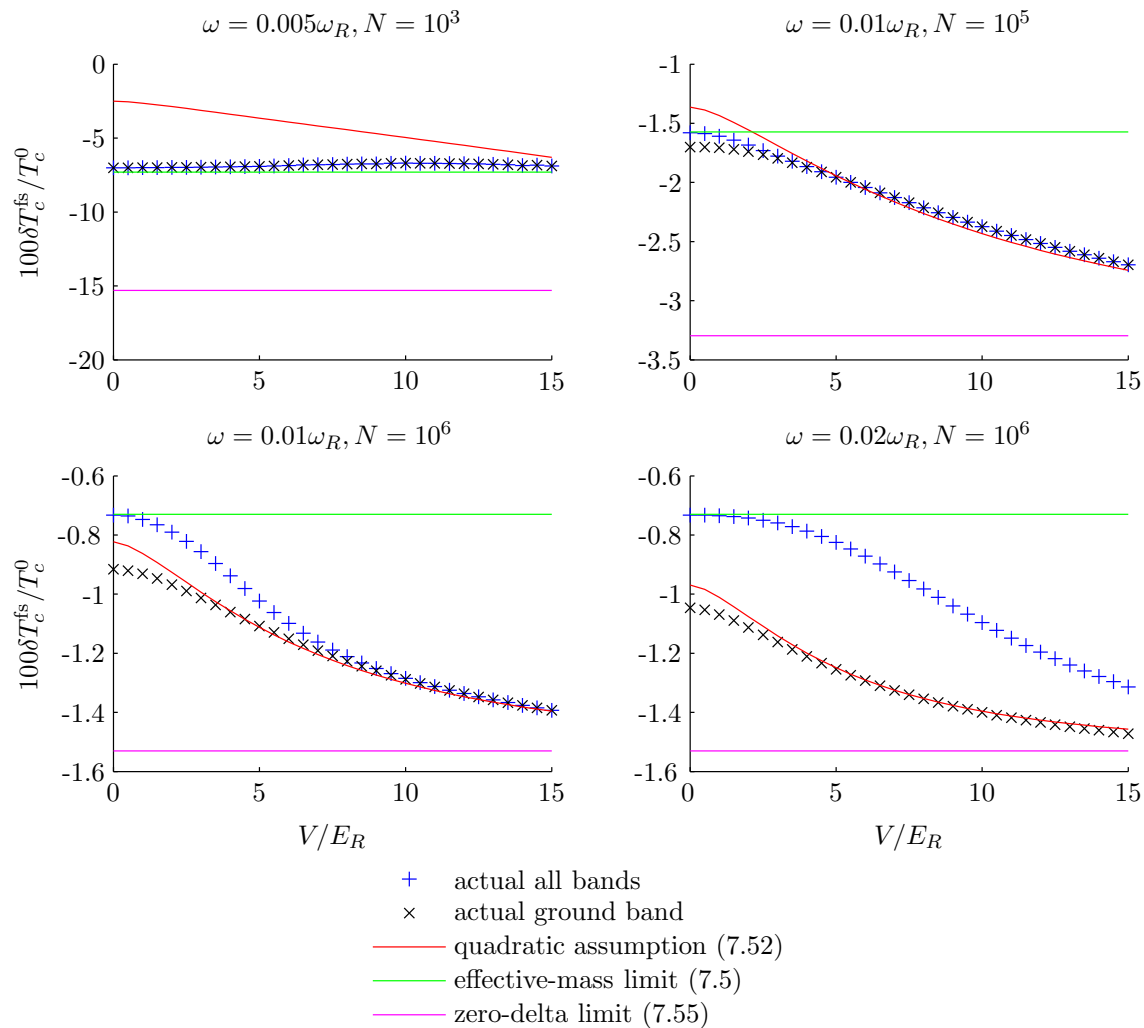
Figure 7.12: Finite-size effect on the combined harmonic non-interacting ground-band critical temperature

7.6   Mean-field critical temperature

In this section we find the effect of ground-band mean-field interactions on the critical temperature: $\delta T_c = T_c - T_c^0$ where T_c is the critical temperature of a interacting gas in a three-dimensional combined harmonic lattice. We allow for interactions within the ground band only. We do not estimate the translationally-invariant lattice interacting critical temperature, since there is no mean-field shift, the leading order correction being due to critical fluctuations.

We will use a Taylor series expansion of the number of thermal atoms about the critical point. Our overall approach is similar to the work of [54] for the trapped, no lattice

case.[10] However, in our case, the non-interacting gas has some divergent properties at condensation ($\mu \to 0$) in the limit $w \to 0$. For example, the density at the centre of the harmonic trap from (7.10) and the derivative of the thermal number with respect to μ from (7.50) are both infinite as $w \to 0$.[11] At $V = 15E_R$, we have from figure 7.4 that $W \approx 0.1E_R$ and from figure 7.11 $k_B T_c^0$ at $V = 15E_R$ is up to $2E_R$ (for the trap frequencies and atom numbers we consider), so that the thermal width is close to zero, $w \approx 0.05$. The effect of repulsive interactions is to force atoms away from the centre of the trap and, as we shall see, decrease the critical temperature. As we initially turn on the interaction parameter, U, the effect of moving away from the near-divergent properties is significant. Further increasing the interaction parameter has a more moderate effect. We want to use a linear Taylor series expansion. If we were to use the central density and derivatives at the non-interacting critical temperature when calculating the interaction effect, the result would be significantly overstated, particularly for deep lattices. We therefore use the first terms in a Taylor series about the interacting critical temperature T_c (what we are solving for, analogous to the Brillouin-Wigner perturbation expansion given in [118]) rather than about the non-interacting critical temperature, T_c^0 to get:

$$\tilde{N}_{T_c^0}^0(0) \approx \tilde{N}_{T_c}^U(\mu) - \delta T_c \left[\frac{\partial \tilde{N}_T^U(\mu)}{\partial T} \right]_{T=T_c} - \mu \left[\frac{\partial \tilde{N}_{T_c}^U(\mu)}{\partial \mu} \right]_\mu - U \left[\frac{\partial \tilde{N}_{T_c}^U(\mu)}{\partial U} \right]_U . \quad (7.57)$$

By the definition of the respective critical temperatures, we have $\tilde{N}_{T_c^0}^0(0) = N = \tilde{N}_{T_c}^U(\mu)$ so that:

$$\delta T_c \approx -\frac{\mu \left[\dfrac{\partial \tilde{N}_{T_c}^U(\mu)}{\partial \mu} \right]_\mu + U \left[\dfrac{\partial \tilde{N}_{T_c}^U(\mu)}{\partial U} \right]_U}{\left[\dfrac{\partial \tilde{N}_T^U(\mu)}{\partial T} \right]_{T=T_c}}. \quad (7.58)$$

However, to first order in U and μ, this result can be simplified by considering:

$$\left[\frac{\partial \tilde{N}_T^U(\mu)}{\partial T} \right]_{T=T_c} \approx \left[\frac{\partial \tilde{N}_T^0(0)}{\partial T} \right]_{T=T_c} + U \left[\frac{\partial^2 \tilde{N}_T^U(0)}{\partial T \partial U} \right]_{\substack{T=T_c \\ U=0}} + \mu \left[\frac{\partial^2 \tilde{N}_T^0(\mu)}{\partial T \partial \mu} \right]_{\substack{T=T_c \\ \mu=0}} . \quad (7.59)$$

---

[10]Our presentation, for example our (7.61), is somewhat different from that of [54], but we would get the same final result using their method.

[11]We note that the finite-size effect does not have the same problem as $w \to 0$, since although $\partial \tilde{N}/\partial \mu$ is divergent, we also have $\mu_{\text{fs}} \to 0$ and their product is finite, as shown in (7.55). We include the finite-size effect in this interaction calculation for a coherent treatment, but if the finite-size effect alone is being calculated, the methods of the previous section are sufficient.

By substituting (7.59) into (7.58) and expanding the reciprocal, to first order in U and μ we can ignore the last two terms in (7.59). Using similar equations for the other derivatives in (7.58), we find:

$$\delta T_c \approx -\frac{\mu \left[\dfrac{\partial \tilde{N}_{T_c}^0(\mu)}{\partial \mu}\right]_{\mu=0} + U \left[\dfrac{\partial \tilde{N}_{T_c}^U(0)}{\partial U}\right]_{U=0}}{\left[\dfrac{\partial \tilde{N}_T^0(0)}{\partial T}\right]_{T=T_c}}. \tag{7.60}$$

Above the critical temperature, to zeroth order in U and μ (since this will be multiplied by U), from (3.42):

$$\frac{\partial E_0(\mathbf{k}, \mathbf{r})}{\partial U} = -2\tilde{n}_T^U(\mathbf{r}, \mu)\frac{\partial E_0(\mathbf{k}, \mathbf{r})}{\partial \mu}. \tag{7.61}$$

So, by differentiating (4.4) with respect to U, then using (7.61) and using the derivative of (4.4) with respect to μ:

$$\frac{\partial \tilde{n}_T^U(\mathbf{r}, \mu)}{\partial U} = -2\tilde{n}_T^U(\mathbf{r}, \mu)\frac{\partial \tilde{n}_T^U(\mathbf{r}, \mu)}{\partial \mu}. \tag{7.62}$$

Integrating with respect to $\mathbf{r}$:

$$\frac{\partial \tilde{N}_T^U(\mu)}{\partial U} = -\frac{2}{a^3} \int \mathrm{d}\mathbf{r}\, \tilde{n}_T^U(\mathbf{r}, \mu)\frac{\partial \tilde{n}_T^U(\mathbf{r}, \mu)}{\partial \mu}. \tag{7.63}$$

Condensation occurs when the chemical potential reaches value of the lowest energy (interacting) state of the Hamiltonian, which from (3.42) (coming from above the critical temperature) is when $\mu \to \mu_{\mathrm{fs}} + 2U\tilde{n}_T^0(\mathbf{0}, 0)$ to lowest order in U. Then we have (in the same form as the trapped, no lattice shift of [54]):

$$\delta T_c = -\left\{\mu_{\mathrm{fs}} + 2U[1 - S(w_c)]\tilde{n}_{T_c}^0(\mathbf{0}, 0)\right\} \frac{\left[\dfrac{\partial \tilde{N}_{T_c}^0(\mu)}{\partial \mu}\right]_{\mu=0}}{\left[\dfrac{\partial \tilde{N}_T^0(0)}{\partial T}\right]_{T=T_c}}, \tag{7.64}$$

where we have defined $w_c \equiv W/k_B T_c$ and the spread function $S(w)$ considered in the next section.

7.6.1 Spread function

The function $S(w)$ measures of the spread of the number density weighted by its rate of change with respect to the chemical potential:

$$S(w) \equiv \frac{\int \mathrm{d}\mathbf{r}\, \tilde{n}_T^0(\mathbf{r}, 0) \left[\frac{\partial \tilde{n}_T^0(\mathbf{r}, \mu)}{\partial \mu} \right]_{\mu=0}}{\int \mathrm{d}\mathbf{r}\, \tilde{n}_T^0(\mathbf{0}, 0) \left[\frac{\partial \tilde{n}_T^0(\mathbf{r}, \mu)}{\partial \mu} \right]_{\mu=0}} = \frac{\int \mathrm{d}\mathbf{r}\, \tilde{n}_T^0(\mathbf{r}, 0) \left[\frac{\partial \tilde{n}_T^0(\mathbf{r}, \mu)}{\partial \mu} \right]_{\mu=0}}{a^3 \tilde{n}_T^0(\mathbf{0}, 0) \left[\frac{\partial \tilde{N}_T^0(\mu)}{\partial \mu} \right]_{\mu=0}}. \tag{7.65}$$

Since any change of the variables $\mathbf{r}$ in the integrals of $S(w)$ gives the same factor in the numerator and the denominator, we note that $S(w)$ depends on W and T only through the ratio w (since other T dependence is as a multiple of r_i) and on the band shape assumed (for example centred-delta, quadratic or triangular). In particular, $S(w)$ is independent of the harmonic trap frequencies ω_i.

We note that for a gas with no lattice in a three-dimensional harmonic trap we have [54]:

$$S = \frac{1}{\zeta(3/2)\zeta(2)} \sum_{j,k=1}^{\infty} \frac{1}{\sqrt{j}[k(j+k)]^{3/2}} = 0.281. \tag{7.66}$$

In appendix L we derive the following analytic formula for $S(w)$ in the centred-delta approximation (we note that the Bose functions $\zeta_{-1/2}(e^{-w/2})$ and $\zeta_{1/2}(e^{-w/2})$ are finite for $w > 0$):

$$S(w) = \frac{e^{w/2} - 1}{2} \left[\frac{\zeta_{-1/2}(e^{-w/2})}{\zeta_{1/2}(e^{-w/2})} - 1 \right]. \tag{7.67}$$

Using (I.8) we get following series, which is convergent for $w < 4\pi$:

$$S(w) = \frac{1}{4} - \frac{\zeta(1/2)}{4\sqrt{2\pi}}\sqrt{w} - \left[\frac{3}{16} - \frac{\zeta(1/2)^2}{8\pi} \right] w + O(w^{3/2}). \tag{7.68}$$

So, for the zero-delta approximation, $S(0) = 1/4$. From (I.1) we get the expansion for $w \gg 1$, although we note that the centred-delta approximation is poor for $w \gg 1$:

$$S(w) = \frac{1}{2\sqrt{2}} - \left(\frac{1}{4} + \frac{1}{2\sqrt{2}} - \frac{1}{\sqrt{3}} \right) e^{-w/2} + O(e^{-w}). \tag{7.69}$$

The rectangular band assumption, due to its finite density of states at zero energy, is not sufficiently representative of the actual density of states to give a reasonable

estimate for $S(w)$. For that assumption we show in appendix L that $S(w) = 0$ and from (7.16), we note that $\tilde{n}_T^0(\mathbf{0}, 0)$ is divergent even for $w > 0$.

As we show in appendix L, for both the quadratic and triangular band assumptions, as $w \to \infty$ we have:

$$S(w) \to \frac{1}{\zeta(2)\zeta(5/2)} \sum_{j,k=1}^{\infty} \frac{1}{j^2 k(j+k)^{3/2}} \approx 0.325. \tag{7.70}$$

We have evaluated $S(w)$ numerically as shown in figure 7.13 below. We only show the result for $w < 2\pi$ since the expansions we will use below are valid only in that region. We see from figure 7.13 that as $w \to 0$, $S(w) \to 0.24$ for both the quadratic and triangular cases. In both cases we always have $0.240 < S(w) < 0.325$.
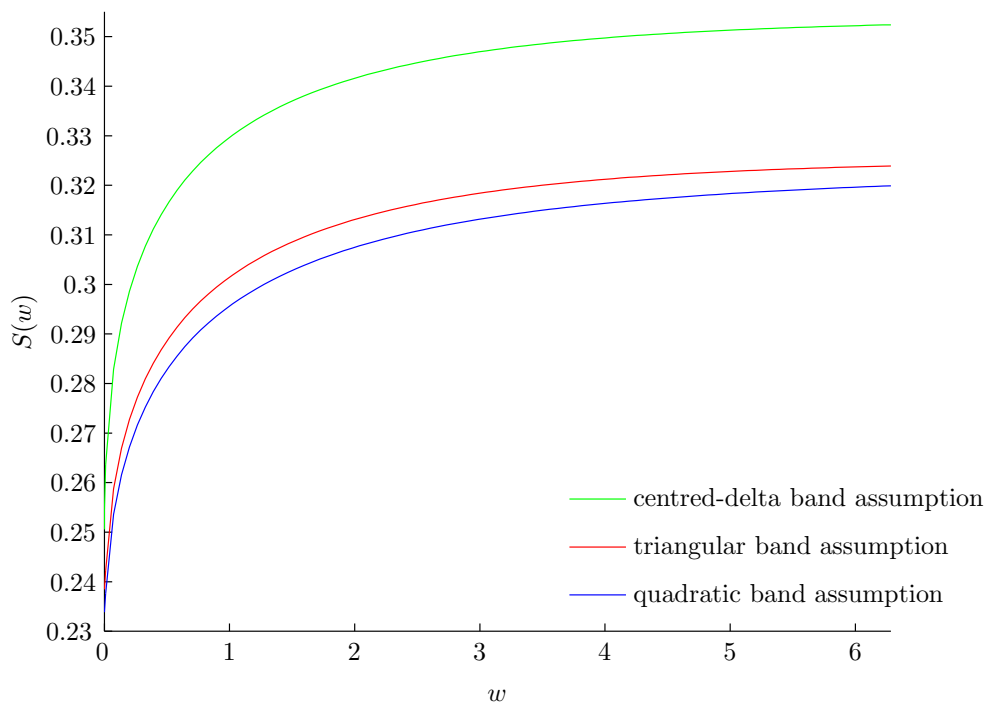
Figure 7.13: $S(w)$

7.6.2 Interaction shift

For the centred delta case, we have from (7.64), (7.10), (7.67), (K.1) and (K.3) we get the analytic result:

$$
\delta T_c = -\frac{\left(\mu_{\mathrm{fs}} + \dfrac{2U}{e^{w_c/2} - 1}\right) 2\zeta_{1/2}\left(e^{-w_c/2}\right) - 2U\left[\zeta_{-1/2}\left(e^{-w_c/2}\right) - \zeta_{1/2}\left(e^{-w_c/2}\right)\right]}{k_B\left[3\zeta_{3/2}\left(e^{-w_c/2}\right) + w_c\zeta_{1/2}\left(e^{-w_c/2}\right)\right]} \tag{7.71}
$$

$$
= -\left(\mu_{\mathrm{fs}} + 3\frac{U}{w_c}\right)\frac{2\sqrt{2\pi}}{3\zeta(3/2)k_B\sqrt{w_c}} + O(\mu_{\mathrm{fs}}) + O\left(\frac{U}{w_c}\right)
$$

$$
\approx -0.6\frac{\mu_{\mathrm{fs}}}{k_B}\sqrt{\frac{k_B T_c}{W}} - 1.9\frac{U}{k_B}\left(\frac{k_B T_c}{W}\right)^{3/2},
$$

where in the series expansion in w_c using (I.8), we have taken first terms for each of the μ_{fs} and U components. We follow the same approach for the expansions for the quadratic and triangular cases below.

For the quadratic case, we have from (7.19) and (I.8):

$$
\tilde{n}_T^0(\mathbf{0}, 0) = \frac{3}{w} - \frac{1}{2} + O(w). \tag{7.72}
$$

From (7.50), (7.51), (7.64) and (7.72) we get (we omit the higher order terms in (7.53) which could be included if accurate calculations of $S(w_c)$ are used):

$$
\delta T_c \approx -\left\{\mu_{\mathrm{fs}} + 6\frac{U[1 - S(w_c)]}{w_c}\right\}\frac{16\sqrt{\pi}}{15\zeta(3/2)k_B\sqrt{w_c}}
$$

$$
\approx -0.72\frac{\mu_{\mathrm{fs}}}{k_B\sqrt{w_c}} - 4.34\frac{U[1 - S(w_c)]}{k_B w_c^{3/2}}. \tag{7.73}
$$

From this result, it is clear why we cannot get a result for the interaction shift in the zero-delta band assumption, $w_c \to 0$ limit. In appendix K.3, we derive similar results for the triangular band assumption:

$$
\delta T_c = -\left\{\mu_{\mathrm{fs}} + 8\ln 2\frac{U[1 - S(w_c)]}{w_c}\right\}\frac{16(2 - \sqrt{2})\sqrt{\pi}}{9\zeta(3/2)k_B\sqrt{w_c}}
$$

$$
\approx -0.71\frac{\mu_{\mathrm{fs}}}{k_B\sqrt{w_c}} - 3.92\frac{U[1 - S(w_c)]}{k_B w_c^{3/2}}. \tag{7.74}
$$

Using the approximation $S(w_c) \approx 0.3$, we get the approximate shift for both the quadratic and triangular cases:

$$
\delta T_c = T_c - T_c^0 \approx -0.7\frac{\mu_{\mathrm{fs}}}{k_B}\sqrt{\frac{k_B T_c}{W}} - 3\frac{U}{k_B}\left(\frac{k_B T_c}{W}\right)^{3/2}, \tag{7.75}
$$

which we need to solve self-consistently for T_c.

7.6.3   Excited bands

When interaction in excited bands is significant, the approximate methods we present in this chapter are not adequate. However, over a wide regime of experimental interest, it will be sufficient to treat the small excited-band occupation that occurs as non-interacting. We note that the interacting critical temperature is often significantly reduced from the ideal value, so that the influence of excited bands may be very different at T_c compared to T_c^0. Therefore, we may not simply take T_c^0 from (7.47) and add δT_c from (7.75). The approach we use is:

1. Calculate an initial estimate of the non-interacting critical temperature, T_c^0.

2. Calculate the ground-band interaction shift δT_c using (7.75). We do not adjust δT_c in the remainder of the calculation.

3. Calculate the ground-band number N_0 from (7.47), but using the temperature $T_c^0 + \delta T_c$.

4. Recalculate the non-interacting critical temperature, T_c^0 using N_0. We do not use a δT_c adjustment in this calculation (other than the adjusted N_0 from step 3), so that if the effect of excited bands is insignificant, the resulting interacting critical temperature is as in (7.75) as intended.

5. Iterate steps 3 and 4 to find T_c^0 if necessary.

6. The critical temperature allowing for interactions in the ground band, with an adjustment for non-interacting excited bands is then $T_c^0 + \delta T_c$.

7.6.4   Results

We compare our ground-band only and all-bands approximations to the results from the full numerical calculation in figure 7.14. We have ignored the finite-size effect which was considered in figure 7.12. We have used $a = 425$ nm as in [76] and a scattering length of $a_s = 5.77$ nm. The approximate results for the $\omega = 0.005\omega_R, N = 10^3$ case are poor since the series expansion used is invalid in that region. Otherwise, for high V/E_R, the approximate results are good because the critical temperature is so low that excited bands are unimportant. For low V/E_R the approximate results are good when excited bands are insignificant, and still fair when excited bands have some effect, since
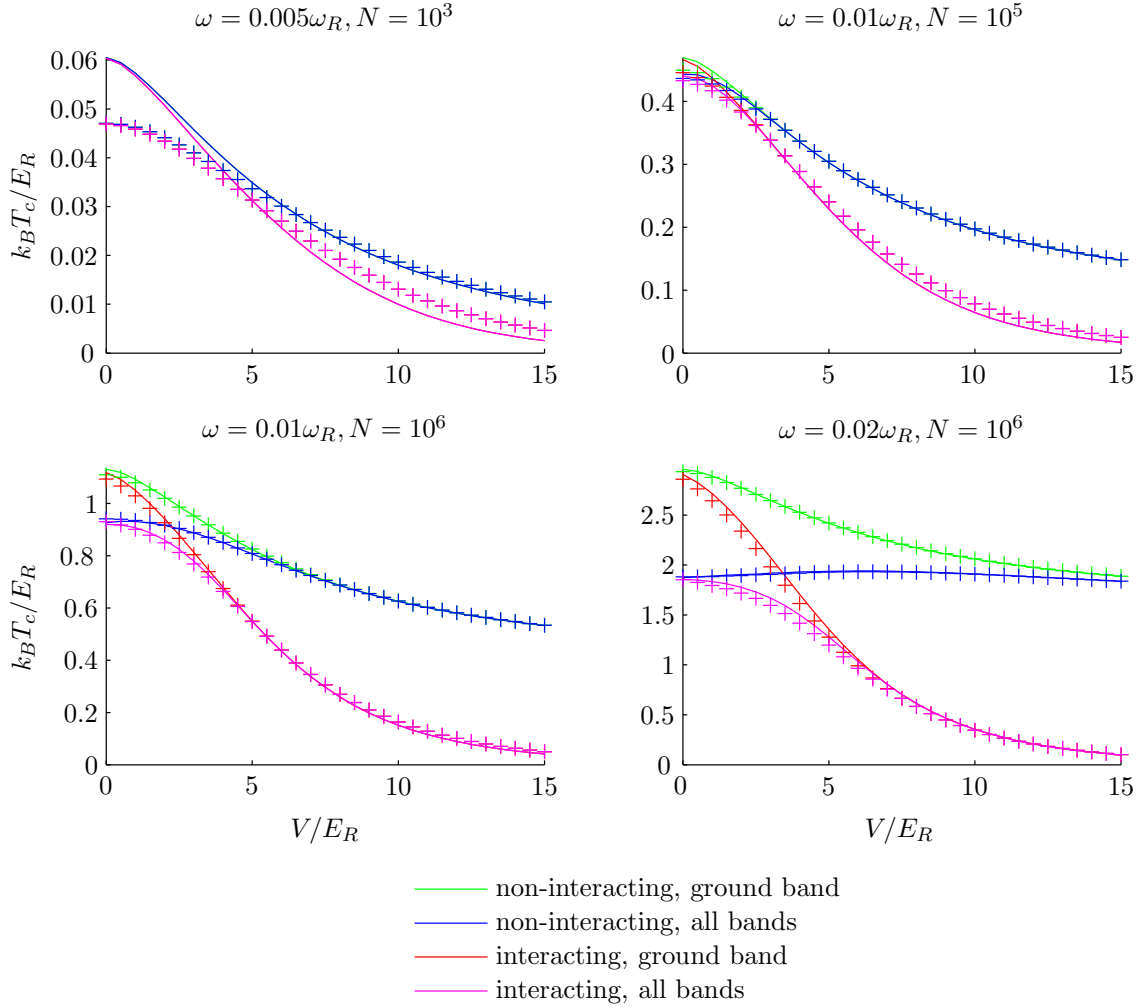
Figure 7.14: Solid lines use the quadratic approximation, + results are from the full numerical calculation

interactions have less impact for low V/E_R. We must emphasise that the full numerical interacting calculation itself uses significant approximations in the low V/E_R region, particularly when excited bands are significant, as discussed in previous chapters.

We see from (7.75) and figure 7.14 that the effect of interactions increases as the lattice depth increases and w decreases. The resulting decrease in critical temperature means that the effect of excited bands on the critical temperature decreases as the lattice depth increases.

7.7   Summary

We have analytically derived novel, practical formulae for the critical temperature in an optical lattice by using simplified shapes for the density of states. We have considered both the translationally-invariant lattice and the combined harmonic lattice. For the non-interacting case we have shown that our validity range (low to moderate thermal width) is complementary to that of the effective-mass approximation (high thermal width). By using the average energy of the band to calculate the width in (7.7), we have extended the validity range, at least for the non-interacting case, into shallow lattices. We have considered a number of possible approximate band shapes: the extreme simplicity of the centred-delta and rectangular shapes and the reasonable fit of the quadratic and triangular cases.

We have compared our results to full numerical calculations and have generally found good agreement. When calculating critical temperatures by solving the Bose functions, for example in (7.20), we get very good agreement and when we use the simple formulae, for example (7.40) we get generally good results for $w \ll 2\pi$.

We have derived a simple, effective adjustment for excited bands (7.47) and a simple formula for the finite-size effect (7.52). We have derived an adjustment for mean-field interactions in the ground band (7.75) which is valid whenever the simplified band shape is valid. This result is fully analytically derived in the centred-delta case and analytically derived in the quadratic and triangular cases except for the spread function for which we have analytically derived the large w limit and numerically shown it to vary over the moderate range $0.240 < S(w) < 0.325$ in a well behaved fashion.

We have described a practical scheme for simultaneously adjusting the critical temperature for both ground-band interactions and non-interacting excited bands.

What we leave for future work includes further investigation into the one and two-dimensional cases and the effect of mean-field interactions: in a shallow lattice, in excited bands and in a translationally-invariant lattice.

Chapter 8

Conclusions

8.1 Summary

Ground-breaking experiments have shown that bosons in optical lattices provide a physical system with an unprecedented degree of control, that they can generate strongly correlated states, allow for simulation of many-body Hamiltonians and may be a useful vehicle for quantum computing.

In contrast to the trapped gas with no lattice, few thermodynamic results for cold bosons in an optical lattice have yet been observed or calculated.

In this thesis, we have used an extended Bose-Hubbard Hamiltonian which goes beyond the usual Bose-Hubbard approach, and is valid for shallower lattices and higher temperatures, by allowing for beyond nearest-neighbour hopping and excited bands, and we have considered an approximate interpolative scheme for off-site interactions. We have carefully considered the extended Bose-Hubbard model parameters, including the hopping matrix elements, the harmonic trap and interaction coefficients and have investigated the approximations often used to obtain the Bose-Hubbard model parameters.

We have derived the equations of the Popov approximation to the Hartree-Fock-Bogoliubov method for our extended Bose-Hubbard Hamiltonian, and have diagonalised these equations in the LDA.

We have examined the density of states of the optical lattice in detail and in various limits. We have derived new results on the structure of the combined harmonic lattice

density of states. We have compared the non-interacting LDA density of states with these limits and with the full diagonalisation of the combined harmonic lattice.

We have made an efficient numerical implementation of our theory and compared the thermodynamic results with the full diagonalisation (for the non-interacting case) and with the limited experimental results currently available. We have considered the significance of beyond nearest-neighbour hopping and excited bands and illustrated the properties of our model.

For the trapped gas with no lattice, the non-interacting critical temperature, the finite-size effect and the mean-field interaction shift are all well known. In this work, we have produced the first practical formula for these results in a lattice. In particular, we have analytically derived an expression for the critical temperature in an optical lattice by using simplified shapes for the density of states. We have considered both the translationally-invariant lattice and the combined harmonic lattice. We have derived simple corrections for the influence of excited bands and finite-size effects. We have also derived a correction for mean-field interactions in the ground band, which is typically a large effect in the lattice system. We have described a practical scheme for simultaneously adjusting the critical temperature for both ground-band interactions and non-interacting excited bands. In all of these cases, we have compared our results to full numerical calculations and have shown that the validity range of our method is complementary to that of the effective-mass approximation, so that the simple descriptions extend over a wide range.

8.2 Outlook

Experimental work in optical lattices is continuing apace. The lack of attention to the finite temperature thermodynamics in a lattice has been partly due to the inability of experiments to measure temperature in the lattice system. However, recently a practical scheme for measuring temperature in an optical lattice has been demonstrated [1], so it is likely that the critical temperature will be measured in the near future.

We are planning several avenues for extending this work.

First, our methods will be applied to other thermodynamic quantities. For example,

we have used our numerical results to calculate the entropy:

$$\frac{S}{k_B} = \sum_b \int d\mathbf{r} \int dK g_b(K) \left\{ \beta E_b(K, \mathbf{r}) \bar{n}_{\mathrm{BE}} \left[E_b(K, \mathbf{r}) \right] - \log \left[1 - e^{-\beta E_b(K, \mathbf{r})} \right] \right\}, \quad (8.1)$$

and from that the specific heat, $C(T) = T \left(\partial S / \partial T \right)_N$, and then the energy, can be obtained. From these quantities, much useful information can be gained about the lattice system. For example, this allows us to understand the change in temperature when the atoms are adiabatically loaded into an optical lattice (as is done in experiments). Also, our formalism would allow the momentum density of the expanded distribution to be calculated and afford greater understanding of the emergence of interference patterns (currently the role of condensation in this interference is being debated in the literature [57, 58, 93, 119]). We also believe that analytical results for these thermodynamic quantities will be possible with simplified band shape approximations.

Second, we will investigate further the effects of the approximations inherent in the LDA and, more generally, in the mean-field approach. Emerging experimental results will be particularly useful for judging the significance of these approximations. One extension to our work would be to include the next term in the semiclassical series beyond the LDA [120]. The number of particles and sites in [53] could be increased to allow comparison between our results and the discrete Popov approximation to the Hartree-Fock-Bogoliubov method, with the Gross-Pitaevskii equation for the condensate. Also, we will compare to beyond mean-field results using, for example, a stochastic Gross-Pitaevskii approach [121]. A possible, but computationally difficult, extension is an improved treatment of off-site interactions.

Finally, the physical regimes for our methods will be extended. We will modify the approach of this thesis for a gas of superfluid fermions in an optical lattice. We will also further investigate the one and two-dimensional cases, using simplified band shapes that approximate their true structure. Possible work would be to further develop the interacting effective-mass approximation to improve the modelling of interacting particles in shallow lattices.

We believe that impressive experiments with cold gases in optical lattices will continue to motivate much future physical discovery.

References

[1] D. McKay, M. White, and B. DeMarco. *Lattice thermodynamics for ultracold atoms.* Phys. Rev. A **79**, 063605 (2009).

[2] S. N. Bose. *Plancks Gesetz und Lichtquantenhypothese (Planck's law and the light quantum hypothesis).* Z. Phys. **26**, 178 (1924).

[3] I. Duck and E. C. G. Sudarshan, *Pauli and the spin-statistics theorem* (World Scientific, Singapore, 1997).

[4] A. Einstein. *Quantentheorie des einatomigen idealen Gases (Quantum theory of monatomic ideal gases).* S.B.d. Preuss. Akad. Wiss. Ber. **22**, 261 (1924).

[5] A. Einstein. *Quantentheorie des einatomigen idealen Gases. Zweite Abhandlung (Quantum theory of monatomic ideal gases, part two).* S.B.d. Preuss. Akad. Wiss. Ber. **1**, 3 (1925).

[6] F. London. *The λ-phenomenon of liquid helium and the Bose-Einstein degeneracy.* Nature **141**, 643 (1938).

[7] F. London. *On the Bose-Einstein condensation.* Phys. Rev. **54**, 947 (1938).

[8] N. Bogoliubov. *On the theory of superfluidity.* J. Phys. (USSR) **11**, 23 (1947).

[9] de Groot, S. R., Hooyman, G. J., and ten Seldam, C. A. *On the Bose-Einstein condensation.* Proc. Roy. Soc. London Ser. A **203**, 266 (1950).

[10] E. P. Gross. *Structure of a quantized vortex in boson systems.* Nuovo Cimiento **20**, 454 (1961).

[11] L. P. Pitaevskii. *Vortex lines in an imperfect Bose gas.* Sov. Phys. JETP **13**, 451 (1961).

References

[12] M. H. Anderson, J. R. Ensher, M. R. Matthews, C. E. Wieman, and E. A. Cornell. *Observation of Bose-Einstein condensation in a dilute atomic vapor.* Science **269**, 198 (1995).

[13] URL `patapsco.nist.gov/imagegallery/details.cfm?imageid=193`.

[14] K. B. Davis, M. O. Mewes, M. R. Andrews, N. J. van Druten, D. S. Durfee, D. M. Kurn, and W. Ketterle. *Bose-Einstein condensation in a gas of sodium atoms.* Phys. Rev. Lett. **75**, 3969 (1995).

[15] C. C. Bradley, C. A. Sackett, J. J. Tollett, and R. G. Hulet. *Evidence of Bose-Einstein condensation in an atomic gas with attractive interactions.* Phys. Rev. Lett. **75**, 1687 (1995).

[16] M. R. Andrews, C. G. Townsend, H.-J. Miesner, D. S. Durfee, D. M. Kurn, and W. Ketterle. *Observation of interference between two Bose condensates.* Science **275**, 637 (1997).

[17] M.-O. Mewes, M. R. Andrews, D. M. Kurn, D. S. Durfee, C. G. Townsend, and W. Ketterle. *Output coupler for Bose-Einstein condensed atoms.* Phys. Rev. Lett. **78**, 582 (1997).

[18] M. R. Matthews, B. P. Anderson, P. C. Haljan, D. S. Hall, C. E. Wieman, and E. A. Cornell. *Vortices in a Bose-Einstein condensate.* Phys. Rev. Lett. **83**, 2498 (1999).

[19] D. S. Jin, J. R. Ensher, M. R. Matthews, C. E. Wieman, and E. A. Cornell. *Collective excitations of a Bose-Einstein condensate in a dilute gas.* Phys. Rev. Lett. **77**, 420 (1996).

[20] E. A. Donley, N. R. Claussen, S. L. Cornish, J. L. Roberts, E. A. Cornell, and C. E. Wieman. *Dynamics of collapsing and exploding Bose-Einstein condensates.* Nature **412**, 295 (2001).

[21] J. L. Roberts, N. R. Claussen, S. L. Cornish, E. A. Donley, E. A. Cornell, and C. E. Wieman. *Controlled collapse of a Bose-Einstein condensate.* Phys. Rev. Lett. **86**, 4211 (2001).

[22] P. Courteille, R. S. Freeland, D. J. Heinzen, F. A. van Abeelen, and B. J. Verhaar. *Observation of a Feshbach resonance in cold atom scattering.* Phys. Rev. Lett. **81**, 69 (1998).

[23] J. L. Roberts, N. R. Claussen, J. P. Burke, C. H. Greene, E. A. Cornell, and C. E. Wieman. *Resonant magnetic field control of elastic scattering in cold ^{85}Rb.* Phys. Rev. Lett. **81**, 5109 (1998).

[24] V. Vuletić, A. J. Kerman, C. Chin, and S. Chu. *Observation of low-field Feshbach resonances in collisions of cesium atoms.* Phys. Rev. Lett. **82**, 1406 (1999).

[25] E. A. Burt, R. W. Ghrist, C. J. Myatt, M. J. Holland, E. A. Cornell, and C. E. Wieman. *Coherence, correlations, and collisions: What one learns about Bose-Einstein condensates from their decay.* Phys. Rev. Lett. **79**, 337 (1997).

[26] M. Greiner, C. A. Regal, and D. S. Jin. *Emergence of a molecular Bose-Einstein condensate from a Fermi gas.* Nature **426**, 537 (2003).

[27] S. Jochim, M. Bartenstein, A. Altmeyer, G. Hendl, S. Riedl, C. Chin, J. Hecker Denschlag, and R. Grimm. *Bose-Einstein condensation of molecules.* Science **302**, 2101 (2003).

[28] I. Bloch. *Ultracold quantum gases in optical lattices.* Nat. Phys. **1**, 23 (2005).

[29] H. Feshbach. *Unified theory of nuclear reactions.* Ann. Phys. (N.Y.) **5**, 357 (1958).

[30] S. Inouye, M. R. Andrews, J. Stenger, H. J. Miesner, D. M. Stamper-Kurn, and W. Ketterle. *Observation of Feshbach resonances in a Bose-Einstein condensate.* Nature **392**, 151 (1998).

[31] D. B. M. Dickerscheid, U. Al Khawaja, D. van Oosten, and H. T. C. Stoof. *Feshbach resonances in an optical lattice.* Phys. Rev. A **71**, 043604 (2005).

[32] J. Hubbard. *Electron correlations in narrow energy bands.* Proc. Roy. Soc. London Ser. A **276**, 238 (1963).

[33] M. P. A. Fisher, P. B. Weichman, G. Grinstein, and D. S. Fisher. *Boson localization and the superfluid-insulator transition.* Phys. Rev. B **40**, 546 (1989).

[34] D. Jaksch, C. Bruder, J. I. Cirac, C. W. Gardiner, and P. Zoller. *Cold bosonic atoms in optical lattices.* Phys. Rev. Lett. **81**, 3108 (1998).

[35] K. Berg-Sørensen and K. Mølmer. *Bose-Einstein condensates in spatially periodic potentials.* Phys. Rev. A **58**, 1480 (1998).

References

[36] O. Penrose and L. Onsager. *Bose-Einstein condensation and liquid helium.* Phys. Rev. **104**, 576 (1956).

[37] S. Stringari, *Bose-Einstein condensation and superfluidity in trapped atomic gases* (2001), URL `arxiv.org/abs/cond-mat/0101299v1`.

[38] D. van Oosten, P. van der Straten, and H. T. C. Stoof. *Quantum phases in an optical lattice.* Phys. Rev. A **63**, 053601 (2001).

[39] M. Greiner, O. Mandel, T. Esslinger, T. W. Hänsch, and I. Bloch. *Quantum phase transition from a superfluid to a Mott insulator in a gas of ultracold atoms.* Nature **415**, 39 (2002).

[40] K. Xu, Y. Liu, D. E. Miller, J. K. Chin, W. Setiawan, and W. Ketterle. *Observation of strong quantum depletion in a gaseous Bose-Einstein condensate.* Phys. Rev. Lett. **96**, 180405 (2006).

[41] B. Paredes, A. Widera, V. Murg, O. Mandel, S. Folling, I. Cirac, G. V. Shlyapnikov, T. W. Hansch, and I. Bloch. *Tonks-Girardeau gas of ultracold atoms in an optical lattice.* Nature **429**, 277 (2004).

[42] F. Gerbier, S. Fölling, A. Widera, O. Mandel, and I. Bloch. *Probing number squeezing of ultracold atoms across the superfluid-Mott insulator transition.* Phys. Rev. Lett. **96**, 090401 (2006).

[43] S. Trotzky, P. Cheinet, S. Folling, M. Feld, U. Schnorrberger, A. M. Rey, A. Polkovnikov, E. A. Demler, M. D. Lukin, and I. Bloch. *Time-resolved observation and control of superexchange interactions with ultracold atoms in optical lattices.* Science **319**, 295 (2008).

[44] I. Bloch. *Quantum coherence and entanglement with ultracold atoms in optical lattices.* Nature **453**, 1016 (2008).

[45] U. Schnorrberger, J. D. Thompson, S. Trotzky, R. Pugatch, N. Davidson, S. Kuhr, and I. Bloch. *Electromagnetically induced transparency and light storage in an atomic mott insulator.* Phys. Rev. Lett. **103**, 033003 (2009).

[46] S. Wessel, F. Alet, M. Troyer, and G. G. Batrouni. *Quantum Monte Carlo simulations of confined bosonic atoms in optical lattices.* Phys. Rev. A **70**, 053615 (2004).

[47] B. Capogrosso-Sansone, N. V. Prokof'ev, and B. V. Svistunov. *Phase diagram and thermodynamics of the three-dimensional Bose-Hubbard model.* Phys. Rev. B **75**, 134302 (2007).

[48] U. Schollwöck. *The density-matrix renormalization group.* Rev. Mod. Phys. **77**, 259 (2005).

[49] L. Urba, E. Lundh, and A. Rosengren. *One-dimensional extended Bose-Hubbard model with a confining potential: a DMRG analysis.* J. Phys. B **39**, 5187 (2006).

[50] J. Jordan, R. Orús, and G. Vidal. *Numerical study of the hard-core Bose-Hubbard model on an infinite square lattice.* Phys. Rev. B **79**, 174515 (2009).

[51] D. A. W. Hutchinson, E. Zaremba, and A. Griffin. *Finite temperature excitations of a trapped Bose gas.* Phys. Rev. Lett. **78**, 1842 (1997).

[52] A. M. Rey, G. Pupillo, and J. V. Porto. *The role of interactions, tunneling, and harmonic confinement on the adiabatic loading of bosons in an optical lattice.* Phys. Rev. A **73**, 023608 (2006).

[53] B. G. Wild, P. B. Blakie, and D. A. W. Hutchinson. *Finite-temperature treatment of ultracold atoms in a one-dimensional optical lattice.* Phys. Rev. A **73**, 023604 (2006).

[54] S. Giorgini, L. P. Pitaevskii, and S. Stringari. *Condensate fraction and critical temperature of a trapped interacting Bose gas.* Phys. Rev. A **54**, R4633 (1996).

[55] S. Giorgini, L. P. Pitaevskii, and S. Stringari. *Scaling and thermodynamics of a trapped Bose-condensed gas.* Phys. Rev. Lett. **78**, 3987 (1997).

[56] S. Giorgini, L. P. Pitaevskii, and S. Stringari. *Thermodynamics of a trapped Bose-condensed gas.* J. Low Temp. Phys. **109**, 309 (1997).

[57] W. Yi, G.-D. Lin, and L.-M. Duan. *Signal of Bose-Einstein condensation in an optical lattice at finite temperature.* Phys. Rev. A **76**, 031602(R) (2007).

[58] G.-D. Lin, W. Zhang, and L.-M. Duan. *Characteristics of Bose-Einstein condensation in an optical lattice.* Phys. Rev. A **77**, 043626 (2008).

[59] S. Yoshimura, S. Konabe, and T. Nikuni. *Adiabatic cooling and heating of cold bosons in three-dimensional optical lattices and the superfluid-normal phase transition.* Phys. Rev. A **78**, 015602 (2008).

References

[60] M. Cramer, S. Ospelkaus, C. Ospelkaus, K. Bongs, K. Sengstock, and J. Eisert. *Do mixtures of bosonic and fermionic atoms adiabatically heat up in optical lattices?* Phys. Rev. Lett. **100**, 140409 (2008).

[61] A. Griffin. *Conserving and gapless approximations for an inhomogeneous Bose gas at finite temperatures.* Phys. Rev. B **53**, 9341 (1996).

[62] P. B. Blakie and W.-X. Wang. *Bose-Einstein condensation in an optical lattice.* Phys. Rev. A **76**, 053620 (2007).

[63] D. Baillie and P. B. Blakie, *Finite-temperature theory of bosons in optical lattices* (2009), arxiv.org:0906.4606.

[64] D. Baillie and P. B. Blakie, *Critical temperature of a Bose gas in an optical lattice* (2009), arxiv.org:0905.4783.

[65] R. N. Bisset, D. Baillie, and P. B. Blakie. *Analysis of the Holzmann-Chevallier-Krauth theory for the trapped quasi-two-dimensional Bose gas.* Phys. Rev. A **79**, 013602 (2009).

[66] V. W. Scarola and S. D. Sarma. *Quantum phases of the extended Bose-Hubbard Hamiltonian: Possibility of a supersolid state of cold atoms in optical lattices.* Phys. Rev. Lett. **95**, 033003 (2005).

[67] G. Mazzarella, S. M. Giampaolo, and F. Illuminati. *Extended Bose Hubbard model of interacting bosonic atoms in optical lattices: From superfluidity to density waves.* Phys. Rev. A **73**, 013625 (2006).

[68] J. Larson, A. Collin, and J.-P. Martikainen. *Multiband bosons in optical lattices.* Phys. Rev. A **79**, 033603 (2009).

[69] K. Yamamoto, S. Todo, and S. Miyashita. *Successive phase transitions at finite temperatures toward the supersolid state in a three-dimensional extended Bose-Hubbard model.* Phys. Rev. B **79**, 094503 (2009).

[70] K. I. Petsas, A. B. Coates, and G. Grynberg. *Crystallography of optical lattices.* Phys. Rev. A **50**, 5173 (1994).

[71] P. B. Blakie and C. W. Clark. *Wannier states and Bose-Hubbard parameters for 2D optical lattices.* J. Phys. B **37**, 1391 (2004).

[72] D. A. Steck, *Rubidium-87 D line data, version 2.1* (2008), date accessed: 1 October 2008, URL http://steck.us/alkalidata.

[73] D. A. Steck, *Sodium D line data, version 2.1* (2008), date accessed: 1 October 2008, URL http://steck.us/alkalidata.

[74] M. Greiner, O. Mandel, T. W. Hänsch, and I. Bloch. *Collapse and revival of the matter wave field of a Bose-Einstein condensate.* Nature **419**, 51 (2002).

[75] S. Folling, F. Gerbier, A. Widera, O. Mandel, T. Gericke, and I. Bloch. *Spatial quantum noise interferometry in expanding ultracold atom clouds.* Nature **434**, 481 (2005).

[76] F. Gerbier, A. Widera, S. Fölling, O. Mandel, T. Gericke, and I. Bloch. *Phase coherence of an atomic Mott insulator.* Phys. Rev. Lett. **95**, 050404 (2005).

[77] F. Gerbier, A. Widera, S. Fölling, O. Mandel, T. Gericke, and I. Bloch. *Interference pattern and visibility of a Mott insulator.* Phys. Rev. A **72**, 053606 (2005).

[78] C. Schori, T. Stöferle, H. Moritz, M. Köhl, and T. Esslinger. *Excitations of a superfluid in a three-dimensional optical lattice.* Phys. Rev. Lett. **93**, 240402 (2004).

[79] K. Xu, Y. Liu, J. R. Abo-Shaeer, T. Mukaiyama, J. K. Chin, D. E. Miller, W. Ketterle, K. M. Jones, and E. Tiesinga. *Sodium Bose-Einstein condensates in an optical lattice.* Phys. Rev. A **72**, 043604 (2005).

[80] A. L. Fetter and J. D. Walecka, *Quantum theory of many-particle systems* (McGraw-Hill, San Francisco, 1971).

[81] K. Huang and C. N. Yang. *Quantum-mechanical many-body problem with hard-sphere interaction.* Phys. Rev. **105**, 767 (1957).

[82] C. J. Pethick and H. Smith, *Bose-Einstein condensation in dilute gases* (Cambridge University Press, Cambridge, 2002).

[83] A. Isacsson and S. M. Girvin. *Multiflavor bosonic Hubbard models in the first excited Bloch band of an optical lattice.* Phys. Rev. A **72**, 053604 (2005).

References

[84] A. M. Rey, G. Pupillo, C. W. Clark, and C. J. Williams. *Ultracold atoms confined in an optical lattice plus parabolic potential: A closed-form approach.* Phys. Rev. A **72**, 033616 (2005).

[85] S. Goldstein. *On the asymptotic expansion of the characteristic numbers of the Mathieu equation.* Proc. Roy. Soc. Edin. **49**, 210 (1929).

[86] I. Bloch, J. Dalibard, and W. Zwerger. *Many-body physics with ultracold gases.* Rev. Mod. Phys. **80**, 885 (2008).

[87] A. Albus, F. Illuminati, and J. Eisert. *Mixtures of bosonic and fermionic atoms in optical lattices.* Phys. Rev. A **68**, 023606 (2003).

[88] D. Boers, C. Weiss, and M. Holthaus. *Bogoliubov speed of sound for a dilute Bose-Einstein condensate in a 3d optical lattice.* Europhys. Lett. **67**, 887 (2004).

[89] W. Zwerger. *Mott-Hubbard transition of cold atoms in optical lattices.* J. Opt. B **5**, S9 (2003).

[90] G. G. Batrouni, R. T. Scalettar, and G. T. Zimanyi. *Quantum critical phenomena in one-dimensional Bose systems.* Phys. Rev. Lett. **65**, 1765 (1990).

[91] G. G. Batrouni, V. Rousseau, R. T. Scalettar, M. Rigol, A. Muramatsu, P. J. H. Denteneer, and M. Troyer. *Mott domains of bosons confined on optical lattices.* Phys. Rev. Lett. **89**, 117203 (2002).

[92] M. Rigol, R. T. Scalettar, P. Sengupta, and G. G. Batrouni. *Time-of-flight observables and the formation of Mott domains of fermions and bosons on optical lattices.* Phys. Rev. B **73**, 121103 (2006).

[93] Y. Kato, Q. Zhou, N. Kawashima, and N. Trivedi. *Sharp peaks in the momentum distribution of bosons in optical lattices in the normal state.* Nat. Phys. **4**, 617 (2008).

[94] O. Gygi, H. G. Katzgraber, M. Troyer, S. Wessel, and G. G. Batrouni. *Simulations of ultracold bosonic atoms in optical lattices with anharmonic traps.* Phys. Rev. A **73**, 063606 (2006).

[95] A. L. Fetter. *Nonuniform states of an imperfect Bose gas.* Ann. Phys. (N.Y.) **70**, 67 (1972).

[96] A. M. Rey, K. Burnett, R. Roth, M. Edwards, C. J. Williams, and C. W. Clark. *Bogoliubov approach to superfluidity of atoms in an optical lattice.* J. Phys. B **36**, 825 (2003).

[97] P. O. Fedichev and G. V. Shlyapnikov. *Finite-temperature perturbation theory for a spatially inhomogeneous Bose-condensed gas.* Phys. Rev. A **58**, 3146 (1998).

[98] S. A. Morgan. *A gapless theory of Bose-Einstein condensation in dilute gases at finite temperature.* J. Phys. B **33**, 3847 (2000).

[99] S. A. Morgan. *A gapless theory of Bose-Einstein condensation in dilute gases at finite temperature.* Ph.D. thesis, University of Oxford (1999).

[100] K. Burnett, M. Edwards, C. W. Clark, and M. Shotter. *The Bogoliubov approach to number squeezing of atoms in an optical lattice.* J. Phys. B **35**, 1671 (2002).

[101] T. Gericke, P. Wurtz, D. Reitz, T. Langen, and H. Ott. *High-resolution scanning electron microscopy of an ultracold quantum gas.* Nat. Phys. **4**, 949 (2008).

[102] J. Reidl, A. Csordás, R. Graham, and P. Szépfalusy. *Finite-temperature excitations of Bose gases in anisotropic traps.* Phys. Rev. A **59**, 3816 (1999).

[103] N. W. Ashcroft and N. D. Mermin, *Solid state physics* (Saunders College/Harcourt College Publishers, Fort Worth, 1976).

[104] M. Abramowitz and I. A. Stegun, *Handbook of mathematical functions* (Dover, New York, 1970).

[105] N. W. McLachlan, *Theory and application of Mathieu functions* (Dover, New York, 1964).

[106] T. Müller-Seydlitz, M. Hartl, B. Brezger, H. Hänsel, C. Keller, A. Schnetz, R. J. C. Spreeuw, T. Pfau, and J. Mlynek. *Atoms in the lowest motional band of a three-dimensional optical lattice.* Phys. Rev. Lett. **78**, 1038 (1997).

[107] C. Hooley and J. Quintanilla. *Single-atom density of states of an optical lattice.* Phys. Rev. Lett. **93**, 080404 (2004).

[108] G. B. Arfken and H. J. Weber, *Mathematical methods for physicists* (Harcourt/Academic Press, San Diego, 2001), 5th ed.

References

[109] W. H. Press, *Numerical recipes: The art of scientific computing* (Cambridge University Press, Cambridge, UK, 2007), 3rd ed.

[110] C. Gies, B. P. van Zyl, S. A. Morgan, and D. A. W. Hutchinson. *Finite-temperature theory of the trapped two-dimensional Bose gas*. Phys. Rev. A **69**, 023616 (2004).

[111] H. Kleinert, S. Schmidt, and A. Pelster. *Reentrant phenomenon in the quantum phase transitions of a gas of bosons trapped in an optical lattice*. Phys. Rev. Lett. **93**, 160402 (2004).

[112] P. B. Blakie and J. V. Porto. *Adiabatic loading of bosons into optical lattices*. Phys. Rev. A **69**, 013603 (2004).

[113] S. Grossmann and M. Holthaus. *On Bose-Einstein condensation in harmonic traps*. Phys. Lett. A **208**, 188 (1995).

[114] L. P. Pitaevskii and S. Stringari, *Bose-Einstein condensation* (Clarendon Press, Oxford, 2003).

[115] L. Viverit, C. Menotti, T. Calarco, and A. Smerzi. *Efficient and robust initialization of a qubit register with fermionic atoms*. Phys. Rev. Lett. **93**, 110401 (2004).

[116] G. Muradyan and J. R. Anglin. *Finite-temperature coherence of the ideal Bose gas in an optical lattice*. Phys. Rev. A **78**, 053628 (2008).

[117] J. E. Robinson. *Note on the Bose-Einstein integral functions*. Phys. Rev. **83**, 678 (1951).

[118] J. M. Ziman, *Elements of advanced quantum theory* (Cambridge University Press, Cambridge, 1969).

[119] R. B. Diener, Q. Zhou, H. Zhai, and T.-L. Ho. *Criterion for bosonic superfluidity in an optical lattice*. Phys. Rev. Lett. **98**, 180404 (2007).

[120] A. Smerzi. *Semiclassical expansion theory in phase space*. Phys. Rev. A **52**, 4365 (1995).

[121] P. B. Blakie, A. S. Bradley, M. J. Davis, R. J. Ballagh, and C. W. Gardiner. *Dynamics and statistical mechanics of ultra-cold Bose gases using c-field techniques*. Adv. Phys. **57**, 363 (2008).

114

[122] W. Pauli. *Über den Einfluß der Geschwindigkeitsabhängigkeit der Elektronenmasse auf den Zeemaneffekt (About the relationship of the closing of electron shells in atoms with the complex structure of the spectrum).* Z. Phys. **31**, 765 (1925).

[123] W. Heisenberg. *Mehrkörperproblem und Resonanz in der Quantenmechanik (Many-body problem and resonance in quantum mechanics).* Z. Phys. **38**, 411 (1926).

[124] P. A. M. Dirac. *On the theory of quantum mechanics.* Proc. Roy. Soc. London Ser. A **112**, 661 (1926).

[125] E. Fermi. *Zur Quantelung des idealen einatomigen Gases (On the quantization of the ideal monatomic gas).* Z. Phys. **36**, 902 (1926).

[126] M. Fierz. *Über die relativistische Theorie kräftefreier Teilchen mit beliebigem Spin (About the relativistic theory of force free particles with arbitrary spin).* Helv. Phys. Acta **12**, 3 (1939).

[127] W. Pauli. *The connection between spin and statistics.* Phys. Rev. **58**, 716 (1940).

[128] C. Cohen-Tannoudji, J. Dupont-Roc, and G. Grynberg, *Atom-photon interactions: Basic processes and applications* (J. Wiley, New York, 1992).

[129] R. Grimm, M. Weidemüller, and Y. Ovchinnikov. *Optical dipole traps for neutral atoms.* Adv. At. Mol. Opt. Phys. **42**, 95 (2000).

[130] C. J. Foot, *Atomic physics* (Oxford University Press, Oxford, 2005).

[131] D. Jaksch and P. Zoller. *The cold atom Hubbard toolbox.* Ann. Phys. (N.Y.) **315**, 52 (2005).

[132] C. P. Enz, *A course on many-body theory applied to solid-state physics* (World Scientific, Singapore, 1992).

[133] J. M. Ziman, *Principles of the theory of solids* (Cambridge University Press, Cambridge, 1972), 2nd ed.

Appendix A

Spin and statistics

After the statement of Pauli's exclusion principle in 1925 [122], that 'there can never be two or more equivalent elections in an atom', Heisenberg [123] and Dirac [124] showed that there are two types of identical particles possible in quantum mechanics: bosons which are symmetric under exchange and allow any number of particles in each quantum state and fermions [125] which are anti-symmetric under exchange and satisfy Pauli's exclusion principle. In 1940, the spin-statistics theorem was proven: 'particles with arbitrary half-integer spin' are fermions and 'particles with arbitrary integer spin' are bosons [126, 127]. Atoms are composite bosons, being composed of an even total number of fermions (electrons and nucleons). The energies we will consider are far below any of the dissociation energies, so the composite nature of our atoms has negligible effect.

Appendix B

Lattice potential

To form an optical lattice, in each direction, the standing wave is created by two opposing lasers. We consider one of the dimensions. The laser frequency, ω_L, is off-resonant with respect to an atomic transition from an unperturbed ground state ($|g\rangle$ with energy E_g) to an unperturbed excited state ($|e\rangle$ with energy E_e), the detuning being $\Delta \equiv \omega_L - (E_e - E_g)/\hbar$.[1] The ground state is perturbed by the resulting a.c. Stark shift which we now consider using the rotating wave approximation, for $|\Delta| \ll (E_e - E_g)/\hbar$.

The reactive force on the atom due to the standing wave is, from the optical Bloch equations [128]:

$$F = -\frac{\hbar\Delta}{4}\frac{\nabla(\Omega^2)}{\Delta^2 + \Gamma^2/4 + \Omega^2/2},\qquad\text{(B.1)}$$

where Γ is the decay rate of the excited state, Ω is the Rabi frequency. In our case, for a standing wave (for distances much smaller than the beam waist of the laser [86]), the Rabi frequency is $\Omega = \Omega_0 \sin(2\pi x/\lambda)$ where $\lambda = 2\pi c/\omega_L$ is the laser wavelength. The potential corresponding to the reactive force, $F = -\nabla V_{\text{latt}}(\mathbf{r})$, gives:

$$\begin{aligned}
V_{\text{latt}}(x) &= \frac{\hbar\Delta}{2}\ln\left(1 + \frac{\Omega^2/2}{\Delta^2 + \Gamma^2/4}\right)\\
&\approx \frac{\hbar\Delta}{4}\frac{\Omega^2}{\Delta^2 + \Gamma^2/4} \approx \frac{\hbar\Omega^2}{4\Delta}\\
&= V\sin^2(2\pi x/\lambda),\qquad\text{(B.2)}
\end{aligned}$$

since $|\Delta| \gg \Gamma$, assuming $\Omega^2 \ll 2\Delta^2$, and where $V = \hbar\Omega_0^2/4\Delta$.

---

[1]In the experiments we consider in table 2.1, the beam is red detuned, $\Delta < 0$.

Appendix B. Lattice potential

With orthogonal polarisation vectors and (at least) slightly different wavelengths, the standing waves in each direction are independent [86], giving, in d dimensions:

$$V_{\text{latt}}(\mathbf{r}) = \sum_{j=1}^{d} V_j \sin^2 \left(2\pi r_j / \lambda_j\right), \tag{B.3}$$

where V_j is the lattice depth, λ_j is the wavelength in direction j.

The decay rate is given by [129]:

$$\Gamma = \frac{(E_e - E_g)^3}{3\pi\epsilon_0 \hbar^4 c^3} \left|\langle e| d |g\rangle\right|^2, \tag{B.4}$$

where d is the dipole operator. So, $\Gamma \propto \Omega_0^2$ and the lattice depth is proportional to Γ/Δ. The spontaneous emission rate is [128, 130]:

$$\frac{\Gamma}{2} \frac{\Omega^2/2}{\Delta^2 + \Gamma^2/4 + \Omega^2/2} \approx \frac{\Gamma\Omega^2}{4\Delta^2} \propto \left(\frac{\Gamma}{\Delta}\right)^2. \tag{B.5}$$

Therefore, to minimise spontaneous emission (hence realising a conservative potential), the detuning is chosen large enough so that $|\Delta| \gg \Gamma$ [131].

Appendix C

Bloch wavefunctions

As discussed in section 4.2, the potential of the non-interacting lattice is separable, so we consider Schrödinger's equation for the one-dimensional, non-interacting, translationally-invariant lattice which is:

$$-\frac{\hbar^2}{2m}\frac{\mathrm{d}^2\psi_{b,k}(x)}{\mathrm{d}x^2} + V\sin^2\left(\frac{\pi x}{a}\right)\psi_{b,k}(x) = K_b(k)\psi_{b,k}(x). \tag{C.1}$$

This is Mathieu's equation with amplitude $q = -V/4E_R$ and 'characteristic value' $(K_b(k) - \frac{1}{2}V)/E_R$ [104]. We require that $\psi_{b,k}$ is a Bloch solution such that:

$$\psi_{b,k}(x) = e^{\mathrm{i}kx}u_{b,k}(x), u_{b,k}(x+na) = u_{b,k}(x) \implies \psi_{b,k}(x+na) = e^{\mathrm{i}kna}\psi_{b,k}(x), \tag{C.2}$$

for integer n and k in the first Brillouin Zone (which we label BZ) which is $-\pi/a \leq k < \pi/a$. We use the Born-von Karman boundary condition, with N_s sites:

$$\psi_{b,k}(x+N_sa) = \psi_{b,k}(x) \text{ so that } \psi_{b,k}(x+N_sa) = e^{\mathrm{i}kN_sa}\psi_{b,k}(x), \tag{C.3}$$

then (we assume N_s even):

$$e^{\mathrm{i}N_ska} = 1 \implies k = 2\pi n/N_sa, n = -N_s/2, ..., 0, ..., N_s/2 - 1. \tag{C.4}$$

C.1 Mathieu solutions

For non-negative integer $b = 0, 1, \ldots$ we define the position in recoil units $\bar{x} = x\pi/a$ and the extended zone scheme quasi-momentum, or characteristic exponent:

$$\nu = ka/\pi + \mathrm{sgn}(k)b' \text{ where } b' = \begin{cases} b & b \text{ even,} \\ -(b+1) & b \text{ odd.} \end{cases} \tag{C.5}$$

The general solution to (C.1) is:

$$c_1 \, \mathrm{ce}_{|\nu|}(\bar{x}, q) + c_2 \, \mathrm{se}_{|\nu|}(\bar{x}, q), \tag{C.6}$$

where ce and se are the even and odd Mathieu functions, respectively. For $\nu > 0$, from [104], the Bloch solution to (C.1) is:

$$\psi_{b,k}(x) = A\left[\mathrm{ce}_\nu(\bar{x}, q) + \mathrm{i}\,\mathrm{se}_\nu(\bar{x}, q)\right] = e^{\mathrm{i}\nu\bar{x}} u_{b,k}(x). \tag{C.7}$$

We note that if $\psi_{b,k}(x) = e^{\mathrm{i}\nu\bar{x}} u_{b,k}(x)$ where $u_{b,k}(x + a) = u_{b,k}(x)$ then $\psi_{b,k}(x) = e^{\mathrm{i}kx}\tilde{u}_{b,k}(x)$ is a Bloch function where $\tilde{u}_{b,k}(x) = e^{\mathrm{i}\,\mathrm{sgn}(k)b'x} u_{b,k}(x) \implies \tilde{u}_{b,k}(x+a) = \tilde{u}_{b,k}(x)$ since b' is always even.

For $\nu = 0$, $\mathrm{se}_\nu(\bar{x}, q)$ is not defined, so we must have $\psi_{0,0}(x) = A\,\mathrm{ce}_0(\bar{x}, q)$.

For $\nu < 0$, we define $\mathrm{ce}_\nu(\bar{x}, q) \equiv \mathrm{ce}_{-\nu}(\bar{x}, q)$ and $\mathrm{se}_\nu(\bar{x}, q) \equiv -\mathrm{se}_{-\nu}(\bar{x}, q)$ so that (C.7) still applies which is consistent with [104].[1]

For the no lattice, $q = 0$, case we have [105], $\mathrm{ce}_\nu(\bar{x}, 0) = \cos\nu\bar{x}$ and $\mathrm{se}_\nu(\bar{x}, 0) = \sin\nu\bar{x}$ so that $\psi_{b,k}(x) = Ae^{\mathrm{i}\nu\bar{x}}$.

C.2 Normalisation

We note [105] that, for $ka/\pi = \pm p/s$ where the natural numbers p and s have no common multiples, $\psi_{b,k}(x)$ has period $2as$ ($|\psi_{b,k}(x)|^2 = |u_{b,k}(x)|^2$ has period a) and that the normalisation of ce and se is:

$$\int_0^{2as} \mathrm{ce}^2_{b+p/s}(\bar{x}, q)\mathrm{d}x = \int_0^{2as} \mathrm{se}^2_{b+p/s}(\bar{x}, q)\mathrm{d}x = sa, \qquad \int_0^{2as} \mathrm{ce}_\kappa(\bar{x}, q)\mathrm{se}_\nu(\bar{x}, q)\mathrm{d}x = 0, \tag{C.8}$$

and for $\kappa \neq \nu$:

$$\int_0^{2as} \mathrm{ce}_\kappa(\bar{x}, q)\mathrm{ce}_\nu(\bar{x}, q)\mathrm{d}x = \int_0^{2as} \mathrm{se}_\kappa(\bar{x}, q)\mathrm{se}_\nu(\bar{x}, q)\mathrm{d}x = 0, \tag{C.9}$$

---

[1]Although this isn't stated explicitly in [104], it is consistent with their 20.5.2 which is stated 'for all ν' other than zero. We note that with our Mathieu function definition for $\nu < 0$, (C.6) is the general solution since the characteristic value is even in ν so that the positive and negative quasi-momentum solutions are degenerate in energy and the two positive momentum eigenfunctions form a complete set for a given energy. Also, (C.7) is the Bloch solution for $\nu < 0$ from (C.7) since $\mathrm{ce}_{-\nu}(\bar{x}, q)$ is even in x and $\mathrm{se}_{-\nu}(\bar{x}, q)$ is odd in x.

so we have:

$$\int_0^{2as} |\psi_{b,k}(x)|^2 \mathrm{d}x = 2as|A|^2, \tag{C.10}$$

so that we set $A = 1/\sqrt{a}$ to normalise over a single lattice site (subject to an overall phase which we will utilise for our Wannier functions) so that the normalised Bloch function is:

$$\psi_{b,k}(x) = \frac{1}{\sqrt{a}}[\mathrm{ce}_\nu(\bar{x}, q) + \mathrm{i}\,\mathrm{se}_\nu(\bar{x}, q)] = e^{\mathrm{i}\nu\bar{x}} u_{b,k}(x), \tag{C.11}$$

and our normalisation, in three dimensions is:

$$\int \mathrm{d}\mathbf{r}\, \psi_{b,\mathbf{k}}^*(\mathbf{r})\psi_{b',\mathbf{k}'}(\mathbf{r}) = N_s \delta_{bb'}\delta_{\mathbf{k}\mathbf{k}'}. \tag{C.12}$$

Appendix D

Wannier functions

We show some results for Wannier functions for a general periodic potential in section D.1, we consider the resulting hopping matrix in section D.2 and give the Wannier function for the optical lattice in section D.3.

D.1 General properties

We define the Wannier function for band b, localised at site $\mathbf{R}_i$ as:[1]

$$w_b(\mathbf{r} - \mathbf{R}_i) \equiv \frac{1}{N_s} \sum_{\mathbf{k} \in \text{BZ}} e^{-i\mathbf{k} \cdot \mathbf{R}_i} \psi_{b,\mathbf{k}}(\mathbf{r}). \tag{D.1}$$

were BZ refers to the first Brillouin zone. We define $N_{s,j}$ to be the number of sites in direction j. If $\mathbf{k}$ is on the reciprocal lattice then $\mathbf{K} \cdot \mathbf{R}_i = 1$ for all i so that $\sum_{i=1}^{N_s} e^{i\mathbf{k} \cdot \mathbf{R}_i} = N_s$. Otherwise, if $k_j = 2\pi n'_j / N_{s,j} a_j$, and picking any direction l for which n'_l is not an integer multiple of $N_{s,l}$ (correcting [132]):

$$\sum_{i=1}^{N_s} e^{i\mathbf{k} \cdot \mathbf{R}_i} = \prod_{j=1}^{d} \sum_{n_j=0}^{N_{s,j}-1} e^{2\pi i n_j n'_j / N_{s,j}} \propto \frac{1 - e^{2\pi i n'_l}}{1 - e^{2\pi i n'_l / N_{s,l}}} = 0, \tag{D.2}$$

so, for $\mathbf{k} \in \text{BZ}$:

$$\sum_{i=1}^{N_s} e^{i\mathbf{k} \cdot \mathbf{R}_i} = N_s \sum_{\mathbf{K}} \delta_{\mathbf{k},\mathbf{0}}, \tag{D.3}$$

---

[1]We choose the asymmetric form in (D.1), rather than $1/\sqrt{N_s}$, since our Bloch functions are normalised over a single site from (C.12).

Appendix D. Wannier functions

and we then have:

$$\psi_{b,\mathbf{k}}(\mathbf{r}) = \sum_{i=1}^{N_s} e^{i\mathbf{k}\cdot\mathbf{R}_i} w_b(\mathbf{r} - \mathbf{R}_i). \tag{D.4}$$

If $\mathbf{R}_i = \mathbf{0}$ then $\sum_{\mathbf{k}\in\mathrm{BZ}} e^{i\mathbf{k}\cdot\mathbf{R}_i} = N_s$, the number of wavevectors in BZ. Otherwise, if $\mathbf{R}_i \neq \mathbf{0}$ is a lattice site, then $n_j = R_{i,j}/a_j$ is not an integer multiple of $N_{s,j}$ so that:

$$\sum_{\mathbf{k}\in\mathrm{BZ}} e^{i\mathbf{k}\cdot\mathbf{R}_i} = \prod_{j=1}^{d} \sum_{n'_j=0}^{N_{s,j}-1} e^{2\pi i n_j n'_j/N_{s,j}} \propto \frac{1 - e^{2\pi i n_l}}{1 - e^{2\pi i n_l/N_{s,l}}} = 0, \tag{D.5}$$

so for $\mathbf{R}_i$ on the lattice:

$$\sum_{\mathbf{k}\in\mathrm{BZ}} e^{i\mathbf{k}\cdot\mathbf{R}_i} = N_s \delta_{\mathbf{R}_i,\mathbf{0}}, \tag{D.6}$$

and we have, using also (C.12):

$$\int d\mathbf{r}\, w_b^*(\mathbf{r} - \mathbf{R}_i) w_{b'}(\mathbf{r} - \mathbf{R}_{i'}) = \frac{1}{N_s^2} \sum_{\mathbf{k},\mathbf{k}'\in\mathrm{BZ}} e^{i(\mathbf{k}\cdot\mathbf{R}_i - \mathbf{k}'\cdot\mathbf{R}_{i'})} \int d\mathbf{r}\, \psi_{b,\mathbf{k}}^*(\mathbf{r}) \psi_{b',\mathbf{k}'}(\mathbf{r})$$

$$= \frac{1}{N_s} \delta_{bb'} \sum_{\mathbf{k}\in\mathrm{BZ}} e^{i\mathbf{k}\cdot(\mathbf{R}_i - \mathbf{R}_{i'})}$$

$$= \delta_{bb'} \delta_{ii'}. \tag{D.7}$$

The set of Wannier functions $w_b(\mathbf{r} - \mathbf{R}_i)$ is a complete set, since, from the completeness of the energy eigenfunctions we can write $f(\mathbf{r}) = \sum_{b,\mathbf{k}} c_{b,\mathbf{k}} \psi_{b,\mathbf{k}}(\mathbf{r})$ so that if we define $c_{b,i} \equiv \sum_{\mathbf{k}\in\mathrm{BZ}} c_{b,\mathbf{k}} e^{i\mathbf{k}\cdot\mathbf{R}_i}$ then from (D.4):

$$f(\mathbf{r}) = \sum_{b,i} c_{b,i} w_b(\mathbf{r} - \mathbf{R}_i). \tag{D.8}$$

The Wannier functions are a decomposition of the Dirac delta function:

$$\sum_{b,i} w_b(\mathbf{r} - \mathbf{R}_i) w_b^*(\mathbf{r}' - \mathbf{R}_i) = \delta(\mathbf{r} - \mathbf{r}'), \tag{D.9}$$

in the sense that:

$$\int d\mathbf{r}'\, f(\mathbf{r}') \sum_{b,i} w_b(\mathbf{r} - \mathbf{R}_i) w_b^*(\mathbf{r}' - \mathbf{R}_i) = \sum_{b,i} w_b(\mathbf{r} - \mathbf{R}_i) \int d\mathbf{r}'\, f(\mathbf{r}') w_b^*(\mathbf{r}' - \mathbf{R}_i) = f(\mathbf{r}),$$

$$\tag{D.10}$$

from (D.8) and since $w_b(\mathbf{r} - \mathbf{R}_i)$ is orthonormal from (D.7).

If the potential is separable, so that $\psi_{b,\mathbf{k}}(\mathbf{r}) = \prod_{j=1}^{d} \psi_{b,k_j}(r_j)$ then:

$$w_b(\mathbf{r} - \mathbf{R}_i) = \prod_{j=1}^{d} \frac{1}{N_{s,j}} \sum_{k_j \in \mathrm{BZ}_j} e^{-ik_j R_{i,j}} \psi_{b_j,k_j}(r_j) = \prod_{j=1}^{d} w_{b_j}(r_j - R_{i,j}), \tag{D.11}$$

since the sum over $\mathbf{k} \in \mathrm{BZ}$ includes all possible combinations of $k_j \in \mathrm{BZ}_j$.

The integral approximation to the Wannier functions is:

$$w_b(\mathbf{r} - \mathbf{R}_i) = \left(\frac{a}{2\pi}\right)^d \int_{\mathrm{BZ}} \mathrm{d}\mathbf{k}\, e^{-i\mathbf{k} \cdot \mathbf{R}_i} \psi_{b,\mathbf{k}}(\mathbf{r}), \tag{D.12}$$

since we have, for constant $N_s a^3$:

$$\lim_{N_s \to \infty} \sum_{\mathbf{k}} = \lim_{N_s \to \infty} \sum_{\mathbf{n}} = \int \mathrm{d}\mathbf{n} = \frac{N_s a^d}{(2\pi)^d} \int \mathrm{d}\mathbf{k}. \tag{D.13}$$

D.2 Hopping matrix

Since $H\psi_{b,\mathbf{k}}(\mathbf{r}) = K_b(\mathbf{k})\psi_{b,\mathbf{k}}(\mathbf{r})$, where $H = -\hbar^2 \nabla^2/2m + V_{\mathrm{latt}}(\mathbf{r})$, we have (as in [133]):

$$
\begin{aligned}
Hw_b(\mathbf{r} - \mathbf{R}_{i'}) &= \frac{1}{N_s} \sum_{\mathbf{k} \in \mathrm{BZ}} e^{-i\mathbf{k} \cdot \mathbf{R}_{i'}} H\psi_{b,\mathbf{k}}(\mathbf{r}) \\
&= \sum_{i=1}^{N_s} \left[\frac{1}{N_s} \sum_{\mathbf{k} \in \mathrm{BZ}} e^{-i\mathbf{k} \cdot (\mathbf{R}_{i'} - \mathbf{R}_i)} K_b(\mathbf{k}) \right] w_b(\mathbf{r} - \mathbf{R}_{i'}) \\
&= -\sum_{i=1}^{N_s} J_{b,i,i'} w_b(\mathbf{r} - \mathbf{R}_i),
\end{aligned}
\tag{D.14}
$$

where hopping matrix, defined as (2.6), is:

$$J_{b,i,i'} = -\int \mathrm{d}\mathbf{r}\, w_b^*(\mathbf{r} - \mathbf{R}_i) H w_b(\mathbf{r} - \mathbf{R}_{i'}) = -\frac{1}{N_s} \sum_{\mathbf{k} \in \mathrm{BZ}} e^{-i\mathbf{k} \cdot (\mathbf{R}_{i'} - \mathbf{R}_i)} K_b(\mathbf{k}), \tag{D.15}$$

is the Fourier transform of the energy. In particular, $-J_{b,i,i} = \sum_{\mathbf{k} \in \mathrm{BZ}} K_b(\mathbf{k})/N_s$ is the average energy in the band.

Using (C.12)

$$\int \mathrm{d}\mathbf{r}\, w_b^*(\mathbf{r} - \mathbf{R}_i) H w_{b'}(\mathbf{r} - \mathbf{R}_{i'}) = \frac{\delta_{bb'}}{N_s} \sum_{\mathbf{k} \in \mathrm{BZ}} e^{-i\mathbf{k} \cdot (\mathbf{R}_{i'} - \mathbf{R}_i)} K_b(\mathbf{k}), \tag{D.16}$$

so that there is no inter-band hopping and the hopping matrix depends only on the difference $\mathbf{R}_i - \mathbf{R}_{i'}$. We can invert (D.15) to write the dispersion relation as a Fourier series:

$$K_b(\mathbf{k}) = -\sum_{i'=1}^{N_s} J_{b,i,i'}\, e^{i\mathbf{k} \cdot (\mathbf{R}_{i'} - \mathbf{R}_i)} = -\sum_{i=1}^{N_s} J_{b,i,0}\, e^{-i\mathbf{k} \cdot \mathbf{R}_i}. \tag{D.17}$$

Appendix D. Wannier functions

For the one-dimensional case, if the spectrum is even in k_x then:

$$K_{b_x}(k_x) = -J^0_{b_x,x} - 2\sum_{l>0} J^l_{b_x,x}\cos(lk_xa_x). \tag{D.18}$$

We demonstrate the Fourier cosine series for the translationally-invariant lattice spectrum in figure D.1. For $V = E_R$, we can see that a few terms are needed for the series to approach the nearly free-particle dispersion. By $V = 5E_R$, the ground band is well described by nearest neighbours. For the first excited band, the approach to nearest-neighbour dispersion with increasing V/E_R is somewhat slower.
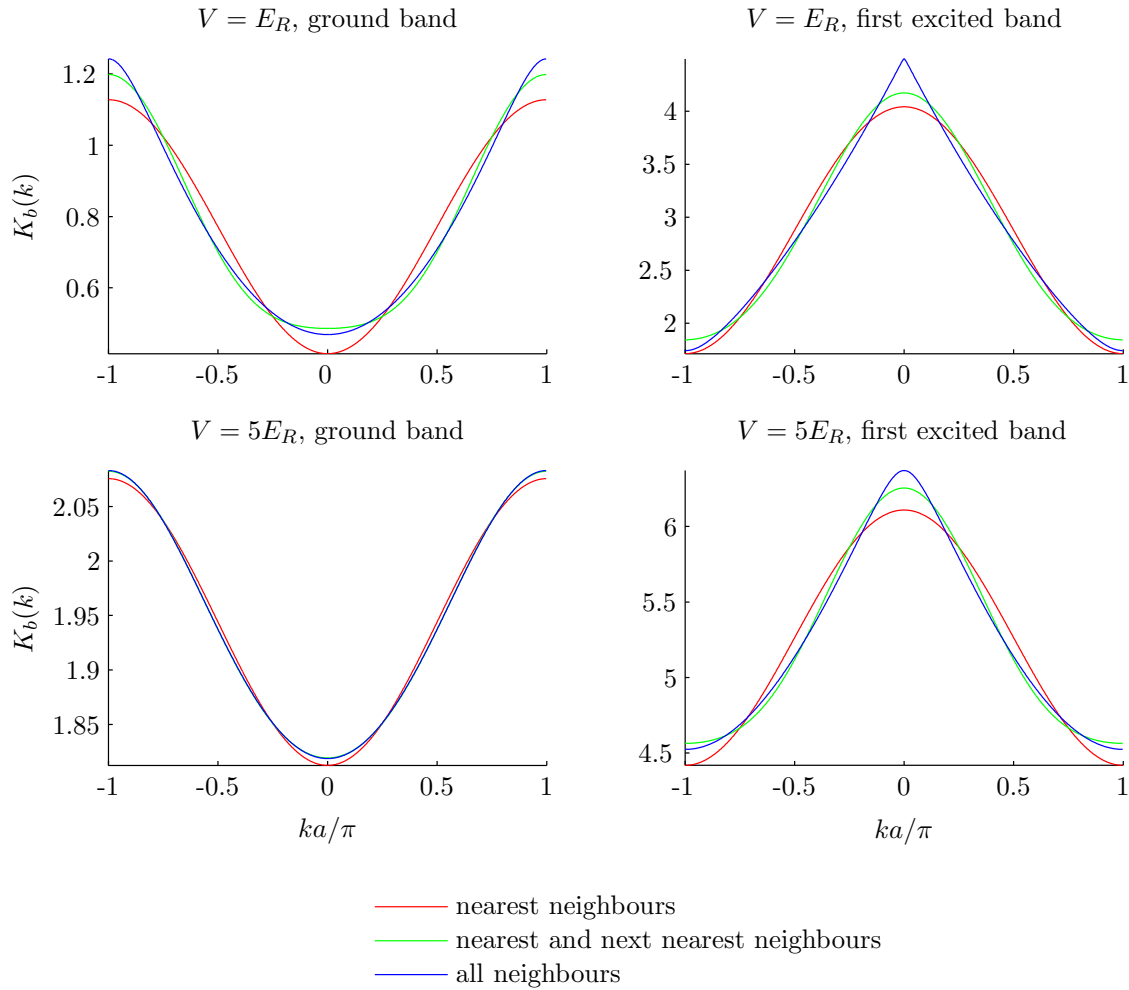
Figure D.1: Fourier series for the one-dimensional translationally-invariant lattice spectrum

The width of band b_x is:

$$\left| K_{b_x}\left(\frac{\pi}{a_x}\right) - K_{b_x}(0) \right| = 2 \left| \sum_{l>0} J^l_{b_x,x}[\cos(l\pi) - 1] \right| = 4 \left| \sum_{l>0}^{\infty} J^{2l-1}_{b_x,x} \right|, \qquad (D.19)$$

so, for any number of dimensions:

$$K_b(\mathbf{k}) = -\sum_j \left[J^0_{b_j,j} + 2\sum_{l>0} J^l_{b_j,j} \cos(lk_j a_j) \right], \qquad (D.20)$$

and the width of band b is:

$$K_b^{\max} - K_b^{\min} = 4\sum_j \left| \sum_{l>0} J^{2l-1}_{b_j,j} \right|. \qquad (D.21)$$

In the tight-binding case where $l = 1$ dominates, the bandwidth is $4\sum_j \left| J^1_{b_j,j} \right|$.

D.3   Optical-lattice Wannier functions

Due to the separability, from (D.11), we consider one dimension. We apply a phase factor, ϕ where $\phi = 1$ for b even and when b is odd, $\phi^+ = i$ when $k > 0$ and $\phi^- = -i$ when $k < 0$ (using (D.1), (C.5) and (D.13)):

$$w_b(x - X_i) = \frac{1}{N_{s,x}} \sum_{k \in \mathrm{BZ}^+} \left[\phi^+ e^{-ikX_i} \psi_{b,k}(x) + \phi^- e^{ikX_i} \psi_{b,-k}(x) \right]$$

$$= \frac{2}{N_{s,x}\sqrt{a}} \sum_{k \in \mathrm{BZ}^+} \begin{cases} \cos(kX_i)\mathrm{ce}_\nu(\bar{x}, q) + \sin(kX_i)\mathrm{se}_\nu(\bar{x}, q) & b \text{ even,} \\ \sin(kX_i)\mathrm{ce}_\nu(\bar{x}, q) - \cos(kX_i)\mathrm{se}_\nu(\bar{x}, q) & b \text{ odd,} \end{cases}$$

$$\approx \frac{\sqrt{a}}{\pi} \int_0^{\pi/a} dk \begin{cases} \cos(kX_i)\mathrm{ce}_\nu(\bar{x}, q) + \sin(kX_i)\mathrm{se}_\nu(\bar{x}, q) & b \text{ even,} \\ \sin(kX_i)\mathrm{ce}_\nu(\bar{x}, q) - \cos(kX_i)\mathrm{se}_\nu(\bar{x}, q) & b \text{ odd.} \end{cases} \qquad (D.22)$$

For the no lattice limit, using: $\mathrm{ce}_\nu(\bar{x}, 0) = \cos\nu\bar{x}$, $\mathrm{se}_\nu(\bar{x}, 0) = \sin\nu\bar{x}$ and (D.22):

$$w_0(x - X_i) = \frac{\sqrt{a}}{\pi} \int_0^{\pi/a} dk \, \cos\left[k(x - X_i)\right] = \frac{1}{\sqrt{a}} \mathrm{sinc}\left[(x - X_i)\frac{\pi}{a}\right], \qquad (D.23)$$

and in general for the no lattice limit:

$$w_b(x - X_i) = \frac{\sqrt{a}}{\pi} \int_0^{\pi/a} dk \begin{cases} \cos\left[\left(k + b\frac{\pi}{a}\right)x - kX_i\right] & b \text{ even,} \\ -\sin\left\{\left[k - (b+1)\frac{\pi}{a}\right]x - kX_i\right\} & b \text{ odd,} \end{cases} \qquad (D.24)$$

$$= \frac{\sqrt{a}}{(x - X_i)\pi} \begin{cases} \sin\left\{\left[(b+1)x - X_i\right]\frac{\pi}{a}\right\} - \sin\left(bx\frac{\pi}{a}\right) & b \text{ even,} \\ \cos\left[(bx + X_i)\frac{\pi}{a}\right] - \cos\left[(b+1)x\frac{\pi}{a}\right] & b \text{ odd,} \end{cases} \qquad (D.25)$$

Appendix D. Wannier functions

and:

$$w_b(x) = \frac{1}{\sqrt{a}} \begin{cases} (b+1)\operatorname{sinc}\left[(b+1)x\frac{\pi}{a}\right] - b\operatorname{sinc}\left(bx\frac{\pi}{a}\right) & b \text{ even,} \\ \left\{\cos\left(bx\frac{\pi}{a}\right) - \cos\left[(b+1)x\frac{\pi}{a}\right]\right\}/(x\pi/a) & b \text{ odd,} \end{cases} \tag{D.26}$$

and we note that $w_b(0) = 1/\sqrt{a}$ for even b and $w_b(0) = 0$ for odd b.

We show the Wannier function for the ground band in figure D.2 (the Gaussian approximation is taken from (2.18)) and for the first and second excited band in one dimension in figure D.3 (the harmonic oscillator approximation is similar to (2.18), but takes the next two excited states). The Gaussian approximation, while reasonable for deep lattices, overstates the peak height at the expense of the tails, and misses the detailed structure of the Wannier functions.
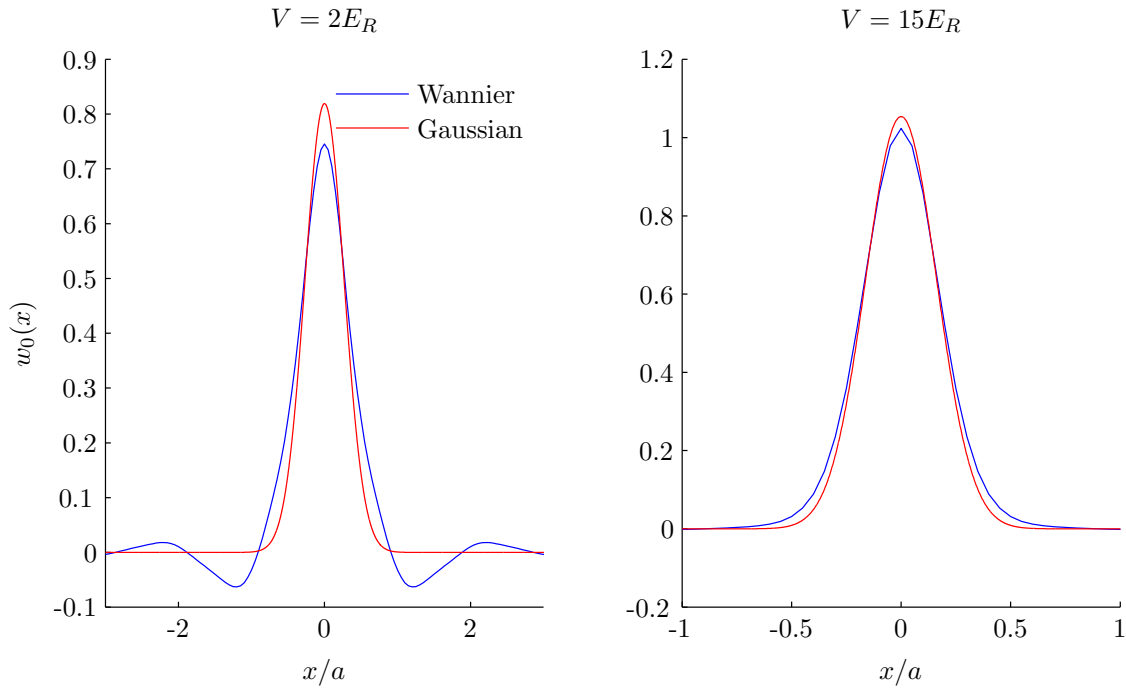

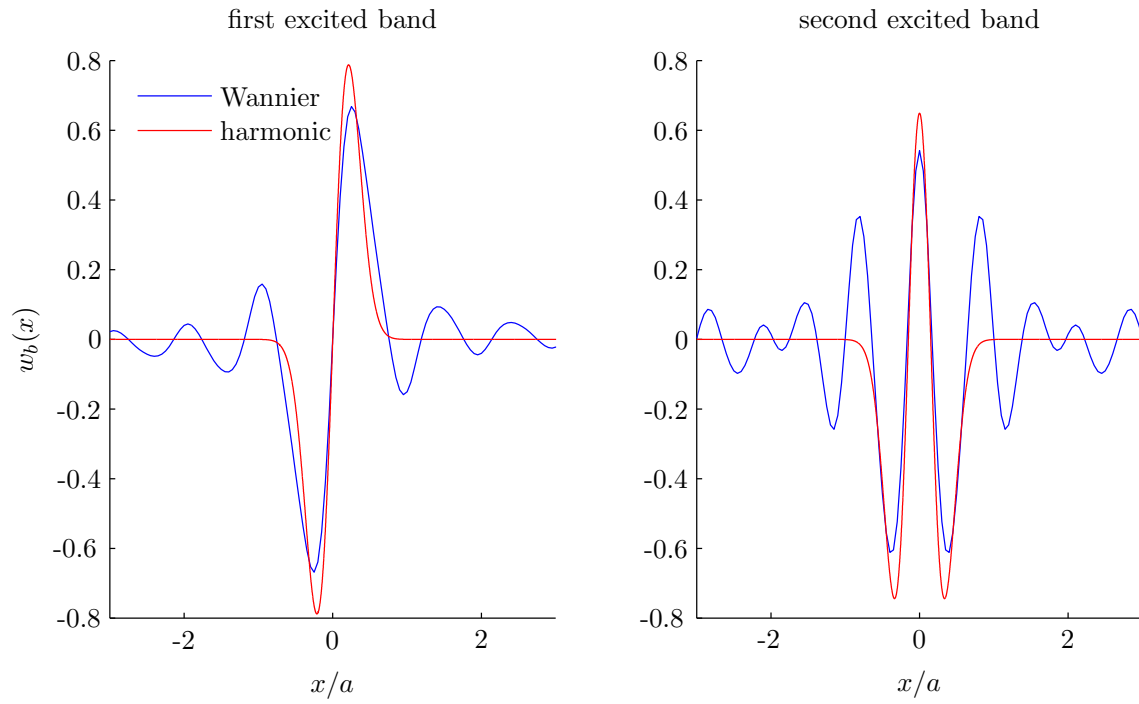Figure D.2: Ground-band Wannier functions compared to the Gaussian approximation

Figure D.3: Wannier function for the first and second excited bands for $V = 5E_R$ compared to the harmonic oscillator approximation

Appendix E

Gaussian hopping matrix

We consider the Gaussian approximation to the nearest-neighbour hopping matrix for a cubic lattice. Shifting the potential of (2.1) so that a barrier is at the origin (which doesn't change the result but improves the symmetry for this calculation) we get:

$$V_{\text{latt}}(\mathbf{r}) = \sum_{j=1}^{d} V_j \sin^2\left(\frac{r_j \pi}{a_j} + \frac{\pi}{2}\right) \approx \sum_{j=1}^{d} V_j \left[1 - \left(\frac{r_j \pi}{a_j}\right)^2\right] = V\left[d - \left(\frac{r\pi}{a}\right)^2\right]. \quad \text{(E.1)}$$

Using the Gaussian approximation from (2.18), we have:

$$\nabla^2 w_0(\mathbf{r}) = w_0(\mathbf{r})\left[\frac{V}{E_R}\left(\frac{\pi}{a}\right)^4 r^2 - d\sqrt{\frac{V}{E_R}}\left(\frac{\pi}{a}\right)^2\right], \quad \text{(E.2)}$$

so that:

$$
\begin{aligned}
J &= -\int d\mathbf{r}\, w_0^*\left(\mathbf{r} - \frac{a}{2}\hat{\mathbf{x}}\right)\left[-\frac{\hbar^2}{2m}\nabla^2 + V_{\text{latt}}(\mathbf{r})\right] w_0\left(\mathbf{r} + \frac{a}{2}\hat{\mathbf{x}}\right) \\
&= \left(\frac{V\pi^4}{E_R a^4}\right)^{d/4}\int_{-\infty}^{\infty} dr\, \frac{2r^{d-1}}{\Gamma(d/2)} e^{-\sqrt{\frac{V}{E_R}}\left[\left(\frac{r\pi}{a}\right)^2 + \frac{\pi^2}{4}\right]}\left\{V\left[2\left(\frac{r\pi}{a}\right)^2 + \frac{\pi^2}{4} - d\right] - d\sqrt{VE_R}\right\} \\
&= \left(\frac{\pi^2}{4} - d\right) V \exp\left(-\frac{\pi^2}{4}\sqrt{\frac{V}{E_R}}\right). \quad \text{(E.3)}
\end{aligned}
$$

The Gaussian approximation does correctly predict that, for large V/E_R, $J \sim e^{-c\sqrt{V/E_R}}$ for some c. However, as shown in (2.16) and (2.17), this the prediction for c is incorrect, and consequently, as shown in figure 2.4 the resulting approximation is poor. The overall constant multiplier depends on d, and changes sign from $d = 2$ to $d = 3$, which cannot be correct. The problem is that the Gaussian approximation, unlike the Wannier

functions themselves, are not orthogonal. In fact the overlap integral is:

$$
\begin{aligned}
I &= \int \mathrm{d}\mathbf{r}\, w_0^* \left(\mathbf{r} - \frac{a}{2}\hat{\mathbf{x}} \right) w_0 \left(\mathbf{r} + \frac{a}{2}\hat{\mathbf{x}} \right) \\
&= \left(\frac{\pi}{a^2} \sqrt{\frac{V}{E_R}} \right)^{d/2} e^{-\sqrt{V/E_R}\frac{\pi^2}{4}} \int \mathrm{d}\mathbf{r}\, e^{-\sqrt{V/E_R}(\pi r/a)^2} \\
&= \exp\left(-\frac{\pi^2}{4} \sqrt{\frac{V}{E_R}} \right).
\end{aligned}
\tag{E.4}
$$

If we orthogonalise the approximate Wannier functions with Gram-Schmidt:

$$
w_0' \left(\mathbf{r} + \frac{a}{2}\hat{\mathbf{x}} \right) = \frac{w_0 \left(\mathbf{r} + \frac{a}{2}\hat{\mathbf{x}} \right) - I w_0 \left(\mathbf{r} - \frac{a}{2}\hat{\mathbf{x}} \right)}{\sqrt{1 - I^2}},
\tag{E.5}
$$

then we find that $J = 0$ since:

$$
-\int \mathrm{d}\mathbf{r}\, w_0^* \left(\mathbf{r} - \frac{a}{2}\hat{\mathbf{x}} \right) \left[-\frac{\hbar^2}{2m}\nabla^2 + V_{\mathrm{latt}}(\mathbf{r}) \right] w_0 \left(\mathbf{r} - \frac{a}{2}\hat{\mathbf{x}} \right) = \left(\frac{\pi^2}{4} - d \right) V.
\tag{E.6}
$$

We note that this calculation should not be taken out of context, since our approximation for $V_{\mathrm{latt}}(\mathbf{r})$ has no barrier at $x = -a$.

We reach the same conclusion, that $J = 0$, with the symmetric orthogonalisation:

$$
w_0' \left(\mathbf{r} \pm \frac{a}{2}\hat{\mathbf{x}} \right) = \frac{w_0 \left(\mathbf{r} \pm \frac{a}{2}\hat{\mathbf{x}} \right) - c\, w_0 \left(\mathbf{r} \mp \frac{a}{2}\hat{\mathbf{x}} \right)}{\sqrt{1 - 2cI + c^2}},
\tag{E.7}
$$

where $c = 1/I - \sqrt{1/I^2 - 1} \approx I/2$ for $I \ll 1$.

These results suggest the Gaussian approximation has to be used with care and should always be verified with an explicit numerical calculation.

Appendix F

Off-site interactions approximation

We start from the interaction term of the extended Bose-Hubbard Hamiltonian (2.9):

$$\frac{1}{2} \sum_{b_1,b_2,b_3,b_4} \hat{a}^{\dagger}_{b_1,i_1} \hat{a}^{\dagger}_{b_2,i_2} \hat{a}_{b_3,i_3} \hat{a}_{b_4,i_4} U_{\substack{i_1,i_2,i_3,i_4 \\ b_1,b_2,b_3,b_4}}$$

$$= \frac{1}{2} z^*_{i_1} z^*_{i_2} z_{i_3} z_{i_4} U_{\substack{i_1,i_2,i_3,i_4 \\ 0,0,0,0}} + \sum_b \left[z^*_{i_1} z^*_{i_2} z_{i_3} \hat{\delta}_{b,i_4} + z^*_{i_1} z_{i_2} z_{i_3} \hat{\delta}^{\dagger}_{b,i_4} \right] U_{\substack{i_1,i_2,i_3,i_4 \\ 0,0,0,b}}$$

$$+ \sum_{b,b'} \left[\frac{1}{2} z^*_{i_1} z^*_{i_2} \hat{\delta}_{b,i_3} \hat{\delta}_{b',i_4} + \frac{1}{2} z_{i_1} z_{i_2} \hat{\delta}^{\dagger}_{b,i_3} \hat{\delta}^{\dagger}_{b',i_4} + 2 z^*_{i_1} z_{i_2} \hat{\delta}^{\dagger}_{b,i_3} \hat{\delta}_{b',i_4} \right] U_{\substack{i_1,i_2,i_3,i_4 \\ 0,0,b,b'}}$$

$$+ \sum_{b_2,b_3,b_4} \left[z^*_{i_1} \hat{\delta}^{\dagger}_{b_2,i_2} \hat{\delta}_{b_3,i_3} \hat{\delta}_{b_4,i_4} + z_{i_1} \hat{\delta}^{\dagger}_{b_2,i_2} \hat{\delta}^{\dagger}_{b_3,i_3} \hat{\delta}_{b_4,i_4} \right] U_{\substack{i_1,i_2,i_3,i_4 \\ 0,b_2,b_3,b_4}}$$

$$+ \frac{1}{2} \sum_{b_1,b_2,b_3,b_4} \hat{\delta}^{\dagger}_{b_1,i_1} \hat{\delta}^{\dagger}_{b_2,i_2} \hat{\delta}_{b_3,i_3} \hat{\delta}_{b_4,i_4} U_{\substack{i_1,i_2,i_3,i_4 \\ b_1,b_2,b_3,b_4}} . \tag{F.1}$$

For the quartic term, we make the mean-field approximation as in section 3.2:

$$\hat{\delta}^{\dagger}_{b_1,i_1} \hat{\delta}^{\dagger}_{b_2,i_2} \hat{\delta}_{b_3,i_3} \hat{\delta}_{b_4,i_4} \approx \left\langle \hat{\delta}^{\dagger}_{b_1,i_1} \hat{\delta}^{\dagger}_{b_2,i_2} \right\rangle \hat{\delta}_{b_3,i_3} \hat{\delta}_{b_4,i_4} + \left\langle \hat{\delta}^{\dagger}_{b_1,i_1} \hat{\delta}_{b_3,i_3} \right\rangle \hat{\delta}^{\dagger}_{b_2,i_2} \hat{\delta}_{b_4,i_4} \tag{F.2}$$

$$+ \left\langle \hat{\delta}^{\dagger}_{b_1,i_1} \hat{\delta}_{b_4,i_4} \right\rangle \hat{\delta}^{\dagger}_{b_2,i_2} \hat{\delta}_{b_3,i_3} + \left\langle \hat{\delta}^{\dagger}_{b_2,i_2} \hat{\delta}_{b_3,i_3} \right\rangle \hat{\delta}^{\dagger}_{b_1,i_1} \hat{\delta}_{b_4,i_4} \tag{F.3}$$

$$+ \left\langle \hat{\delta}^{\dagger}_{b_2,i_2} \hat{\delta}_{b_4,i_4} \right\rangle \hat{\delta}^{\dagger}_{b_1,i_1} \hat{\delta}_{b_3,i_3} + \left\langle \hat{\delta}_{b_3,i_3} \hat{\delta}_{b_4,i_4} \right\rangle \hat{\delta}^{\dagger}_{b_1,i_1} \hat{\delta}^{\dagger}_{b_2,i_2} . \tag{F.4}$$

We again make a Popov approximation to eliminate the terms $\left\langle \hat{\delta}^{\dagger}_{b_1,i_1} \hat{\delta}^{\dagger}_{b_2,i_2} \right\rangle \hat{\delta}_{b_3,i_3} \hat{\delta}_{b_4,i_4}$ and $\left\langle \hat{\delta}_{b_3,i_3} \hat{\delta}_{b_4,i_4} \right\rangle \hat{\delta}^{\dagger}_{b_1,i_1} \hat{\delta}^{\dagger}_{b_2,i_2}$. As in the on-site case, we ignore collisional couplings between bands in the many body-state, since interactions are assumed perturbative with respect to the band gap energy scale. Since this is the non-condensate, we also ignore collisional coupling that relies on coherences between sites (that is, requiring two

Appendix F. Off-site interactions approximation

indices at two sites) in the many-body state, to find:

$$\sum_{\substack{i_1,i_2,i_3,i_4 \\ b_1,b_2,b_3,b_4}} \hat{\delta}^\dagger_{b_1,i_1} \hat{\delta}^\dagger_{b_2,i_2} \hat{\delta}_{b_3,i_3} \hat{\delta}_{b_4,i_4} U_{\substack{i_1,i_2,i_3,i_4 \\ b_1,b_2,b_3,b_4}} \approx 4 \sum_{i,b,b'} \hat{\delta}^\dagger_{b,i} \hat{\delta}_{b,i} \sum_{i'} \tilde{n}_{b',i'} U_{\substack{i,i',i,i' \\ b,b',b,b'}}. \tag{F.5}$$

We assume that the density varies sufficiently slowly that $\tilde{n}_{b,i} \approx \tilde{n}_{b,j}$ for sites $\mathbf{R}_j$ near $\mathbf{R}_i$. In the following, we will sum over all sites, by assuming that where the approximation $\tilde{n}_{b,i} \approx \tilde{n}_{b,j}$ is poor, due to the sites being far apart, these terms will be suppressed by the negligible Wannier function overlap. Then we have:

$$\sum_{\substack{i_1,i_2,i_3,i_4 \\ b_1,b_2,b_3,b_4}} \hat{\delta}^\dagger_{b_1,i_1} \hat{\delta}^\dagger_{b_2,i_2} \hat{\delta}_{b_3,i_3} \hat{\delta}_{b_4,i_4} U_{\substack{i_1,i_2,i_3,i_4 \\ b_1,b_2,b_3,b_4}} \approx 4g \sum_{i,b,b'} \hat{\delta}^\dagger_{b,i} \hat{\delta}_{b,i} \tilde{n}_{b',i} \sum_{i'} \int \mathrm{d}\mathbf{r} \, |w_b(\mathbf{r}) w_{b'}(\mathbf{r} - \mathbf{R}_{i'})|^2$$

$$= 4 \sum_{i,b,b'} \hat{\delta}^\dagger_{b,i} \hat{\delta}_{b,i} \tilde{n}_{b',i} U'_{bb'}, \tag{F.6}$$

which is the same as (3.12) with $U'_{bb'}$ substituted for $U_{bb'}$ where:

$$U'_{bb'} = g \sum_{i'} \int \mathrm{d}\mathbf{r} \, |w_b(\mathbf{r}) w_{b'}(\mathbf{r} - \mathbf{R}_{i'})|^2. \tag{F.7}$$

For a coherent state, such as the condensate, we assume that the complex amplitude, varies sufficiently slowly that $z_i \approx z_j$, for sites $\mathbf{R}_j$ near $\mathbf{R}_i$ (exactly true in the translationally-invariant case). As above, we assume that contributions between sites far apart are suppressed by the negligible Wannier function overlap. We have, for site $\mathbf{R}_{i_1}$:

$$\sum_{i_2,i_3,i_4} z^*_{i_1} z^*_{i_2} z_{i_3} z_{i_4} U_{\substack{i_1,i_2,i_3,i_4 \\ 0,0,0,0}}$$

$$= g \sum_{i_2,i_3,i_4} z^*_{i_1} z^*_{i_2} z_{i_3} z_{i_4} \int \mathrm{d}\mathbf{r} \, w^*_0(\mathbf{r} - \mathbf{R}_{i_1}) w^*_0(\mathbf{r} - \mathbf{R}_{i_2}) w_0(\mathbf{r} - \mathbf{R}_{i_3}) w_0(\mathbf{r} - \mathbf{R}_{i_4}) \tag{F.8}$$

$$\approx g \, |z_{i_1}|^4 \sum_{i_2,i_3,i_4} \int \mathrm{d}\mathbf{r} \, w^*_0(\mathbf{r} - \mathbf{R}_{i_1}) w^*_0(\mathbf{r} - \mathbf{R}_{i_2}) w_0(\mathbf{r} - \mathbf{R}_{i_3}) w_0(\mathbf{r} - \mathbf{R}_{i_4})$$

$$= g \, |z_{i_1}|^4 \int \mathrm{d}\mathbf{r} \, w^*_0(\mathbf{r} - \mathbf{R}_{i_1}) \left[\sum_{i_2} w^*_0(\mathbf{r} - \mathbf{R}_{i_2}) \right] \left[\sum_{i_3} w_0(\mathbf{r} - \mathbf{R}_{i_3}) \right] \left[\sum_{i_4} w_0(\mathbf{r} - \mathbf{R}_{i_4}) \right]$$

$$= g \, |z_{i_1}|^4 \int \mathrm{d}\mathbf{r} \, w_0(\mathbf{r}) \, [\psi_{0,\mathbf{0}}(\mathbf{r})]^3$$

$$= |z_{i_1}|^4 U''_{00},$$

where we have used $\sum_i w_b(\mathbf{r} - \mathbf{R}_i) = \psi_{b,\mathbf{0}}(\mathbf{r})$ from (D.4), that $\psi_{0,\mathbf{0}}(\mathbf{r}) = \mathrm{ce}_0(\bar{z}, q)$ is real and periodic on the lattice from section C, and that $w_0(\mathbf{r})$ is real from (D.22). The

result again takes the same form as (3.12) with U_{00}'' substituted for U_{00} where:

$$U_{00}'' = g \int \mathrm{d}\mathbf{r}\, w_0(\mathbf{r}) \left[\psi_{0,\mathbf{0}}(\mathbf{r})\right]^3 . \tag{F.9}$$

Similar arguments could be used for the terms involving interactions between the condensate and the non-condensate. The above results are appropriate for the pure thermal gas, for example, for finding the critical temperature from above, and for the pure condensate at zero temperature. To quantify the effect of off-site interactions on the thermal depletion, terms for interactions between the condensate and the non-condensate would be needed.

F.1 Interaction coefficients

In this section, we compare the behaviour of the interaction coefficients $U_{bb'}$, $U_{bb'}'$ and U_{00}''.

Both all-sites interaction coefficients, $U_{bb'}'$ and U_{00}'', include their corresponding on-site component, $U_{bb'}$, in their sums, (F.7) and (F.8). For the non-condensate interaction coefficient, since we have excluded interference, all other terms in the sum are positive, so that off-site interactions always increase the interaction coefficient (relative to $U_{bb'}$).

For the condensate, interference is included in the sum, so the effect of off-site interactions depends on the integrand[1] $w_0(\mathbf{r})[\psi_{0,\mathbf{0}}(\mathbf{r})]^3$ compared to $[w_0(\mathbf{r})]^4$ which we plot in figure F.1 (since the potential is separable we consider the one-dimensional case – for higher-dimensional cases, differences between the coefficients are accentuated, since the d-th power of each integral is taken).

For $V = 0$, there is no interference at $x = 0$,[2] but interference elsewhere is significant and positive. For $V = 10E_R$, the all-sites integrand is lower at $x = 0$, due to interference from neighbouring sites, and the interference elsewhere is less significant. As shown in figure F.2, the overall effect of off-site interactions is to reduce the condensate interaction coefficient for moderate lattice depths.

---

[1] The functions $\psi_{0,\mathbf{0}}(\mathbf{r})$ and $w_0(\mathbf{r})$ are real from section C.1 and from (D.22).

[2] Since the Wannier functions in the sum, $\sum_i w_0(\mathbf{r} - \mathbf{R}_i) = \psi_{0,\mathbf{0}}(\mathbf{r})$, are then sinc functions which are zero at neighbouring sites.

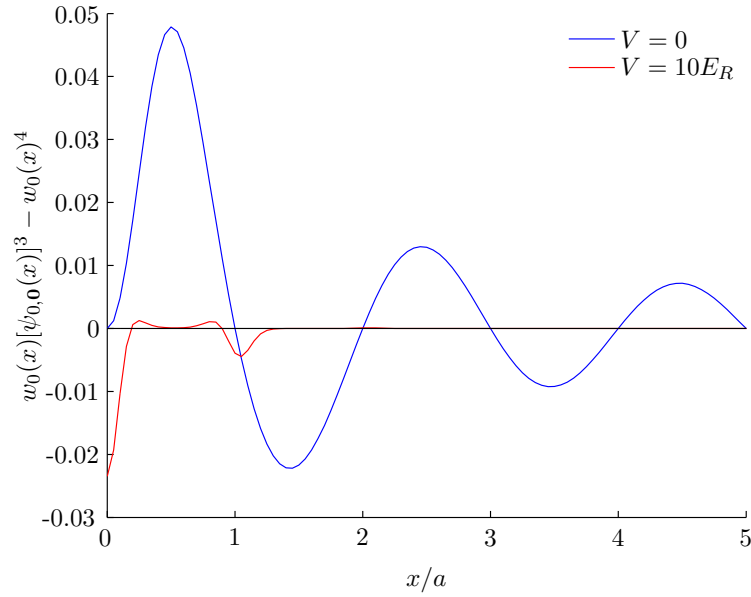# Appendix F. Off-site interactions approximation

Figure F.1: Difference between all-site and on-site integrands for the one-dimensional condensate interaction coefficients
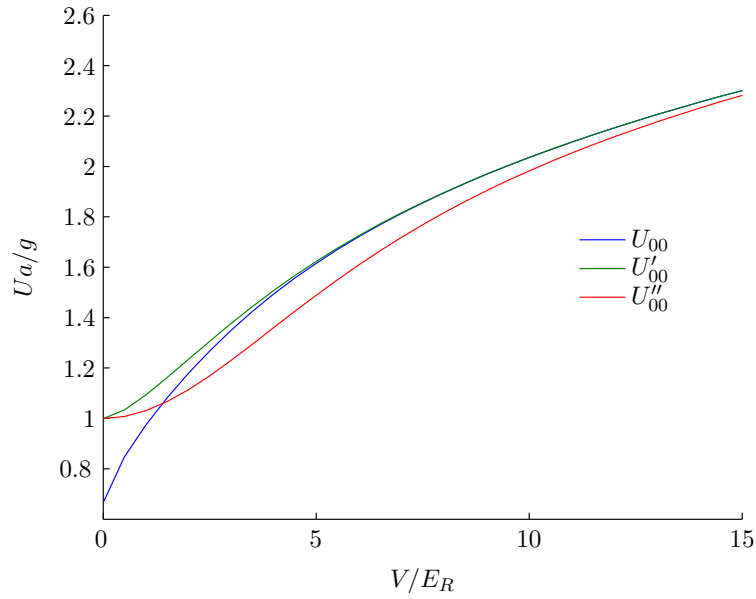
Figure F.2: Comparison of on-site to all-sites interaction coefficients for the ground band in one dimension

We show the ground-band interaction coefficients in three dimensions in figure 2.8.

The excited-band interaction coefficients are shown in figure 2.9. The effect of off-site interactions is significant for much deeper lattices for excited bands than for the ground band reflecting the greater spread of the excited-band Wannier functions.

F.2 No lattice limit

We consider the LDA formulae from section 3.6 when there is no lattice. The Hamiltonian (3.34) would give us $K_b(\mathbf{k}) = \hbar^2 k^2 / 2m$. If we were to have $U_{bb'} = g/a^d$ for all b, b' then $U_{0b} n_c(\mathbf{r}) = g n_c(\mathbf{r})/a^d$ and:

$$\sum_{b'} U_{bb'} \tilde{n}_{b'}(\mathbf{r}) = g \frac{\tilde{n}(\mathbf{r})}{a^d}, \tag{F.10}$$

where the divisor a^d converts our per-site densities into per-volume, and if we also treat $n_c(\mathbf{r})$ and $\tilde{n}_b(\mathbf{r})$ as the condensate and non-condensate densities (rather than as envelope functions, with densities defined by (3.3) and (3.5), although the total condensate and non-condensate numbers do not depend on this distinction, from (3.4) and (3.6)) then all of our LDA equations would be the same as we would get from a no lattice calculation [56], in spite of our expansion of the field operators in a Wannier function basis. From our results of section 2.10, we see that this is not the case for on-site interactions only.

Including off-site interactions, we can easily see that the condensate gives the correct limit from (F.9):

$$U_{00}'' = g \prod_{j=1}^{d} \frac{1}{a_j^2} \int_{-\infty}^{\infty} \mathrm{d}r_j \, \mathrm{sinc}\left(\frac{r_j \pi}{a_j}\right) = \frac{g}{a^d}, \tag{F.11}$$

since $\psi_{0,0}(r_j) = 1/\sqrt{a_j}$ from section C.1 and $w_0(r_j) = \mathrm{sinc}\,(r_j \pi/a_j)/\sqrt{a_j}$ from (D.23).

For the non-condensate, we include only paired terms in the sum (F.5), so that the calculation is somewhat more involved. We define the following integral:

$$I_{bb'}(n) = \int_{-\infty}^{\infty} w_b^2(x) w_{b'}^2(x - na) \mathrm{d}x. \tag{F.12}$$

From the calculations behind section 2.10.3 that $I_{00}(0) = 2/3a$ and for $b > 0$, $I_{0b}(0) = 5/12a$ and $I_{bb}(0) = 1/2a$. We also have $I_{00}(n) = 1/(n^2 \pi^2 a)$ so that, using $\zeta(2) = \pi^2/6$, we have $I_{00}(1+) \equiv \sum_{n=1}^{\infty} I_{00}(n) = 1/6a$ where . The ground-band interaction coefficient in one dimension then gives the correct limit $U_{00}' = g(2/3a + 2/6a) = g/a$. The ground-

Appendix F. Off-site interactions approximation

band interaction coefficient in three dimensions also gives the correct limit:

$$
\begin{aligned}
\frac{U'_{00}}{g} &= I_{00}^3(0) + 6 \sum_{\substack{n_1>0 \\ n_2=n_3=0}} \prod_j I_{00}(n_j) + 12 \sum_{\substack{n_1>0,n_2>0 \\ n_3=0}} \prod_j I_{00}(n_j) + 8 \sum_{n_j>0} \prod_j I_{00}(n_j) \\
&= I_{00}(0)^3 + 6 I_{00}(0)^2 I_{00}(1+) + 12 I_{00}(0) I_{00}^2(1+) + 8 I_{00}^3(1+) \\
&= \left(\frac{2}{3a}\right)^3 + 6\left(\frac{2}{3a}\right)^2 \frac{1}{6a} + 12\frac{2}{3a}\left(\frac{1}{6a}\right)^2 + 8\left(\frac{1}{6a}\right)^3 \\
&= \frac{1}{a^3}.
\end{aligned} \tag{F.13}
$$

For excited bands, off-site interaction calculations are not so simple, but we recognise numerically:

$$
I_{10}(n) = \int_{-\infty}^{\infty} w_1^2(x) w_0^2(x-na)\mathrm{d}x = \frac{1}{n^2\pi^2 a}
\begin{cases}
2 & n \text{ odd}, \\
1 & n \text{ even},
\end{cases} \tag{F.14}
$$

$$
I_{11}(n) = \int_{-\infty}^{\infty} w_1^2(x) w_1^2(x-na)\mathrm{d}x = \frac{1}{n^2\pi^2 a}
\begin{cases}
1 & n \text{ odd}, \\
3 & n \text{ even}.
\end{cases} \tag{F.15}
$$

So, for the ground-first-excited band interactions in one dimension:

$$
\begin{aligned}
I_{10}(1+) &= \sum_{n=1}^{\infty} \int w_1^2(x) w_0^2(x-na)\mathrm{d}x = \frac{1}{\pi^2 a}\left\{2\left[\zeta(2) - \frac{\zeta(2)}{4}\right] + \frac{\zeta(2)}{4}\right\} = \frac{7}{24a}, \\
&\implies U'_{10} = g\left(\frac{5}{12a} + 2\frac{7}{24a}\right) = \frac{g}{a}.
\end{aligned} \tag{F.16}
$$

And, for the intra-first-excited interactions in one dimension:

$$
I_{11}(1+) = \sum_{n=1}^{\infty} \int w_1^2(x) w_1^2(x-na)\mathrm{d}x = \frac{1}{\pi^2 a}\left[\zeta(2) - \frac{\zeta(2)}{4} + \frac{3\zeta(2)}{4}\right] = \frac{1}{4a}, \tag{F.17}
$$

$$
\implies U'_{11} = g\left(\frac{1}{2a} + 2\frac{1}{4a}\right) = \frac{g}{a}. \tag{F.18}
$$

The general integral in three dimensions is:

$$
\begin{aligned}
\frac{U'_{abc,ijk}}{g} = &\, I_{ai}(0) I_{bj}(0) I_{ck}(0) \\
&+ 2 I_{ai}(1+) I_{bj}(0) I_{ck}(0) + 2 I_{ai}(0) I_{bj}(1+) I_{ck}(0) + 2 I_{ai}(0) I_{bj}(0) I_{ck}(1+) \\
&+ 4 I_{ai}(1+) I_{bj}(1+) I_{ck}(0) + 4 I_{ai}(1+) I_{bj}(0) I_{ck}(1+) + 4 I_{ai}(0) I_{bj}(1+) I_{ck}(1+) \\
&+ 8 I_{ai}(1+) I_{bj}(1+) I_{ck}(1+).
\end{aligned} \tag{F.19}
$$

So, ground-first-excited-band interactions in three dimensions give the correct limit:

$$\frac{a^3 U'_{000,001}}{g} = \left(\frac{2}{3}\right)^2 \frac{5}{12} + 4\frac{1}{6}\frac{2}{3}\frac{5}{12} + 2\left(\frac{2}{3}\right)^2 \frac{7}{24} + 8\frac{2}{3}\frac{1}{6}\frac{7}{24} + 4\left(\frac{1}{6}\right)^2 \frac{5}{12} + 8\left(\frac{1}{6}\right)^2 \frac{7}{24}$$
$$= 1,$$
$$\frac{a^3 U'_{001,001}}{g} = \left(\frac{2}{3}\right)^2 \frac{1}{2} + 4\frac{1}{6}\frac{2}{3}\frac{1}{2} + 2\left(\frac{2}{3}\right)^2 \frac{1}{4} + 4\left(\frac{1}{6}\right)^2 \frac{1}{2} + 8\frac{1}{6}\frac{2}{3}\frac{1}{4} + 8\left(\frac{1}{6}\right)^2 \frac{1}{4}$$
$$= 1,$$
$$\frac{a^3 U'_{010,001}}{g} = \frac{2}{3}\left(\frac{5}{12}\right)^2 + 2\frac{1}{6}\left(\frac{5}{12}\right)^2 + 4\frac{2}{3}\frac{5}{12}\frac{7}{24} + 8\frac{1}{6}\frac{7}{24}\frac{5}{12} + 4\frac{2}{3}\left(\frac{7}{24}\right)^2 + 8\frac{1}{6}\left(\frac{7}{24}\right)^2$$
$$= 1. \tag{F.20}$$

Appendix G

Bogoliubov diagonalisation

To calculate the tunnelling term, we first consider a property of the shift operator, $\hat{S}_{i',i}$, defined on page 33. Since $J_{b,i,i'} = J^*_{b,i',i}$, we have:

$$\sum_i \sum_{i'} x_i^* J_{b,i,i'} \hat{S}_{i',i} y_i = \sum_{i,i'} x_i^* J_{b,i,i'} y_{i'} = \sum_{i,i'} \left(J_{b,i',i} \hat{S}_{i,i'} x_{i'} \right)^* y_{i'}$$

$$= \sum_i \sum_{i'} \left(J_{b,i,i'} \hat{S}_{i',i} x_i \right)^* y_i, \qquad \text{(G.1)}$$

by interchanging the roles of the dummy variables. This result continues to apply if we exclude, for example, beyond nearest or beyond next-nearest neighbours by symmetrically setting $J_{b,i,i'} = 0$ for hopping terms not required. From (3.16), since the diagonal terms in $\hat{\mathcal{L}}$ are real, we therefore have[1] $\sum_i x_i^* \hat{\mathcal{L}}_{b,i} y_i = \sum_i \left(\hat{\mathcal{L}}_{b,i} x_i \right)^* y_i$ so that:

$$\sum_i x_i^* \hat{\mathcal{L}}_{b,i} y_i = \frac{1}{2} \left[\sum_i \left(\hat{\mathcal{L}}_{b,i} x_i \right)^* y_i + \sum_i x_i^* \hat{\mathcal{L}}_{b,i} y_i \right], \qquad \text{(G.2)}$$

and, from (3.27):

$$\sum_i \hat{K}_{2,b,i} = \frac{1}{2} \sum_{i,j,k}{}' \left[(E_{b,j} + E_{b,k}) \left(\hat{\alpha}^\dagger_{b,j} \hat{\alpha}_{b,k} u^*_{b,i,j} u_{b,i,k} - \hat{\alpha}_{b,j} \hat{\alpha}^\dagger_{b,k} v_{b,i,j} v^*_{b,i,k} \right) \right.$$

$$\left. - (E_{b,j} - E_{b,k}) \left(\hat{\alpha}_{b,j} \hat{\alpha}_{b,k} v_{b,i,j} u_{b,i,k} - \hat{\alpha}^\dagger_{b,j} \hat{\alpha}^\dagger_{b,k} u^*_{b,i,j} v^*_{b,i,k} \right) \right]. \qquad \text{(G.3)}$$

First considering the term $(E_{b,j} - E_{b,k}) \left(\hat{\alpha}_{b,j} \hat{\alpha}_{b,k} v_{b,i,j} u_{b,i,k} - \hat{\alpha}^\dagger_{b,j} \hat{\alpha}^\dagger_{b,k} u^*_{b,i,j} v^*_{b,i,k} \right)$, this is clearly zero for $j = k$ and from $v_{b,i,k} \times (3.28) + u_{b,i,k} \times (3.29)$ and applying $\hat{\mathcal{L}}$ to the left:

$$(E_{b,j} + E_{b,k})(u_{b,i,j} v_{b,i,k} - v_{b,i,j} u_{b,i,k}) = 0, \qquad \text{(G.4)}$$

---

[1]This result shows that $\hat{\mathcal{L}}$ is Hermitian under the inner product $\langle x | y \rangle = \sum_i x_i^* y_i$

so, for $j \neq k$ we have:

$$v_{b,i,j} u_{b,i,k} = u_{b,i,j} v_{b,i,k}, \tag{G.5}$$

since $E_{b,k}$ is non-negative [95]. Therefore, the sum of each pair of opposite off-diagonal elements of the coefficients of $\hat{\alpha}_{b,j} \hat{\alpha}_{b,k}$ is zero. The same argument works for the off-diagonal coefficients of $\hat{\alpha}^\dagger_{b,j} \hat{\alpha}^\dagger_{b,k}$ using the complex conjugate of (G.5).

Now considering the term:

$$
\sum_{j,k} (E_{b,j} + E_{b,k}) \left(\hat{\alpha}^\dagger_{b,j} \hat{\alpha}_{b,k} u^*_{b,i,j} u_{b,i,k} - \hat{\alpha}_{b,j} \hat{\alpha}^\dagger_{b,k} v_{b,i,j} v^*_{b,i,k} \right)
$$
$$
= \sum_{j,k} (E_{b,j} + E_{b,k}) \left[\hat{\alpha}^\dagger_{b,j} \hat{\alpha}_{b,k} \left(u^*_{b,i,j} u_{b,i,k} - v^*_{b,i,j} v_{b,i,k} \right) - \delta_{jk} |v_{b,i,j}|^2 \right]. \tag{G.6}
$$

where we have used (3.19) and exchanged the dummy variables j and k for the $\hat{\alpha}_{b,j} \hat{\alpha}^\dagger_{b,k}$ terms. From $u^*_{b,i,k} \times (3.28) + v^*_{b,i,k} \times (3.29)$ and applying $\hat{\mathcal{L}}$ to the left:

$$(E_{b,j} - E_{b,k})(u_{b,i,j} u^*_{b,i,k} - v_{b,i,j} v^*_{b,i,k}) = 0, \tag{G.7}$$

so taking the complex conjugate for $j \neq k$ we have $u^*_{b,i,j} u_{b,i,k} = v^*_{b,i,j} v_{b,i,k}$, eliminating the off-diagonal terms, and using (3.26) for the diagonal terms we are left with:

$$\sum_i \hat{K}_{2,b,i} = \sum_j{}' E_{b,j} \hat{\alpha}^\dagger_{b,j} \hat{\alpha}_{b,j} - \sum_j{}' E_{b,j} \sum_i |v_{b,i,j}|^2 . \tag{G.8}$$

The Hamiltonian is therefore reduced to the diagonal form:

$$\hat{K} = -\sum_{i,i'} J_{0,i,i'} z^*_i z_{i'} + \sum_i \left[v_i - \mu + \frac{U_{00}}{2} |z_i|^2 \right] |z_i|^2 + \sum_{b,j}{}' E_{b,j} \left[\hat{\alpha}^\dagger_{b,j} \hat{\alpha}_{b,j} - \sum_i |v_{b,i,j}|^2 \right]. \tag{G.9}$$

Appendix H

Effective mass

We will use the derivative, (4.9), for our calculations, unless otherwise stated. We consider the accuracy of analytic approximations to the ground-band effective mass in the shallow and deep lattice limits. For $|k_x| \ll \pi/a_x$ [104]:

$$\frac{K_0(k_x)}{E_{R,x}} = \frac{V_x}{2E_{R,x}} + \left(\frac{a_x k_x}{\pi}\right)^2 + \frac{(V_x/4E_{R,x})^2}{2\left[(a_x k_x/\pi)^2 - 1\right]} + O\left(\frac{V_x}{E_{R,x}}\right)^4, \qquad \text{(H.1)}$$

so for $V_j < 4E_{R,j}$ we have:

$$\frac{m}{m_j^*} = 1 - \frac{V_j^2}{32E_{R,j}^2} + O\left(\frac{V_j}{E_{R,j}}\right)^4. \qquad \text{(H.2)}$$

In the opposite, $V_j \gg E_{R,j}$ limit, from (4.9) and (D.20):

$$\frac{m}{m_j^*} = \frac{\pi^2}{E_{R,j}} \sum_{l>0} l^2 J_{0,j}^l, \qquad \text{(H.3)}$$

which, in the tight-binding limit becomes:

$$\frac{m}{m_j^*} = \frac{\pi^2 J_{0,j}^1}{E_{R,j}}. \qquad \text{(H.4)}$$

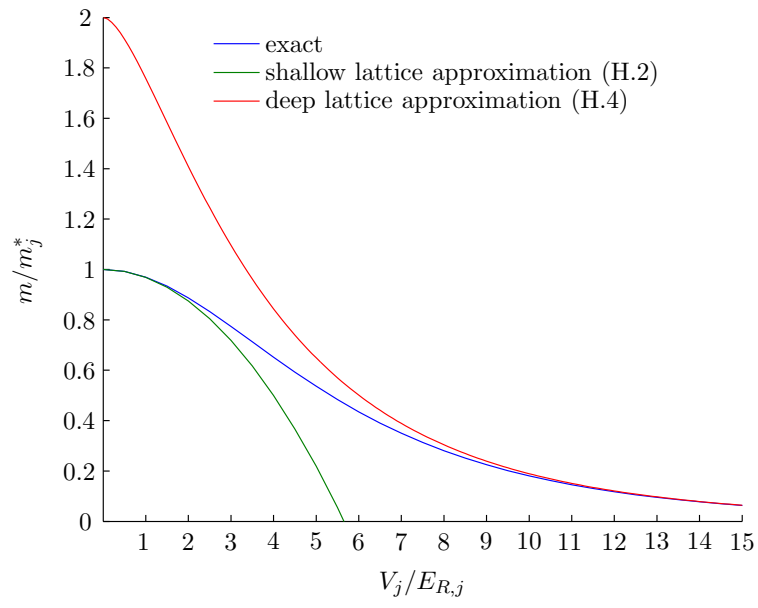A comparison of these approximations for the ratio of the mass to the effective mass is shown in figure H.1.

Figure H.1: Ratio of mass to effective mass

Appendix I

Bose function

We define the Bose function as:

$$\zeta_\alpha(z) \equiv \frac{1}{\Gamma(\alpha)} \int_0^\infty \frac{du\, u^{\alpha-1}}{z^{-1}e^u - 1}, \tag{I.1}$$

where $0 \leq z \leq 1$, analytically continued over the entire complex α-plane, except for the singularity (the harmonic series) when $\alpha = 1$ and $z = 1$ [117]. For $\alpha > 0$ and $z < 1$ we have (for $z = 1$ and $\alpha < 1$ we use the analytically continued form):

$$\zeta_\alpha(z) = \sum_{n=1}^\infty \frac{z^n}{\Gamma(\alpha)} \int_0^\infty du\, u^{\alpha-1} e^{-nu} = \sum_{n=1}^\infty \frac{z^n}{n^\alpha}. \tag{I.2}$$

From d'Alembert's test, this last form of $\zeta_\alpha(z)$ converges if $0 \leq z < 1$ since the ratio of successive terms $\to z$ as $n \to \infty$. From analytic continuation, this last form also applies for $\alpha \leq 0$ if $z < 1$.

We define the Riemann zeta function $\zeta(\alpha) \equiv \zeta_\alpha(1)$ and see that:

$$\zeta_\alpha(z) \to z \text{ as } z \to 0 \text{ or as } \alpha \to \infty, \tag{I.3}$$

$$\zeta_\alpha(z) \to \frac{z}{1-z} \text{ as } \alpha \to 0, \tag{I.4}$$

$$\zeta_\alpha(1) = \zeta(\alpha) = \sum_{n=1}^\infty n^{-\alpha} \text{ for } \alpha > 1, \tag{I.5}$$

$$\zeta_1(z) = -\ln(1-z). \tag{I.6}$$

We have, from (I.2):

$$\frac{\partial \zeta_\alpha\big(e^{f(x)}\big)}{\partial x} = \zeta_{\alpha-1}\big(e^{f(x)}\big) f'(x). \tag{I.7}$$

Appendix I. Bose function

A useful series expansion for $-2\pi < x < 0, \alpha \geq 0$ is:

$$\zeta_\alpha(e^x) = \begin{cases} 1/(e^{-x} - 1) & \alpha = 0, \\ \dfrac{x^{\alpha-1}}{(\alpha-1)!}[H_{\alpha-1} - \ln(-x)] + \displaystyle\sum_{n=0,n\neq\alpha-1}^{\infty} \dfrac{\zeta(\alpha-n)}{n!}x^n & \alpha = 1, 2, 3, 4, 5, \ldots, \\ \Gamma(1-\alpha)(-x)^{\alpha-1} + \displaystyle\sum_{n=0}^{\infty} \dfrac{\zeta(\alpha-n)}{n!}x^n & \text{otherwise,} \end{cases}$$

(I.8)

where we have converted from the form of [117] using:

$$H_{\alpha-1} = \frac{d}{2} + \frac{\Gamma'(\alpha)}{\Gamma(\alpha)}, H_n = \sum_{m=1}^{n} \frac{1}{m}, H_0 = 0.$$

(I.9)

For expansions up to order $\alpha - 2$, the $x^{\alpha-1}$ term in (I.8) can be ignored.

Appendix J

Translationally-invariant lattice integrand

In this appendix, we consider the numerics of the translationally-invariant lattice calculation and justify the accuracy of the effective-mass critical temperatures. We consider the case when the integrand for the ground-band density is $g_0(K)/(e^{K/k_B T} - 1)$ (for example at or below the critical temperature for a non-interacting gas with $\mu \to 0$, or at the critical temperature for an interacting gas, so that $\mu \to 2 \sum_{b'} U_{bb'} \tilde{n}_{b'}(\bar{r})$, where we ignore the finite-size effect for a translationally-invariant lattice). For low K, the effective-mass approximation is reasonable from section 4.4, so that the integrand is then:

$$\int_0^K \frac{g_0(K')\mathrm{d}K'}{e^{K'/k_B T} - 1} \propto \int_0^K K'^{d/2-2}\mathrm{d}K' \propto K^{d/2-1}, \tag{J.1}$$

so that, even for the three-dimensional case, the integrand has a divergence at $K = 0$ (and the integral is divergent for one dimension reflecting the lack of condensation in that case), so that this low energy region is very important to the integral.

To improve the numerical calculations, we transform the above integral using $K = u^4$ in three dimensions so that:

$$\int_0^K \frac{g_0(K')\mathrm{d}K}{e^{K'/k_B T} - 1} = \int_0^u \frac{g_0(u'^4)}{e^{u'^4/k_B T} - 1}4u'^3\mathrm{d}u' \propto \int_0^u u'\mathrm{d}u' \propto u^2 = \sqrt{K}, \tag{J.2}$$

so that the integrand is zero at the origin and initially linear thereafter. We could substitute $K \propto p^2$ so that the integrand is initially constant, but an initially zero integrand improves numerics.

Appendix J. Translationally-invariant lattice integrand

We consider the deep lattice case, $V = 15E_R$, where the actual and effective-mass density of states are very different, except for the low energy region, as shown in figure J.1. We note that the first excited band does not start until $K > 6E_R$ which emphasises just how different the effective-mass density of states is and ensures that the excited bands will not be significant for the temperatures we are considering (in figure 7.2).
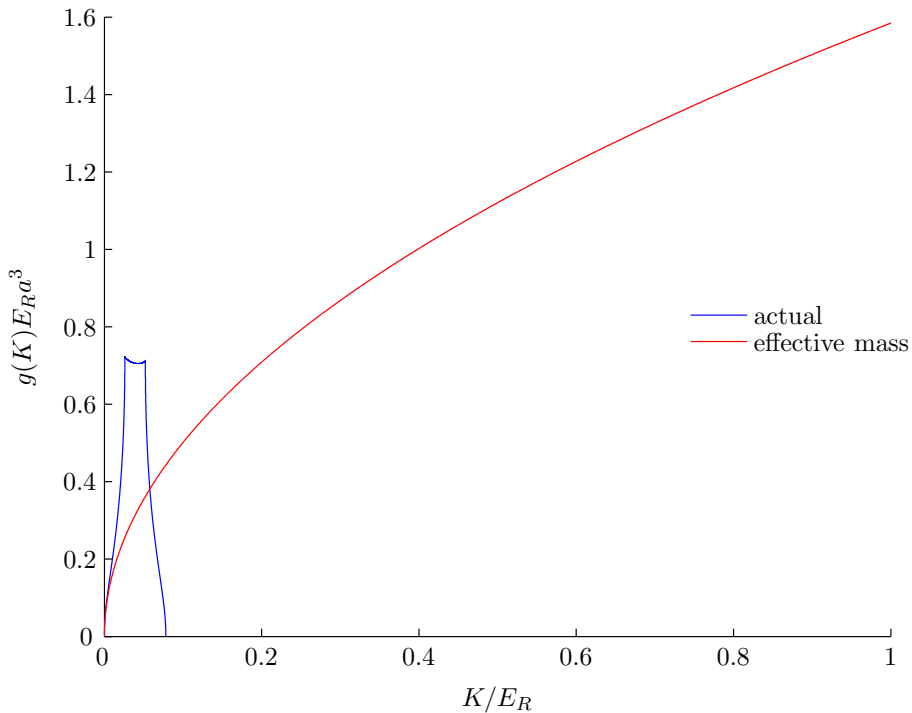

Figure J.1: Comparison of three-dimensional density of states for $V = 15E_R$

Since the integrand is divergent, we cannot see the important region by plotting it directly. Instead we plot the transformed integrand of (J.2) in figure J.2. We have used the same horizontal scale in both cases (the interval $K/E_R \in [0, 1]$ in figure J.1 is equivalent to $u/E_R^{1/4} \in [0, 1]$ in figure J.2). We use $k_B T = 0.1E_R$, a typical critical temperature for this lattice depth. We see that the integrands are rather different in shape, but the linear region (the effective-mass region) where they agree has some importance, the high energy region is exponentially suppressed by the temperature and the integral or area under the curves is similar.
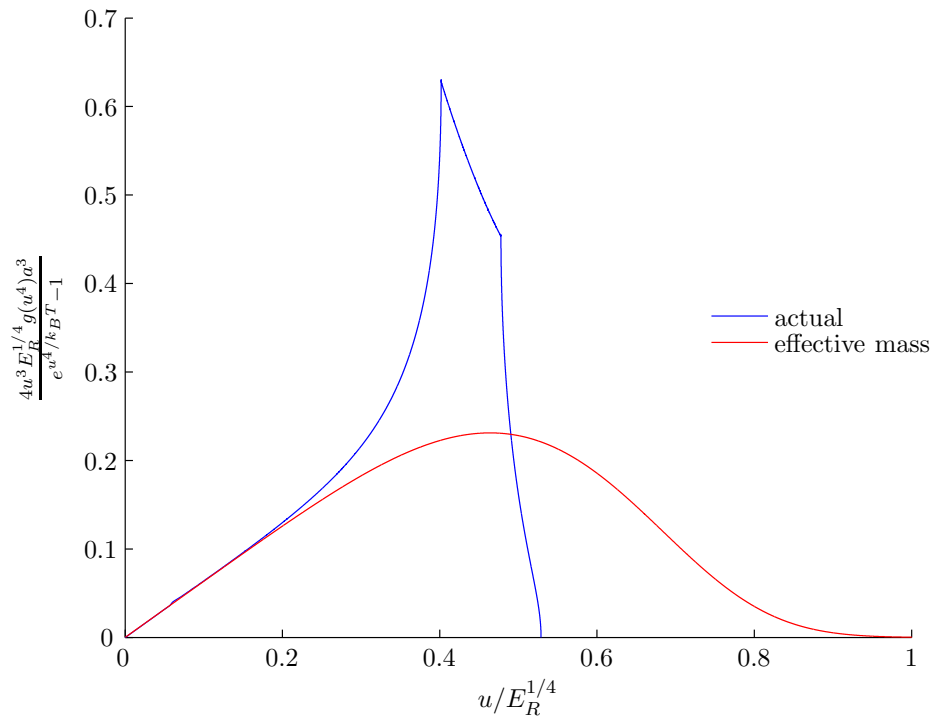
Figure J.2: Integrand of (J.2) for $V = 15E_R$ at $k_B T = 0.1E_R$

Appendix K

Simplified ground-band shape finite-size effect

We consider the finite-size effect for the three-dimensional combined harmonic lattice, extending the results of section 7.5 by giving the derivatives in terms of the Bose function forms which are valid for higher w than the series expansion, and we derive the finite-size effect for each of the band shapes.

K.1 Centred-delta

From (7.11), (I.7) and (I.8) the derivatives are:

$$\left[\frac{\partial \tilde{N}_0(\mu)}{\partial \mu}\right]_{\mu=0} = N_s \beta \zeta_{1/2}\big(e^{-w/2}\big) \tag{K.1}$$

$$= N_s \beta \left[\sqrt{\frac{2\pi}{w}} + \zeta(1/2) - \frac{\zeta(-1/2)}{2}w + O\big(w^2\big)\right], \tag{K.2}$$

$$\frac{\partial \tilde{N}_0(0)}{\partial T} = \frac{N_s}{T}\left[\frac{3}{2}\zeta_{3/2}\big(e^{-w/2}\big) + \frac{w}{2}\zeta_{1/2}\big(e^{-w/2}\big)\right] \tag{K.3}$$

$$= \frac{N_s}{T}\left[\frac{3}{2}\zeta(3/2) - \sqrt{2\pi w} - \frac{\zeta(1/2)}{4}w + O\big(w^2\big)\right]. \tag{K.4}$$

From (7.49), (K.1) and (K.3) we get:

$$\delta T_c^{\text{fs}} = -\frac{\mu_{\text{fs}}}{k_B} \frac{2\zeta_{1/2}\left(e^{-w_c^0/2}\right)}{3\zeta_{3/2}(e^{-w_c^0/2}) + w_c^0\zeta_{1/2}(e^{-w_c^0/2})} \tag{K.5}$$

$$= -\frac{\mu_{\text{fs}}}{k_B} \left[\frac{2\sqrt{2\pi}}{3\zeta(3/2)\sqrt{w_c^0}} + \frac{8\pi}{9\zeta(3/2)^2} + \frac{2\zeta(1/2)}{3\zeta(3/2)} + O\left(\sqrt{w_c^0}\right) \right]. \tag{K.6}$$

K.2   Rectangular

From (7.17), (I.7) and (I.8) the derivatives are:

$$\left[\frac{\partial \tilde{N}_T^0(\mu)}{\partial \mu} \right]_{\mu=0} = \frac{N_s\beta}{w} \left[\zeta(3/2) - \zeta_{3/2}\left(e^{-w}\right) \right] \tag{K.7}$$

$$= N_s\beta \left[2\sqrt{\frac{\pi}{w}} + \zeta(1/2) - \frac{\zeta(-1/2)w}{2} + O\left(w^2\right) \right], \tag{K.8}$$

$$\frac{\partial \tilde{N}_T^0(0)}{\partial T} = \frac{N_s}{wT} \left[\frac{5}{2}\zeta(5/2) - \frac{5}{2}\zeta_{5/2}\left(e^{-w}\right) - w\zeta_{3/2}\left(e^{-w}\right) \right] \tag{K.9}$$

$$= \frac{N_s}{T} \left[\frac{3}{2}\zeta(3/2) - \frac{4\sqrt{\pi w}}{3} - \frac{\zeta(1/2)w}{4} + O\left(w^2\right) \right]. \tag{K.10}$$

From (7.49), (K.7) and (K.9) we get:

$$\delta T_c^{\text{fs}} = -\frac{\mu_{\text{fs}}}{k_B} \frac{\zeta(3/2) - \zeta_{3/2}\left(e^{-w_c^0}\right)}{\frac{5}{2}\zeta(5/2) - \frac{5}{2}\zeta_{5/2}(e^{-w_c^0}) - w_c^0\zeta_{3/2}(e^{-w_c^0})} \tag{K.11}$$

$$= -\frac{\mu_{\text{fs}}}{k_B} \left[\frac{4\sqrt{\pi}}{3\zeta(3/2)\sqrt{w_c^0}} + \frac{32\pi}{27\zeta(3/2)^2} + \frac{2\zeta(1/2)}{3\zeta(3/2)} + O\left(\sqrt{w_c^0}\right) \right]. \tag{K.12}$$

K.3   Quadratic

From (7.20), (I.7) and (I.8) the derivatives are:

$$\left[\left(\frac{\partial \tilde{N}}{\partial \mu}\right)_T\right]_{\mu=0} = \frac{6N_s\beta}{w^3}\left[w\zeta(5/2) - 2\zeta(7/2) + w\zeta_{5/2}\left(e^{-w}\right) + 2\zeta_{7/2}\left(e^{-w}\right)\right] \quad \text{(K.13)}$$

$$= N_s\beta\left[\frac{8\sqrt{\pi}}{5\sqrt{w}} + \zeta(1/2) - \frac{\zeta(-1/2)w}{2} + O(w^2)\right], \quad \text{(K.14)}$$

$$\left[\left(\frac{\partial \tilde{N}}{\partial T}\right)_\mu\right]_{\mu=0} = \frac{27N_s}{w^3 T}\left[w\zeta(7/2) - 2\zeta(9/2) + w\zeta_{7/2}\left(e^{-w}\right) + 2\zeta_{9/2}\left(e^{-w}\right)\right]$$

$$- \frac{6N_s}{w^2 T}\left[\zeta(7/2) - \zeta_{7/2}\left(e^{-w}\right) - w\zeta_{5/2}\left(e^{-w}\right)\right] \quad \text{(K.15)}$$

$$= \frac{N_s}{T}\left[\frac{3}{2}\zeta(3/2) - \frac{48\sqrt{\pi w}}{35} - \frac{\zeta(1/2)w}{4} + O(w^2)\right]. \quad \text{(K.16)}$$

From (7.49), (K.13) and (7.51) we get:

$$\delta T_c^{\text{fs}} = -\frac{\mu_{\text{fs}}}{k_B}\left[\frac{16\sqrt{\pi}}{15\zeta(3/2)\sqrt{w_c^0}} + \frac{2\zeta(1/2)}{3\zeta(3/2)} + \frac{512\pi}{525\zeta(3/2)^2} + O\left(\sqrt{w_c^0}\right)\right]. \quad \text{(K.17)}$$

K.4   Triangular

From (7.25), (I.7) and (I.8) the derivatives are:

$$\left[\frac{\partial \tilde{N}_T^0(\mu)}{\partial \mu}\right]_{\mu=0} = \frac{4N_s}{k_B T w^2}\left[\zeta(5/2) - 2\zeta_{5/2}\left(e^{-w/2}\right) + \zeta_{5/2}\left(e^{-w}\right)\right] \quad \text{(K.18)}$$

$$= \frac{4N_s}{k_B T}\left[\frac{2\sqrt{\pi}\left(2 - \sqrt{2}\right)}{3\sqrt{w}} + \frac{\zeta(1/2)}{4} + O(w)\right], \quad \text{(K.19)}$$

$$\frac{\partial \tilde{N}_T^0(0)}{\partial T} = \frac{14N_s}{w^2 T}\left[\zeta(7/2) - 2\zeta_{7/2}\left(e^{-w/2}\right) + \zeta_{7/2}\left(e^{-w}\right)\right]$$

$$+ \frac{4N_s}{wT}\left[-\zeta_{5/2}\left(e^{-w/2}\right) + \zeta_{5/2}\left(e^{-w}\right)\right] \quad \text{(K.20)}$$

$$= \frac{N_s}{T}\left[\frac{3}{2}\zeta(3/2) - \frac{8\sqrt{\pi}}{15}\left(4 - \sqrt{2}\right)\sqrt{w} - \frac{\zeta(1/2)}{4}w + O(w^2)\right]. \quad \text{(K.21)}$$

From (7.49), (K.18) and (K.21) we get:

$$\delta T_c^{\text{fs}} = -\frac{\mu_{\text{fs}}}{k_B}\left[\frac{16(2 - \sqrt{2})\sqrt{\pi}}{9\zeta(3/2)\sqrt{w_c^0}} + \frac{2\zeta(1/2)}{3\zeta(3/2)} + \frac{512(5 - 3\sqrt{2})\pi}{405\zeta(3/2)^2} + O\left(\sqrt{w_c^0}\right)\right].$$

$$\text{(K.22)}$$

Appendix L

Spread function

We derive some results for the spread function for the three-dimensional combined harmonic lattice.

L.1 Centred delta

From (7.10) we have:

$$\left[\frac{\partial \tilde{n}_T^0(\mathbf{r}, \mu)}{\partial \mu}\right]_{\mu=0} = \frac{\beta \exp[\beta V_{\mathrm{tr}}(\mathbf{r}) + w/2]}{\{\exp[\beta V_{\mathrm{tr}}(\mathbf{r}) + w/2] - 1\}^2}. \tag{L.1}$$

We recognise that, only for the centred delta shape, the product of the density and its derivative takes the following easy to integrate form:

$$\tilde{n}_T^0(\mathbf{r}, \mu)\frac{\partial \tilde{n}_T^0(\mathbf{r}, \mu)}{\partial \mu} = \frac{1}{2}\left(\frac{1}{\beta}\frac{\partial^2}{\partial \mu^2} - \frac{\partial}{\partial \mu}\right)\tilde{n}_T^0(\mathbf{r}, \mu), \tag{L.2}$$

so that we have:

$$\frac{1}{a^3}\int d\mathbf{r}\,\tilde{n}_T^0(\mathbf{r}, 0)\left[\frac{\partial \tilde{n}_T^0(\mathbf{r}, \mu)}{\partial \mu}\right]_{\mu=0} = \frac{1}{2}\left[\left(\frac{1}{\beta}\frac{\partial^2}{\partial \mu^2} - \frac{\partial}{\partial \mu}\right)\tilde{N}_T^0(\mu)\right]_{\mu=0}$$

$$= \frac{N_s\beta}{2}\left[\zeta_{-1/2}\big(e^{-w/2}\big) - \zeta_{1/2}\big(e^{-w/2}\big)\right], \tag{L.3}$$

where we have used (K.1) and we get the following analytic result for the spread function:

$$S(w) = \frac{e^{w/2} - 1}{2}\left[\frac{\zeta_{-1/2}\big(e^{-w/2}\big)}{\zeta_{1/2}\big(e^{-w/2}\big)} - 1\right]. \tag{L.4}$$

L.2 Rectangular

We show that a rectangular band assumption would lead us to the incorrect conclusion for the spread function. The ratio $\tilde{n}_T^0(\mathbf{r}, 0)/\tilde{n}_T^0(\mathbf{0}, 0) = 1$ if $\mathbf{r} = \mathbf{0}$. For any other $\mathbf{r}$, the numerator is finite and the denominator is infinite from (7.16) so that $\tilde{n}_T^0(\mathbf{r}, 0)/\tilde{n}_T^0(\mathbf{0}, 0) = 0$. As $\mathbf{r} \to \mathbf{0}$:

$$\left[\frac{\partial \tilde{n}_T^0(\mathbf{r}, \mu)}{\partial \mu} \right]_{\mu=0} \to \frac{\beta}{w} \left[\frac{1}{V_{\mathrm{tr}}(\mathbf{r})} - \frac{1}{e^w - 1} \right], \tag{L.5}$$

so that $r^2 \left[\partial \tilde{n}_T^0(\mathbf{r}, \mu)/\partial \mu \right]_{\mu=0}$ is finite. Also $\left[\partial \tilde{N}_T^0(\mu)/\partial \mu \right]_{\mu=0}$ is finite from (K.7) so that we would falsely conclude that $S(w) = 0$.

L.3 Quadratic

The integrand of the numerator of the spread function is:

$$\left[\tilde{n}(\mathbf{r}) \left(\frac{\partial \tilde{n}(\mathbf{r})}{\partial \mu} \right)_T \right]_{\mu=0} = \frac{36\beta}{w^6 a^6}$$

$$\times \left[w\zeta_2 \left(e^{-\beta V_{\mathrm{tr}}(\mathbf{r})} \right) - 2\zeta_3 \left(e^{-\beta V_{\mathrm{tr}}(\mathbf{r})} \right) + w\zeta_2 \left(e^{-\beta V_{\mathrm{tr}}(\mathbf{r})-w} \right) + 2\zeta_3 \left(e^{-\beta V_{\mathrm{tr}}(\mathbf{r})-w} \right) \right]$$

$$\times \left[w\zeta_1 \left(e^{-\beta V_{\mathrm{tr}}(\mathbf{r})} \right) - 2\zeta_2 \left(e^{-\beta V_{\mathrm{tr}}(\mathbf{r})} \right) + w\zeta_1 \left(e^{-\beta V_{\mathrm{tr}}(\mathbf{r})-w} \right) + 2\zeta_2 \left(e^{-\beta V_{\mathrm{tr}}(\mathbf{r})-w} \right) \right]. \tag{L.6}$$

As $w \to \infty$, using (7.19), (7.65), (7.50) and (L.6):

$$S(w) \to \frac{1}{\zeta(2)\zeta(5/2)} \sum_{j,k=1}^{\infty} \frac{1}{j^2 k (j+k)^{3/2}} \approx 0.325, \tag{L.7}$$

where we have used:

$$\frac{1}{a^3 N_s} \int d\mathbf{r}\, \zeta_2 \left(e^{-\beta V_{\mathrm{tr}}(\mathbf{r})} \right) \zeta_1 \left(e^{-\beta V_{\mathrm{tr}}(\mathbf{r})} \right) = \frac{1}{a^3 N_s} \sum_{j,k=1}^{\infty} \frac{1}{j^2 k} \int d\mathbf{r}\, \exp \left[-(j+k)\beta V_{\mathrm{tr}}(\mathbf{r}) \right]$$

$$= \sum_{j,k=1}^{\infty} \frac{1}{j^2 k (j+k)^{3/2}} \approx 0.7173. \tag{L.8}$$

L.4 Triangular

The integrand of the numerator of the spread function is:

$$\left[\tilde{n}(\mathbf{r})\left(\frac{\partial\tilde{n}(\mathbf{r})}{\partial\mu}\right)_T\right]_{\mu=0} = \frac{16\beta}{w^4 a^6}$$

$$\times\left[\zeta_2\left(e^{-\beta V_{\mathrm{tr}}(\mathbf{r})}\right) - 2\zeta_2\left(e^{-\beta V_{\mathrm{tr}}(\mathbf{r})-w/2}\right) + \zeta_2\left(e^{-\beta V_{\mathrm{tr}}(\mathbf{r})-w}\right)\right]$$

$$\times\left[\zeta_1\left(e^{-\beta V_{\mathrm{tr}}(\mathbf{r})}\right) - 2\zeta_1\left(e^{-\beta V_{\mathrm{tr}}(\mathbf{r})-w/2}\right) + \zeta_1\left(e^{-\beta V_{\mathrm{tr}}(\mathbf{r})-w}\right)\right]. \quad (L.9)$$

As $w \to \infty$, using (7.24), (7.65), (K.18), (L.8) and (L.9):

$$S(w) \to \frac{1}{\zeta(2)\zeta(5/2)} \sum_{j,k=1}^{\infty} \frac{1}{j^2 k(j+k)^{3/2}}, \quad (L.10)$$

as in the quadratic case.